Design, Construction and Commissioning of a Transonic Test-Turbine Facility

J. Erhard

Doctoral Thesis at the Institute of

Thermal Turbomachinery and Machine Dynamics

Graz University of Technology, Austria

First Expert : **Prof. Dr. techn. H. Jericha**
Institute of Thermal Turbomachinery and Machine Dynamics
Technical University of Graz, Austria

Second Expert : **Prof. Dr. techn. W. Sanz**
Institute of Thermal Turbomachinery and Machine Dynamics
Technical University of Graz, Austria

Graz, May 2000

Acknowledgements

The author gratefully acknowledge the support of the Austrian Science Foundation (FWF) in the project S6801-TEC, "Efficiency improvement by flow optimisation". The work summarised here is also part of the BRITE EURAM project DITTUS ("Development of Industrial Transonic Turbine Stages"), in which our institute had to adapt the whole test rig for testing new turbine stages in full similarity but also got the chance to employ the following persons the author would also like to thank : Mr. G. Kulhanek for the proper alignment and balancing of the machine train, the brake compressors inlet filter and venturi nozzle and for his help in countless detail work on the test rig assembly. Mr. F. Neumayer for the transient FEM verification of the casing above the running blades, the overflow pipe and the exhaust line handling and the final construction of the suction blower. Mr. A. Seyr for his precious contribution to the conventional measurement concept, the compressor station supply pipe and the brake compressors IGV´s drive. Thanks also to Mr. N. Mayrhofer for his contribution to the automatic machine train speed control and Mr. Woisetschläger for the vibrometer and holographic measurements on the bladed disc.

With thankfulness towards Mr. A. Gehrer I will commend his work in CFD optimisation of the final TTM-stage design, his help in Quasi 3D simulation for different load condition calculation, his GLAGER present for tilting pad bearing recalculation and his availability in technical discussions.

Thanks also to Prof. Jericha who gave me the vision for having some national and also international turbomachinery industry in our test hall in Austria.

Finally I want to dedicate this doctoral thesis to all engineers having their strength in God and not in their own limited power to serve the creation he gave us.

Abstract

This doctoral thesis describes the design concept and construction of a continuous operating cold flow transonic test turbine facility, which is a unique combination of a 2 MW axial test turbine and a direct coupled brake compressor. To cover the losses additional air is provided by a separate electrically driven compressor station and fed into the turbine inlet casing via special mixer inserts which are also fed by the hot compressed air from the brake compressor. The main test rig dimensions and its capabilities are outlined.

A description of the design illustrated at some test rig features is presented starting from the first conceptual ideas up to the latest plant development for special testing conditions enabling performance measurements at industrial transonic turbine stages. The aerodynamic and structural design of the internally developed transonic single turbine stage (TTM-Stage) is shown in detail and some results of the respective flow simulations are presented.

A summary of the test rig commissioning, final conclusions and an appendix containing the most important simulation model parameters and some drawings conclude this detailed information.

Contents

1. Introduction

1.1 Starting point

The Institute for Thermal Turbomachinery and Machine Dynamics (TTM) planned to start some research on industrial turbines, because first turbine technology was more interesting for our national industry and second turbine aerothermal design technology has not reached the ultimate level in comparison to compressor technology which has evolved to high loading, high pressure ratio designs with a limited number of stages.

The most advanced turbines at present are those employed by aircraft engines. For the high pressure turbine section single highly loaded stages are typically used on military engines, where low weight rather than very high efficiency and lifetime is really the target. The civil aero engine low pressure turbines used to drive the engine fan at low speed are made up of multiple, low Mach number stages having almost no relationship with the kind of high speed low pressure stages needed on the industrial gas turbines.

The market trend towards higher efficiency on industrial gas turbines at constant and possibly decreasing costs per kW shaft power led to advanced 3-D aerodynamic designs for higher pressure ratios and increasing maximum cycle temperatures associated with advanced cooling techniques and hot part materials [1]. For reduction of the substantial increases in manufacturing costs especially the very expensive parts of the turbine hot section up to now show considerable potential through stage number reduction at comparable efficiencies. This calls for an increase of total enthalpy drop per stage. Blade peripheral speeds could not increase that much keeping high reliability and long life design criteria within hot part stress and metal temperature constraints. This indicates the need for higher loading coefficients with considerably higher Mach number level. This leads to severe supersonic shock activity which has to be optimised by suitable aero design strongly supported by nonsteady flow analysis and testing to provide still acceptable stage efficiencies. To allow better observation to this shock activity in rotor-stator interaction and its influence on stage performance it was decided to build up a transonic test turbine facility for continuous operation of highly loaded turbine stages under full flow similarity.

Since the University of Graz had decided many years ago to build new premises for its new Institute for Thermal Turbomachinery and Machine Dynamics (TTM) a great environment was already prepared for building up such new test facilities [2].

In the large test hall a modular designed turbomachinery foundation was prepared for a machine train consisting of an old back pressure turbine from the dismantled Technical University heating and power station with a step-down gear to its former generator. A big exhaust air tower including silencers was installed and in the second basement a large compressor and cooling station had been installed to supply the new test stand with pressurized air and cooling water.

Moreover the national refinery ÖMV made a great industry present to our institute in 1993 as a big centrifugal compressor in their FCC-plant was replaced by a bigger one. This three stage centrifugal compressor GHH G5-6/3L was originally rated at 11175rpm at a pressure ratio from 0.99 to 4.1bar with an airflow of 9.0kg/s at 1.9 MW.

To overcome the efforts to feed back the electrical energy from the synchronized turbine driven generator to the electrical grid there now was a new possibility to use this centrifugal compressor instead of the generator. In addition this machines could be connected as a free running turbo group feeding back the pressurized air from the brake compressor to the supply system. Since only the losses of this continuous running machine train had to be covered from the TTM compressor station it seemed to be worth examining it in more detail.

1.2 Mission

As I first noticed this idea in the Design Exercise at TTM in 1992 and I already knew something about the characteristics of such a configuration it was another step to start my diploma thesis on August 1993 as a part of a preliminary study.

Due to cost reasons we first examined the old industrial steam turbine with the two Curtis wheels to be adapted with a new blading. But the calculations of the shaft bending modes and the bearing stability of this design did not allow to run it above 9000 rpm. So we decided to build a new test turbine that could satisfy our high demands in a wide adjustable speed range between 7000 and 11500 rpm.

To get the right machine scale without cost overruns a principle decision was made to manufacture a high number of parts our own. Prof. Jericha gave me the vision for having some national and also international turbomachinery industry in our test hall if this transonic test turbine facility would be valuable enough for their test configurations. But without God´s wonderful help I would have been lost in fighting my continuous stretching time schedule because of doing too much work alone with limited power.

1.3 Comparison with other test facilities

Existing low speed air test turbines do have their big advantages in scale but in flow similarity condition they are restricted to subsonic flows. But test turbines which also could operate in continuous transonic flow are often limited in the available power for testing highly loaded transonic stages in full flow similarity.

In the field of test turbine rigs in the last years there was a tendency for building short duration machines with very advanced high time resolved measurements which needs less operation power in comparison to the continuous running facilities. But also the state of the art compression tube turbine facilities at the VKI and MIT which can achieve full flow similarity for the main flow and perhaps even cooling effectiveness have too short continuous operation time to observe all flow details researchers looking for.

To complement the collection of test turbine facilities Prof. Jericha decided well to build up a test rig for continuous operation at full scale and transonic flow ability with blade interaction and pressurised air as flow medium in an open cycle.

To give a brief overview to present test rig facility technology the four most common types are described on one example each :

(1) The Low Speed Research Turbine in open cycle configuration from [3] serves the possibility for very detailed measurements down to real boundary layer effects because of large scale bladings. If geometrically similar scaled blade models moved through a fluid with the same orientation at similar Mach and Reynolds number will experience the same dimensionless forces due to aerodynamic similarity. Since the large scale test blading could only be tested up to about a Mach number of 0.12 and the blading in the real engine runs at Mach numbers of 0.6 to 0.8 a second approach has to be added to compensate for the different Mach numbers in the compressible fluid. To behave the same aerodynamically effects at different Mach numbers the incidence angle of the blading relative to the approaching air, the camber (curvature) of the blading and the thickness distribution along the balding has to be prescribed. Also looking carefully at the same scaled surface roughness and turbulence intensity the low-speed airfoils are said to be “aerodynamically similar“ to the high-speed airfoils. Although the greater accuracy at large scale and the lower costs through less power consumption and less expensive materials have a great contribution to low pressure turbine research the LSRT (see Fig. 1) concept cannot provide the environment for transonic flows from its definition.

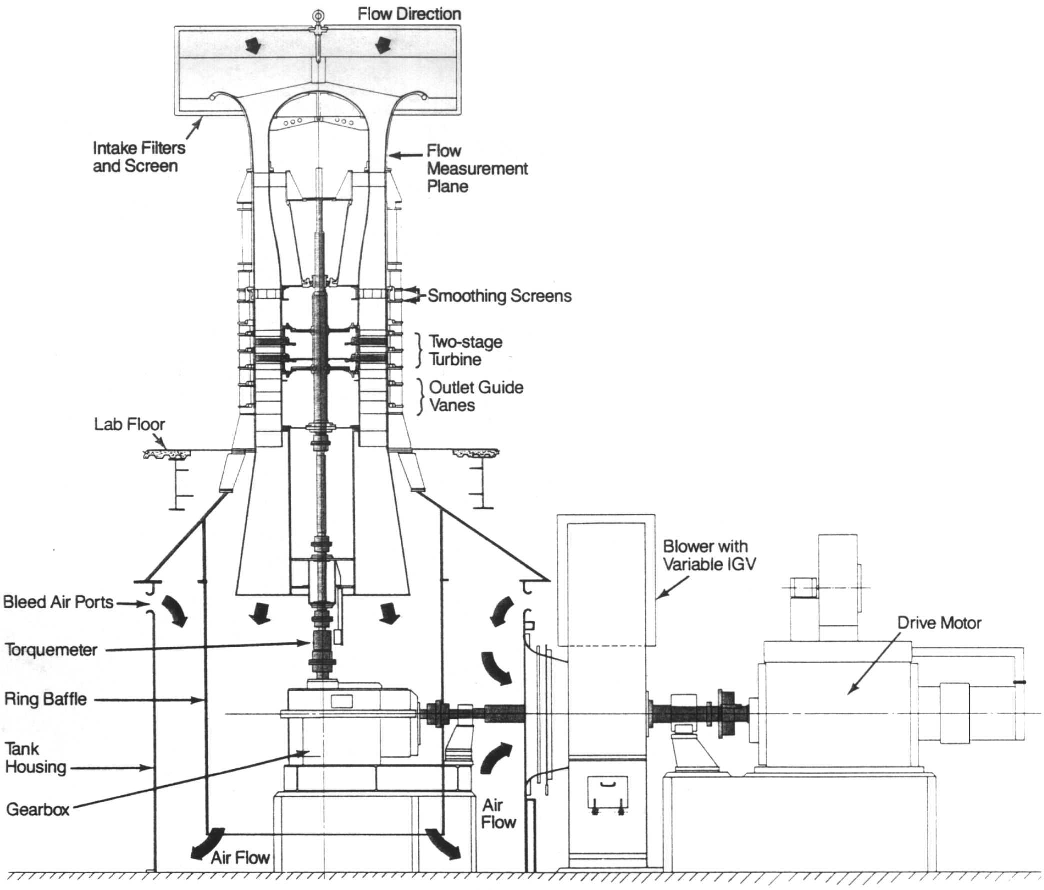

Fig. 1 Schematic of a Low Speed Research Compressor (LSRT in GE-ARL) in a two stage configuration

(2) Some test stands built in wind tunnel configurations as closed cycle facilities have the advantage of adjustable pressure and temperature level for independent variation of Mach and Reynolds number [4]. The flow medium (dried air) is driven in an closed wind tunnel cycle by an compressor with a variable speed electric motor and additional bypass valves. In order to maintain a constant temperature in the system a water cooled heat exchanger is used to achieve elevated temperatures a test section inlet. The pressure ratio of 6 provides testing capabilities up to Mach numbers of 1.8 (in the relative system). The maximum compressor power of 1MW at total inlet pressures of 10...150kPa and total inlet temperature of 15...50°C therefore enables Reynolds numbers up to 50 000 (based upon exit conditions) at a mean diameter of 512mm and 36mm blade height. In comparison the new test stand at the ETH Zürich [5] enables 800mm tip diameter at 90mm blade height, but since it is not possible to pressurise this test stand the Mach and Reynolds number are directly coupled since velocity variations can only be affected through variations of inlet mass flow. However in reality for loss studies in shock free flows Mach number variations are of less importance. Enabling comparable Reynolds numbers for transitional boundary layers this test rig provides interesting results for CFD evaluation at best controlled inlet boundary conditions (see Fig. 2).

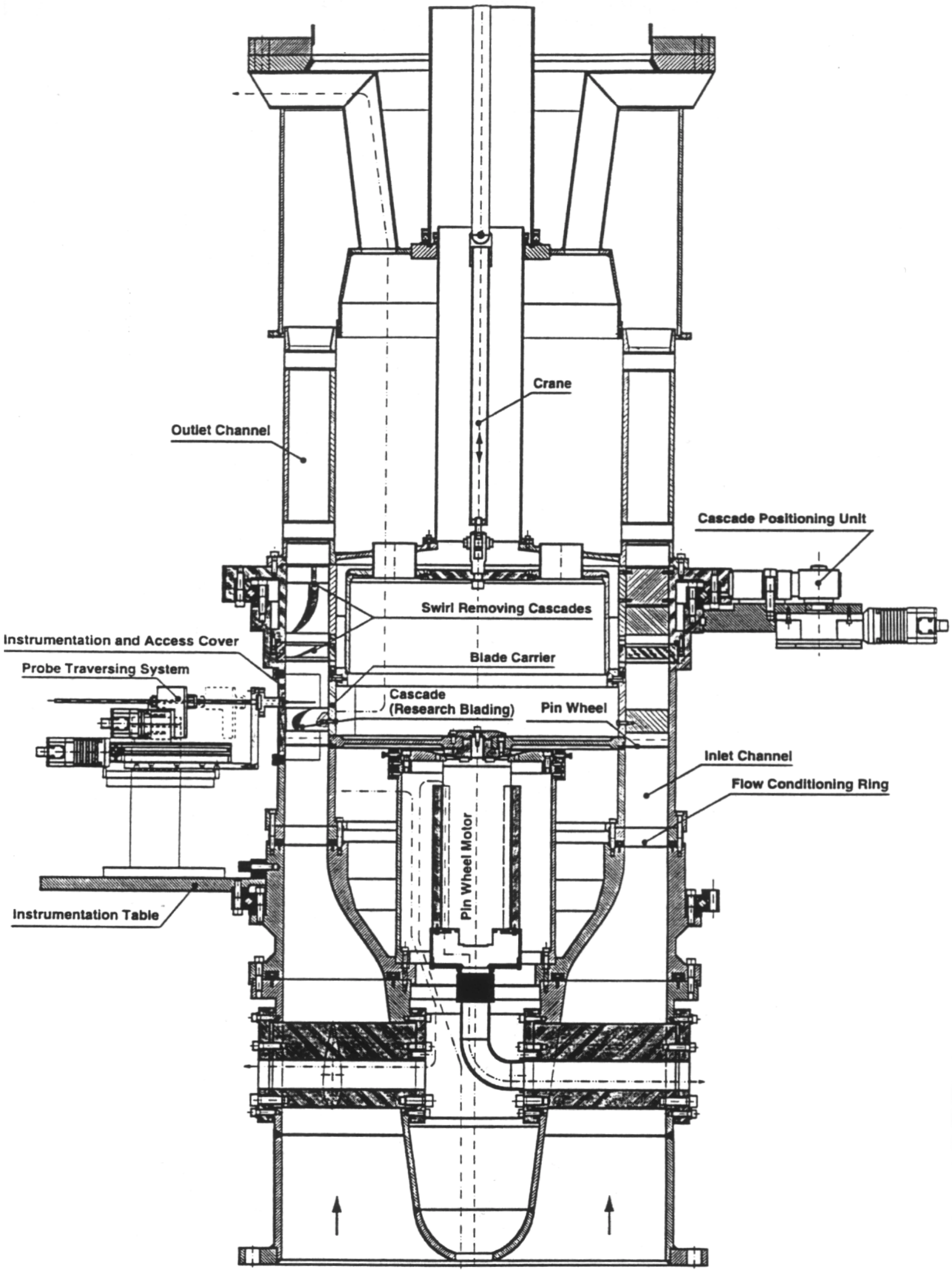

Fig. 2 Test section of test stand at ETH-Zürich

(3) Compression Tube Facilities like the one used at the VKI [6] are short duration test machines with highly sophisticated operation and measurement techniques investigating 1:1scaled transonic test stages under full flow and perhaps cooling flow similarity. A typical blowdown after stabilising the rotor on test speed continues about 0.5s, the measurement averaging time at constant stage parameters is about 0.1s. Since this test facilities are equipped with high time resolution equipment they are predestined to unsteady measurements. Although the step from continuous to short duration measurement enables testing of highly loaded transonic industrial stages at less power demand this technique is hardly used for performance mapping.

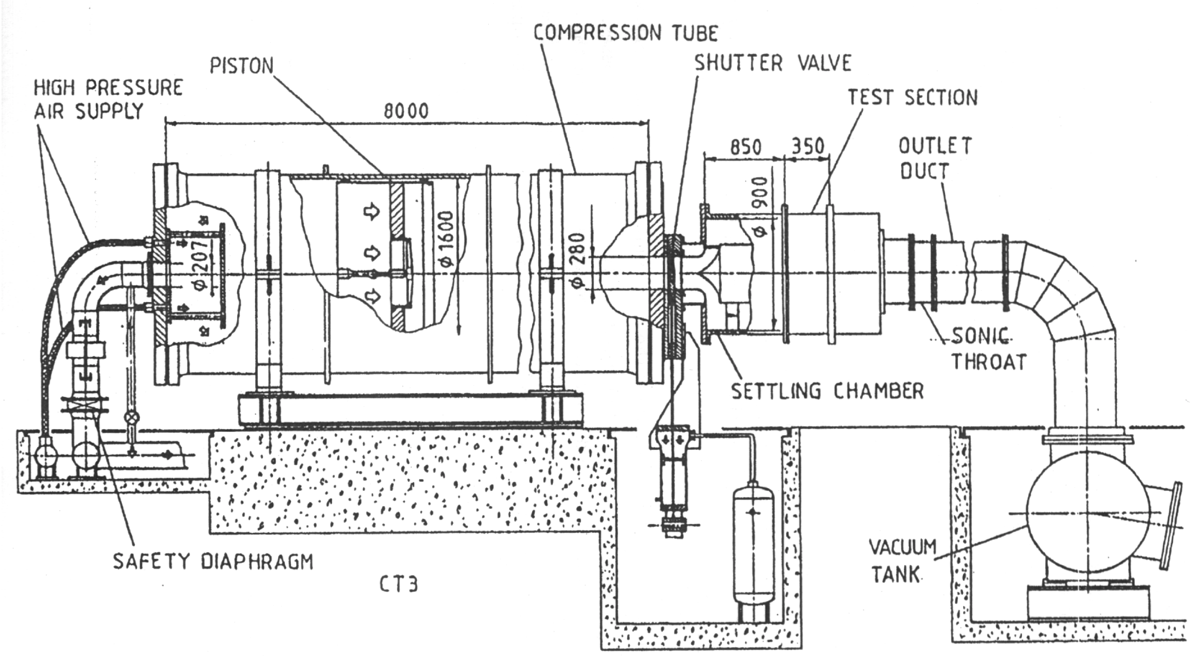

Fig. 3 Main elements of a compression tube facility

(4) Test rigs in industry often use real machine components and people there on first priority have to explore if the performance goals are met for scheduled manufacturing and customer dates and if the explored configuration may have an aerodynamic risk of performance penalty or could lead in difficulties at a major engine program. In Fig. 4 a part of the test section of a cold test rig for performance investigations on the High Work Research Turbine (HWRT) [7] is shown. Pratt and Whittney Canada investigated in the tests of this aggressive transonic stage design the influence of speed and limit load pattern on performance maps comparing cooled and uncooled efficiency with real engine data measured on a High Technology Demonstrator Engine (HDTE).

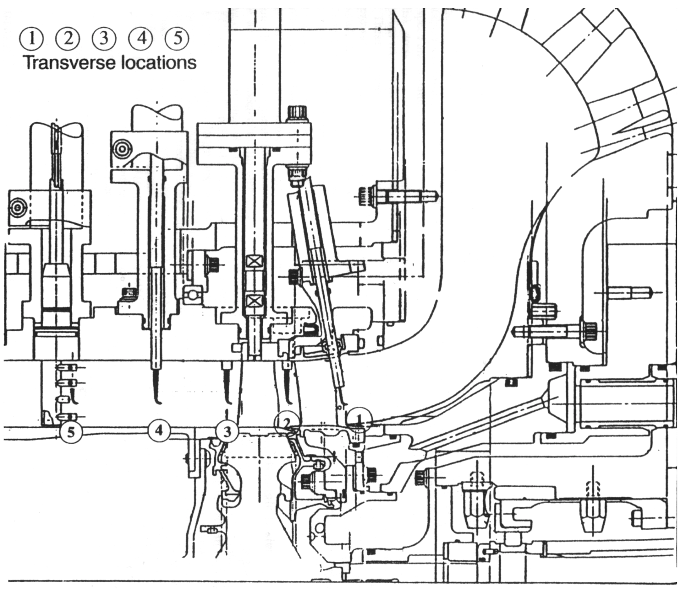

Fig. 4 Test section of High Work Research Turbine (HWRT)

2. Operation concept

2.1 Capabilities

At our institute a compressor station is located in the second basement consisting of two turbo and one double screw compressor with two coolers. The electrically driven machines can be connected in a highly flexible configuration so that air can be provided continuously from 2.5kg/s up to nearly 16.0kg/s with a pressure ratio up to 2.9 bar in parallel operation and 7.0kg/s at 10.0bar in serial operation [2].

The compressed air temperature can be adjusted from about 150°C down to ambient temperature +15°C in the coolers (t_{min} = 20°C). Alternatively the test turbine supply pipe (350mm diameter) with its venturi nozzle for mass flow measurement connects the 3bar low pressure or the high pressure line to the test turbine inlet casing at a maximum of 5bar. Mixing with the additional air from the brake compressor and straightened up in the vertical direction through a tandem cascade the flow enters the inlet housing, accelerates further downstream to the nozzle and generates up to about 2.0MW power in the blading of the test turbine, see Fig. 5.

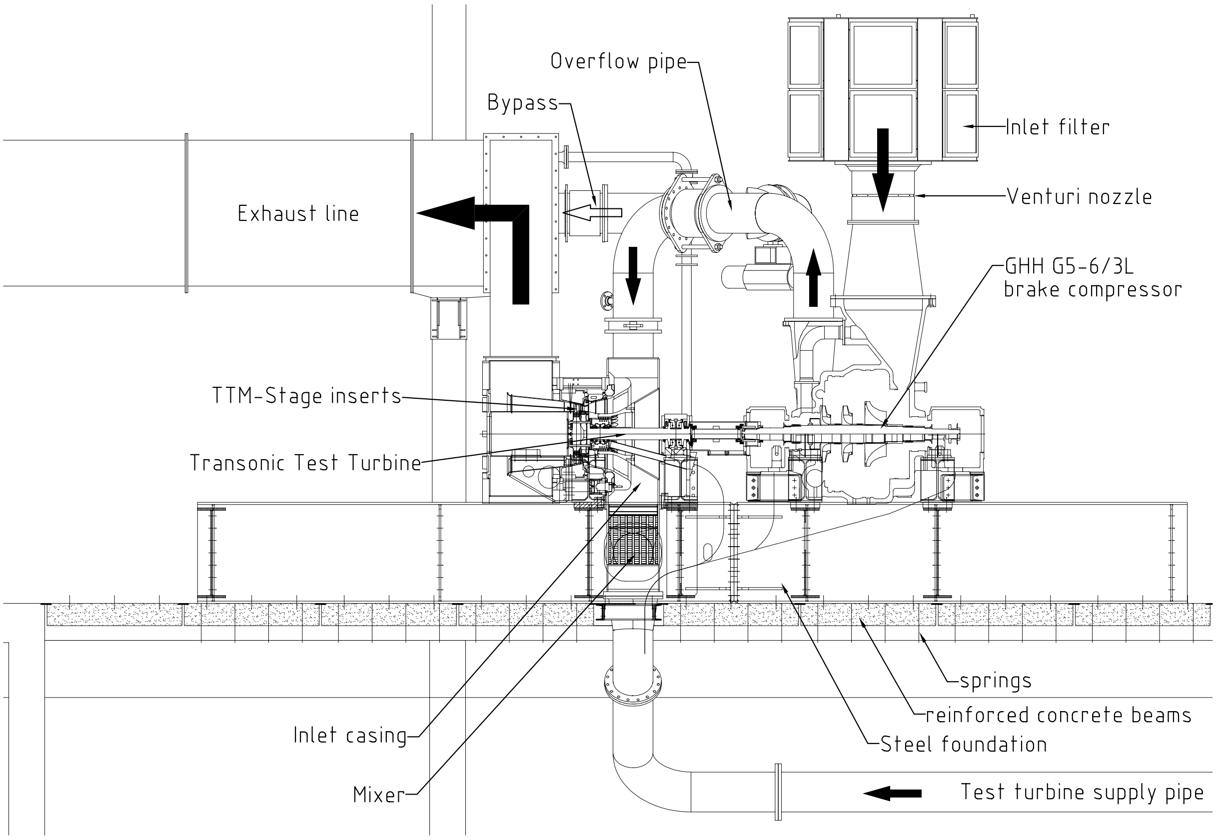

Fig. 5 Transonic test-turbine facility section

A membran type coupling directly transmits this turbine shaft power to our three stage centrifugal compressor GHH G5-6/3L. We got this machine in 1993 and found it suitable as a brake and an additional air supply after recovery of the rusty stator parts and the replacement of the old rotor by a new spare one. This machine sucks air from the test hall through a large filter, a venturi nozzle for mass flow measurement and adjustable inlet guide vanes, which can be manually controlled by a stepping motor to adjust the absorbing brake power. At operating conditions it also can be switched to control the speed of the machine train automatically.

The air compressed through this machine can be used for driving the test turbine if the pressure ratio is lower than approximately 4 and the running speed of the stage to be tested is high enough. Through the overflow pipe (350mm diameter) connecting the GHH brake compressor with the turbine the pressurised air is fed to the mixer in the bottom of the turbine inlet casing to provide the smallest possible temperature distortion in the stage inlet. The use of the compressed air in the test turbine enables us more than doubling the mass flow of our compressor station, which is a big advantage in testing high loaded turbine stages in full similarity.

The overflow pipe first planned as a simple connection between brake compressor and turbine was supplemented with the following capabilities :

(1) Bypass from the overflow pipe to the exhaust line through a DN350 bleeder for pressure independent throttling mode of the brake compressor (also used for test rig start up procedure at low speeds). In this case the DN350 connection valve between the turbine inlet and the brake compressor has always to be shut for clear mass flow balancing and real pressure independent test turbine operation, see Fig. 6.
(2) Emergency bleeder valves for safety reasons for quick unloading of both machines (both valves in parallel fully opened through spring forces in less than 0.5s).
(3) DN50 throttling valve with a from the turbine inlet to the exhaust line for fine mass flow adjustments.

Because the GHH compressor has the same speed as the test turbine shaft, the brake air has to be bypassed to the exhaust line at the above mentioned throttling mode capability, if the inlet pressure for the test stage is higher than maximum possible exit pressure of the brake compressor at test speed. Since the brake compressors pressure ratio mainly depends on the machine train speed the throttling mode could also be necessary at lower turbine inlet pressure ratios if the turbine is limited to low speed regarding flow similarity conditions.

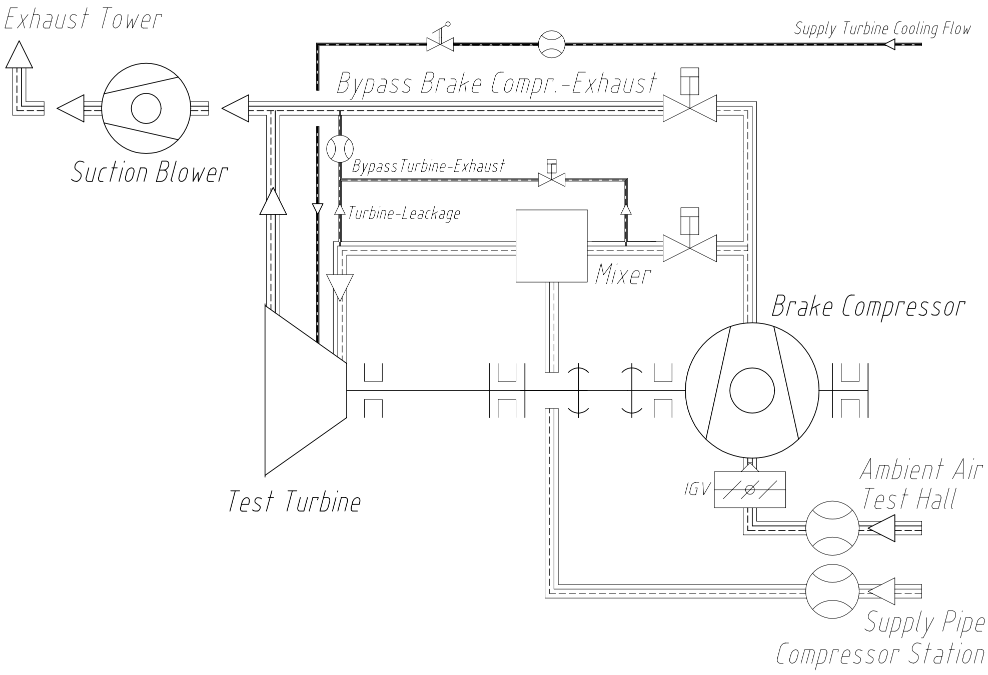

Fig . 6 Transonic test-turbine facility flow scheme

Normally the exit condition after the diffuser with its 90° flow bend upwards in the diffuser collector is set to ambient pressure. But for some more freedom in pressure ratio and power we have designed and built up a suction blower assembly, which can be put into the exhaust line in front of our exhaust tower if necessary.

Since electrical power supply was limited due to the high electrical power requirements of our compressor station and a frequency converter solution for less power consumption and variable speed control for an electrical motor was too expensive it was decided to drive the blower rather unconventionally through an old helicopter engine RR GNOME H.1200 Mk.610, which was used in an Agusta-Bell 204B helicopter rated at 750kW. The 6600rpm power output is now reduced to the 3000rpm subcritical blower shaft assembly by means of a 250mm wide high speed flat belt drive, a design reducing the costs for this transmission assembly below 50% of the conventional high speed gear drive solution with coupling.

Besides the stage main flow also leakage and cooling flows can be provided. For this purpose 16 pipes of 15mm inner diameter are connected to the inner inlet section of the test turbine forming groups of four pipes leading to one quadrant each (1,2,3,4 see Fig. 7). Next to group 1 is the leakage outlet piping and next to group 4 the cooling flow inlet pipe. Each group can be connected or also disconnected via open rings or straight discs to each other respectively to the leakage outlet or the cooling inlet. Additionally pipes between these four groups may increase the number of possible combinations. So if required in some pipes leakage mass flow from the test stage is guided through a measurement orifice to the exit line and at the same time cooling flow can be pressed in parallel through the other pipes. The cooling air mass flow can be covered from the compressed-air ductwork system up to mass flow ratios of about 0.1kg/s, higher cooling mass flow rates with higher pressure ratios will require additional air supplies such as mobile diesel driven units with cooler and drier (up to 0.7kg/s per unit).

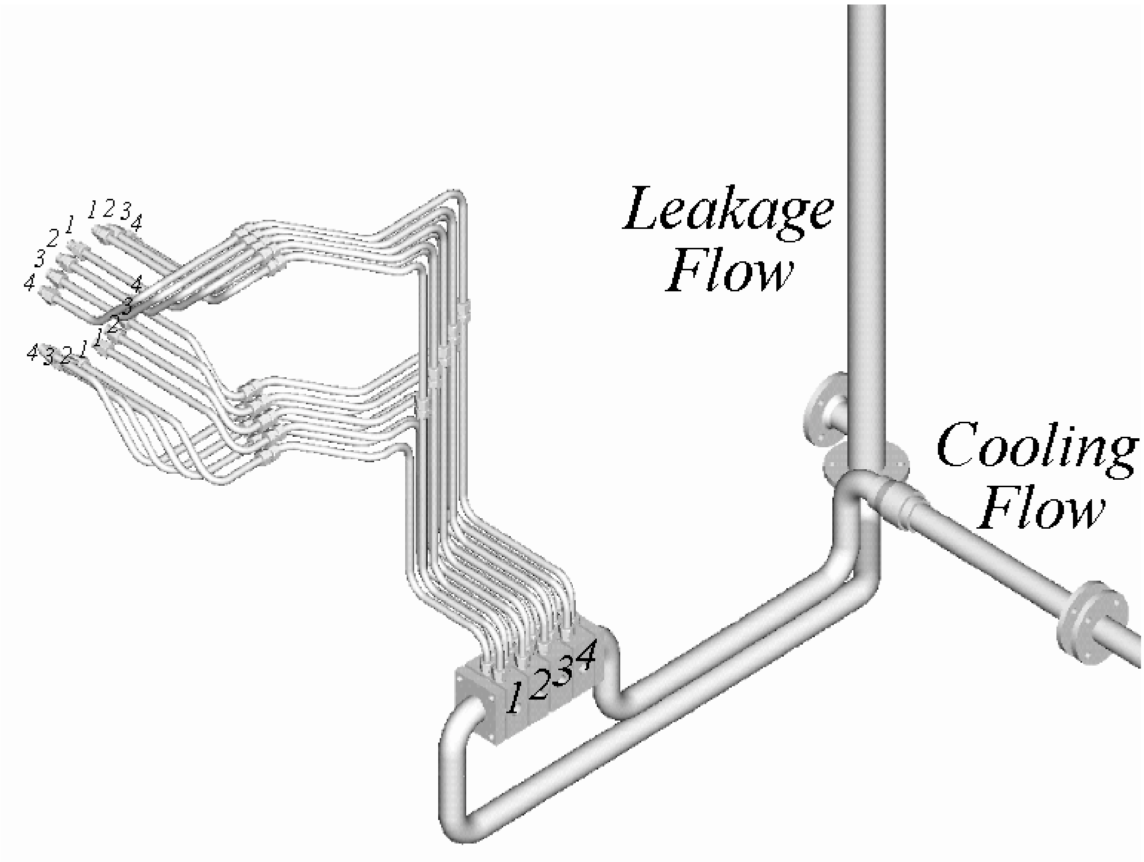

Fig . 7 Leakage and cooling flow scheme

2.2 Mechanical & operational concept

- Continuous operating cold flow test facility in open cycle
- Use of a compressor as brake for multiplying mass flow
- Wide adjustable speed range of the test rig with the first bending modes of the two shafts beyond 7000 rpm and the second bending mode sufficiently higher than the maximum speed of 11550 rpm
- Stable tilting pad bearings also at the turbine shaft
- Overhung type turbine shaft for easy disk assembling
- All casing parts horizontally split for easy maintenance (except diffuser inserts)
- Modular design for quick modification in test setup
- Test section with high flexibility in meridional path [mm]:
  Stage inlet adapters starting at $D_i = 360$, $D_a = 620$
  Test section inserts maximum diameter $D_s = 800$
  Diffuser insert flanges $D_i = 720$
  Test section length $L_{Test} = 406$
  Diffuser length $L_{Diff} = 620$
- Test turbine stage boundaries (with suction blower) :
  Inlet pressure max. 4.7bar
  Inlet temperature max. 185°C
  Outlet pressure 0.97 (minimum 0.77bar with suction blower) :
- GHH brake compressor :
  nominal speed 11175rpm
  nominal outlet temperature 229°C
  maximum coupling power 2.5MW at -15° IGV´s
- Flexible Membran Coupling TSJE0420 :
  maximum axial displacement +/-2.0mm & angular displacement 18´

Important notes on operation concept of the Transonic Test-Turbine Facility :

On test stages with sufficient overspeed capability the maximum nominal speed of the GHH brake compressor may be increased to 11550rpm. But because the wheel and sleeve shrink seats of this brake compressor shaft have less overspeed capability the shaft vibration amplitudes have to be watched very carefully to detect any change from best balanced machine train condition.

So looking at vibration amplitudes, bearing temperatures and thermal displacements in the coupling and rotor clearances the overload capability of the transonic test turbine facility may reach 2.75MW at 11550rpm.

2.3 Measurements

- Speed, Torque and Power at membran type coupling
- Mass flow, pressure and temperature for
  - compressor station supply pipe
  - GHH-brake compressor inlet and outlet
  - stage leakage flow outlet
  - stage cooling flow inlet
  - bearing oil supplies inlet and outlet
- Inlet casing pressure and temperature for turbine total inlet parameters
- Diffuser exit condition in pressure and temperature
- Suction blower pressure difference to ambient
- Four measurement planes for more detailed investigation each depending on stage inserts and testing to be performed (see Fig. 8)
  - A in front of the guide vanes for stage inlet
  - B between guide vanes and running blades
  - C behind the blades for stage outlet
  - D axial diffuser exit
- Rotatable stator ring (+/-180°) for simple radial-circumferential traversing access and in the special case of our TTM stage also different vane trailing edge positions
- Best optical access to the TTM-Stage starting from the vane exit to the diffuser inlet

2.4 Safety concept

Exceeding preset danger values each one of the following signals release an automatic emergency shutdown of the machine train through cut-off the compressor station and fast opening (0.4s from 0% to 100%) of the two main valves in the overflow pipe to the bypass into the exhaust line.

- Electric circuit interruption to emergency supply
- 2 channel overspeed system on turbine shaft coupling end
- XY Orbit / relative shaft displacement in the four bearing planes
- Axial displacement at each axial bearing for thrust control
- Temperature measurement of all tilting pad bearings
- Inlet pressure control for all four bearing supply pipes
- Pressure control for the main and the auxiliary electrical oil pump
- Temperature and oil level control of the oil tank
- Overpressure of the Turbine inlet casing

In the worst case the free accelerating turbine (e.g. because of coupling break up due to a severe rub in the brake compressor) should be caught at about 25% overspeed.

The two main valves are opened through spring forces and the most important monitoring systems are supplied from the electrical emergency grid to store the shutdown data for later analysis.

Because the oil pumps are electrically driven only, they are automatically switched to an independent emergency supply in the case of any electric circuit interruption to supply the bearings with oil during shut down, run out and cooling phase.

3. Structural design and construction

3.1 Design for optical access

3.1.1 TTM-Stage meridional section

The meridional shape of the gas path (see Fig. 8) was strongly dictated from the requirements of the straight optical windows (see Fig. 9) and a cylindrical hub flow path for optical reflection capability. The TTM flow path aero design therefore looks different than most unshrouded single stage turbine flow paths usually avoiding difficulties with accurately controlling the conical tip clearance.

Although having one window over the guide vane exit to the blade midst promises good optical access to the unsteady rotor stator interaction and to elongate the window over the blade to the exit measurement plane C (see Fig. 8) was not that more expenditure. The 50mm radius tangentially connects the inlet and the conical gaspath opening over the blade the angle of which was determined through the stage expansion ratio respectively the demand for keeping constant axial velocity. The inner meridional contour was designed to be manufactured cylindrically for use as optical reflection surface. This advantage also has the high price of a conical window and clearance at the outer meridional contour and severe nozzle wall curvature usually requires local tailoring of several spanwise sections to obtain a good pressure distribution on the air foil.

However as the need for optical measurements had a high priority in design decisions the above mentioned features were realized in a meridional section shown in Fig. 8.

The technical challenge was to provide small clearance in proper thermal alignment between the running blade and the glass window also at transient conditions. The next difficulty was the rotation of the vanes to allow for quasi 3D measurements in planes spread through an axial and a radial vector. The rotation of such a traverse ring is state of the art but the free cut guide vanes under the window were a new experiment which has to be proven (see chapter 3.4.2 and 5.3).

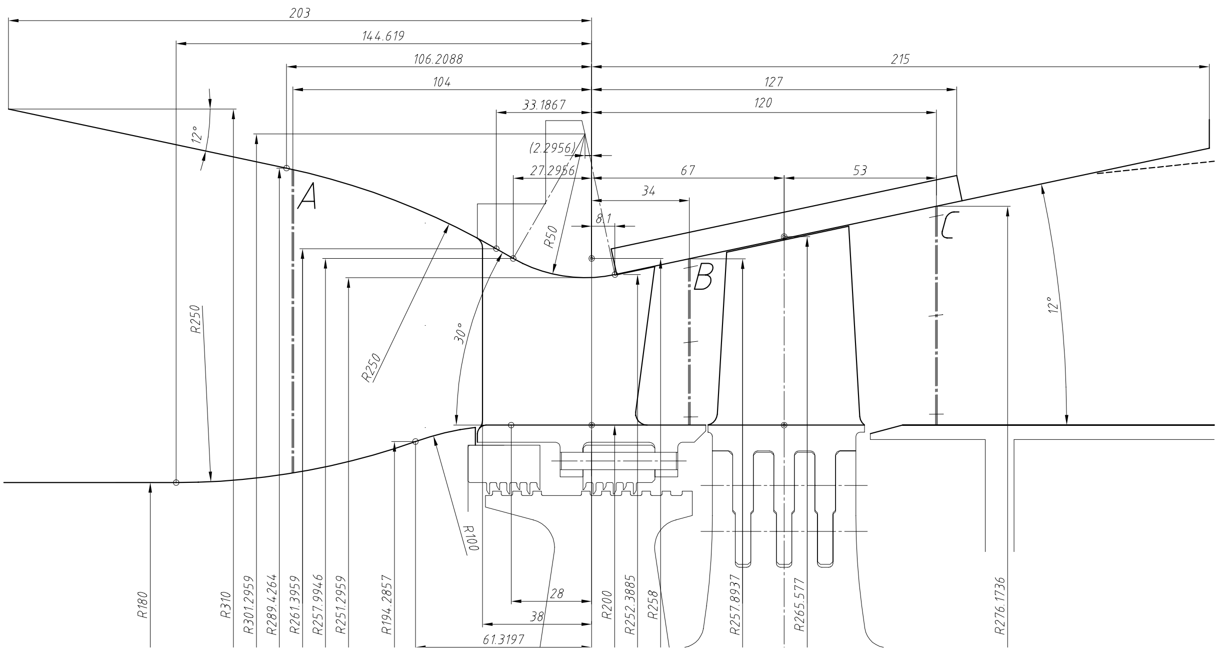

Fig. 8 Meridional section TTM-Stage

3.1.2 Optical windows

Two types of optical windows are used in the upper half of the turbine casing: A long narrow one for Laser Doppler Velocimetry (LDV) and a large one for Particle Image Velocimetry (PIV). This technique can be used as an alternative or complementary approach to LDV reducing testing time at comparable accuracy on multiple measurement points enabling the study both transient and steady state flow phenomena. In a recent publication [8] successful application of the PIV technique to transonic axial compressor and the end diffuser region of a high speed centrifugal compressor is presented. Different to the transonic axial compressor in our test stage the light sheet has to be implemented between the vanes and the blades to catch the real rotor stator interaction. To avoid disturbance of the vane exit flow this light sheet probe must be mounted in another vane exit channel or much better but also more complicated it has to be insert into a guide vane itself. Observing the rotor exit flow is much more easier, because into the low pressure diffuser at low temperatures and no clearance requirements a light sheet can be guided easily through a planar window in the diffuser end plate. The stereoscopic PIV cameras could be mounted in the arrangement above the rotor blades looking through the conical window (see Fig. 9).

The implementation of this large conical PIV-window in our rotor casing was not that easy, because our machine runs not at ambient temperature and therefore any cut in the casing shell will deform the ideal geometry at transient temperature condition. To guarantee safety operation this challenging task is solved step by step, first using metal covers instead of the optical windows for some operation experience. The next step could be the optical windows - first the smaller and then the bigger - with a second outer protection shield and at least the final window assembly used only if all works well on remote control and optical measurements are on schedule.

For optimum optical access with PIV instruments in our application one of the two PIV-window inserts were build in a small 1:1 test section model of our TTM-stage. This model now is used in the laboratories of Dantec and will come back on the TTM-stage for PIV measurements.

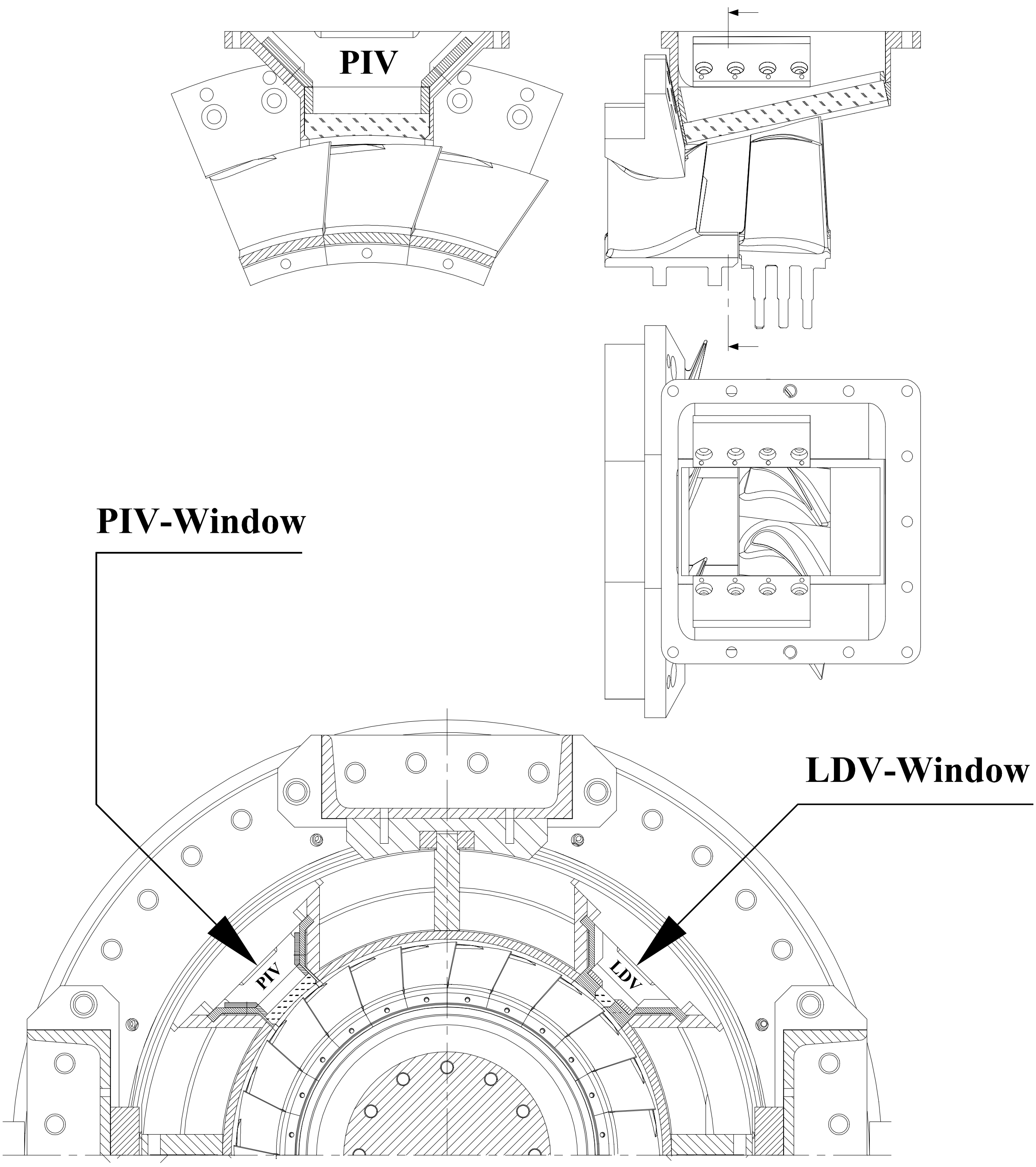

Fig. 9 Particle Image Velocimetry (PIV) and Laser Doppler Anemometry (LDA) window in TTM-Stage

3.2 Design for ease of assembly

3.2.1 Facility main components

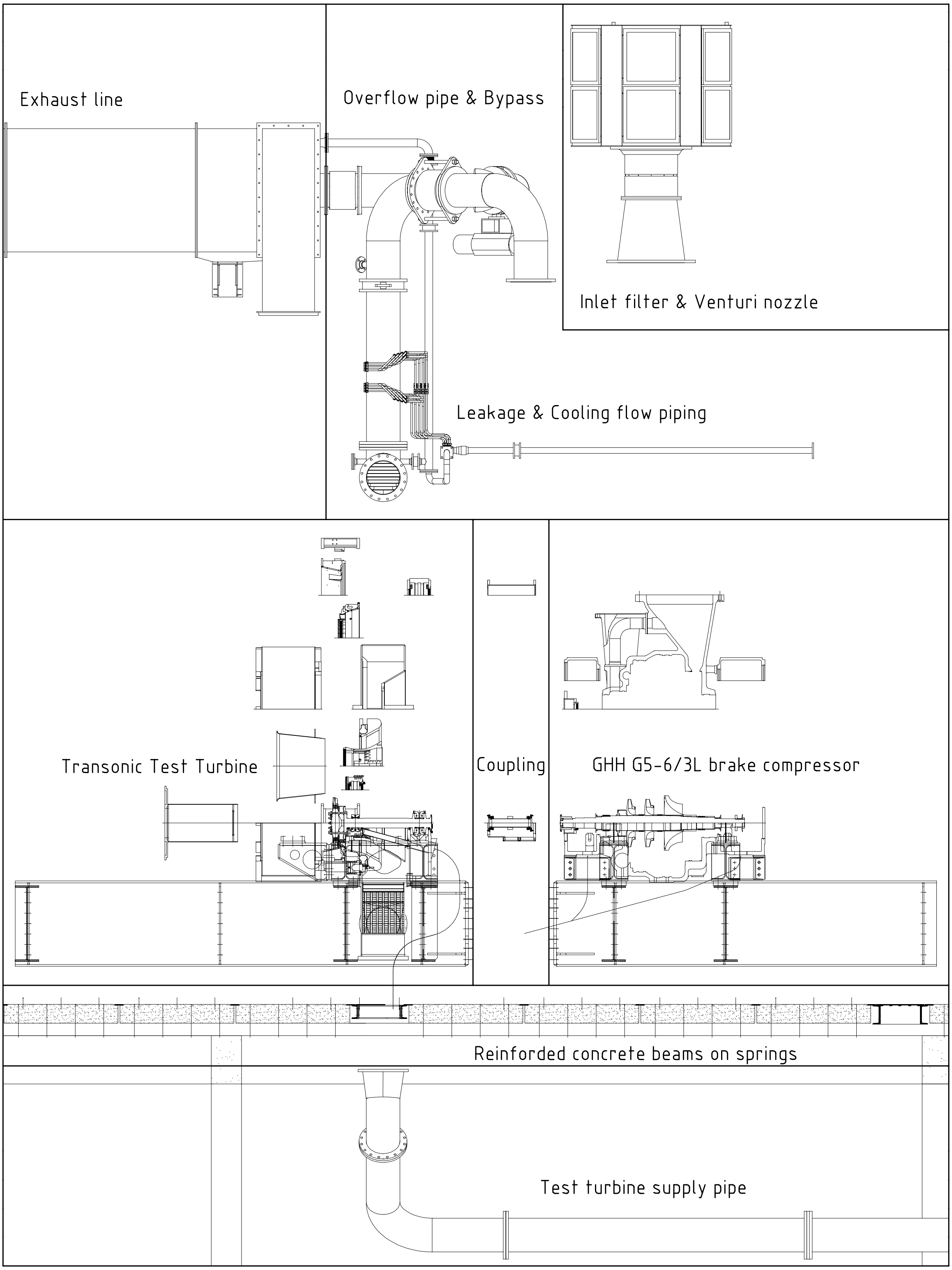

Fig. 10 Transonic test-turbine facility main assemblies and joint faces

In Fig. 10 besides the main components of the Transonic Test-Turbine Facility also the major joint faces of the test facility are shown:

The transonic test turbine and the GHH brake compressor are each mounted one there separate steel foundation, so that the GHH compressor can be replaced by another machine (axial compressor, generator,...) without modification of the test turbine assembly. On the other side an extension of the single stage test turbine to a two shaft arrangement would have not that much influence on the brake compressor side of the facility.

The horizontal split plane of the hole facility (except TTM-Stage diffuser inserts) provides ease of maintenance, which is further improved through the modular design of the test turbine. The overhung test turbine shaft in combination with the two vertical split planes of the struts between the inlet and the diffuser casing gives best accessibility for the test section with high flexibility in meridional path.

After removing the upper strut between the inlet and the diffuser casing in the case of the split TTM-stage inserts there is the possibility to lift up the upper rotor and guide vane casing parts to look for the clearances. Pulling out the inner diffuser there is also full axial access to the bladed disk.

However if stage inserts due to cost reasons are not horizontally split the hole change from one test stage to another can be performed after removing the first exhaust line knee and the upper half of the diffuser collector without even opening the turbine inlet casing, because all test stage parts can be mounted axially.

Removing the coupling cover the flexible membran type coupling with its Bently torque measurement system can be observed and lifting up the bearing cover of the test turbine combined axial and radial bearing at the turbine coupling flange there is access to this bearing.

The bearings of the GHH brake compressor are easy accessible although the observation of the hole GHH rotor takes more time, because before opening the brake compressors upper casing half the inlet filter, the venturi nozzle and the overflow pipe have to be removed.

3.2.2 Fitting dimensions for test stage inserts

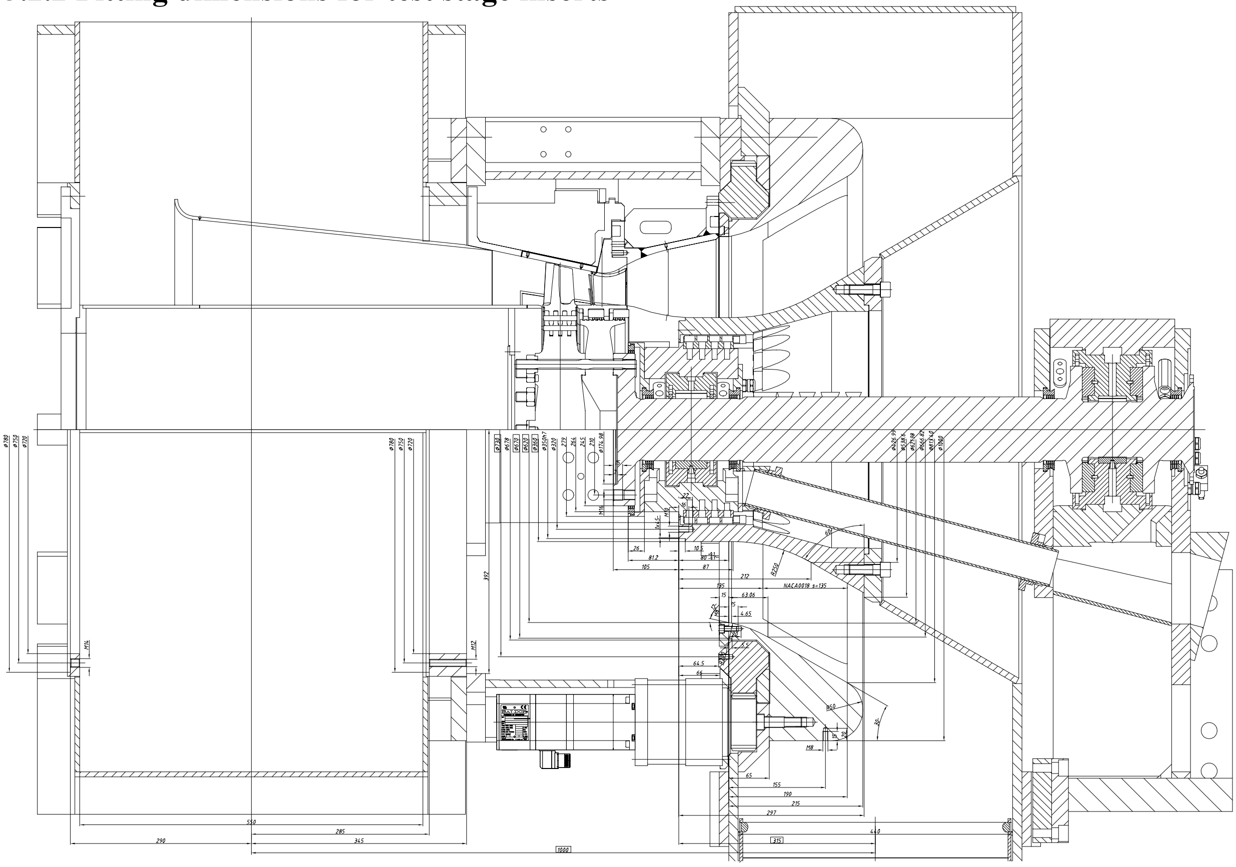

Fig.11 Transonic test turbine facility with TTM-Stage (upper half)
and fitting dimensions for test stage inserts (bottom half)

In Fig. 11 the main joint faces for test stage inserts are shown and as an example the TTM-stage inserts are shown in the upper half. The M16-bolts for the rotor disk have to be carefully tighten hydraulically to guarantee even forces and the rotor clearances have to be adjusted before turning the rotor train first by hand and then second through pressurised air through the test turbine supply pipe.

3.3 Design for strength

3.3.1 Overspeed capability

Just to get the highest operational reliability the test turbine design was straightened to the worst case of a free accelerating turbine shaft. As mentioned above in the safety concept the possible maximum speed is about 25% above the operational speed. So in the case of maximum speed at 11500rpm the TTM-Stage would accelerate to about 14300rpm. For the worst case of a further accelerating rotor the machine is caught through breaking off pins in the blade foot to disc fitting between 14300 and 15000rpm (the pan of the blade itself is to short respectively strength), so that it is guaranteed that the rotor disc assembly can not reach critical values (see material properties in Table 1).

	blades	***disks***	***pins***
R_m [N/mm^2]	930	790	924
$R_{p0,2}$ [N/mm^2]	750	570	764

Table 1 Certified material properties

For testing the bladed disk it was spun for 1 minute at 12660rpm in vacuum (see Fig. 12). That corresponds to 15% overspeed (based on operational speed 11000rpm respectively 10% overspeed for 11500rpm maximum). After the spin test the blades could be measured to be moved max. 0.02mm.

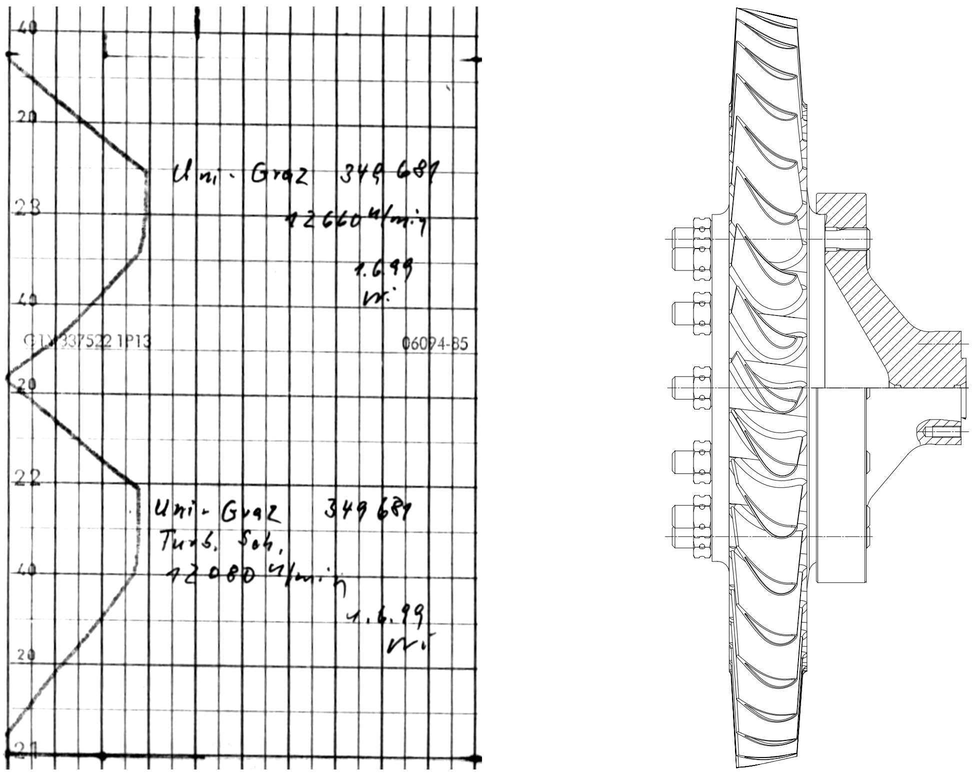

Fig. 12 Spin test of bladed TTM disk at GHH-BORSIG in Oberhausen

In case of a blade crash no parts are allowed to leave the casing. The unbalanced mass that could appear after such a scenario was set to about 5% of the 36 blades mass. This worst case hypothesis in case of our TTM-Stage leads to an unbalance force of 450kN rotating at 14300rpm (one blade with its blade foot is equal to 0.55kg at 201mm Radius)!

This utmost high load would exceed the apparent limit of elasticity of the turbine shaft bending in the front bearing at about 300kN, but the bending shaft could be held in the surrounding bearing and inner casing although the screws would be on limit load at 450kN.

3.3.2 Turbine inlet casing

For safety management of parts conducting pressurized fluids not only the piping had to be examined but also the big turbine inlet casing had to be tested. As mentioned above in chapter 2.2 the test stage boundaries given through the inlet casing condition is given to : **pressure < 4.7bar, temperature < 185°C**

These limits of our transonic test turbine facility are values calculated from the TTM compressor station and GHH brake compressor exit conditions and power boundaries. Because the yield strength of steel is a function of temperature, the permissible pressure in the inlet casing has to be reduced with a reduction factor $K_{p\,T}$.

$K_{p\,T} = R_{p\,T} / R_{p\,RT}$	$R_{p\,T}$ ...	yield strength at operating temperature T	= 185°C
	$R_{p\,RT}$ ...	yield strength at ambient temperature RT	= 20°C
	$K_{p\,T}$ ...	reduction factor	= 0.784

The qualified pressure stage PN is then compared to the calculated cold pressure p_{RT}, which must be less or equal than pressure stage PN.

$PN \geq p_{RT} = p / K_{p\,T}$	p ...	permissible hot inlet pressure	= 4.7bar
	p_{RT} ...	cold pressure p_{RT}	= 6.0bar
	PN ...	pressure stage	= 6.0bar

Finally the system test pressure p_p is set to be 30% higher than the cold pressure p_{RT} for pressure tests with water (10% higher for tests with gas) and must be lower or equal the measured effective pressure p_{eff}.

$p_p = 1.3\ p_{RT}$	p_p ...	system test pressure	= 7.8bar
$p_{eff} \geq p_p$	p_{eff} ...	measured effective pressure	= 8.0bar

For pressure testing a special inlet casing assembling arrangement was used to close this vessel which usually is in open connection to the compressor station supply pipe at the bottom, the GHH overflow pipe on the side and the annular outlet to the turbine stage. The feeding ports where closed with blind flanges and the connection to the guide vane casing and inner adapter was closed with a special cover, which was also used as an positioning device for the manufacturing of the inner turbine casing (see Fig. 13).

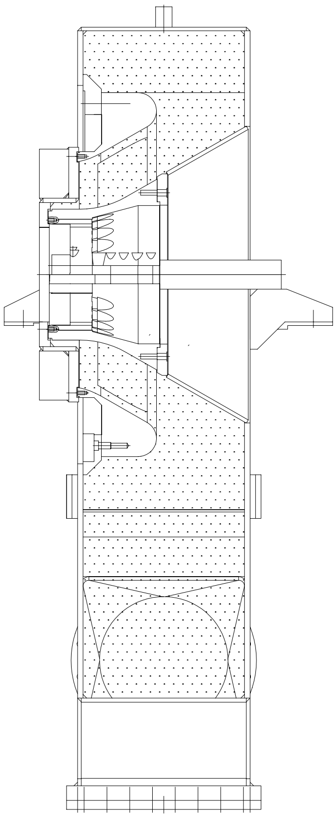

Fig.13 Pressure testing of turbine inlet casing

3.4 Design to accommodate thermal expansion

3.4.1 Centerline support for clearance control

As mentioned before in the Mechanical & Operational Concept above the test turbine facility was designed with all casing parts split for easy maintenance (except diffuser inserts). Furthermore this continuous operating cold flow test facility runs in open cycle at turbine inlet temperatures up to 185°C. Additionally the TTM flow path aero design looks different than most unshrouded single stage turbine flow paths. The hub flow path is cylindrical for optical reflection and the outer flow path is conical, which for practical applications is usually avoided due to difficulties with accurately controlling the tip clearance.

Using a casing part concept which additional to axial joints uses horizontally split planes unfortunately implies not only easy maintenance but this additional flanges also have to be closed and sealed. Due to their departure from the ideal thin rotational shell these casings are causing more deflections at transient thermal operation and also at steady temperature gradients.

Although the simple open flow concept in comparison to closed ones saves investments in back cooling and drying systems and therefore enables higher power capability it has also the inevitable disadvantage of humid air as flow medium. To avoid condensation during thermodynamic expansion the turbine inlet temperature in comparison to other cold test rigs depending on test stage pressure ratio has to be quite high. Otherwise condensation would falsify the thermodynamic enthalpy drop respectively stage efficiency calculated at measured total to static temperature difference. To escape from this problem the turbine outlet temperature has to be approximately equal or higher than ambient temperature leading to turbine inlet temperatures above 140°C for transonic testing.

To obtain good thermal behaviour at these inlet temperatures and to properly adjust all clearances between rotating and stationary parts the old concept of centerline support was used to accommodate for the different thermal expansions. Although this concept is generally used at higher temperature applications we used it for this cold test rig to keep best control of the small clearances at thermal expansions in the same range (approximately 0.6mm at 500mm Radius and 100°C temperature difference). Since the common designs with abradable materials or an active clearance control system are useless in a test stage using big optical windows we were motivated to this high expenditure solution for keeping small tip clearances during performance testing to guarantee that the rotor tip does not rub at off-design condition.

So in principal the hole test rig assembly with turbine and compressor is carried in centerline supports to minimize deflections due to thermal gradients. Depending on thermal growth the machines are sliding on ground plates mounted on the connecting steel frame in an horizontal plane with 140mm offset to the horizontal machine split plane. In their thermal expansion the machines are guided through feather and key ways in all three possible directions of motion hanging on their claws with their own weight only protected against lifting up through big washers in a vertical distance of about 0.2mm.

For axial displacement control the GHH compressor with its integrated bearing housings in the lower casing half is fixed at the hot exit plane. The resultant coupling end displacement at the GHH brake compressor rotor depends on the temperature distribution respectively difference between the rotor itself and the thick cast iron casing, since the thrust bearing is located on the cold inlet side. This causes an axial compression of the membran type coupling at fast start ups and also at high speed ratings which has to be carefully observed as there is no automatic alarm system indicating to high axial displacements.

The turbine casing concept (see Fig. 14) separates the cold axial thrust bearing from the hot inlet casing and fixes it to the cold steel foundation. So the hot big inlet casing is fixed in the axial direction near the front bearing and expands thermally free towards the thrust bearing. The turbine casing itself is fixed in another centerline supporting device mounted on the connection struts between the inlet casing and the diffuser collector allowing the rotor casing to minimize the clearance reduction. When the rotor casing grows at about 0.15mm relative to its axial fixing, the connection struts expand about 0.1mm from this point to the inlet casing axial fixing plane and we estimate to have a comparable temperature behaviour of the claws and the rest of the connection struts towards the inlet respectively if this casing parts behave neutral then the relative movement of the rotor casing is about 0.25mm. Assuming the steel foundation to keep cold the warming up turbine rotor grows out of the fixed axial thrust bearing. Depending on the rotor temperature distribution for example 75°C from the thrust bearing to the disk flange and 130°C till the midst of the disk the thermal expansion would come up to 0.65mm. This allows the turbine disk to move outwards the conical turbine casing depending on the thermal growth of the turbine shaft minus the rotor casing displacement. So this turbine casing concept allows only minor axial displacements between the turbine disk and the turbine casing partly compensating each other to maximum 0.4mm. So finally

the tip clearance during performance testing is increasing about maximum 0.08mm due to this expected axial displacement of the rotor tip to the rotor casing.
The second challenge in our TTM-stage is the turbine casing structure itself. Because there are deep axial cuts in the conical housing for the large window assemblies we also have to tackle with radial deflections of the ideal shell geometry at transient operation.

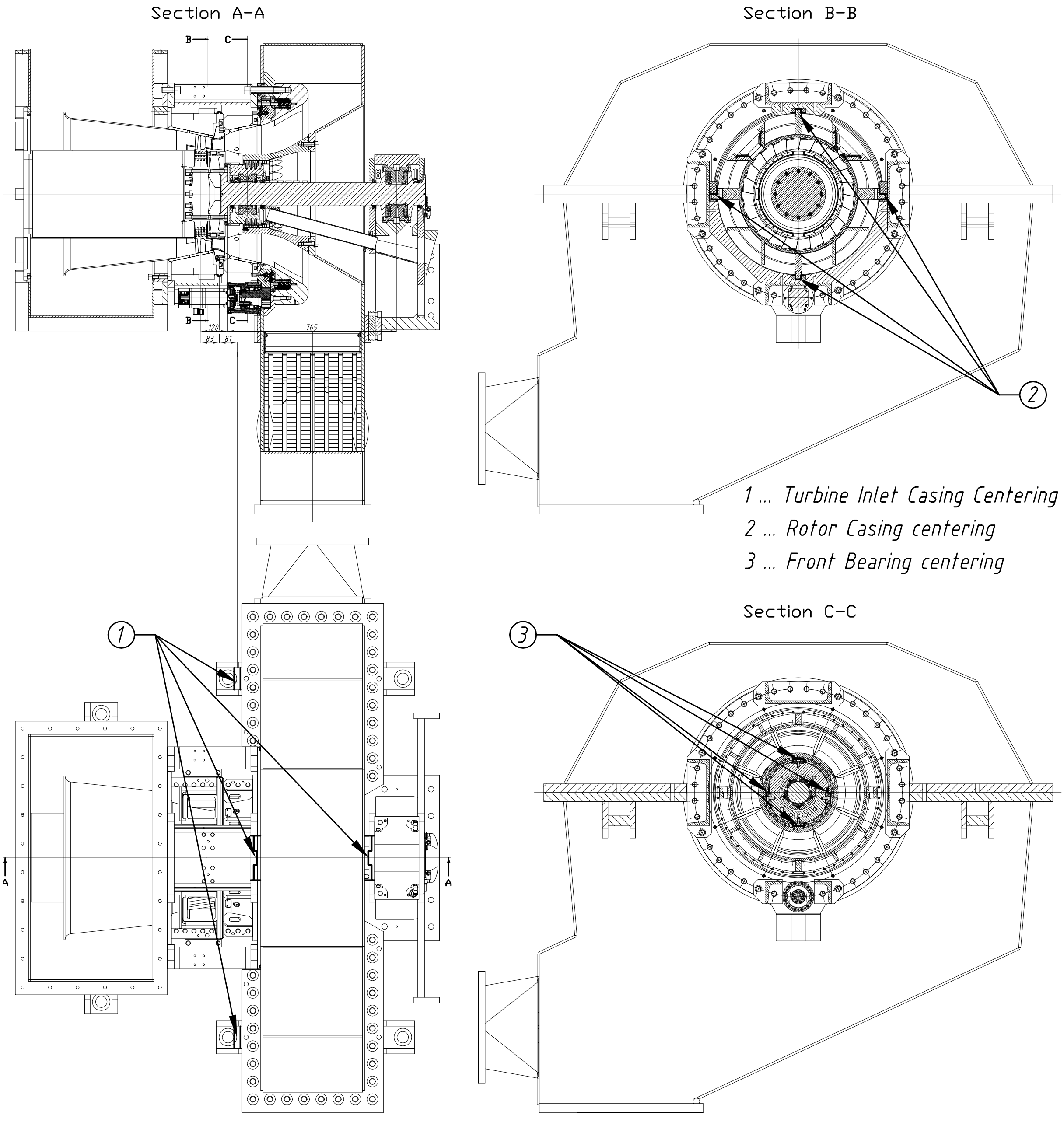

Fig. 14 Centerline support concept at transonic test turbine
Section B-B test section and radial fixing of rotor casing
Section C-C front bearing plane and adjustable thermal centering

A short summary of the radial displacement effects [mm] :

(1) The exact radial mounting position of all centerline supports to the rotor is +/-0.05mm with a turbine disk vertical eccentricity of 0.1 at 0rpm to compensate for the turbine shaft radial shift in the sliding bearings. The measured alignment values are documented and then compared to the shaft average positions which are continuously logged in the Bently ADRE system.

(2) The axial displacement of the turbine rotor due to the temperature of the rotor shaft (hot discs and bearings) and the axial thermal growth of the turbine casing are partially compensating each other to a resultant axial rotor shift of maximal 0.4 out of the cone respectively 0.08 radial at steady state condition.
(3) The transient rotor casing thermal behaviour results only in about 0.05 clearance reduction at the windows through deformation of the conical geometry, but depending on the turbine inlet temperature there possibly is also a unsteady casing contracting effect in the range of 0.1 through the temperature lag of the outer parts. In steady state operation a temperature difference of the outer casing parts to the turbine inlet temperature will also lead to clearance reductions of about 0.1 at 30°C. Additionally some care has to be taken on the horizontal split plane screws, because these free cut thread joints tend to contract the casing in vertical direction through deforming its original conical geometry (0.05).
(4) The blade tips are also growing towards the rotor casing first due to elastic strain of centrifugal forces acting on the rotor disk and the blades (0.2 at 11000rpm) and second through the thermal expansion where the blades are the faster reacting component in comparison to the disk. So the time delayed reaction of the disk is dangerous to high test stage inlet temperature gradients especially in a cooling down phase.
(5) Fortunately the blades are on lower temperature because of the low reaction, and so the rotor disk temperature is estimated to stage exit temperature plus about half of the stage static temperature drop (-0.15).

The cold clearance (ambient temperature, 0rpm) at steady design load condition (see chapter 4.2.2.1) is reduced with [mm]

+0.05	assembling tolerance for centerline support
+0.05	rotor eccentricity due to sliding bearings
+0.10	rotor casing thermal lag
+0.05	assembling tolerance for rotor casing split plane
+0.20	elastic centrifugal blade tip displacement
- 0.15	tip diameter reduction through lower rotor temperature
+0.30	cold clearance reduction at design load condition (181.3°C, 11000rpm)

Therefore the small steady state warm clearance (design load condition) of 0.5mm (respectively 0.72% clearance to blade exit height) would have to be enlarged with 0.30mm.

To control the rotor tip clearance at transient operation such as cold quick start (or inlet temperature reduction)

+0.05	cold short turbine shaft lags axially 0.25 to rotor casing (-0.08 at steady design load condition)
+0.15	estimated deformation and reduction of conical rotor casing due to unsteady thermal behaviour

I would suggest to enlarge the clearance for another 0.2mm, which only would set the steady state warm clearance to 0.7mm, equivalent to 1% clearance/span, an often published clearance value for such turbine stages.
The resultant radial cold clearance to be adjusted in the TTM-stage assembling would therefore aggregate to 1.0mm (in the horizontal plane, 1.1 vertical up and 0.9 down to compensate for the turbine shaft radial shift in the sliding bearings).

3.4.2 Turbine inlet measurement system

Established in the measurement concept the rotatable stator ring (+/-180°) for radial-circumferential traversing access is one of the key features of this test rig to optimise the inlet measurement plane in terms of circumferential distribution analysis. This is important first for the special case of our transonic test turbine facility, because our turbine concept with its 90° flow bends in the inlet casing and the diffuser collector is more similar to a real machine than the common implementation of such test rigs in wind tunnel like closed circle applications although this will also imply some total pressure distortions. Second the open concept with the uncooled brake compressor air forces the use of a mixer which also is not able to fully equalise the temperature profile. In the special case of our TTM stage also different vane trailing edge positions are requested for the quasi 3D LDV and PIVmeasurements.
So the rotating device is not only part of the TTM-stage but is also used for the hole turbine inlet measurement system to compensate possible distortion problems through better thermodynamic balancing capabilities. To make this device available for all future test stage inserts without major modifications the initial position of the geared ring above the TTM guide vanes was changed and it was located near the inlet casing joints for the test stage inserts.
To rotate the hole guide vane casing during test run an appreciable moment has to be applied. 1612Nm are generated in the 24 guide vanes at design condition and to make the axial flanges leak proof two inflatable silicone seals are applied which also cause some friction torque.

Additional loads to be carried from the rotating device in the case of TTM-stage design load conditions are 45.3 kN axial thrust and 1.1kN eccentric load at 155mm relative to the geared ring axial symmetry plane (see Fig.15). As the turbine inlet temperature is too high for excluding temperature differences respectively displacements a preload cross roller bearing concept was designed to compensate for thermal expansions and load variations. Different from live rings used in cranes which are filled with rollers we applied closed roller bearings for easier maintenance in the vertical plane. The gear ring carries 8 roller bearings on its load side towards the bearing ring and 4 ones towards the preload ring. To tooth this inner bearing ring for additional use as gear ring driven by the servo pinion in the lower casing half was not that big problem in comparison to split all these parts for the horizontal assembling concept.

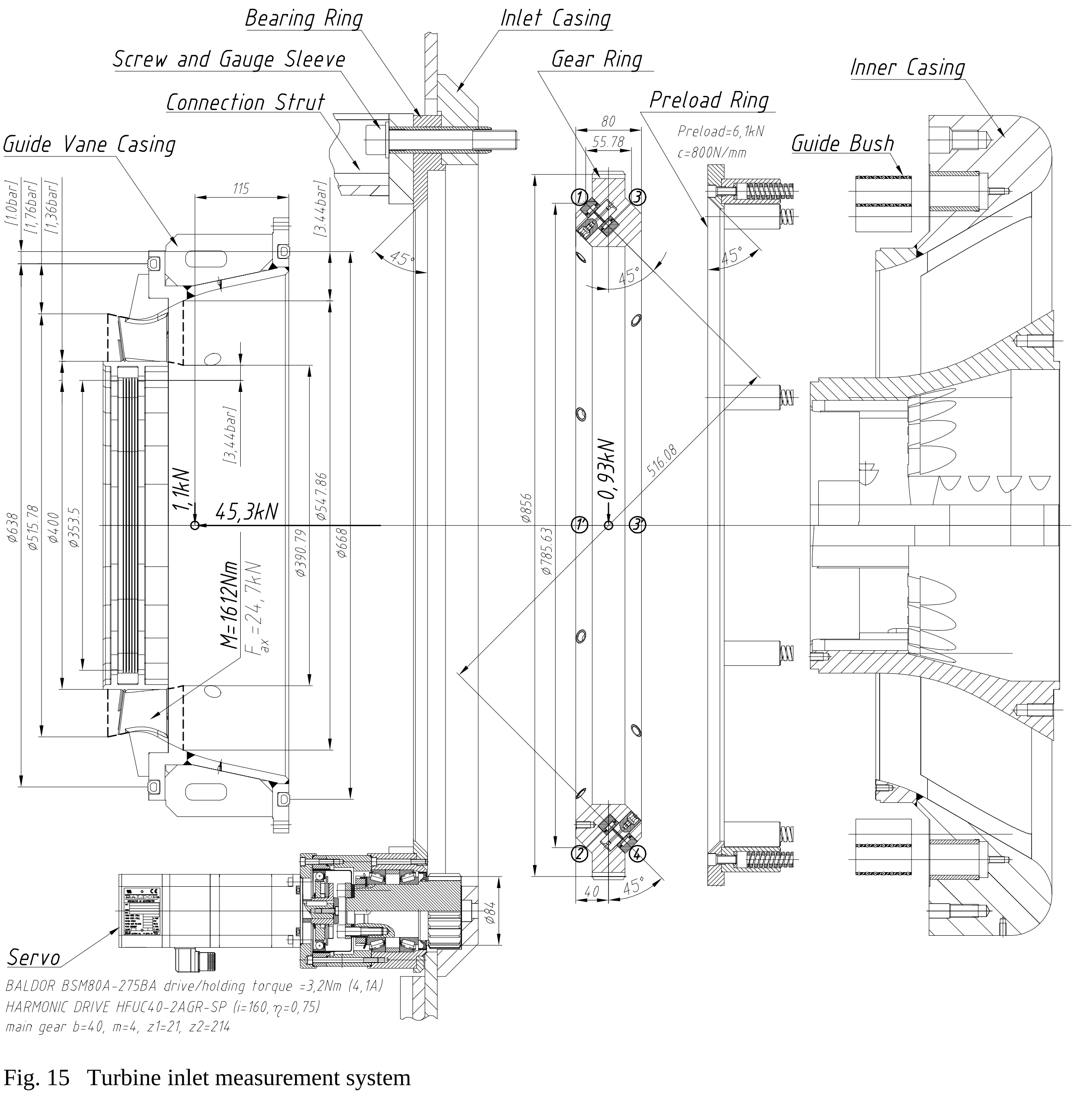

Fig. 15 Turbine inlet measurement system

The high guide vane casing axial thrust of 45.3kN plus the axial spring forces from the preload ring are directly carried from all 8 roller bearings against the bearing ring.
To have some simplification on the other load conditions we assume to have one roller bearing each at point 1,2,3 and 4 respectively four other ones 1´,2´,3´and 4´ in a plane 90° rotated CCW in the rotor axis. This enables for some simple calculations leading to the following results :

(1) Eccentric vertical loads at 155mm (or less) relative to the geared ring axial symmetry plane produce about the same load (100%) at point 4, 2 carries 70.7%, 1 carries 30% and 3 is free. The gear ring own weight of 0.93kN adds 0.66kN at point 2 and 4.

(2) If the guide vane casing gets some torque at testing conditions or through additional movements against the inflated seals the pinion shaft holds respectively moves the gear ring with the circumferential force Fu = M / 0.428 and pushes it vertical upward with the upward force Fr = Fu*tan20°. Fr presses the gear ring in point 1 and 3 with 70.7% of Fr each and Fu stresses point 1´and 3´in the same proportion (70.7% of Fu).
(3) To compensate the resultant axial forces on the preload ring the springs have to be prestressed with 160% of the forces acting in point 3,4 and 3´. Although the guide bushes are of roller type to prevent the preload ring against chocking some margin in higher preload will have some advantage against an eccentric working point at this relative soft bending structure.

3.5 Design for stability

3.5.1 Machine train bending modes

Since in chapter 2.2 a wide adjustable speed range of the test rig above the first bending modes was requested the design had to set the first bending mode of each shaft beyond 7000rpm and the second bending mode sufficiently higher than the maximum speed of 11550rpm for stable operating conditions. The overall behaviour at 11500rpm is shown in Fig. 16 :

Almost independent bending vibration behaviour of the two shafts due to the flexible membran type coupling acting like a rigid body connection between the two machines. This allows for separated dynamic modelling in the case of test rig balancing for instance on a new test stage.

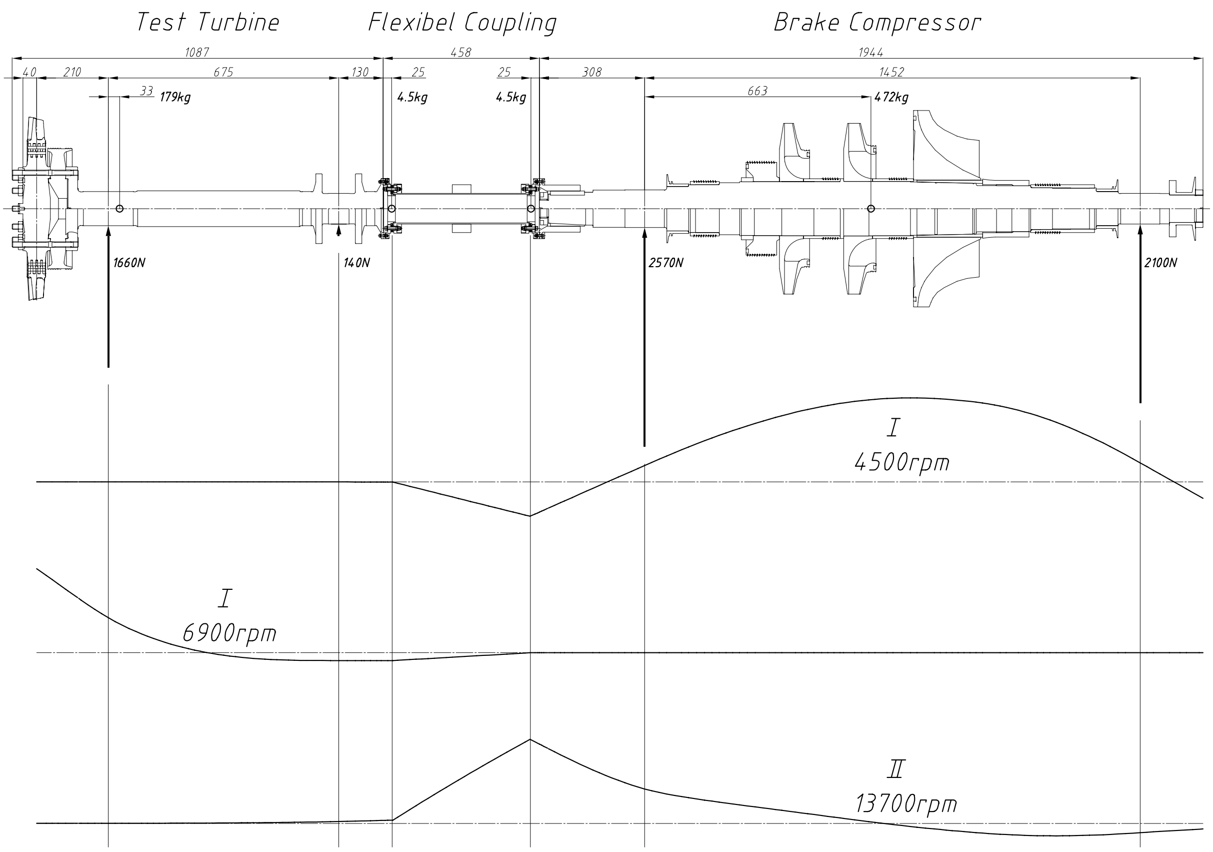

Fig. 16   Transonic Test-Turbine bending modes at 11500rpm

On the GHH brake compressor rotor only minor modifications to its original design were performed. The old RENK TACKE coupling hub (12.7kg with a gravity center 56mm inwards from coupling shaft end) on the old rotor end was replaced at the new spare rotor with one of two new hubs delivered with the flexible Membran Type Coupling TSJE-0420 from FLEXIBOX (7.0kg 61mm inwards). The lateral mass of the pinion shaft from the RENK planetary gear originally between the electrical motor drive and the GHH compressor was estimated to be at the same mass dimension compared to the new shared coupling spacer mass of 4.5kg.

So we could confirm the first critical speed of the brake compressor in the anticipated range of 4700rpm given by GHH BORSIG. This first bending mode only shows less sensitivity to variation in bearing stiffness, so that the 5% difference between the numbers shown in Fig. 16 and the reality have not much influence on the first mode itself. The bearing stiffness difference has two reasons :
(1) We tried to recalculate the stiffness of the radial tilting pad bearings since the values given by GHH in our dynamic rotor model led to about 5% to high frequencies compared to their values. Since we did not know the preload factor of these bearings we set it to 0.5 and got softer bearings.
(2) The modelling of the brake compressor rotor is a difficult task due to its design with a lot of bushes and a conical first stage wheel mounting.

However since we have measured the first bending mode right at 4700rpm (driven up only a little bit at cold start condition) the reality of bearing stiffness will be somewhere in between. In the following diagrams only these values will be used, which I calculated with GLAGER (written and tested against literature by Dr. Gehrer, Reynolds Equations Solver with integral solved oil temperature and viscosity distribution with a 2nd Order Upwind scheme, tilting pad capability, stiffness and damping coefficients calculation at small difference in equilibrium condition). This bearing behaviour documentation for all four rotor supports and their influence on the respective rotor bending modes are listed in more detail in the attached appendix.

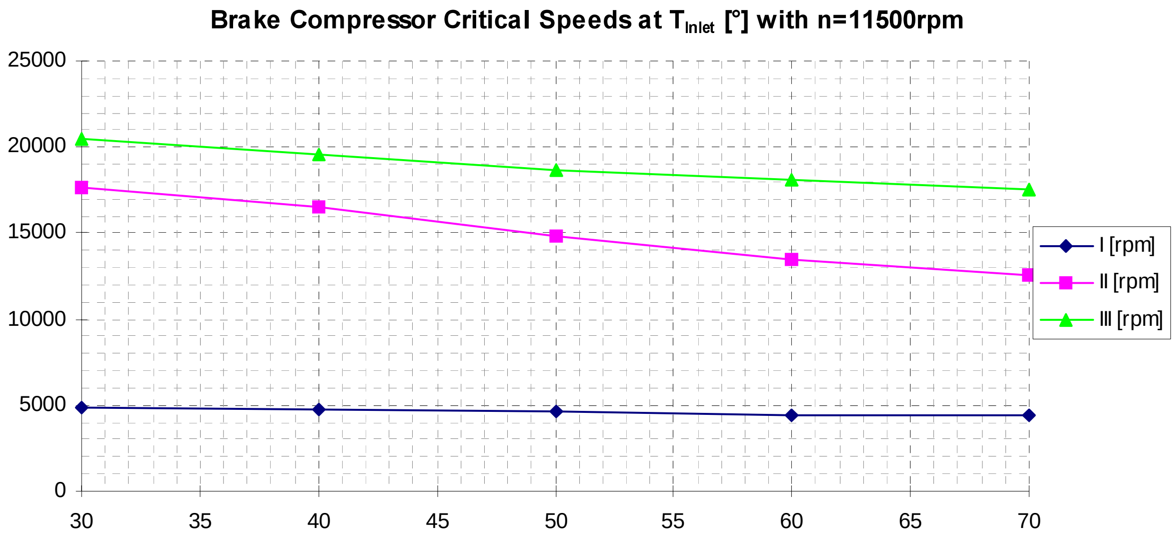

Fig. 17 Brake compressor critical speeds related to 11500rpm at different pad inlet temperatures

The second critical GHH speed in Fig. 17 seems to be much more sensitive to variations in bearing stiffness for instance due to pad inlet temperature than the first one. It can be shown, that there is not very much difference to the maximum running speed of 11500rpm, if the bearing will run with to hot oil. In chapter 8.1.2 it can be shown further more, that the largest amplitude and sensitivity to unbalance (and also balancing) at the second GHH bending mode is given at the coupling shaft end.

The test turbine with its overhung type turbine shaft for easy disk assembling has some similarity to a free running power turbine although the flow direction in our case runs opposite. This is due to the fixed GHH turning direction and the decision to a clockwise running test stage (looking from driver to driven machine).

We luckily tried to get the first turbine bending mode at lowest possible speed and also designed a low weight coupling end with enough margin between maximum machine train speed and the second turbine mode. As we operated the test rig against the calculated first critical during initial test runs we found no change in amplitude and phase, because the first critical was much higher than expected. The turbine bearing stiffness given by the manufacturer were nearly half of the values compared to real running condition. This fact could have been some advantage in another application but in our case it increased the first critical just below acceptable values because this turbine design was very sensitive to that change. Fig. 18 illustrates the variation of the Turbine Front Bearing TLL in stiffness at different pad inlet temperatures at a fixed speed of 11500rpm.

As tilting bearing stiffness show nearly proportional behaviour against speed variation and the test turbine bending modes are sensitive to this effect an additional parameter variation at fixed pad inlet temperature of 60°C was calculated for this machine. This nearly linear stiffness behaviour at fixed pad inlet temperature and decreasing speed is only affected through the “Load between pads“ design of the TLL bearing at low speed (see chapter 8.1.1). However the Turbine Coupling Bearing TFL with “Load on Pad“ design and also both brake compressor bearings really have a proportional decrease in stiffness in respect to speed reduction.

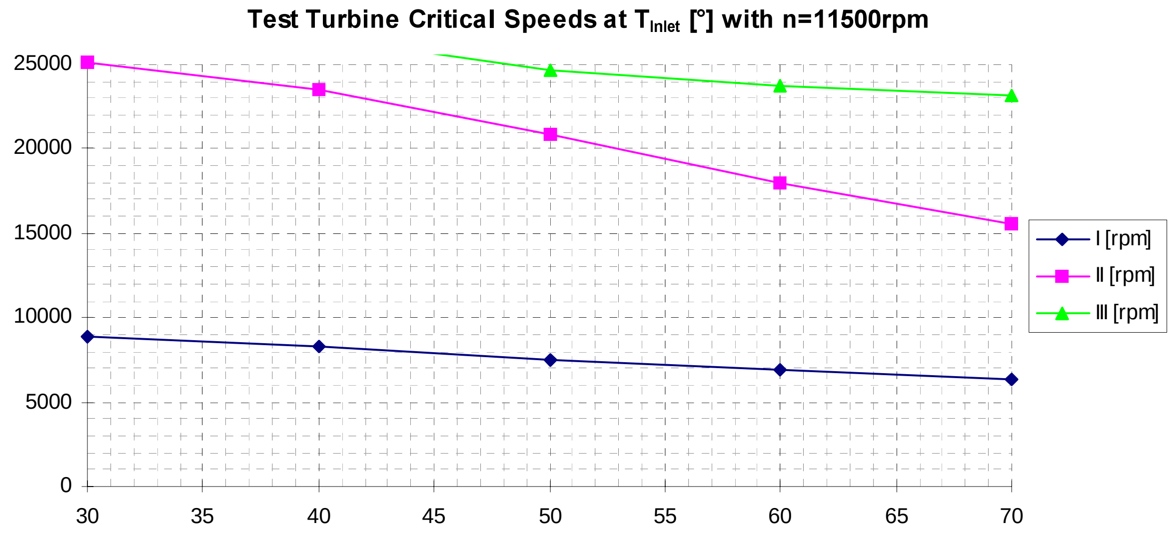

Fig. 18 Test-Turbine critical speeds related to 11500rpm at different pad inlet temperatures

Using the different bearing stiffness as a function of speed the first critical could be well simulated at about 5800rpm in Fig. 19. But because the increasing bearing stiffness at higher speed also leads to increased first bending mode the phase shift occurs over a broad speed range with a flatten peak resonance behaviour. This high sensitivity of the first test turbine bending mode to bearing stiffness changes also causes a considerably higher passage at cold start condition almost driving this first critical up to about 7500rpm see Fig. 18 !

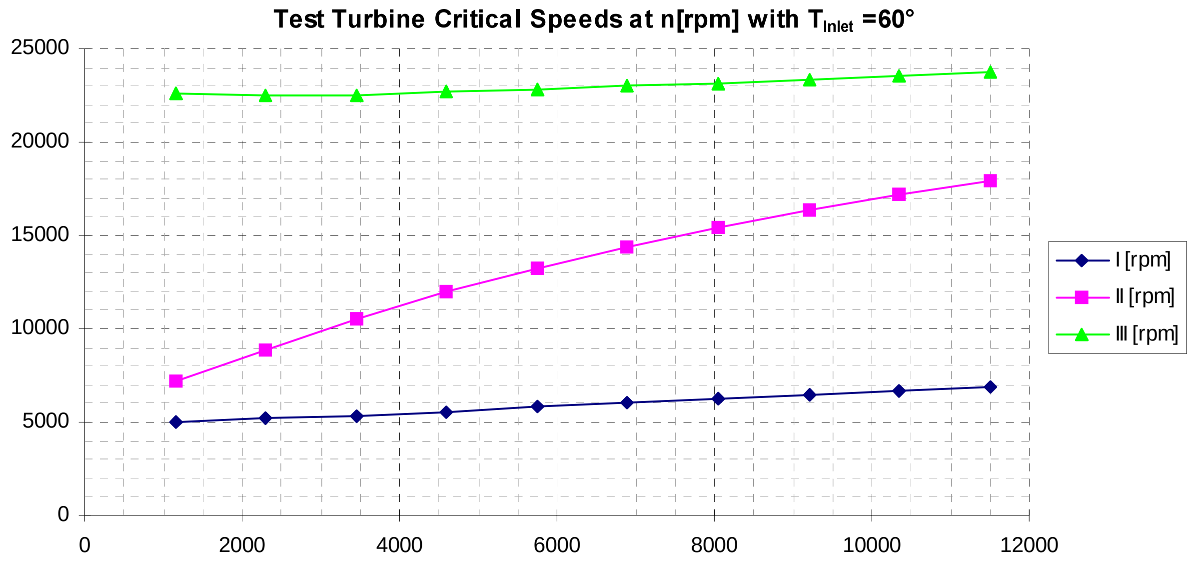

Fig. 19 Test-Turbine critical speeds related to pad inlet temperatures of 60°C and different shaft speeds

So the initial concept of a wide adjustable test rig speed range between 7000rpm and 11500rpm is possible if the shafts are well balanced and the bearing pad inlet temperature at the Brake Compressor Exit Bearing GLL is maximum 60°C. This test speed range could be cut at lower speeds through light test stage discs in combination with a cold Turbine Front Bearing TLL and on higher speeds through operating problems with the brake compressor (poor coupling balancing in conjunction with 2nd bend and hot GHH bearings, overspeed capability). To get some more sense to this parameter pad inlet temperature the following considerations are taken :

Assuming our bearings are low stressed concerning their vertical load and eccentricity ratio to speed, the pad tilting angle is not so much different. From [9] we can estimate, that about 85% outlet flow of the previous pad at its effective temperature (near pad measurement) is ready to fill the next pad inlet gap and the rest of the pad inlet flow is filled with made up lubricant at a temperature somewhere between the inlet and outlet temperatures of the bearing. This means that pad inlet condition will tend to be closer to the measured pad temperature (close to the babbitt metal) than on bearing inlet temperature.

3.5.2 Frequency analyses of the bladed TTM-Stage rotor disk

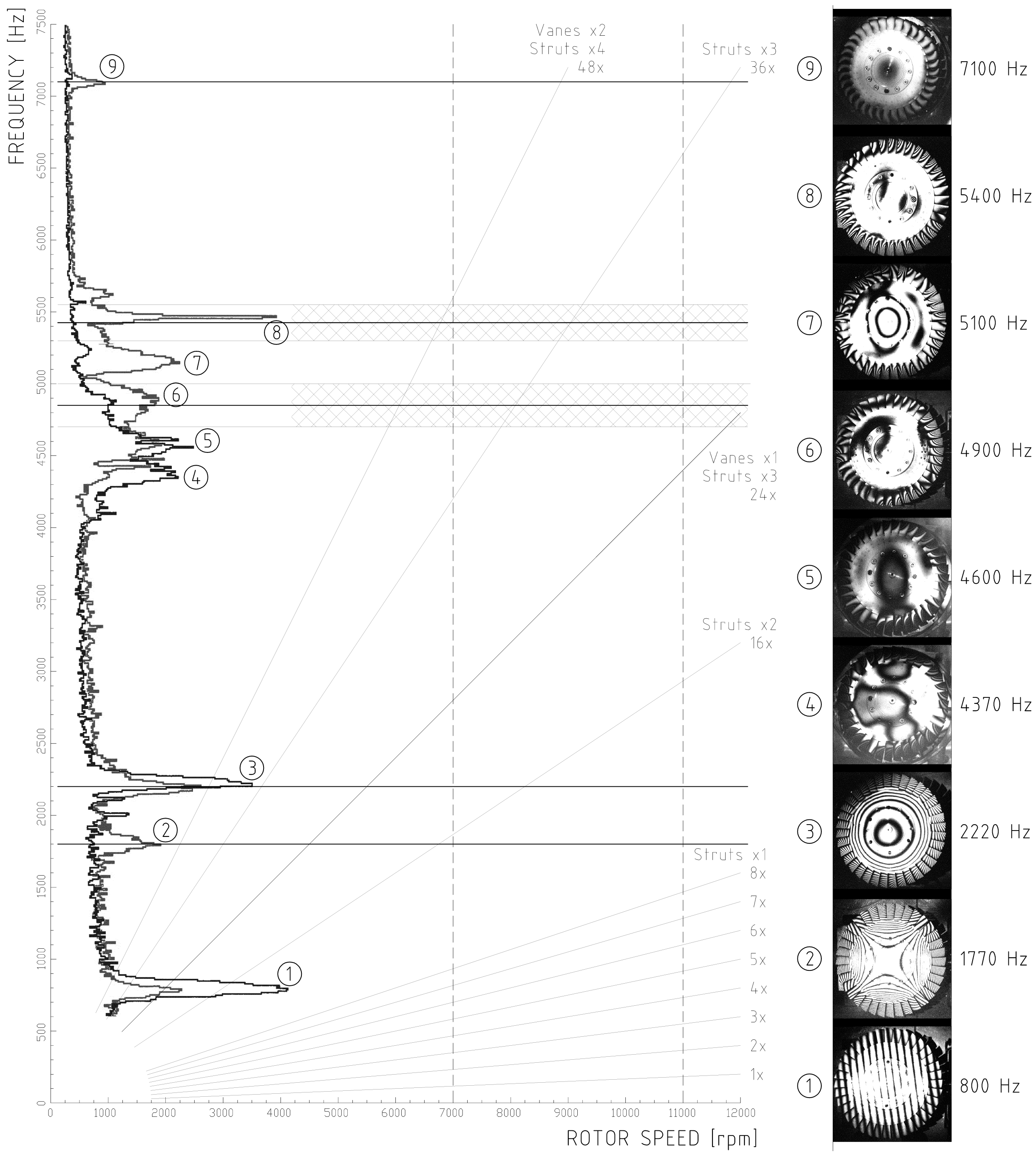

Fig. 20 Campell diagram of the bladed TTM-stage rotor disk

1 ... 800 Hz	Tilting measurement support
2 ... 1770 Hz	Disk mode with two nodal lines
3 ... 2220 Hz	1st Flex rotor blade (low moment of inertia) in connection with first order bell disk mode
4 ... 4370 Hz	Second order disk mode with four nodal lines and excitation of 1st Flex rotor blade (high moment of inertia)
5 ... 4600 Hz	Second order disk mode with six nodal lines and excitation of 1st Flex rotor blade (high moment of inertia)
6 ... 4900 Hz	1st Flex rotor blade (high moment of inertia) and excitation of second order disk mode with six nodal lines
7 ... 5100 Hz	Second torsion disk mode (circumferential) and excitation of 1st Torsion rotor blade
8 ... 5400 Hz	1st Torsion of rotor blade in connection with second order shift disk mode (lateral)
9 ... 7100 Hz	2nd Flex rotor blade (low moment of inertia)

In general the blade aeromechanical behaviour in the operating speed range between 7000rpm and 11000rpm should be o.k., because the blade itself is very stiff and also high stimulations forces will lead to very small amplitudes resulting in low dynamic stress referred to the material high-cycle fatigue limits. This behaviour in connection with the damping in the blade foot to disc fitting leads to the Campell Diagram in Fig. 20, where only a small stimulation from the doubled strut number (=2∗8∗n) could excite the 1st Flex of the rotor blade at a running speed of about 8250rpm. The high order disk modes 4 and 5 with excitation of the 1st Flex of the rotor blade bending over the high moment of inertia could be seen above 4300Hz. However this measurements were taken at 0rpm and less tighten auxiliary bolts held the disk on the measurement support. So in the real machine these disk modes would occur at higher frequencies giving some more distance to the guide vanes frequency (=24∗n) and there will be some frequency increasing effect due to the high centrifugal load. However if one would test the TTM-stage up to the maximum speed of 11500rpm at peak load, this frequency distance has to be tested with some optimised strain gages showing the real behaviour of this complex system for safe operation [10].

4. Aerodynamic design

4.1 Turbine inlet concept

4.1.1 Turbine inlet casing

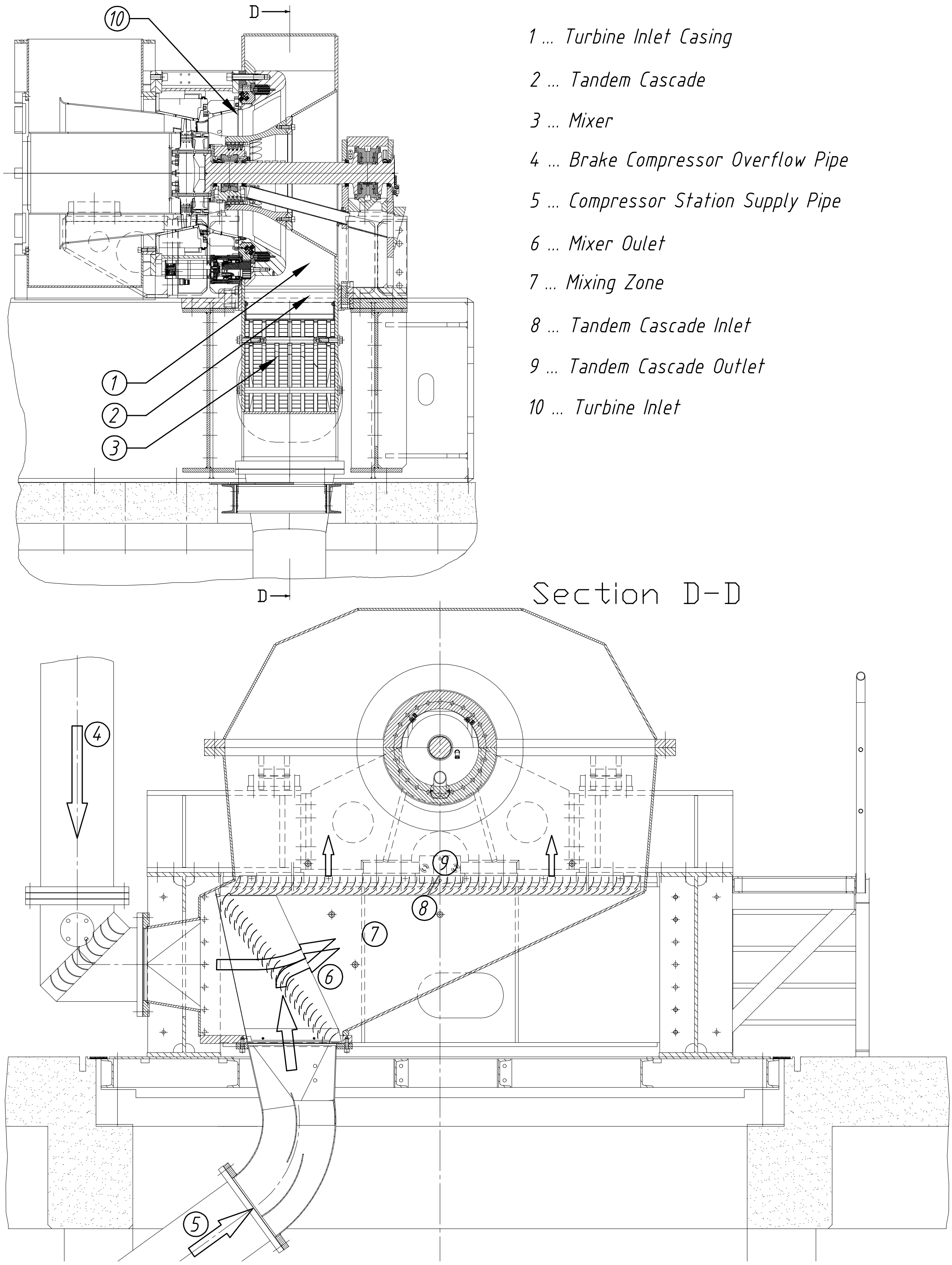

Fig. 21 Turbine inlet concept showing GHH- and compressor station inlets, mixer and tandem cascade in section D-D

Compressor intakes for industrial gas turbines are good examples for effective reduction of flow distortion by modifying the inlet volume, the radial-to-axial bend and additional flow adjustment devices. These efforts are necessary for providing lowest total pressure drop and swirl angle circumferential distributions for the compressor inlet, which is usually designed for flight conditions. So if the perfectly axisymmetric inlet condition of a aeroderivative gas generator is replaced through the commonly used 90° bend intake system with filters and silencers on a new design industrial gas turbine the fully three-dimensional inlet flow has to be properly curbed to avoid severe undermining compressor operation from an aerodynamic-structural standpoint.

Turbine inlets in general are not so sensitive to flow distortions because of the accelerated flow and the thicker blades, but in the case of a test turbine the axisymmetric inlet condition has also to be provided to give some chance for good mass flow and total enthalpy drop balances over the test stage. The more equal the circumferential pressure, temperature, velocity and swirl angle measurements the better the comparison of this data to a small angular segment measured more detailed and the better the comparison to the overall mechanical power transmitted at the coupling.

The first inlet designs of our test turbine intake were kept within the geometric restraints of the milling machine in our workshop, since due to cost reasons we had decided to manufacture this pressure vessel ourselves. As in the initial design the temperature differences between the compressor station supply and the brake compressors delivery were estimated to about 50°C, a simple mixing swirl concept with tangential feeding of the inlet chamber was intended to be sufficient enough for equalising temperature distribution before taking out this swirl through adjustable guide vanes and leading the mixed air in axial direction to the test stage inlet.

When 1997 a big gasturbine manufacturer decided for testing turbine stages in Graz this design was completely changed once more. The new concept led to an inlet casing more than doubling the old volume, designed with the help of CFD calculations on STAR-CD [11] to give better flow acceleration, an enlarged meridional gas path and the implementation of a mixer, since the temperature difference between compressor station delivery and uncooled air from the GHH brake compressor now due to flow similarity conditions could be nearly up to 200°C (see Fig. 21 and 22).

As TTM had already developed their own TTM-Stage to run the machine and to build up the required measurement techniques in conventional and also optical methods, this stage inserts were now used for commissioning the transonic test-turbine facility first in the Brite Euram project “Development of Industrial Transonic Turbine Stages“ within an enlarged and more modular test rig concept now capable for much more different test stage inserts.

First priority on the inlet casing concept was a high flow acceleration providing lowest average total pressure drop and swirl angle circumferential distribution in the measurement plane A in front of the IGV´s at acceptable costs. The enlarged inlet casing now has an inlet flow acceleration factor of about 4 from the tandem cascade outlet (2.0m x 0.44m) to the turbine inlet section (D=0.62m, d=0.18m in front of the stage inner and outer meridional adapters) comparable to an axial compressor inlet casing.

4.1.2 Mixer

Second priority had the optimisation of the inlet temperature profile, because in our mixing concept this task had to be optimised for all test cases in which high temperature differences between the compressor station supply and the brake compressor air would occur. Besides the integral concept of a mixer built into the turbine inlet casing there had been another inlet casing concept with separated casings for more freedom in flow design of the mixer and the turbine inlet. But these two vessels had to be designed on a cold pressure of about 8bar at quite big dimensions and there would have been need for additional big piping. So the first concept with an integral solution of the mixer in the inlet casing was given preference due to cost reasons and we were quite happy about an integral solution. After this concept was accepted from our test partner we started welding this inlet casing ourselves in the test hall handling this growing heavy steel box with the help of the crane and a fork-lift truck since we had to go forward on this task although there was less money (the EU-project for which it was built started half a year later). Although we had some concern about the flow coming from the quite complicated connection piece between supply pipe and the mixer inlet for the compressor station flow, we decided to hold on this concept and to improve it later on if necessary, because there was no time left for further test models or CFD-calculations due to the time schedule depending on the assembling and alignment of the turbine inlet casing.

As the temperature difference to be equalised now was much higher, it was impossible to hold on the original inlet concept of a mixing swirl at relative big dimensions, because the mixing length would have been far to long for acceptable inlet temperature distortions. So the mixer concept now had to provide multiple small zones at higher mixing performance at shorter distances to mix up most of the air before reaching the turbine inlet itself.

To obtain first the necessary velocity difference between the two inlet mass flows for optimal mixing and second the requested high flow acceleration in the turbine inlet casing the following flow scheme was planned :

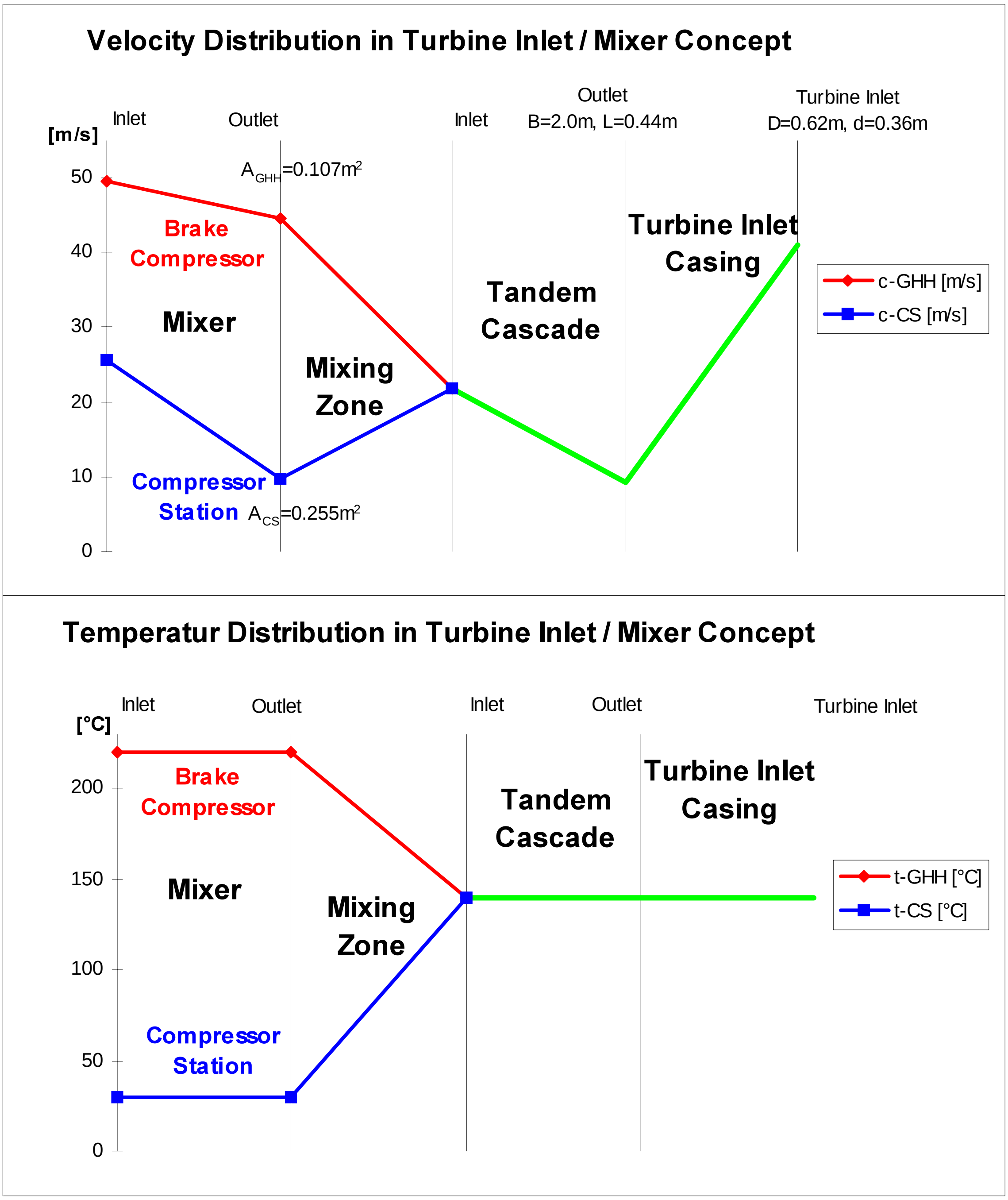

Fig. 22 Velocity and temperature distribution in the turbine inlet and mixer concept

To get the optimum mixer dimensions the most challenging condition was optimised with a matrix of CFD-calculated mixer configurations [11] generating temperature profiles versus mixing length and a one dimensional estimation of pressure loss. The mixing requirements were set to +/-5°C after 300mm mixing length with minimum pressure loss at acceptable design efforts. These boundaries let to a minimum pressure loss in the GHH-slits (depending on the number of GHH-slits) at a number of 7 and after another higher pressure loss zone in between at a higher number of 15. As at seven GHH nozzles the pressure loss was still acceptable it was decided to built in this number, because the minimum slit number was equal to minimum manufacturing expense although the preparation of the mixer insert fixings was designed that way, that it would be possible to realise the doubled number 14, if 7 would fail. This mixer design had to provide +/-5°C after 300mm length also when the uncooled brake would press 230°C hot air through seven 19mm wide slits at high velocity and a pressure loss of about 70mbar to mix up with slow velocity streams in 42mm wide registers fed with cooled air coming from the compressor station at about ambient temperature plus 15°C and a mixer pressure loss of about 30mbar. The requested distortion further downstream at the inlet temperature profile was set to be less than +/- 3°C.

4.2 TTM-Stage

4.2.1 Design history and CFD-development

In 1994 two persons started building up a state-of-the-art test facility and a computational fluid dynamics (CFD) code development in parallel within the project S6801-TEC, "Efficiency improvement by flow optimisation" of the Austrian Science Foundation FWF.

To have the opportunity of free design and publishing data it was decided to build an internally designed transonic turbine stage for our test facility (TTM-Stage). In comparison to the high pressure research turbines shown in [7] the aerodynamic loading was quite high first. The loading factor was set to about 2.0, the pressure ratio at 4.1 and the flow coefficient at about 0.65. This led to a hub to tip reaction variation of 0.25 to 0.50 and average Mach numbers in the midspan section of the vane and the blade exit of about 1.1.

The own developed transonic turbine stage (TTM-Stage) (see Fig. 8, 11, and 26) was designed and optimised first on a five blade sections one dimensional calculation with an estimation of losses from [12] and [13] including the machine characteristics of the compressor station operating conditions and the GHH-brake compressor behaviour. Optimising the parameters speed, meridional path dimensions, turbine inlet parameters at constant vane exit flow angle and specific work distribution over the blade height I got the geometrical data for the stage inlet and outlet boundaries with the corresponding 3D blading design. The system optimisation for maximum coupling power and high efficiency provides effective design point operation for the GHH-brake compressor and the institute´s compressor station which helps in maximising blade height respectively preventing the two end zone loss regions from merging into a single loss structure.

In this first approach the Euler calculations showed very high shock losses and we recognised some problems with our constant vane exit angle at the high design pressure ratio of 4.1. Because it was first decided to keep the constant angle we lowered the total inlet pressure to 3.44 bar to reduce these losses. This reduction also provided a better part load condition at 2.9 bar, so that the high pressure ratio at serial operation of the compressor station would not always be necessary.

In the following iterative cycles between the one-dimensional calculations, the 3D Euler flow and the detailed structural analysis of the stress and vibration modes of the blading the new geometry was optimised and the results of the 3D Euler calculations using an solver with implicit approximate factorisation of Beam and Warming were shown in [14].

In a parallel iteration the flow optimised blade was investigated in finite element method (FEM) stress and vibration calculations and especially its connection to the disk was studied in many different ways to predict the operational behaviour. In spite of all efforts the really measured vibration frequencies of the bladed disk modes surprisingly were to close at the nozzle frequency and so we had to reduce the guide vane number from 29 to 24 to overcome this problem.

For this we designed and calculated [15] a completely new vane using a linear projection of the VKI-LS 82-05 [16] for our hub and tip vane section. To improve the stage efficiency and to keep the maximum Mach number on the vane hub suction surface on a still acceptable value we rejected the constant guide vane angle design and opened the vane at the hub to get some higher reaction. Because the mass flow then increased above the required 18.1kg/s we had to turn the vane somewhat closer at the tip and to scale the blade thickness in the hub and tip design sections. Additionally we increased the design point speed from 10500 to 11000 rpm to have acceptable incidence angles at the already existing running blade. The meridional path and the other machine characteristics fitted well with the new vane design and the turbine coupling power was calculated to about 1.9MW at the old total to static pressure ratio of 3.44 to 1.1bar and total inlet temperature of 454.4K.

Fortunately our CFD codes were built up in parallel so that we could examine the stage design in a first full Navier Stokes calculation sometimes later. The Navier Stokes investigation of the 24 guide vane nozzle in difference to the beautiful inviscid 3D Euler calculation showed severe separation of the hub boundary layer due to the trailing edge shock of the guide vane. Although the manufacturing had already started we redesigned the nozzle once more to get the best we could do in a few days.

The flow solver used in these final design and flow simulations is based on a time-marching Euler code [15],[17]. Here only a brief outline of the main features of the Navier-Stokes code is given from [18].

The 3D-Reynolds/Favre averaged Navier Stokes equations with Spalart and Allmaras [19] turbulence closure are treated in conservative form and discretized in time by applying an implicit method leading to a set of non-linear finite difference equations which is solved by applying a Newton-Raphson relaxation technique.

In stationary simulations convergence is optimized by using a local time step based on a local stability criterion and in addition, by applying a multigrid procedure based on [20],[21]. The convective (Euler) parts are discretized using a third-order-accurate, TVD-upwind, cell-centered finite volume scheme, based on Roe's approximate Riemann solver [15],[22]. In order to construct the numerical viscous flux vector at the cell interfaces, a second order accurate central differencing scheme has been adopted. In the present cell-centered scheme, phantom cells are used to handle all boundaries. According to the theory of characteristics, flow angle, total pressure, total temperature and isentropic relations are used at the subsonic axial inlet. At the subsonic axial outlet the average value of the static pressure is prescribed, density and velocity components are extrapolated. On solid walls, the pressure is extrapolated from the interior points and the non-slip adiabatic condition is used to compute density and total energy.

Quasi-3D nonreflecting boundary conditions for sub-/supersonic in-/outlet, based on the work of Giles [23] and modified by Pieringer [24] are implemented and a simple mixing plane approach has been adopted to model the rotor-stator interaction problem for steady flow analysis.

Structured multiblock grids are used to discretize the flow region. All meshes are generated with an algebraic multi-block grid generator based on Bézier curves and Bézier surfaces [25]. The code is also able to handle moving (e.g. rotating) and deforming grids.

In order to meet the desired design goals, CFD had been included in the design phase of guide vane and rotor blade. Starting with an initial design for the blading geometry, based on one dimensional analytical tools, a series of quasi-3D and full 3D-Euler computations led to a refined geometry which then was further optimised by performing Quasi-3D and full 3D-Navier Stokes simulations.

Most of the computations were done on different grids in order to ensure grid independent solutions. To give an example, a typical O-type mesh, used for 3D-viscous flow analysis is displayed in Fig. 23. The boundary layer is resolved down to the viscous sublayer, therefore the grid is exponentially stretched normal to solid walls such that the size of the first cell at the blade surface is below a y^+-value of about 1.

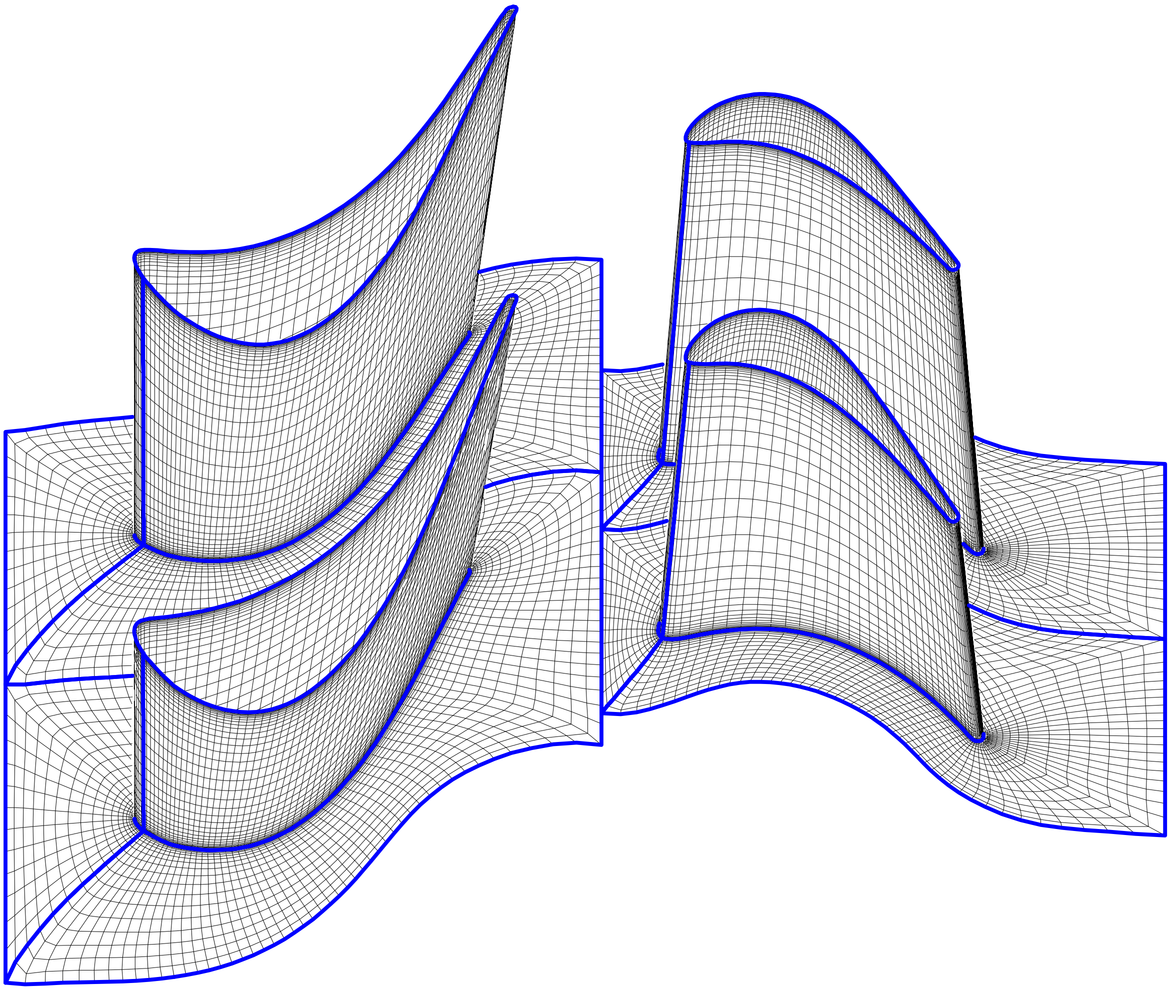

Fig. 23 Structured O-Type grid for 3D-viscous flow analysis (524288 cells in total)

In order to illustrate the flow characteristics at the design point, Mach number contours at midspan predicted by viscous flow simulations are displayed in Fig. 24. Due to the transonic pressure ratio, a strong suction sided trailing edge shock wave at the nozzle exit and a somewhat less pronounced shock at the rotor blade suction side, leading to a strong increase in boundary layer thickness can be observed.

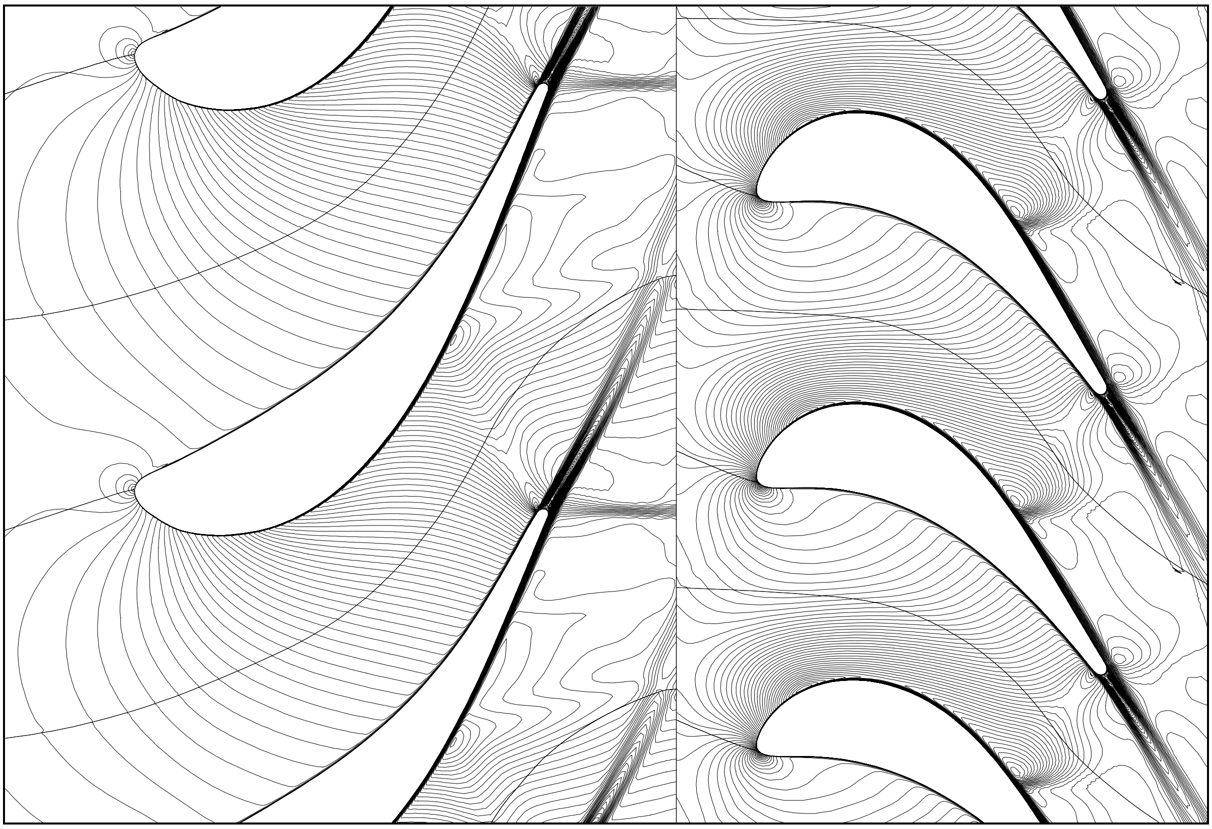

Fig. 24 Mach number contours at midspan predicted by viscous flow simulation (increment 0.02)

It should further be noted that due to the strong trailing edge shock waves, a very big influence of reflecting-nonreflecting boundary conditions had been observed especially at the nozzle exit, as shown by means of pressure contours predicted by quasi 3D inviscid calculations presented in Fig. 25.

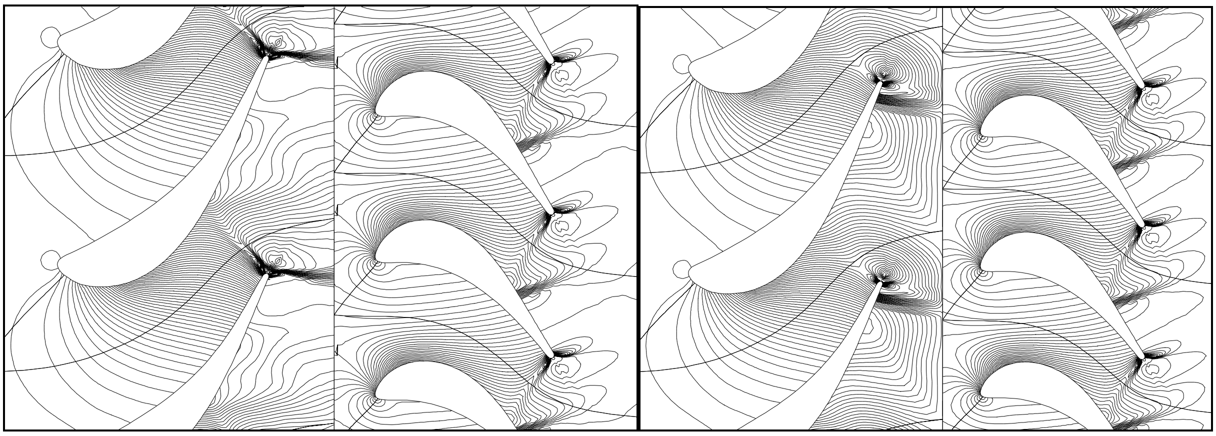

Fig. 25 Q3D-Euler predicted pressure distribution (101, 0.5:4bar) nonreflecting boundaries left, reflecting outlet condition right

4.2.2 Final TTM-Stage design

4.2.2.1 *TTM-Stage parameters*

The initial TTM aero design point was set at a loading factor of 2.0 and a pressure ratio of 4.1 (total to static). After several iterations of increasing design point speed and reducing pressure ratio it was changed to 1.54 and 3.12 (total-to-static), (see Table 2). So I admit that the actual numbers of the presented TTM-stage Navier Stokes Simulation are not that aggressive any more. This is due to the design development in which we stayed on the same design point parameters for this stage due to test rig optimal configuration and due to increasing losses in our blading hub sections at higher Mach numbers.

Nevertheless this low reaction designed TTM-stage has higher limit load capacities and the low values given here as precaution are on the lower boundary of the stages compared in [7]. Checking the TTM-stage with other test stages in this paper our design parameters are best comparable with the DRB of Okapuu (1974) in terms of loading factor, flow factor and reaction but not yet in pressure ratio and the higher exit Mach number.

Boundary Conditions			**Output**	
Inlet (A)	p_{tot} [bar]	3.439	**n [rpm]**	**11000**
	T_{tot} [K]	454.4	**P [MW]**	**1.94**
Outlet (C)	p_{stat} [bar]	1.102	**m [kg/s]**	**18.1**

TTM-Stage Parameters	Hub (5%)	Mean (50%)	Tip (95%)
Pressure Ratio (total to static)		**3.12**	
ψ Loading factor $-\Delta h/u^2$		**1.54**	
ϕ Flow factor c_{ax}/u		**0.54**	
R_{kin} Reaction (hub, mean, tip) [%]	12	**27**	40
Exit swirl (hub, mean, tip) [°]	1	**8**	5
Exit Mach number	0.34	**0.40**	0.37
Reynolds number Vane	2.1E+06	**2.4E+06**	2.6E+06
Reynolds number Blade	1.5E+06	**1.6E+06**	1.6E+06
Airfoil count Vane		**24**	
Airfoil count Blade		**36**	
Aspect ratio Vane		**0.78**	
Aspect ratio Blade		**1.35**	
Zweifel´s Coefficient Vane	0.80	**0.69**	0.67
Zweifel´s Coefficient Blade	0.73	**1.01**	0.94
Trailing Edge Blockage Vane [%]	6.6	**6.9**	7.2
Trailing Edge Blockage Blade [%]	11.6	**9.4**	7.5
Clearance/span [%]		**0.72**	
Stage efficiency (total to static)		**0.85**	

Table 2 TTM-Stage design point parameters as predicted from the latest Navier-Stokes flow simulations
(Reynolds numbers based upon chord length and exit conditions,
stage efficiency total to static isentropic across blading, plane A to C see Fig. 8)

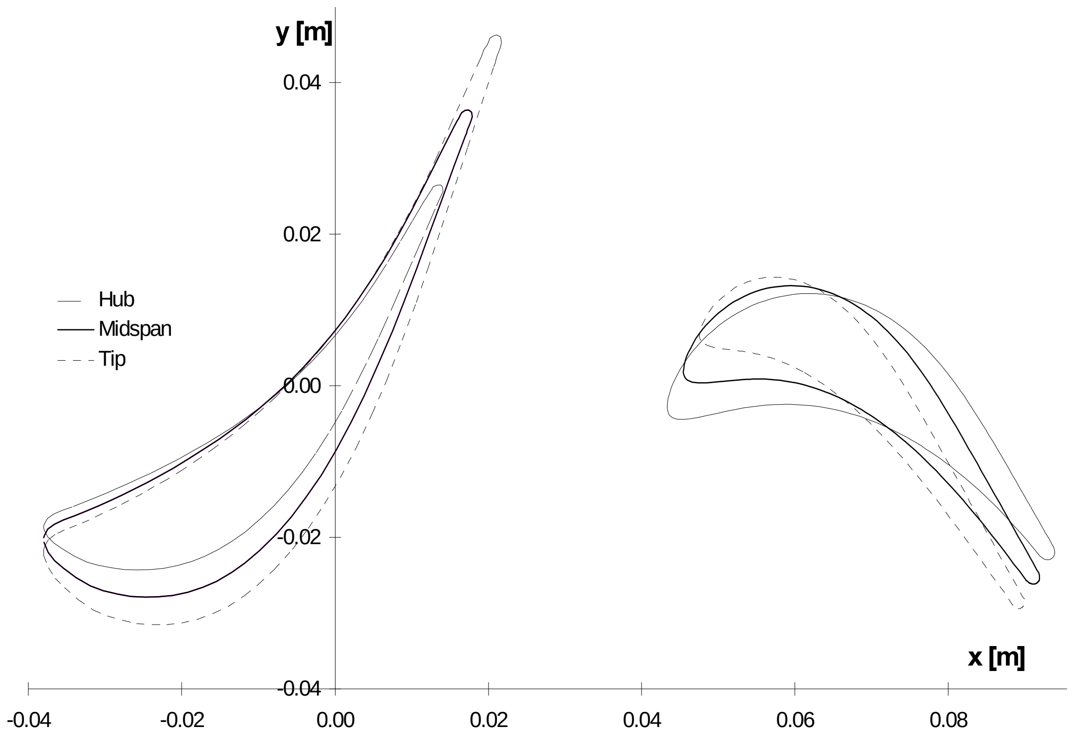

Fig. 26 Hub, midspan and tip sections of TTM-Stage

The blading itself (see Fig. 26) was designed in only two sections each: the two hub sections of the vane and blade are located at the inner diameter of the stage in R200 whereas the tip section of the vane is defined at R258. The blade tip section is defined on R265.577 (see Fig. 8) These sections are wrapped on the corresponding cylinders and then connected with straight lines between the developed hub and tip section points. The surfaces are then cut with the meridional inner and outer contour.

The TTM-stage flow path designed for optical access (see chapter 3.1) led to a severe nozzle wall curvature, which usually requires local tailoring of several spanwise sections to obtain a good pressure distribution on the airfoil. Although the particular airfoil design is a linear interpolation between a hub and tip section the 3D predictions indicate acceptable pressure distribution between the tip and the midspan. Only the nozzle suction surface at the tip shows some small fluctuations in Mach number and pressure and a high acceleration zone at the hub, which could not be avoided in this design regarding nozzle number, angular pitch and meridional section.

However as we had other severe problems with our vane pressure distribution mentioned above (see chapter 4.2.1 Design History and CFD-Development), we were really happy to get this pressure distribution at the original test rig design point with an already manufactured rotor blading after 3 days non stop work, because each day was expensive in production interruption of the new vane manufacturing.

Please look at the following pictures of the surface pressure distribution of our TTM-stage at design point and judge yourself if this simple design gives still acceptable pressure distributions for the first internally developed transonic stage (see Fig. 27):

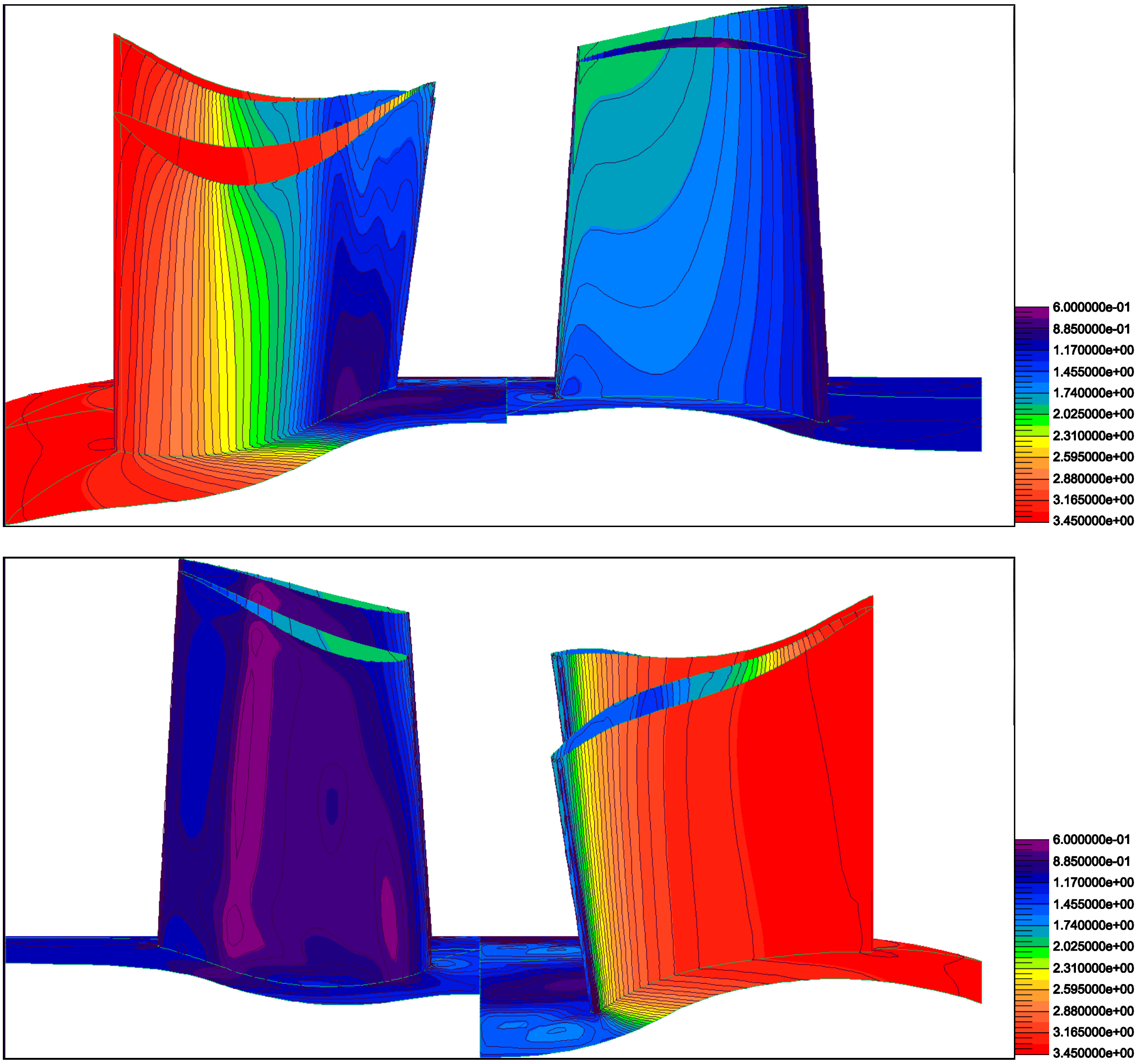

Fig. 27 Pressure distributions of the TTM-stage at design condition (see Table 2)

The stator-to-rotor axial gap was designed at about 0.5 stator axial chord. That is a representative value used in highly loaded stages as a compromise between aerodynamic, mechanical and blade vibration considerations.

The selection of number of airfoils was based on a compromise between optimal loading, minimum trailing edge blockage and secondary losses respectively aspect ratio. Comparing the TTM-Stage to other high loaded stages the guide vane number 24 fits quite well whereas the unconventional small blade number 36 was stressed to give better optical access into a wide blade spacing, but this also led to a high Zweifel coefficient at blade midspan.

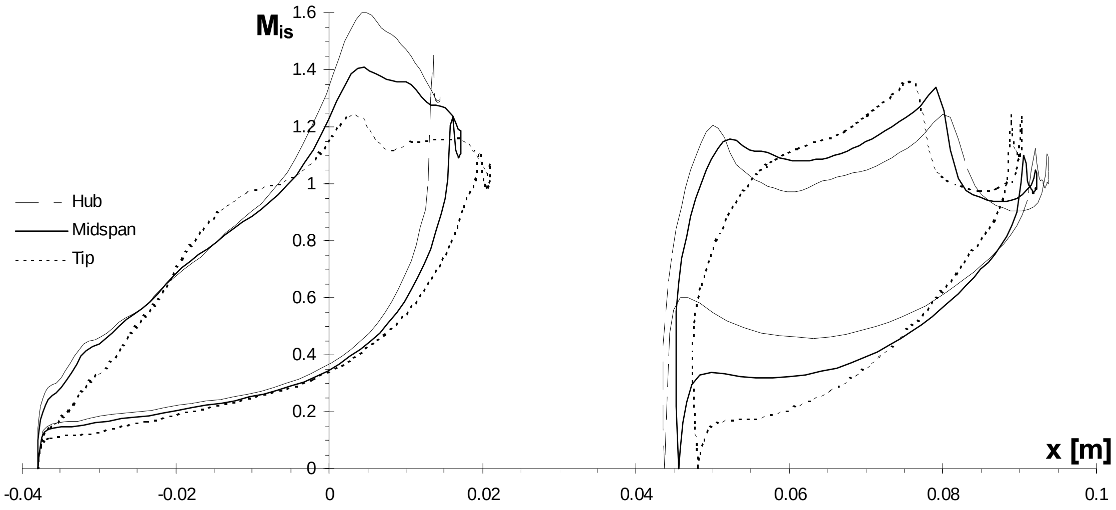

Fig. 28 Vane and blade surface Mach number distributions

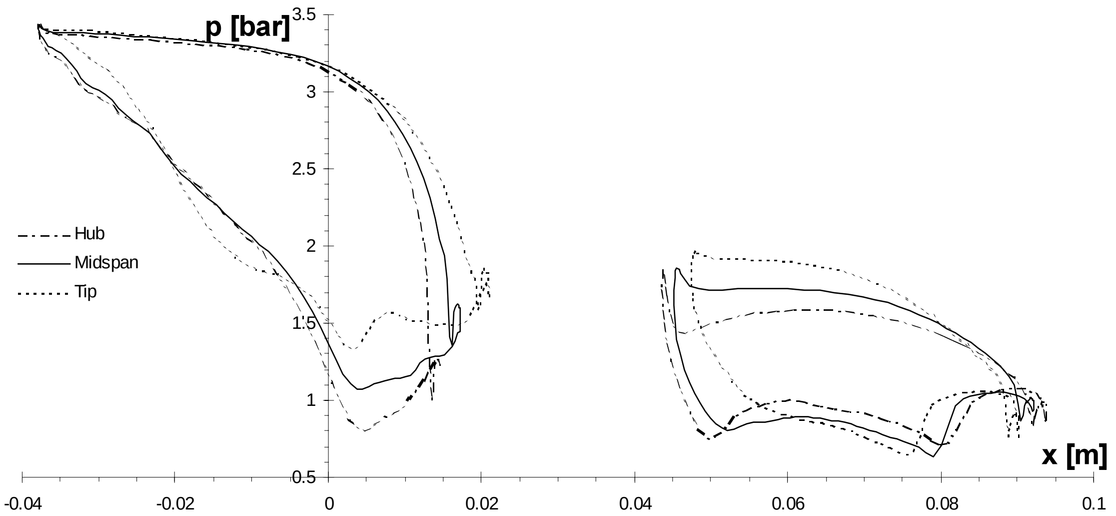

Fig. 29 Vane and blade surface pressure distributions

4.2.2.2 *Nozzle design*

The 24 vanes in their final design (all values in [mm] at Midspan) have an axial chord of 56.1, a pitch-to-chord ratio of 0.76, a turning angle of 69.7° and a mean exit Mach number of 1.11. The trailing edge thickness on midspan section is 1.65 and the throat opening 22.30.

Although the original cooled test case profile with 15° exit angle now is moved to 20.3° and the higher loading at exit Mach number 1.11 (see Fig. 30 compared to 0.9 original design in [16] changes quite a lot, the flow pattern still has some similarity to the original design goal: There is only one strong trailing edge shock at the suction side end and the one on the pressure side is hardly found.

The detailed drawings of the nozzle and blade are given in the appendix.

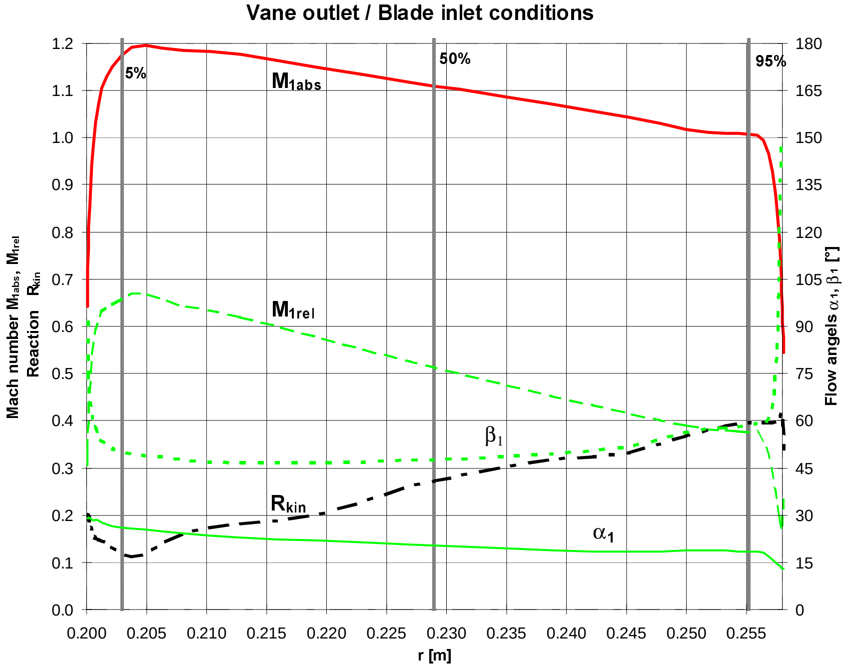

Fig. 30 Vane outlet / Blade inlet conditions

4.2.2.3 *Blade design*

A cooled blade section design implies a larger leading edge for shower head implementation than e.g. a steam turbine profile. In the case of our high inlet relative Mach number of 0.66 at the hub this round leading edge in conjunction with the neighbouring blade suction surface forms a chanal which converges so strong that soon after the leading edge the suction surface exceeds Mach number 1.0 from the hub up to the midspan. This high loading can be seen in the Mach number distribution of the hub blade profile in Fig. 28 and further more on the pressure profiles of the hub suction side, see Fig. 29. At design point there is a 12 to 15% minimum reaction (see Fig. 30) in this region corresponding with low acceleration and a high turning angle of 109°.

The 36 blades (all values in [mm] at Midspan) have an axial chord of 46.8, a pitch-to-chord ratio of 0.75, a turning angle of 106.3°and a mean exit relative Mach number of 0.89, see Fig. 31.

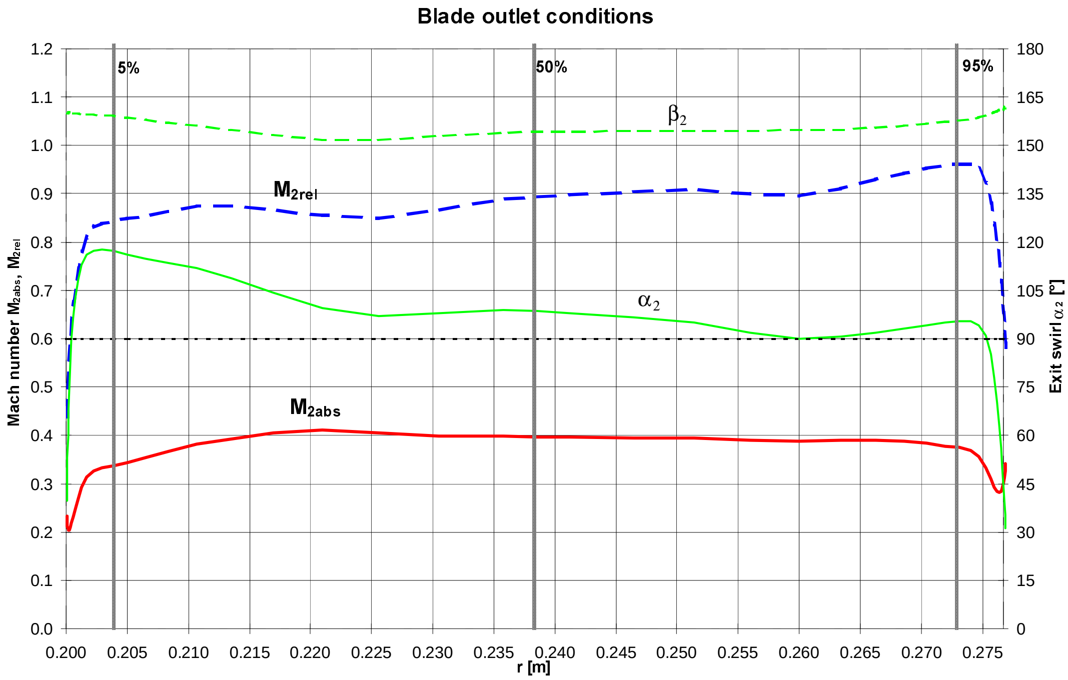

Fig. 31 Blade outlet conditions

4.2.3 Quasi 3D simulation for different load conditions

The following part load investigation was done with the help of a Navier Stokes Solver (see chapter 4.2.1) on a quasi 3D model of the TTM-stage, which consists of the midspan section (50% height) with 10% of respective blade height, see Fig. 32.

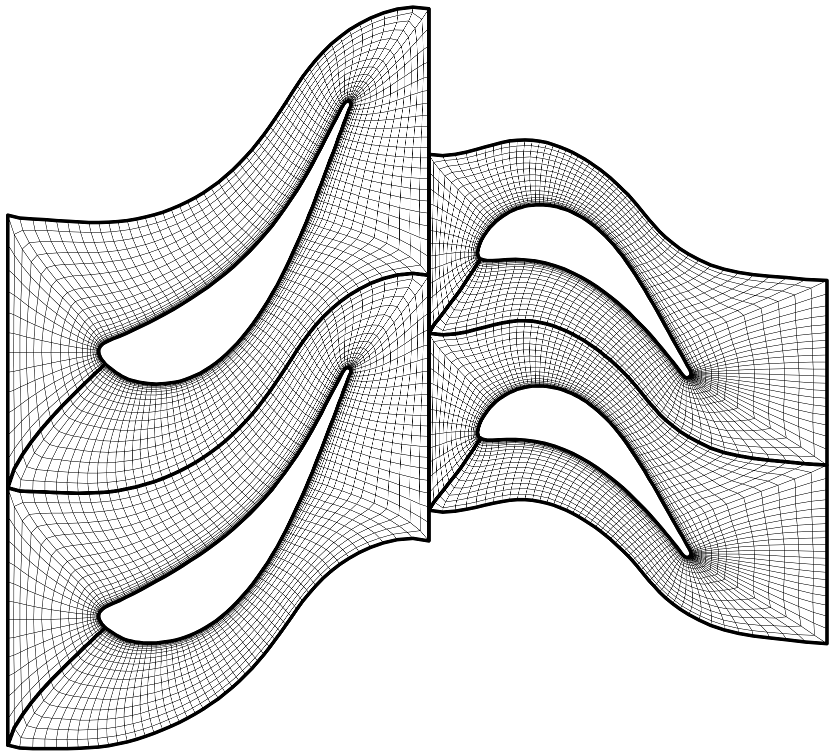

Fig. 32 Periodic O-Type grid: 2x128x32 Cells ($\Delta y_1/t \approx 10^{-6}$ => $y_1^+ \approx 1$)

<u>The following parameter variations were investigated (plane A and C):</u>

Turbine inlet total temperature $t_{0\,tot}$ [°C] :	**181.3, (159.1), 137.0, (116.0), 95.0**
Turbine inlet total pressure $p_{0\,tot}$ [bar] :	**4.0, 3.5, 3.0, 2.5, 2.0**
Speed n [rpm] :	**11550, 11000,10450, 9900 (=105%, 100%, 95%, 90%)**
Turbine outlet static pressure p_2 [bar] :	**1.0**

58 Navier Stokes simulations for different parameter variations were calculated and evaluated. To show some significant examples of TTM-stage part load behaviour the following parameter combinations will be presented :

Fig. 33 **Variation of pressure ratio** at fixed turbine inlet $t_{0\,tot}$ = 137.0°C and speed n = 9900rpm
pressure distribution [bar]

Fig. 34 **Variation of pressure ratio** at fixed turbine inlet $t_{0\,tot}$ = 137.0°C and speed n = 9900rpm
Mach No. distribution

Fig. 35 **Variation of speed** at fixed turbine inlet $p_{0\,tot}$ = 3.0bar and $t_{0\,tot}$ = 137.0°C
Mach No. distribution

To show first the good matching of the TTM-Stage with the GHH brake compressor and TTM compressor station characteristics and second to give some help in checking operational parameters for future tests four **optimal testing configurations of the TTM-Stage from 90% to 105% speed** (11000rpm=100%) are presented in Fig. 36 up to 43. The flow behaviour in the TTM-Stage at these conditions is shown by a Mach number distribution and enclosed detailed evaluation of the characteristic stage parameters such as such as power, mass flow, matching with rotor inlet blade angle, rotor exit swirl, rotor exit static temperature, stator and rotor average Mach number.

To check the parameters for further operating points additional information is given in the appendix at chapter 8.2 and some formulas for the Quasi 3D Navier Stokes evaluation in Fig. 36 up to 40 are shown in 8.4.3.

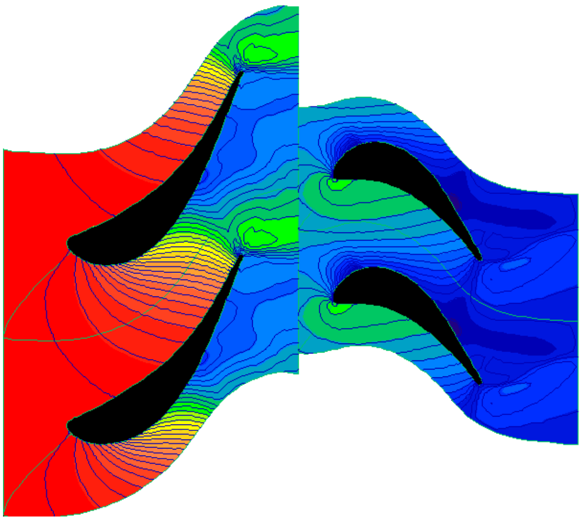

$p_{0\ tot}$ = **4.0bar**, $t_{0\ tot}$ = 137.0°C, n = 9900rpm

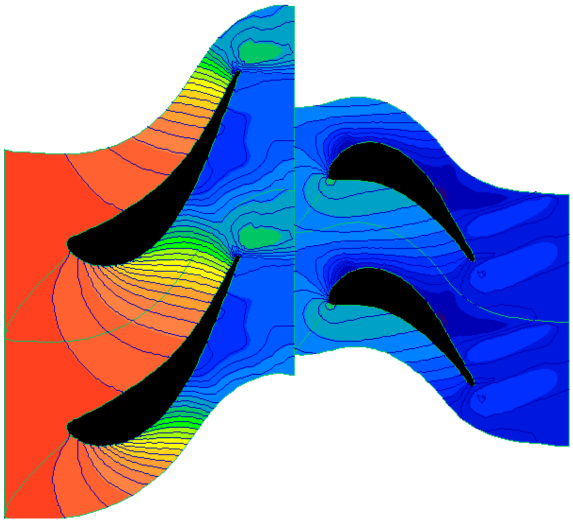

$p_{0\ tot}$ = **3.5bar**, $t_{0\ tot}$ = 137.0°C, n = 9900rpm

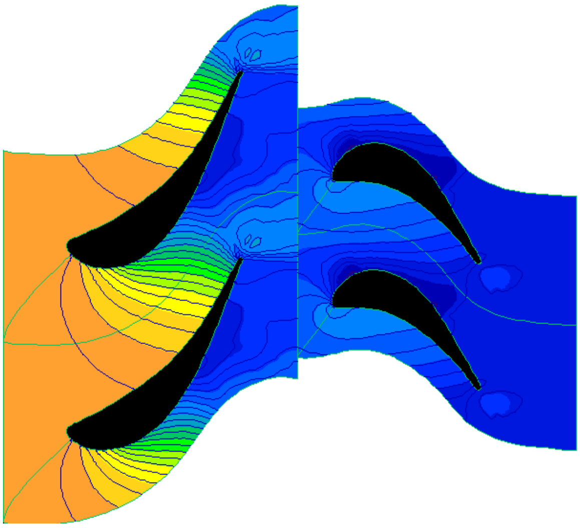

$p_{0\ tot}$ = **3.0bar**, $t_{0\ tot}$ = 137.0°C, n = 9900rpm

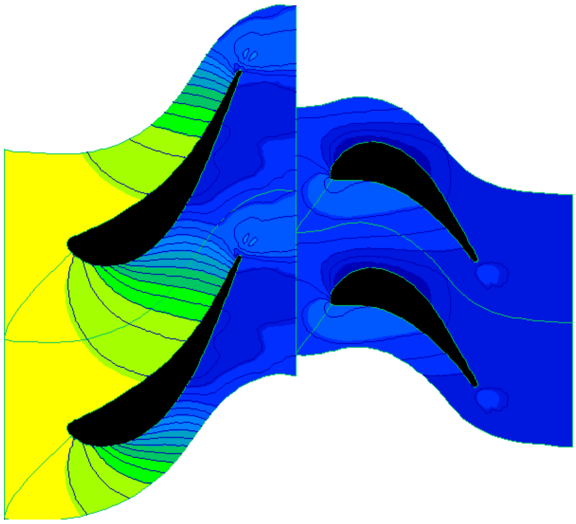

$p_{0\ tot}$ = **2.5bar**, $t_{0\ tot}$ = 137.0°C, n = 9900rpm

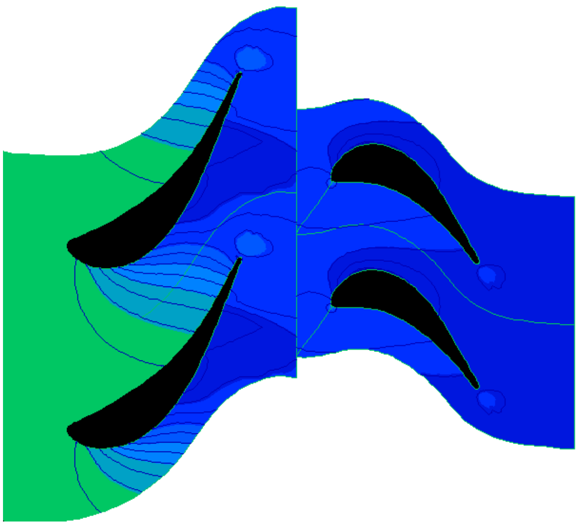

$p_{0\ tot}$ = **2.0bar**, $t_{0\ tot}$ = 137.0°C, n = 9900rpm

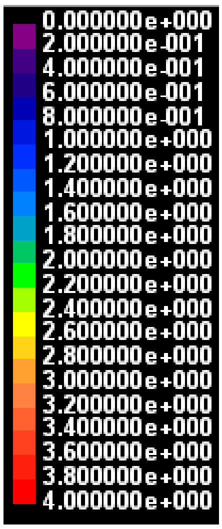

p [bar]

Fig. 33 **Variation of pressure ratio** at fixed turbine inlet $t_{0\ tot}$ = 137.0°C and speed n = 9900rpm **pressure distribution [bar]**

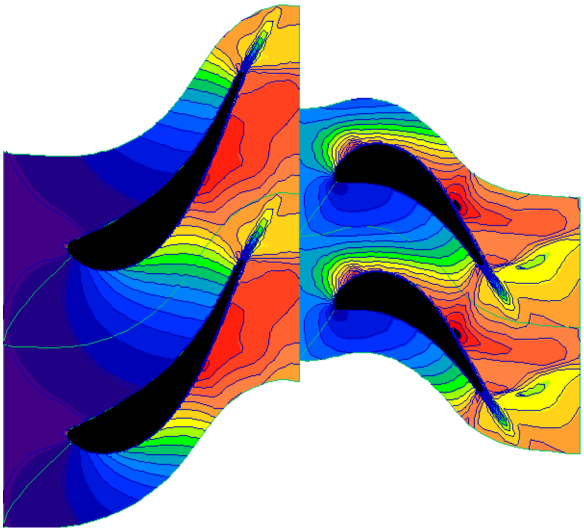

$p_{0\,tot}$ = 4.0bar, $t_{0\,tot}$ = 137.0°C, n = 9900rpm

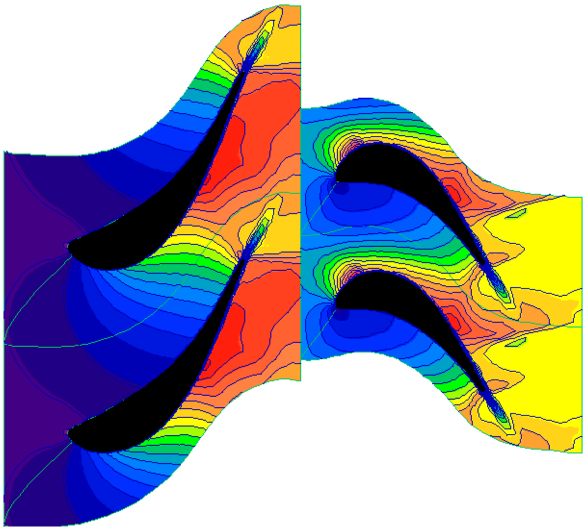

$p_{0\,tot}$ = 3.5bar, $t_{0\,tot}$ = 137.0°C, n = 9900rpm

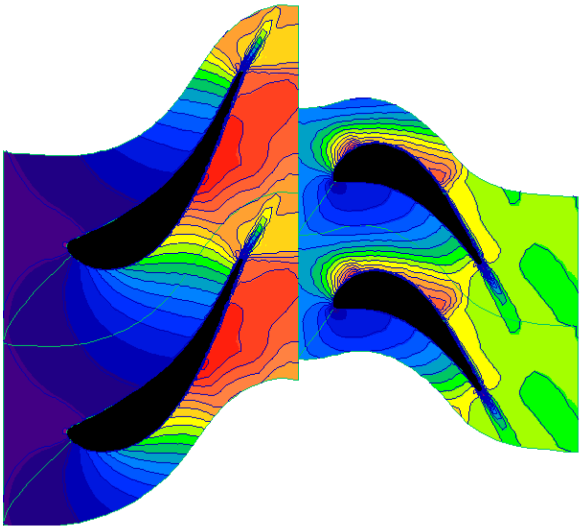

$p_{0\,tot}$ = 3.0bar, $t_{0\,tot}$ = 137.0°C, n = 9900rpm

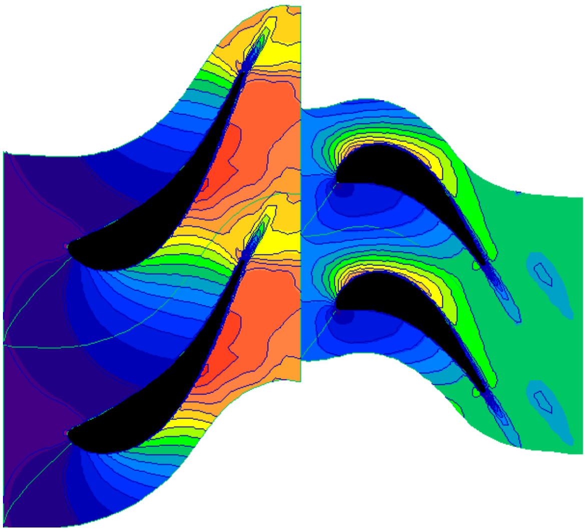

$p_{0\,tot}$ = 2.5bar, $t_{0\,tot}$ = 137.0°C, n = 9900rpm

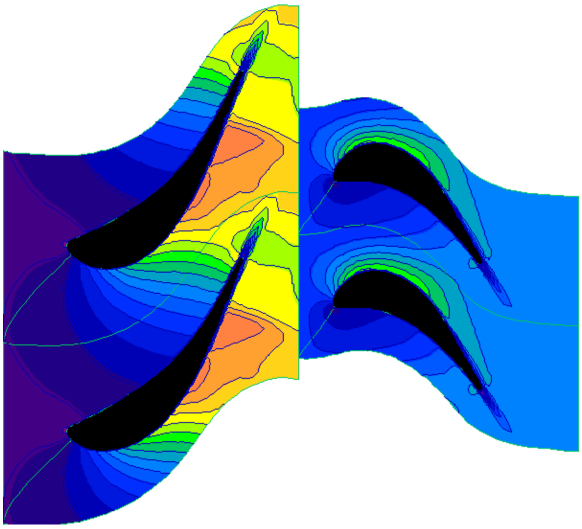

$p_{0\,tot}$ = 2.0bar, $t_{0\,tot}$ = 137.0°C, n = 9900rpm

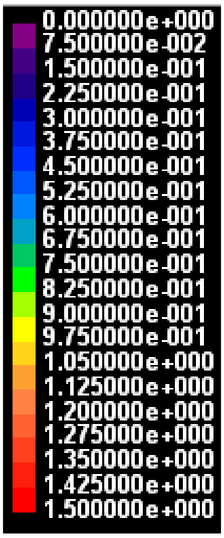

Mach No.

Fig. 34 **Variation of pressure ratio** at fixed turbine inlet $t_{0\,tot}$=137.0°C and speed n=9900rpm
Mach No. distribution

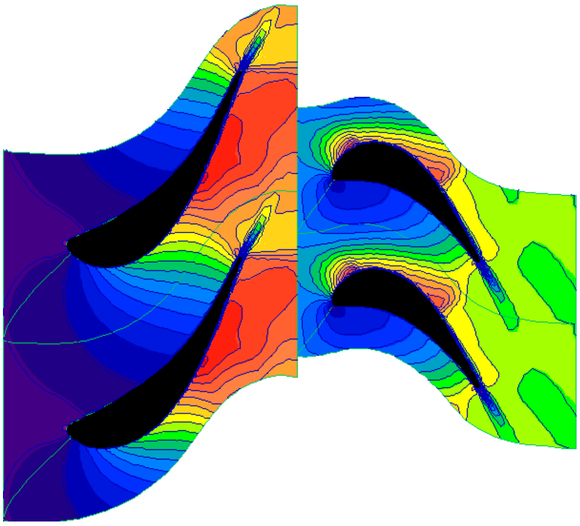

$p_{0\ tot}$ = 3.0bar, $t_{0\ tot}$ = 137.0°C, **n = 9900rpm**

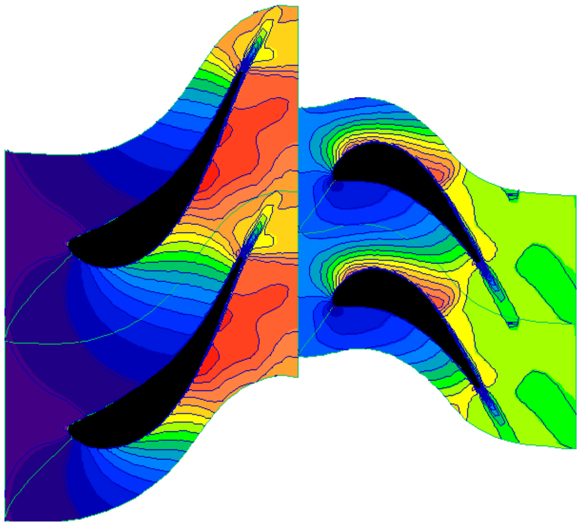

$p_{0\ tot}$ = 3.0bar, $t_{0\ tot}$ = 137.0°C, **n = 10450rpm**

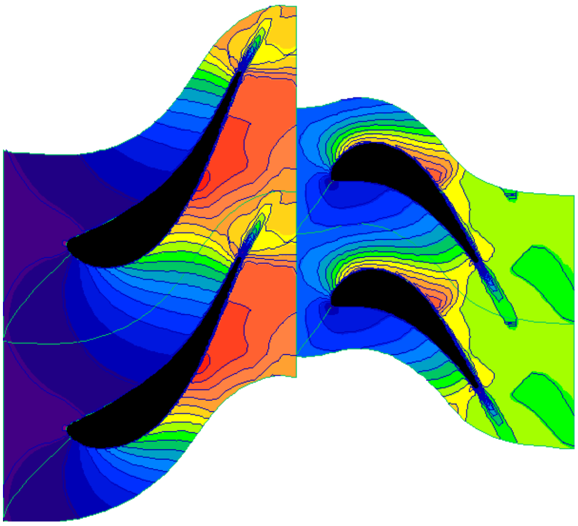

$p_{0\ tot}$ = 3.0bar, $t_{0\ tot}$ = 137.0°C, **n = 11000rpm**

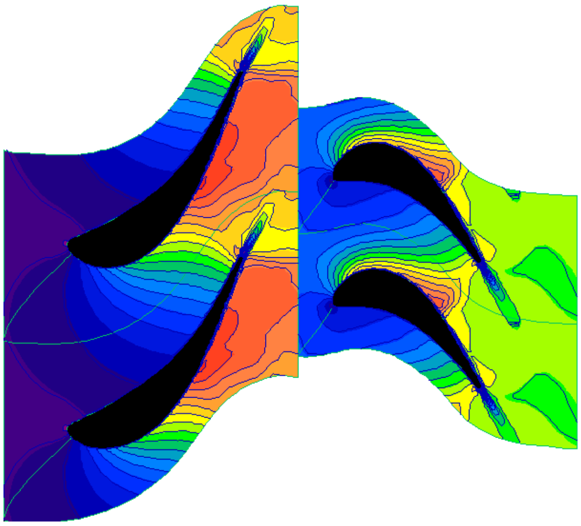

$p_{0\ tot}$ = 3.0bar, $t_{0\ tot}$ = 137.0°C, **n = 11550rpm**

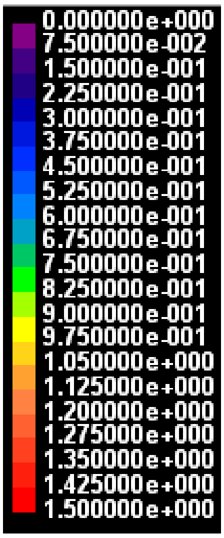

Mach No.

Fig. 35 **Variation of speed** at fixed turbine inlet $p_{0\ tot}$ = 3.0bar and $t_{0\ tot}$ = 137.0°C
Mach No. distribution

4.2.3.1 *Part Load 1 - 9900rpm*

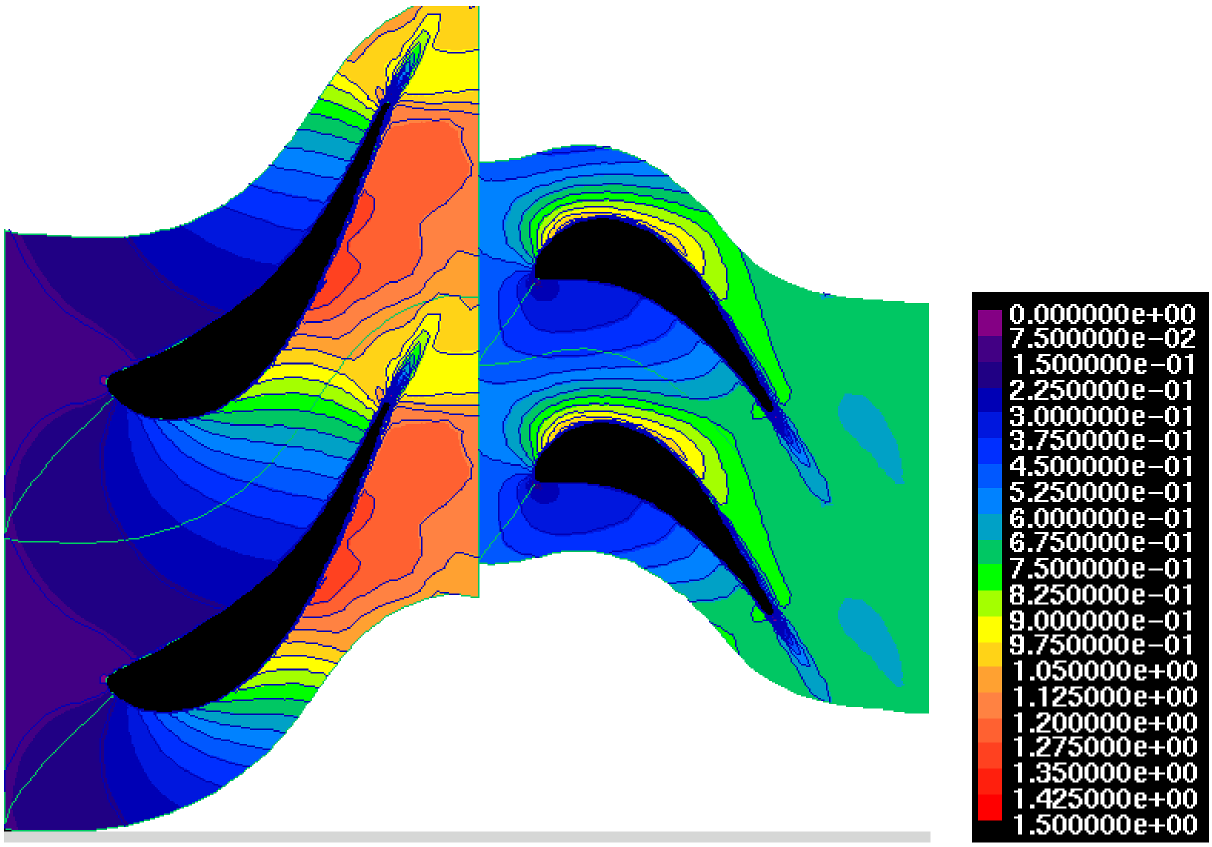

$p_{0\ tot}$ = 2.5bar, $t_{0\ tot}$ = 116.0°C, n = 9900rpm, (simulation job No. 51) **Mach No.**

Job No.	51

Boundary Conditions		Output	
$p_{0\ tot}$ [Pa]	250000	n [rpm]	9900
$T_{0\ tot}$ [K]	389.1	P [kW]	1108
$p_{2\ stat}$ [Pa]	100000	m [kg/s]	14.2

TTM-Stage Parameters			
π Pressure Ratio (total to static)			2.50
η Stage efficiency (total to static)			0.91
ψ Loading factor $-\Delta h/u^2$			1.28
φ Flow factor c_{ax}/u			0.43
R_{kin} Reaction [%]			12.1
		Vane	Blade
Turning angle [°]		70	107
Exit swirl [°]		70	15
Exit Mach number		1.09	0.32
Reynolds number		2.09E+06	1.42E+06
Zweifel´s Coefficient		0.69	1.10
Aspect ratio (true chord)		0.70	1.25
Pitch-to-chord ratio		0.76	0.74
Trailing Edge Blockage [%]		6.9	9.4
Clearance/span [%]			0.72
Airfoil count		24	36
True chord [mm]	s [mm]	78.9	55.9
Pitch [mm]	t [mm]	60.0	41.6
Axial chord [mm]	b_{ax} [mm]	56.1	46.8
Airfoil hight [mm]	h [mm]	55.2	69.8
Trailing edge thickness	d [mm]	1.65	1.94
Throat opening	a [mm]	22.3	18.8

Vane In	r [m]	ρ [kg/m³]	c_{ax} [m/s]	c_u [m/s]	c_r [m/s]	p [Pa]	T [K]
	0.2346876	2.2170026	55.053423	0	0	246614	387.58691
	c_{abs} [m/s]	α [°]	a [m/s]	M_{abs}		p_{tot} [Pa]	T_{tot} [K]
	55.053423	90.00	394.62947	0.1395066		249990	389.1
Vane-Out	r [m]	ρ [kg/m³]	c_{ax} [m/s]	c_u [m/s]	c_r [m/s]	p [Pa]	T [K]
	0.2290334	1.2640203	134.4183	363.27118	16.161842	114619.36	315.95265
	c_{abs} [m/s]	α [°]	a [m/s]	M_{abs}		p_{tot} [Pa]	T_{tot} [K]
	387.67955	20.31	356.30012	1.0880702		241146	390.8
	M_{is}	T_{is} [K]	ρ_{is} [kg/m³]	c_{is} [m/s]	μ_{is} [Ns/m²]	Re	Zweifel´s C.
	1.1170763	311.3831	1.2825699	395.12573	1.915E-05	2088168	0.69
Blade In	r [m]	ρ [kg/m³]	c_{ax} [m/s]	c_u [m/s]	c_r [m/s]	p [Pa]	T [K]
	0.2289003	1.2668576	131.87082	359.90491	15.911881	114744.22	315.58846
	c_{abs} [m/s]	α [°]	a [m/s]	M_{abs}		p_{tot} [Pa]	T_{tot} [K]
	383.63348	20.12	356.09471	1.0773355		238248	388.8
	w_{rel} [m/s]	β [°]	u_1 [m/s]	M_{rel}			
	180.75782	47.09	237.30684	0.5076116			
Blade-Out	r [m]	ρ [kg/m³]	c_{ax} [m/s]	c_u [m/s]	c_r [m/s]	p [Pa]	T [K]
	0.2384778	1.1355175	107.40193	28.584388	12.217743	100000	306.84962
	c_{abs} [m/s]	α [°]	a [m/s]	M_{abs}		p_{tot} [Pa]	T_{tot} [K]
	111.81017	75.10	351.12986	0.3184297		107280	313.1
	w_{rel} [m/s]	β [°]	u_2 [m/s]	M_{rel}			
	243.91189	153.84	247.23608	0.6946487			
	M_{is}	T_{is} [K]	ρ_{is} [kg/m³]	c_{is} [m/s]	μ_{is} [Ns/m²]	Re	Zweifel´s C.
	1.1864036	303.42792	1.1483225	414.25256	1.877E-05	1416455	1.10

Fig. 36 Part Load 1 - 9900rpm in Mach No. and evaluation of Quasi 3D Navier Stokes simulation job No. 51

Part Load 1 - 9900rpm at TTM-Stage and Brake Compressor

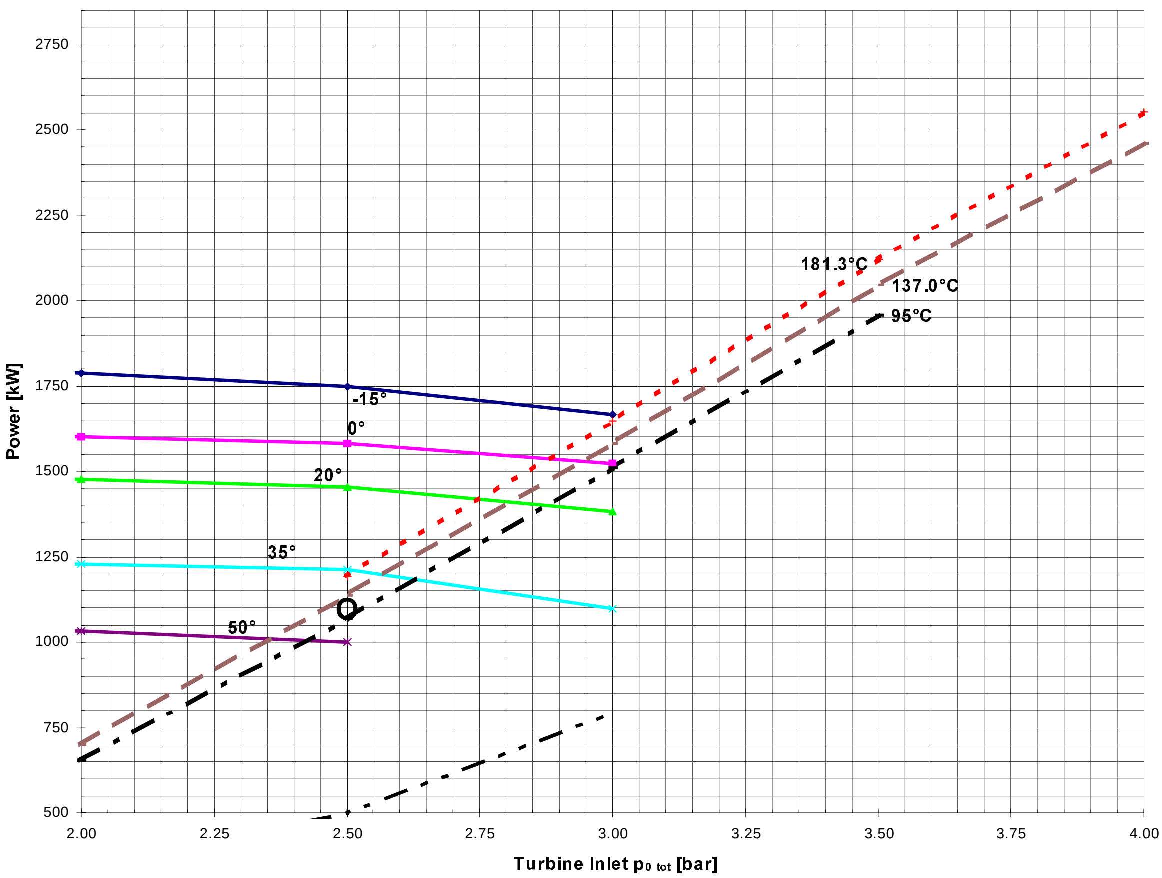

Parameter = f ($p_{0\,to\,t}$ [bar] , $T_{0\,tot}$ [K])			
P [kW]	368	410	454
2.0	653	699	
2.5	1067	1137	1195
3.0	1509	1582	1648
3.5	1958	2045	2122
4.0		2461	2554

Compressor Station TTM :

m_{CS} [kg/s]	368	410	454	t_{CS} [°C]	368	410	454
2.0	6.8	5.8		2.0	61	131	
2.5	7.7	6.4	5.3	2.5	33	107	210
3.0	7.9	6.7	5.6	3.0	7	87	195
3.5				3.5			
4.0				4.0			

Test Turbine TTM-stage :

m[kg/s]	368	410	454	β_1 [°]	368	410	454	α_2 [°]	368	410	454
2.0	11.6	11.0		2.0	57	52		2.0	38	33	
2.5	14.6	13.8	13.1	2.5	49	45	43	2.5	18	12	6
3.0	17.5	16.5	15.7	3.0	47	44	42	3.0	-2	-8	-14
3.5	20.4	19.3	18.3	3.5	47	44	42	3.5	-17	-22	-26
4.0		22.1	21.0	4.0		44	42	4.0		-27	-31
t_2 [°C]	368	410	454	M_{1abs}	368	410	454	M_{2rel}	368	410	454
2.0	34	69		2.0	0.94	0.95		2.0	0.56	0.56	
2.5	17	50	86	2.5	1.08	1.10	1.12	2.5	0.70	0.69	0.69
3.0	4	36	70	3.0	1.13	1.15	1.16	3.0	0.84	0.84	0.84
3.5	-7	24	57	3.5	1.13	1.15	1.16	3.5	0.97	0.97	0.97
4.0		13	44	4.0		1.15	1.16	4.0		1.07	1.07

GHH Brake Compressor :

α_{Drall} [°]	368	410	454	m_{GHH} [kg/s]	368	410	454	t_{GHH} [°C]	368	410	454
2.0	67	66		2.0	4.8	5.2		2.0	143	144	
2.5	45	40	36	2.5	6.9	7.4	7.8	2.5	164	163	162
3.0	7	-10	-14	3.0	9.5	9.8	10.1	3.0	168	171	174
3.5				3.5				3.5			
4.0				4.0				4.0			

Fig. 37 Part Load 1 - 9900rpm at TTM-Stage and brake compressor with test parameter check (m_{CS}, t_{CS}, β_1)

4.2.3.2 *Part Load 2 - 10450rpm*

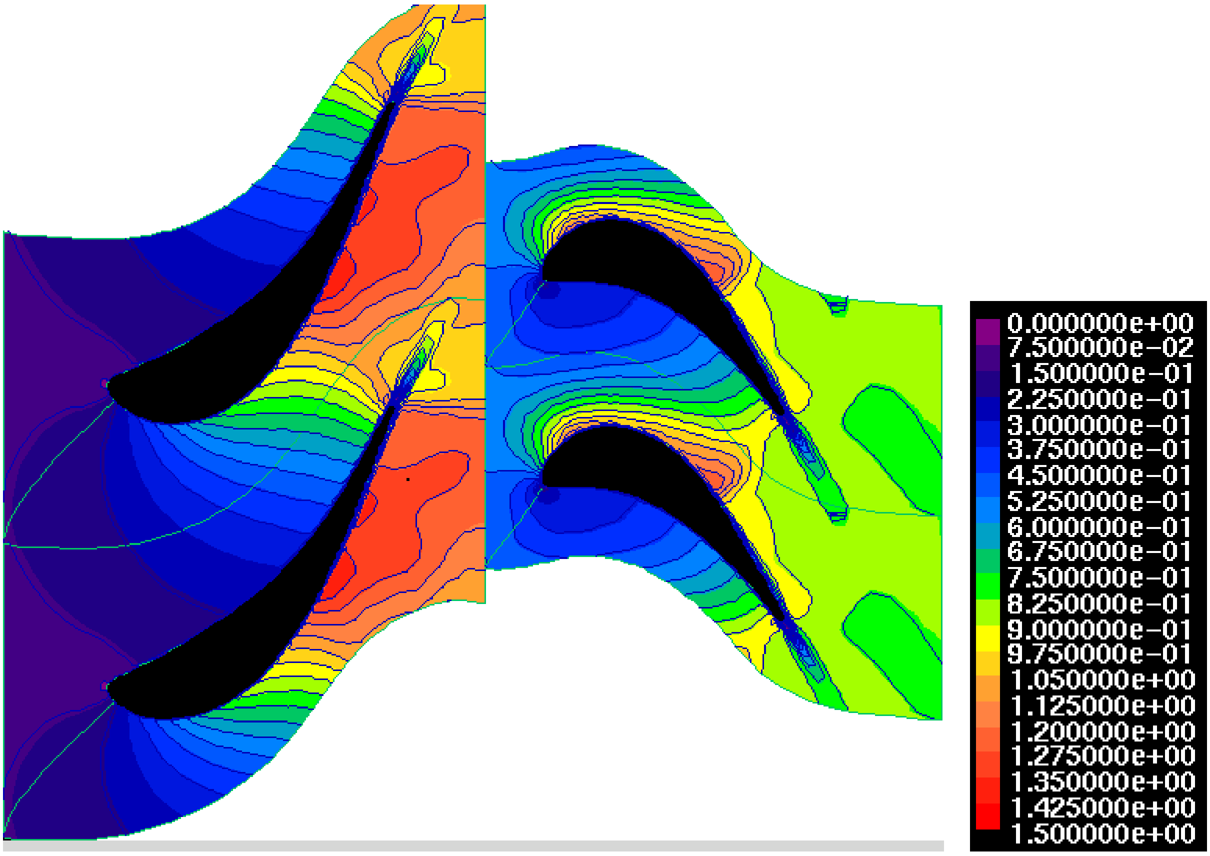

$p_{0\ tot}$ = 3.0bar, $t_{0\ tot}$ = 137.0°C, n = 10450rpm, (simulation job No. 41) **Mach No.**

Job No.	41

Boundary Conditions		Output	
$p_{0\ tot}$ [Pa]	300000	n [rpm]	10450
$T_{0\ tot}$ [K]	410.1	P [kW]	1594
$p_{2\ stat}$ [Pa]	100000	m [kg/s]	16.6

TTM-Stage Parameters			
π Pressure Ratio (total to static)			3.00
η Stage efficiency (total to static)			0.91
ψ Loading factor $-\Delta h/u^2$			1.41
ϕ Flow factor c_{ax}/u			0.48
R_{kin} Reaction [%]			21.2
		Vane	Blade
Turning angle [°]		70	107
Exit swirl [°]		70	-2
Exit Mach number		1.13	0.36
Reynolds number		2.35E+06	1.57E+06
Zweifel´s Coefficient		0.70	1.02
Aspect ratio (true chord)		0.70	1.25
Pitch-to-chord ratio		0.76	0.74
Trailing Edge Blockage [%]		6.9	9.4
Clearance/span [%]			0.72
Airfoil count		24	36
True chord [mm]	s [mm]	78.9	55.9
Pitch [mm]	t [mm]	60.0	41.6
Axial chord [mm]	b_{ax} [mm]	56.1	46.8
Airfoil hight [mm]	h [mm]	55.2	69.8
Trailing edge thickness	d [mm]	1.65	1.94
Throat opening	a [mm]	22.3	18.8

Vane In	r [m]	ρ [kg/m³]	c_{ax} [m/s]	c_u [m/s]	c_r [m/s]	p [Pa]	T [K]
	0.2346876	2.5241749	56.516044	0	0	295937	408.50545
	c_{abs} [m/s]	α [°]	a [m/s]	M_{abs}		p_{tot} [Pa]	T_{tot} [K]
	56.516044	90.00	405.13885	0.139498		299988	410.1
Vane-Out	r [m]	ρ [kg/m³]	c_{ax} [m/s]	c_u [m/s]	c_r [m/s]	p [Pa]	T [K]
	0.2290334	1.3835718	143.27668	383.54815	17.374938	130502.13	328.65027
	c_{abs} [m/s]	α [°]	a [m/s]	M_{abs}		p_{tot} [Pa]	T_{tot} [K]
	409.80396	20.48	363.38915	1.1277275		288462	412.2
	M_{is}	T_{is} [K]	ρ_{is} [kg/m³]	c_{is} [m/s]	μ_{is} [Ns/m²]	Re	Zweiffel´s C.
	1.1586078	323.29807	1.4064769	417.58315	1.97E-05	2352128	0.70

Blade In	r [m]	ρ [kg/m³]	c_{ax} [m/s]	c_u [m/s]	c_r [m/s]	p [Pa]	T [K]
	0.2289003	1.3868274	140.42888	379.6781	17.064983	130575.58	328.06331
	c_{abs} [m/s]	α [°]	a [m/s]	M_{abs}		p_{tot} [Pa]	T_{tot} [K]
	405.1752	20.30	363.06451	1.1159868		284403	409.8
	w_{rel} [m/s]	β [°]	u_1 [m/s]	M_{rel}			
	191.57481	47.39	250.49055	0.5276605			
Blade-Out	r [m]	ρ [kg/m³]	c_{ax} [m/s]	c_u [m/s]	c_r [m/s]	p [Pa]	T [K]
	0.2384778	1.1288808	125.84962	-4.7079463	14.268403	100000	308.65219
	c_{abs} [m/s]	α [°]	a [m/s]	M_{abs}		p_{tot} [Pa]	T_{tot} [K]
	126.74335	92.14	352.15969	0.3599031		109364	316.6
	w_{rel} [m/s]	β [°]	u_2 [m/s]	M_{rel}			
	294.32506	154.65	260.97142	0.8357716			
	M_{is}	T_{is} [K]	ρ_{is} [kg/m³]	c_{is} [m/s]	μ_{is} [Ns/m²]	Re	Zweiffel´s C.
	1.3191248	303.98633	1.1462079	461.01801	1.88E-05	1571241	1.02

Fig. 38 Part Load 2 - 10450rpm in Mach No. and evaluation of Quasi 3D Navier Stokes simulation job No. 41

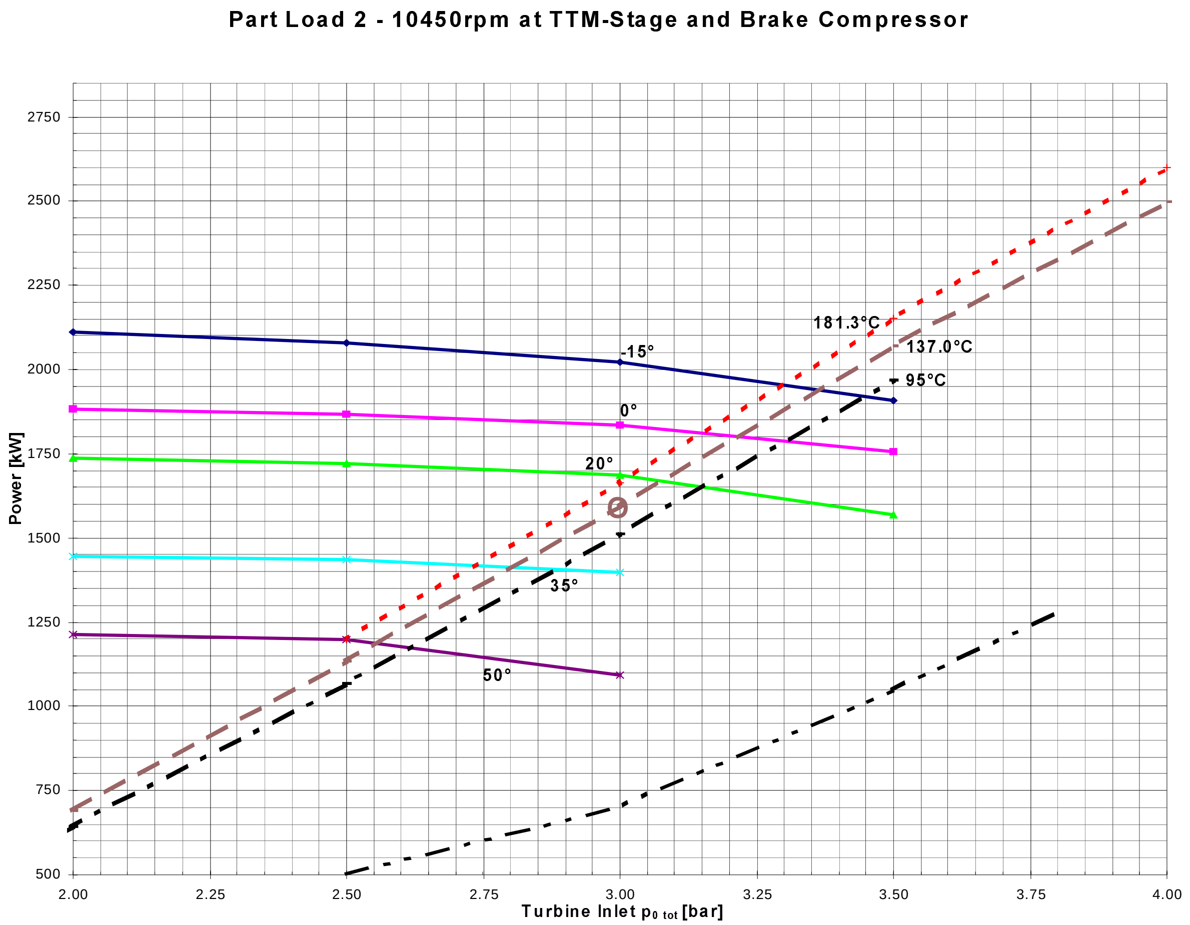

Parameter = f ($p_{0\,tot}$ [bar] , $T_{0\,tot}$ [K])				Compressor Station TTM :							
P [kW]	**368**	**410**	**454**	**m_{CS} [kg/s]**	**368**	**410**	**454**	**t_{CS} [°C]**	**368**	**410**	**454**
2.0	643	690		**2.0**	7.3	6.3		**2.0**	59	124	
2.5	1067	1135	1197	**2.5**	8.0	6.9	5.9	**2.5**	33	101	189
3.0	1512	1594	1665	**3.0**	8.6	7.1	5.8	**3.0**	7	82	187
3.5	1969	2068	2154	**3.5**	10.0			**3.5**	-13		
4.0		2499	2598	**4.0**				**4.0**			

Test Turbine TTM-stage :											
m[kg/s]	**368**	**410**	**454**	**β_1 [°]**	**368**	**410**	**454**	**α_2 [°]**	**368**	**410**	**454**
2.0	11.6	11.0		**2.0**	62	57		**2.0**	43	38	
2.5	14.6	13.8	13.1	**2.5**	53	49	46	**2.5**	24	18	12
3.0	17.5	16.6	15.7	**3.0**	51	47	44	**3.0**	4	-2	-8
3.5	20.4	19.3	18.3	**3.5**	51	47	44	**3.5**	-11	-17	-21
4.0		22.1	21.0	**4.0**		47	44	**4.0**		-23	-27
t_2 [°C]	**368**	**410**	**454**	**M_{1abs}**	**368**	**410**	**454**	**M_{2rel}**	**368**	**410**	**454**
2.0	34	69		**2.0**	0.93	0.94		**2.0**	0.57	0.57	
2.5	17	50	85	**2.5**	1.06	1.08	1.10	**2.5**	0.70	0.70	0.69
3.0	4	36	69	**3.0**	1.11	1.13	1.14	**3.0**	0.84	0.84	0.84
3.5	-7	23	56	**3.5**	1.11	1.13	1.15	**3.5**	0.97	0.97	0.97
4.0		12	44	**4.0**		1.13	1.15	**4.0**		1.07	1.07

GHH Brake Compressor :											
α_{Drall} [°]	**368**	**410**	**454**	**m_{GHH} [kg/s]**	**368**	**410**	**454**	**t_{GHH} [°C]**	**368**	**410**	**454**
2.0	69	68		**2.0**	4.3	4.7		**2.0**	155	155	
2.5	57	53	50	**2.5**	6.6	6.9	7.2	**2.5**	171	174	175
3.0	29	25	21	**3.0**	8.9	9.4	9.9	**3.0**	180	179	178
3.5	-17			**3.5**	10.4			**3.5**	199		
4.0				**4.0**				**4.0**			

Fig. 39 Part Load 2 - 10450rpm at TTM-Stage and brake compressor with test parameter check (m_{CS}, t_{CS}, β_1)

4.2.3.3 *Design Point - 11000rpm*

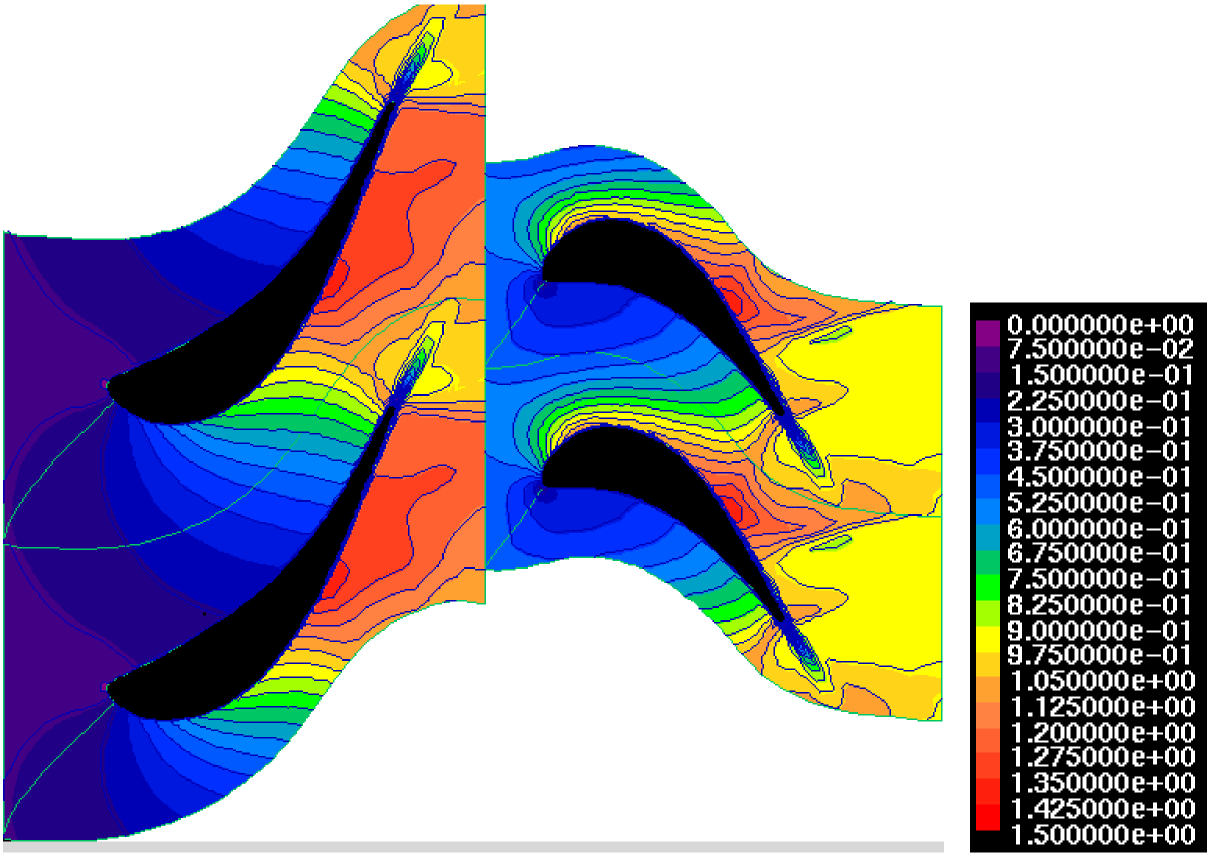

$p_{0\,tot}$ = 3.5bar, $t_{0\,tot}$ = 159.1°C, n = 11000rpm, (simulation job No. 17) **Mach No.**

Job No.	17

Boundary Conditions		Output	
$p_{0\,tot}$ [Pa]	350000	n [rpm]	11000
$T_{0\,tot}$ [K]	432.2	P [kW]	2127
$p_{2\,stat}$ [Pa]	100000	m [kg/s]	18.8

TTM-Stage Parameters			
π Pressure Ratio (total to static)			3.50
η Stage efficiency (total to static)			0.90
ψ Loading factor $-\Delta h/u^2$			1.50
ϕ Flow factor c_{ax}/u			0.53
R_{kin} Reaction [%]			32.4
		Vane	Blade
Turning angle [°]		70	106
Exit swirl [°]		70	-14
Exit Mach number		1.12	0.43
Reynolds number		2.57E+06	1.69E+06
Zweifel´s Coefficient		0.70	0.95
Aspect ratio (true chord)		0.70	1.25
Pitch-to-chord ratio		0.76	0.74
Trailing Edge Blockage [%]		6.9	9.4
Clearance/span [%]			0.72
Airfoil count		24	36
True chord [mm]	s [mm]	78.9	55.9
Pitch [mm]	t [mm]	60.0	41.6
Axial chord [mm]	b_{ax} [mm]	56.1	46.8
Airfoil hight [mm]	h [mm]	55.2	69.8
Trailing edge thickness	d [mm]	1.65	1.94
Throat opening	a [mm]	22.3	18.8

Vane In	r [m]	ρ [kg/m³]	c_{ax} [m/s]	c_u [m/s]	c_r [m/s]	p [Pa]	T [K]
	0.2346876	2.7942804	58.027538	0	0	345258	430.51902
	c_{abs} [m/s]	α [°]	a [m/s]	M_{abs}		p_{tot} [Pa]	T_{tot} [K]
	58.027538	90.00	415.9117	0.1395189		349986	432.2
Vane-Out	r [m]	ρ [kg/m³]	c_{ax} [m/s]	c_u [m/s]	c_r [m/s]	p [Pa]	T [K]
	0.2290334	1.5463664	145.77591	391.16179	17.64226	154187.53	347.4201
	c_{abs} [m/s]	α [°]	a [m/s]	M_{abs}		p_{tot} [Pa]	T_{tot} [K]
	417.81505	20.44	373.622	1.1182828		336798	434.3
	M_{is}	T_{is} [K]	ρ_{is} [kg/m³]	c_{is} [m/s]	μ_{is} [Ns/m²]	Re	Zweiffel´s C.
	1.1487069	341.95205	1.5710939	425.79131	2.055E-05	2568799	0.70

Blade In	r [m]	ρ [kg/m³]	c_{ax} [m/s]	c_u [m/s]	c_r [m/s]	p [Pa]	T [K]
	0.2289003	1.5493877	142.94083	387.43283	17.341158	154225.36	346.82772
	c_{abs} [m/s]	α [°]	a [m/s]	M_{abs}		p_{tot} [Pa]	T_{tot} [K]
	413.32432	20.25	373.30333	1.1072077		332254	431.9
	w_{rel} [m/s]	β [°]	u_1 [m/s]	M_{rel}			
	189.86569	49.11	263.67426	0.5086097			
Blade-Out	r [m]	ρ [kg/m³]	c_{ax} [m/s]	c_u [m/s]	c_r [m/s]	p [Pa]	T [K]
	0.2384778	1.1142919	145.0822	-37.142918	16.572033	99996	312.68251
	c_{abs} [m/s]	α [°]	a [m/s]	M_{abs}		p_{tot} [Pa]	T_{tot} [K]
	150.67539	104.36	354.45145	0.4250946		113227	324.0
	w_{rel} [m/s]	β [°]	u_2 [m/s]	M_{rel}			
	344.34532	155.05	274.70676	0.971488			
	M_{is}	T_{is} [K]	ρ_{is} [kg/m³]	c_{is} [m/s]	μ_{is} [Ns/m²]	Re	Zweiffel´s C.
	1.430517	306.4436	1.1369779	501.96482	1.892E-05	1686591	0.95

Fig. 40 Design Point - 11000rpm in Mach No. and evaluation of Quasi 3D Navier Stokes simulation job No. 17

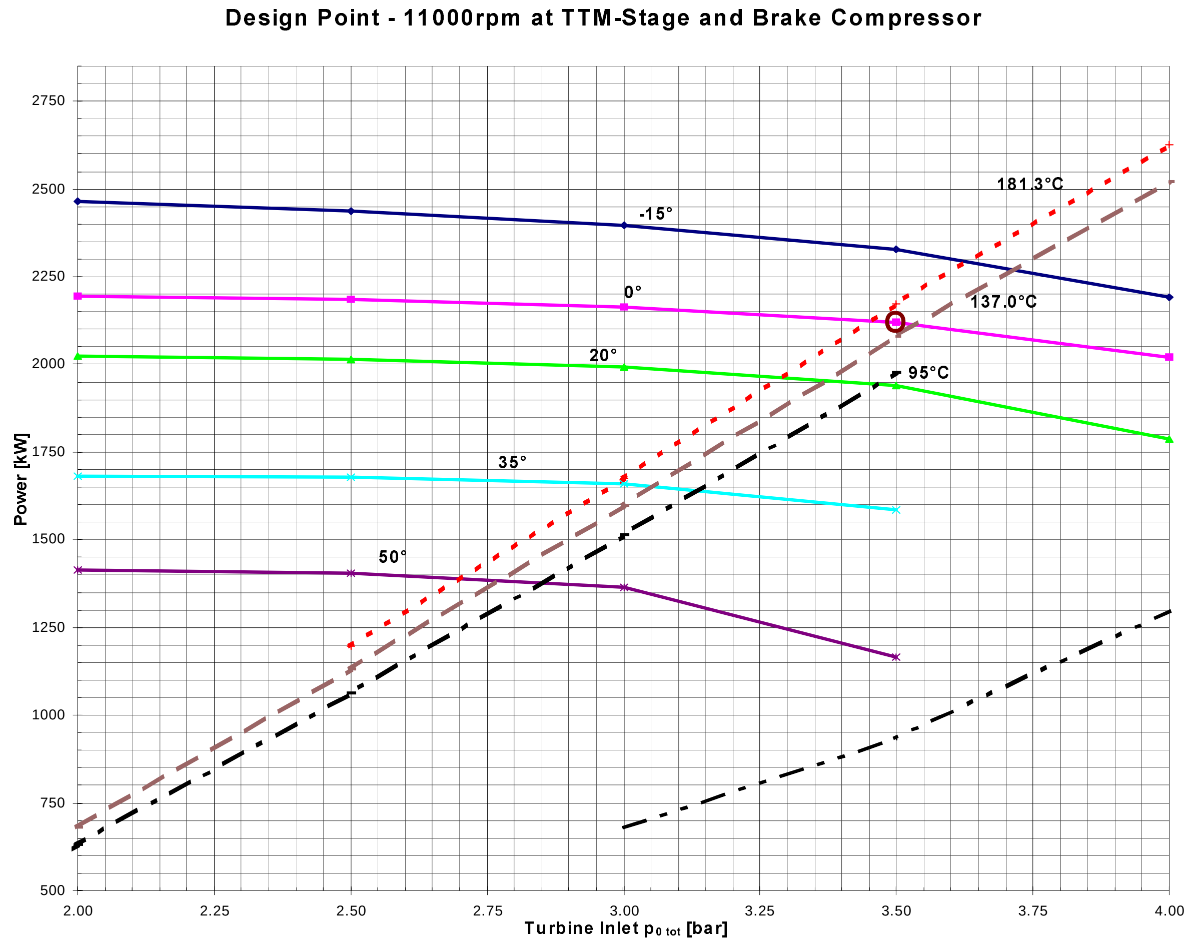

Parameter = f ($p_{0\,tot}$ [bar], $T_{0\,tot}$ [K])				Compressor Station TTM :							
P [kW]	**368**	**410**	**454**	**m_{CS} [kg/s]**	**368**	**410**	**454**	**t_{CS} [°C]**	**368**	**410**	**454**
2.0	629	680		**2.0**	7.7	6.8		**2.0**	58	118	
2.5	1062	1131	1195	**2.5**	8.4	7.2	6.2	**2.5**	33	98	180
3.0	1512	1599	1675	**3.0**	9.5	8.1	6.7	**3.0**	8	74	163
3.5	1975	2080	2172	**3.5**	10.0	8.4	7.2	**3.5**	-14	55	147
4.0		2521	2625	**4.0**				**4.0**			

Test Turbine TTM-stage :											
m[kg/s]	**368**	**410**	**454**	**β_1 [°]**	**368**	**410**	**454**	**α_2 [°]**	**368**	**410**	**454**
2.0	11.6	11.0		**2.0**	68	62		**2.0**	47	43	
2.5	14.6	13.8	13.1	**2.5**	58	53	49	**2.5**	30	24	18
3.0	17.5	16.6	15.7	**3.0**	56	51	47	**3.0**	10	4	-2
3.5	20.4	19.3	18.4	**3.5**	56	51	47	**3.5**	-6	-12	-17
4.0		22.1	21.0	**4.0**		51	47	**4.0**		-19	-23
t_2 [°C]	**368**	**410**	**454**	**M_{1abs}**	**368**	**410**	**454**	**M_{2rel}**	**368**	**410**	**454**
2.0	34	69		**2.0**	0.93	0.93		**2.0**	0.57	0.57	
2.5	17	50	85	**2.5**	1.05	1.06	1.08	**2.5**	0.70	0.70	0.70
3.0	3	35	69	**3.0**	1.09	1.11	1.13	**3.0**	0.84	0.84	0.84
3.5	-7	23	56	**3.5**	1.09	1.11	1.13	**3.5**	0.97	0.97	0.97
4.0		12	43	**4.0**		1.11	1.13	**4.0**		1.07	1.07

GHH Brake Compressor :											
α_{Drall} [°]	**368**	**410**	**454**	**m_{GHH} [kg/s]**	**368**	**410**	**454**	**t_{GHH} [°C]**	**368**	**410**	**454**
2.0	70	70		**2.0**	3.9	4.2		**2.0**	168	168	
2.5	63	61	59	**2.5**	6.2	6.6	6.9	**2.5**	179	180	182
3.0	43	38	34	**3.0**	8.0	8.5	9.0	**3.0**	199	197	195
3.5	18	11	-9	**3.5**	10.4	11.0	11.2	**3.5**	199	199	204
4.0				**4.0**				**4.0**			

Fig. 41 Design Point - 11000rpm at TTM-Stage and brake compressor with test parameter check (m_{CS}, t_{CS}, β_1)

4.2.3.4 *Peak Load - 11550rpm*

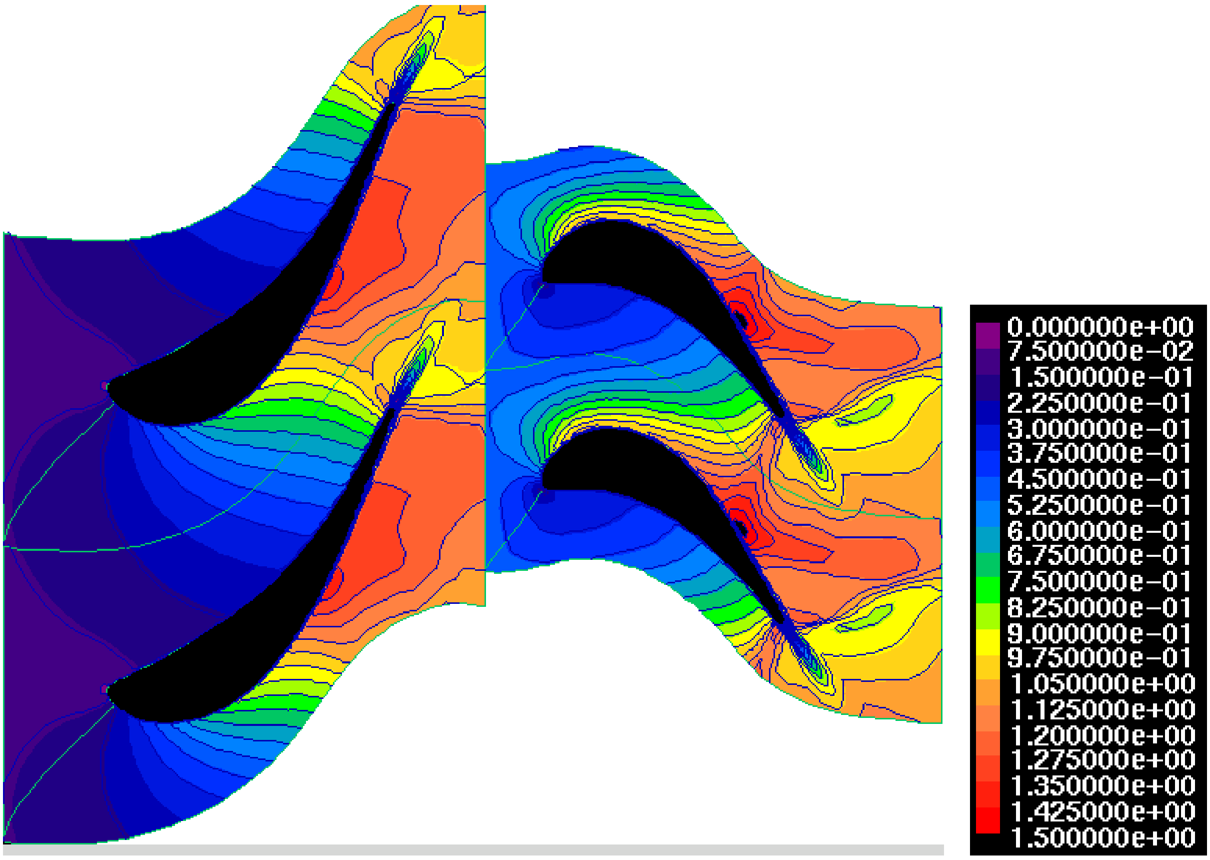

$p_{0\ tot}$ = 4.0bar, $t_{0\ tot}$ = 181.3°C, n = 11550rpm, (simulation job No. 13) **Mach No.**

Job No.	13

Boundary Conditions		Output	
$p_{0\ tot}$ [Pa]	400000	n [rpm]	11550
$T_{0\ tot}$ [K]	454.4	P [kW]	2646
$p_{2\ stat}$ [Pa]	100000	m [kg/s]	21.0

TTM-Stage Parameters			
π Pressure Ratio (total to static)			4.00
η Stage efficiency (total to static)			0.87
ψ Loading factor $-\Delta h/u^2$			1.52
φ Flow factor c_{ax}/u			0.57
R_{kin} Reaction [%]			40.0
		Vane	Blade
Turning angle [°]		70	104
Exit swirl [°]		70	-19
Exit Mach number		1.11	0.49
Reynolds number		2.76E+06	1.77E+06
Zweifel´s Coefficient		0.70	0.92
Aspect ratio (true chord)		0.70	1.25
Pitch-to-chord ratio		0.76	0.74
Trailing Edge Blockage [%]		6.9	9.4
Clearance/span [%]			0.72
Airfoil count		24	36
True chord [mm]	s [mm]	78.9	55.9
Pitch [mm]	t [mm]	60.0	41.6
Axial chord [mm]	b_{ax} [mm]	56.1	46.8
Airfoil hight [mm]	h [mm]	55.2	69.8
Trailing edge thickness	d [mm]	1.65	1.94
Throat opening	a [mm]	22.3	18.8

Vane In	r [m]	ρ [kg/m³]	c_{ax} [m/s]	c_u [m/s]	c_r [m/s]	p [Pa]	T [K]
	0.2346876	3.0374389	59.50496	0	0	394580	452.63233
	c_{abs} [m/s]	α [°]	a [m/s]	M_{abs}		p_{tot} [Pa]	T_{tot} [K]
	59.50496	90.00	426.45946	0.1395325		399984	454.4
Vane-Out	r [m]	ρ [kg/m³]	c_{ax} [m/s]	c_u [m/s]	c_r [m/s]	p [Pa]	T [K]
	0.2290334	1.6942421	148.36646	398.88779	17.925966	178081.22	366.23576
	c_{abs} [m/s]	α [°]	a [m/s]	M_{abs}		p_{tot} [Pa]	T_{tot} [K]
	425.96411	20.40	383.60595	1.110421		385187	456.6
	M_{is}	T_{is} [K]	ρ_{is} [kg/m³]	c_{is} [m/s]	μ_{is} [Ns/m²]	Re	Zweiffel´s C.
	1.1404068	360.60061	1.7207183	434.0882	2.137E-05	2757859	0.70

Blade In	r [m]	ρ [kg/m³]	c_{ax} [m/s]	c_u [m/s]	c_r [m/s]	p [Pa]	T [K]
	0.2289003	1.697107	145.53089	395.22392	17.629015	178085.57	365.62645
	c_{abs} [m/s]	α [°]	a [m/s]	M_{abs}		p_{tot} [Pa]	T_{tot} [K]
	421.53525	20.21	383.28672	1.0997909		380138	454.1
	w_{rel} [m/s]	β [°]	u_1 [m/s]	M_{rel}			
	188.41581	50.88	276.85798	0.4915793			
Blade-Out	r [m]	ρ [kg/m³]	c_{ax} [m/s]	c_u [m/s]	c_r [m/s]	p [Pa]	T [K]
	0.2384778	1.101088	163.72779	-57.238724	18.860408	99941	316.25669
	c_{abs} [m/s]	α [°]	a [m/s]	M_{abs}		p_{tot} [Pa]	T_{tot} [K]
	174.46712	109.27	356.47151	0.489428		117727	331.4
	w_{rel} [m/s]	β [°]	u_2 [m/s]	M_{rel}			
	382.95918	154.66	288.4421	1.0743052			
	M_{is}	T_{is} [K]	ρ_{is} [kg/m³]	c_{is} [m/s]	μ_{is} [Ns/m²]	Re	Zweiffel´s C.
	1.5244259	309.99605	1.1233255	538.00878	1.908E-05	1770340	0.92

Fig. 42 Peak Load - 11550rpm in Mach No. and evaluation of Quasi 3D Navier Stokes simulation job No. 13

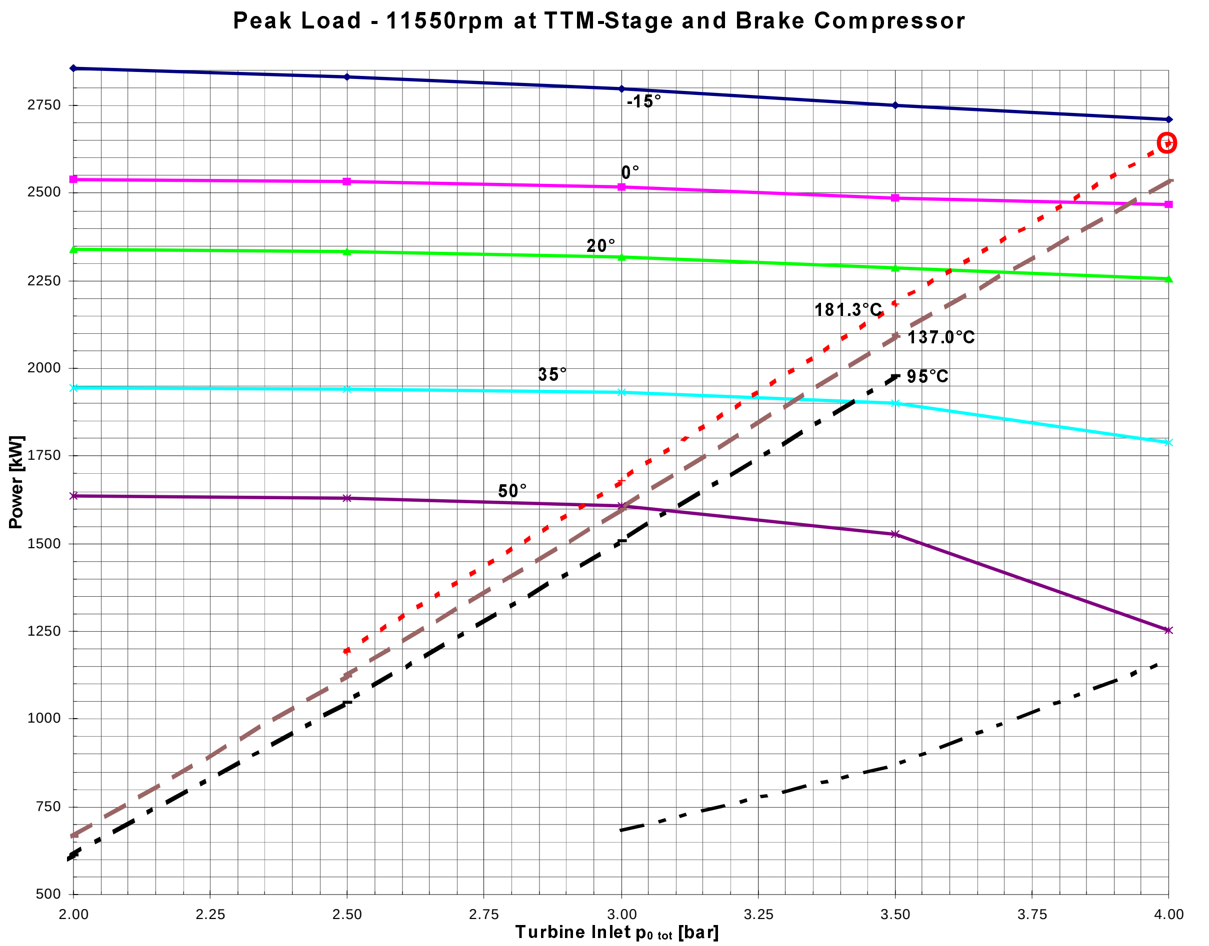

Parameter = f ($p_{0\,tot}$ [bar] , $T_{0\,tot}$ [K])				Compressor Station TTM :							
P [kW]	368	410	454	m_{CS} [kg/s]	368	410	454	t_{CS} [°C]	368	410	454
2.0	613	666		2.0	8.2	7.3		2.0	58	113	
2.5	1049	1124	1190	2.5	8.8	7.7	6.6	2.5	33	94	171
3.0	1509	1598	1678	3.0	10.0	8.7	7.5	3.0	9	70	148
3.5	1980	2090	2185	3.5	10.8	9.1	7.6	3.5	-11	51	138
4.0		2534	2646	4.0		10.4	8.9	4.0		37	118

Test Turbine TTM-stage :											
m[kg/s]	368	410	454	β_1 [°]	368	410	454	α_2 [°]	368	410	454
2.0	11.6	11.0		2.0	75	68		2.0	51	47	
2.5	14.6	13.8	13.1	2.5	63	58	53	2.5	35	30	24
3.0	17.5	16.6	15.7	3.0	61	55	51	3.0	16	10	4
3.5	20.4	19.3	18.4	3.5	60	55	51	3.5	0	-6	-12
4.0		22.1	21.0	4.0		55	51	4.0		-14	-19
t_2 [°C]	368	410	454	M_{1abs}	368	410	454	M_{2rel}	368	410	454
2.0	33	69		2.0	0.92	0.92		2.0	0.57	0.57	
2.5	16	50	85	2.5	1.04	1.05	1.06	2.5	0.70	0.70	0.70
3.0	3	35	69	3.0	1.08	1.10	1.11	3.0	0.84	0.84	0.84
3.5	-7	23	56	3.5	1.08	1.10	1.11	3.5	0.98	0.97	0.97
4.0		12	43	4.0		1.10	1.11	4.0		1.07	1.07

GHH Brake Compressor :											
α_{Drall} [°]	368	410	454	m_{GHH} [kg/s]	368	410	454	t_{GHH} [°C]	368	410	454
2.0	71	71		2.0	3.4	3.7		2.0	183	183	
2.5	66	65	64	2.5	5.8	6.1	6.5	2.5	189	190	191
3.0	54	50	47	3.0	7.5	7.9	8.2	3.0	209	211	212
3.5	32	28	24	3.5	9.6	10.3	10.8	3.5	215	213	212
4.0		-11	-14	4.0		11.7	12.1	4.0		225	228

Fig. 43 Peak Load - 11550rpm at TTM-Stage and brake compressor with test parameter check (m_{CS}, t_{CS}, β_1)

5. Commissioning

5.1 Overall performance

Several obstacles could be detected during the assembling phase, but as the test rig has to be put into commissioning in time, these things were carefully watched during first operation and respective improvement could be planned. For example the inlet casing had been pressurised with water to test its capability for operating condition pressure < 4.7bar, temperature < 185°C. During the water pressure test we noticed some deformation of the casing in a region of low stiffness, but since no essential functions and geometric constraints were changed too much, the plastic deformation in the casing side wall area near the mixer outlet was accepted since the calculation of the horizontal and vertical flanges showed plenty load capability and further plastic deformation could be excluded through the lower maximum operating pressure.

Before putting the TTM-stage into operation, the last measurements of the clearance between the rotor casing and the blades showed a perfect aligned machine, but the cold tip clearance due to manufacturing tolerances was about 0.4, even smaller than the challenging design goal of 0.5mm hot clearance.

But the machine soon was brought on successful low speed operation. The balancing procedure performed on low speeds at the test turbine shaft provided turbine shaft relative vibration below 15µm in both bearings. The brake compressor spare shaft showed some higher but still acceptable values only at machine train maximum speed, since it was already balanced in the GHH manufacturing process (compare to Fig. 44).

One very interesting fact searching for the first critical speed of the test turbine shaft was, that the radial stiffness of the turbine tilting bearings were about double of the values given by the manufacturer. So we found the first turbine bending mode at much higher speed than expected and this natural frequency is now relative sensitive to bearing inlet temperature leading to a more or less stiff front bearing (see 3.5.1).

The test rig oil supply was build up from the old back pressure turbine oil supply (1400liter oil tank with electrically driven auxiliary gear pump and oil cooler from the dismantled Technical University heating and power station see 1.1) and adapted with an additional electrically driven main centrifugal pump, some filters and valves. As the flow temperature of the water coming from the cooling station was higher than respected, the oil flow temperature into our test rig tilting pad bearings was really high at about 55°C at full load in comparison to the recommended 45°C. But since this higher oil inlet temperature seems to be just acceptable from the standpoint of our bearing recalculations we tolerated this condition, although the bearing oil inlet temperature at the brake compressor coupling bearing had to be carefully watched because of the sensitivity of the second bending brake compressor mode (especially at the coupling bearing) to high pad inlet temperature.

The oil cooler moreover showed higher pressure losses due to higher than original mass flow. But since the oil flow recommendations were fulfilled and oil supply pressure was comparable to other operation notes (Glacier suggests 0.5 to 1.0bar oil supply pressure depending upon necessary oil flow for their tilting pad bearings, Bently Nevada Corp. mentions 1.0 to 1.4bar, and GHH wishes about 1.5bar) the values were accepted too. The prescribed supply pressure of 1.5bar for the oil mass flow into the Turbine Coupling Bearing TFL could not be reached even at high flow rates, because the real through flow choked by the floating bearing throttle rings was to high also at low temperatures. However since only the recommended oil mass has to be supplied for thermal balance I would suggest to throttle this oil flow to the original value independent to bearing back pressure, since this gives more margin in the inlet pressure condition of the other bearing supplies.

As some bearing oil tended to leak through the non contacting bearing seals especially at the Turbine Front Bearing TLL above 6000rpm, the oil return piping was set to a depression of about 300mmWS. This is a common used method in oil supply systems although the high suction volume of the little blower may be fed by some filtered bypass air to lower this difference pressure to commonly used 100mmWS. However the cavity between the gasket on the turbine disk flange and the adjacent inner TLL gasket was not buffered enough with cold air to ensure full blockage against hot leakage air. It looks like that some amount of hot air was sucked through the two above mentioned seals into the TLL bearing and the turbine return oil piping increasing the turbine return oil temperature there. Since the difference between this temperature and the turbine bearing oil inlet temperature in conjunction to the respective mass flow is used to calculate the mechanical efficiency of the test turbine this situation has to be treated some more carefully. I would suggest to check the cavity pressure against the leakage flow pressure respectively the flow direction under these seals with a difference pressure measurement installed between the cavity air supply and the leakage outlet collector 1 (see Fig. 7).

However dropping this early life failures the general operation of the test rig under several different load conditions proofed to be on good performance and easy handling. Estimated from different first measurements the characteristics of the three machines matched at the calculated points and the optimal operation conditions of the TTM-stage are within the operational capability of the brake compressor and the TTM compressor station.

The following Fig. 44 shows an example of test rig operation near part load 2 condition (see 4.2.3.2) :

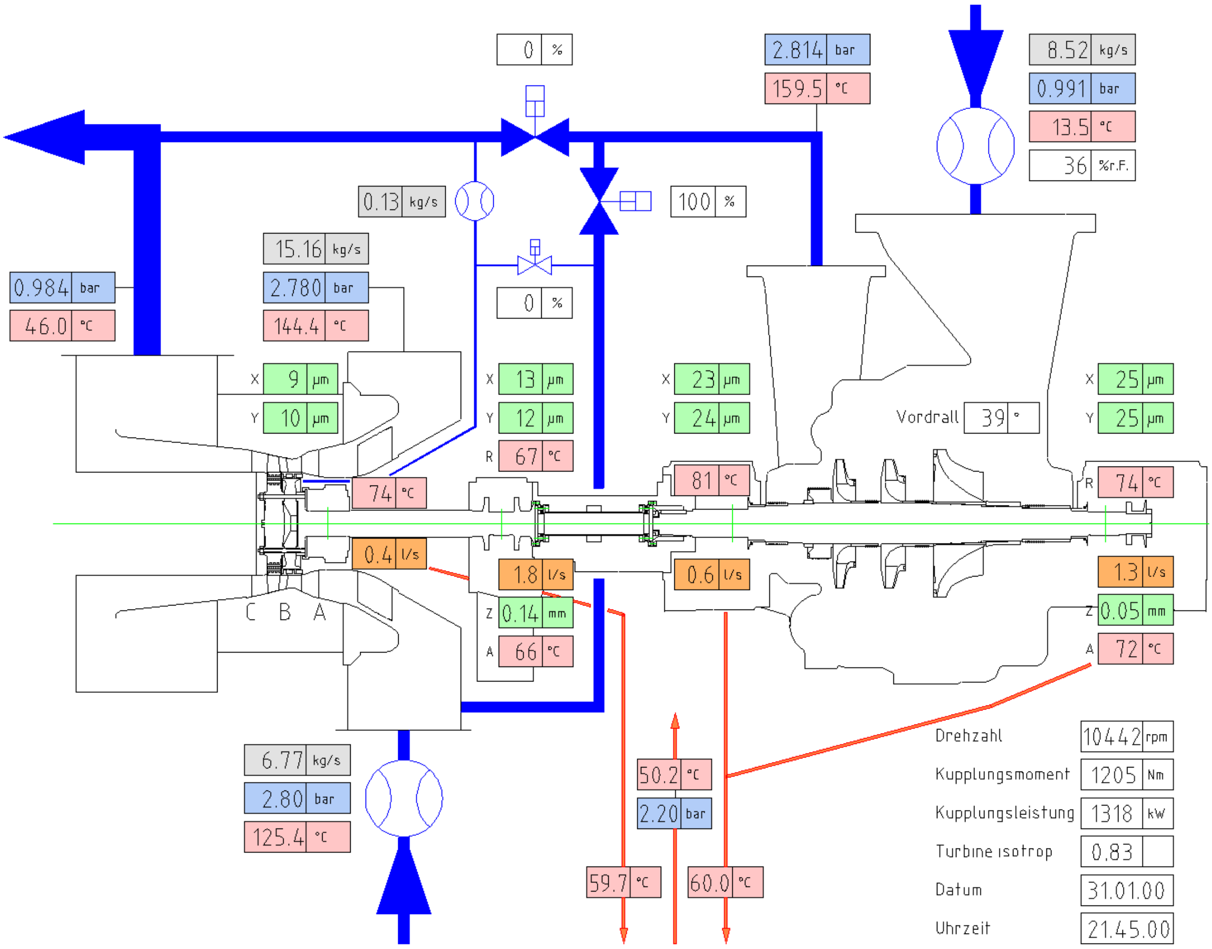

Fig. 44 Transonic test-turbine facility with conventional measurement flow scheme and operational data

The conventional measurement data provided by Mr. Seyr for this figure was corrected on two evident measurement problems. The turbine inlet temperature will not be so far from the thermodynamic mixing temperature of the two mixing chamber inlet flows if the external heat transfer is less than 10% compared to the generated coupling power. More detailed inlet temperature measurement in plane A would be best. The turbine oil discharge temperature seems to be falsified through additional hot air leakage flow (see above) and was set to a comparable value concerning the GHH brake compressor oil discharge.

The operational data in Fig. 44 shows relative good agreement to the models used for design and optimisation, although the following interesting differences could be found :

(1) The GHH brake compressor at equal inlet conditions (0.991bar, 13.5°C, except humidity 36 versus 60%, R_{model} = 289.82 J/kgK), speed and comparable mass flow (+1%) shows better performance in terms of necessary coupling torque and power (-7.3%). To confirm this effect I would suggest to calibrated the brake compressor venturi mass flow measurement and the Bently TORXIMITOR especially on temperature drift of torque measurement in the coupling casing first. A remaining difference after this measures perhaps could become clear in the difference of the actual direct driven TTM configuration in comparison to the assembly at the refinery OMV- Schwechat, where a planetary gear drive was between the electrical motor and the compressor. It is likely that the commissioning data points from Schwechat were measured on the electric motor drive perhaps corrected with motor efficiency and not gear drive mechanical efficiency. This better mechanical efficiency leads to lower brake compressor exit temperatures than calculated in the design models providing a little bit more margin in higher TTM compressor station inlet temperatures at the same turbine inlet testing conditions.

(2) The turbine isotropic efficiency in Fig. 44 is in the designed range but suffers from the poor inlet temperature value and the unclear mechanical efficiency of the turbine shaft. Further on the isotropic turbine efficiency is calculated from total turbine inlet to total diffuser outlet conditions whereas all Navier Stokes simulated values depend on total turbine inlet to static stage outlet values.

Further urgent measures on the conventional measurement system independent on more detailed test stage data at measurement plane A to D for improvement of the test stage thermodynamic balancing will be the replacement of the oil supply pressure transducer and two additional measurement points for total pressure and temperature in the last 90° bend of the exhaust line in front of the exhaust tower respectively the suction blower. First they will show the real exhaust line temperature load in brake compressor throttling mode and second it will be necessary for the suction blower operation support in the conventional measurement flow scheme.

5.2 Turbine inlet distribution

Another difficulty was also early discovered in the assembling period on the mixer concept performance. Proceeding the assembling process with care we first measured the flow distortion from the compressor station outlet of the mixer at open casing condition and we found some severe flow distortion due to simple CFD modelling problems at to small models. The old models did not catch a severe flow separation due to static pressure differences between air stream lines coming from the compressor station supply pipe and having a rather long way between the GHH-nozzle plates and some having only a short distance. As the air took the line of least resistance the equally designed mixer output was not reality. Knowing about this problem in the commissioning phase CFD calculations (about 30 different models !) were performed to force a more equal distribution through guiding the air into this mixer section with the longer distance between the nozzle plates. Looking at the measured temperature inlet profile the flow distribution was greatly improved although it is not best.

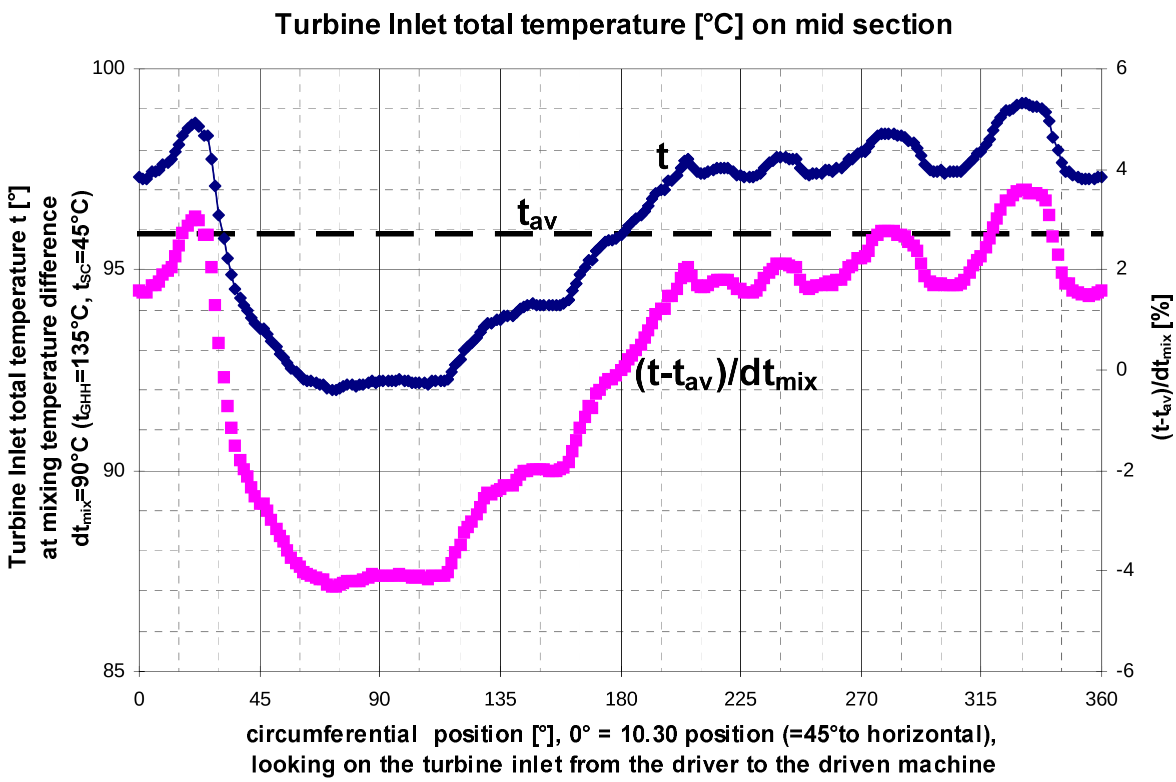

Fig. 45 Mixer performance measurement at turbine inlet measurement plane A

Looking at Fig. 45 still considerable turbine inlet temperature distortion can be detected. Although this result is far better than first measurement results the influence of the colder TTM compressor station flow overhang in the right upper casing part still can be seen from 30 to 180°, because the mixer outlet of this flow remains some preference on the lower and shorter stream lines. As the brake compressor mixer flow tends to do the opposite e.g. finds its line of least resistance on the upper mixer part (against the tandem cascade) this effect is strengthen.

However since the connection piece between the TTM compressor station supply pipe and the turbine inlet casing has less tolerance against further adaptations than the brake compressor inlet I would suggest to correct the second one next. Furthermore adaptations on the brake compressors mixer inlet first could be designed as a simple cover reducing mass flow on the upper mixer inlet area and second could be mounted only disconnecting the 90°bend connection of the brake compressor overflow pipe to the turbine inlet casing.

But as the resultant flow pattern at least not only depends on the above mentioned effects but also on the fact that the half symmetry in the mixer modelling is not fully confirmed through measurement results it is hard to check the different effects. Separating the difference in flow symmetry between the compressor station mixer outlet and the brake compressor flow pressed through the nozzle plates is very difficult since we could not measure the second one at all and there is some distance on different 3D stream lines for the mixed air in between the mixing zone and the inlet measurement plane A shortly behind the turbine inlet (see Fig. 21).

So looking for perfect results I would estimate that 80% improvement was already reached with 20% expense and for further improvements this will be vice versa, but as the design goal for equalising maximum temperature difference is often diminished at less demanding mixer inlet conditions, the resulting temperature distortion will also be better.

Finally checking the turbine inlet also for pressure distribution we found a perfect flow pattern in the mid section of measurement plane A because of the high flow acceleration and the equalising effect of the guide vanes.

5.3 TTM-Stage case of damage

After about 30 starts and about 20 conventional measurements without any bigger operational problem we concentrated on the above mentioned measurements of the inlet temperature distribution at less measurement time conditions first for better thermodynamic balancing and second for some commissioning results on the Brite Euram DITTUS project. Except for one alarm event through a vibration trip on 10350rpm at transient accelerating conditions on 07.12.99 no problems had been detected at the test rig operation. Since the observation of the bladed rotor disk after this event nearly showed any indication for a rub testing was carried on without greater care to the very small clearance between rotor and casing.

On relatively hot tests planned for a series of inlet distribution measurements with increasing temperature difference between the main two turbine feeding air streams we first detected some problems with the turbine inlet measurement system (see3.3.1). Measuring the current of the stepping motor supply we found high torque load on the guide vane casing. From further cold measurements of the clearance between the rotor and the guide vane casing and the different thermal behaviour between them at the auxiliary guide vane casing teflon bearing measured with a thermographic system it was first concluded that different thermal expansion had blocked the guide vane casing leading to high overtorque at the servo motor.

Some days later on a rotor casing inspection during disassembling of the inner diffuser zylinder for application of some pressure tappings the following damages were detected :

(1) Comparing the rubbed surface with a time distance on a watch the rotor blades had rubbed against the rotor casing (maximum depth about 0.3mm) from about 5 to 8 o´clock looking from the drive to the clockwise driven machine.
(2) In addition the absolute failure of the auxiliary teflon bearing enabled an eccentric position of the guide vane to the rotor casing so that the free cut guide vane trailing edges rubbed at the rotor casing. The most severe damaged guide vanes were also found in the 5 to 8 o´clock region with respect to the start position of the guide vane casing.
(3) Later on the disassembling process for this first revision we detected some damage of the tandem cascade fixing due to considerable elastic movement of the turbine inlet casing side walls under load.

Since the turbine bearings were in good shape and with them all respective seals between rotor and inner casing especially the seal under the guide vanes it could be shown that the rotor and the guide vane casing had stayed on their design position. Further measurements confirmed this theory, because the shaft alignment of the turbine shaft in the test turbine inlet casing respectively Front Turbine Bearing and the Turbine Coupling Bearing was unchanged as also the brake compressor has stayed in alignment to the test turbine assembly.

As the diffuser collector has no fully centerline support and is only mounted to the turbine inlet casing through four connection struts, in general the exhaust line forces have to be kept away from this structure. But the first solution for disconnecting the diffuser casing from the exhaust line movements through a thick screwed rubber element seems to be to rigid. So the deflection of this casing respectively the struts carrying the centerline support of the rotor casing may have moved the rotor casing against the rotor blades and the guide vane casing.

The elastic deformation of the inlet casing acts in a comparable way of displacing the rotor casing but this damage mechanism seems not so probably, because this implements also movements of the guide vane casing against the rotor which is not confirmed through the good seal condition.

The high torque load of the servo against a choking guide vane casing may have also resulted in a similar way but could also not be the initial cause of damage.

However to avoid such troublesome problems in future the following corrections have been performed :

(1) Opening up the TTM-stage clearance between the rotor casing and the rotor (Fig. 8 and 3.4.1) respectively the free cut guide vane trailing edges to gain some more margin.
(2) Separation of the turbine diffuser collector from the exhaust line forces and / or moments through a horizontal lubricated sliding plane (system Mr. Kulhanek) and removal of all screws in this connection flange.
Additional elastic centering of turbine diffuser collector on its consoles.
(3) Tie bolts in the turbine inlet casing preventing against asymmetric elastic deformation of this structure under pressure load (Fig. 21).
(4) Servo current display in the control room with additional fuse against overload.

As it was difficult to define the exact damage mechanism or even the probable combination of some above mentioned effects without any further measurements all of this remedial measures were taken to prevent future operation problems.

Looking at the vibration records afterwards once more we could only detect one small amplitude increase for about 6 micrometers during 1.5min at two test runs. But because the peak amplitude was beyond the 20 micrometers alarm level this very small peaks were not detected. One conclusion for further operation will be to minimise alarm level at best balanced shafts and this will for example lead to better balancing of the GHH break compressor shaft . Second the machine condition monitoring must be performed with more diagrams to find such problems earlier although amplitude effects are low.

To prevent the test rig from further damage it will be very advantageous to have better organised test schedules with calculated test points reached under certain transient gradients with definite personnel for the different test tasks under the leadership of a nominated test leader and coordinator. This way will furthermore help to protect the operating personal against injury due to risky actions since also secure systems are rarely foolproof and exploding time schedules should be handled with better methods.

.

1. Conclusion

(1) A great environment already prepared for building up this test facility at the Institute of Thermal Turbomachinery and Machine Dynamics of Graz University of Technology, the industrial present of the GHH brake compressor from the OMV refinery in Schwechat and the institutes financial resources over several years with additional financial resources in national (FWF-S68-01, Start Project Y57) and international (Brite Euram DITTUS) projects enabled this unique facility.

(2) For the intended good optical access to the rotor-stator passage of the TTM-Stage starting from the vane exit to the diffuser inlet two types of optical window inserts had been manufactured for the upper half of the TTM-Stage turbine casing : A long narrow one for Laser Doppler Velocimetry and a large one for Particle Image Velocimetry. A similar PIV window is used in a 1:1 test section model at DANTEC laboratory for optimization and calibration of optical access through the curved window with PIV instruments. Optical access was confirmed and for application of the light sheet between the rotor and the stator a circumferential offset periscope probe will be a solution. The warm clearances will be at 1% blade height for further operation of the TTM-Stage even though the big windows always will be a weak point above a transonic test turbine stage and will have to be carefully used on remote control.

(3) The TTM-Stage clearances had to be corrected since the rotor blade and free cut guide vane trailing edge initially had a to small air gap against the rotor casing. A deflection of the diffuser collector casing respectively the struts carrying the thermal centering of the rotor casing may have moved the rotor casing against the rotor blades and the guide vane casing thus leading to at rotor rub and damage on some free cut vane trailing edges after disabling the auxiliary PTFE-bronze bearing. To avoid such troublesome problems in future the TTM-Stage clearance between the rotor casing and the rotor had to be opened up, the turbine diffuser collector was separated from the exhaust line forces and moments through a horizontal sliding plane and some tie bolts were mounted in the turbine inlet casing for more stiffness against pressure load deformation.

(4) However dropping this early life failures the general operation of the test rig under several different load conditions proofed to be on good performance and easy handling, although due to cost reasons at this machine scale the hole test rig was designed and nearly exclusively build up with TTM personnel. Estimated from different first measurements during commissioning the characteristics of the three machines nearly matched at the calculated points and the optimal operation conditions of the TTM-Stage are within the operational capability of the brake compressor and the TTM compressor station.

(5) Besides the geometrical boundary conditions given in Fig. 11 in general all test stages have to be verified on the test rig operational capabilities (see 2.2). It has to be checked whether it is possible to use the brake compressor air for multiplying mass flow or if pressure independent throttling mode has to be applied. This could be necessary if the inlet pressure for the test stage is higher than 4.2bar at maximum continuous speed 11550rpm or if higher pressure than practical brake compressor exit at another limited machine train speed has to be used regarding test stage flow similarity conditions.

(6) Examining the test rig on the inlet pressure distribution at the test stage inlet we found a perfect flow pattern in the mid section of measurement plane A because of the high flow acceleration and the equalizing effect of the guide vanes. Looking at the measured temperature inlet profile the flow distribution was greatly improved although it is not best at about +/-4% deviation from the average inlet temperature referring to the mixing temperature difference between TTM compressor station and brake compressor inlet flow.

(7) Looking at our own designed TTM-Stage test inserts in more detail the last years showed a stressed design process in building up a highly loaded “measurement machine“ for optical access to transonic shock activity in rotor stator interaction in parallel to the development of the CFD tools necessary for suitable aerodynamic design. Nevertheless it can be shown that the TTM-Stage is comparable to other transonic turbines [5] in loading and flow coefficients although the design pressure ratio is not so high and the blading design is rather simple. The low reaction design in a real engine could be good for low blade metal temperature, low stage exit mach number and low root stagger angle for reduced rotor disk fixing stress and ease of platform fit. To get some better blade hub flow acceleration a higher pressure ratio would help moreover this low reaction design will have higher limit loading.

(8) Although the TTM-Stage parameters are not that aggressive any more the test facility concept itself is still consistent with the mission given in the introduction which stated the indication of the need for higher loading coefficients with considerably higher Mach number level. Looking at the two highly loaded industrial stages soon be tested in our Transonic Test-Turbine Facility our efforts thanks to God´s wonderful help seemed to be successful in having international turbomachinery industry in our test hall at Graz University of Technology.

7. References

[1] **Farmer R., 1997** "Uprating the PGT10 to 12 MW for mechanical drive, 50/60-Hz power“, GAS TURBINE WORLD, September-October 1997

[2] **Pirker H.P., Jericha H., Zhuber-Okrog G., 1995**, „Auslegung und Betriebsverhalten einer Verdichteranlage für die Luftversorgung wissenschaftlicher Versuchseinrichtungen“, VDI Berichte Nr.1208, pp. 331-347

[3] **Low Speed Research Turbine** in GE Aircraft Engines “The Aerodynamics Research Laboratory“

[4] **Amecke J. and F. Kost, 1993,** ***3.2 Rotating Annular Cascade***; in Hirsch, Ch. (Ed.); “Advanced Methods for Cascade Testing“, AGARD AG 328

[5] **Sell M., Treiber M., Althaus P. and Gyarmathy, 1998,** “The Design and Construction of a new Test Stand for the study of basic Turbine Flow Phenomena, Turbomachinery Laboratory“, ETH Swiss Federal Institute of Technology, Zürich , CH

[6] **Dénos,R., 1996,** "Etude aerodynamique et thermique de l’ecoulement instationaire dans un rotor de turbine transonique“, These pour l’obtention du Grade de Docteur These de l’Université de Poitiers

[7] **Vlasic, E.P., Girgis, S., Moustapha, S.H., 1996** "The Design and Performance of a High Work Research Turbine“ ASME Vol. 118

[8] **Wernet, M. P., 2000** "Development of digital particle imaging velocimetry for use in turbomachinery", Experiments in Fluids 28 (2000) 97-115 c Springer-Verlag 2000

[9] **Jones G. J., Martin F. A.,** "Geometry Effects in Tilting-Pad Journal Bearings", AT449/80, Paper presented at the 33rd Annual Meeting in Deerhorn, Michigan, April 1978 and reprinted by kind permission of the American Society of Lubrication Engineers by the Glacier Metal Company Limited, Wembley, Middlesex, England

[10] **Benvenuti E., 1997,** "Design and Test of a New Axial Compressor for the Nuovo Pignone Heavy-Duty Gas Turbines", Journal of Engineering for Gas Turbines and Power, July 1997 Vol. 119 / 633

[11] **Bas P., Mooren A., 1998,** "Optimization of a Mixing Chamber and Intake of the Test Turbine at the Institute of Thermal Turbomachinery and Machine Dynamics“ TME/1997-1998/EE ER, K.U.Leuven, Dept. Werktuigkunde, Afdeling TME, Celestijnenlaan 300A, B-3001 Heverlee (Belgium)

[12] **Traupel, W., 1982,** „Thermische Turbomaschinen“, Band I+II, 3.Auflage, Springer Verlag

[13] **Wilson, D.G., 1987** "New guidelines for the preliminary design and performance prediction of axial-flow turbines“ Proc Instn Mech Engrs Vol 201 No A4

[14] **Paßrucker, H., Sanz, W., Jericha, H., 1998,** "Numerical Calculation of Three-Dimensional Euler Flow Through a Transonic Test Turbine Stage“ ASME Stockholm

[15] **Gehrer, A., 1999,** "Entwicklung eines 3D-Navier-Stokes Codes zur numerischen Berechnung der Turbomaschinenströmung", Doctoral Thesis at the Institute of Thermal Turbomachinery and Machine Dynamics, Technical University of Graz

[16] **Arts, T., Lambert de Rouvroit, M., Rutherford, A. W., 1990,** "Aero-thermal Investigation of a Highly Loaded Transonic Linear Turbine Guide Vane Cascade“, Technical Note 174, von Karman Institute for Fluid Dynamics, Belgium

[17] **Sanz, W., Gehrer, A., Paßrucker, H. 1995,** "An Implicit TVD Upwind Relaxation Scheme for the Unsteady 2D-Euler-Equations", ASME Paper 95-CTP-71

[18] **Erhard J., Gehrer A., 2000,** " Design and Construction of a Transonic Test-Turbine Facility ", ASME Munich 2000

[19] **Spalart, P. R., Allmaras, S. R., 1994**, "A One Equation Turbulence Model for Aerodynamic Flows“, La Recherché Aerospatiale, No.1, pp 5-21

[20] **Jameson, A., Yoon, S.,** 1986, "Multigrid Solution of the Euler Equations Using Implicit Schemes", AIAA Journal, Vol. 24, No. 11, Nov. 1986, p. 1737-1743

[21] **Siikonen, T.,** 1991, "A Three-Dimensional Multigrid Algorithm for the Euler and the Thin-Layer Navier-Stokes Equations", Helsinki University of Technology, Faculty of Mechanical Engineering, Report No. A-12, Series A

[22] **Roe, P. L**. 1981, "Approximate Riemann Solvers, Parameter Vectors, and Differencing schemes", Journal of Computational Physics 43. 357 - 372

[23] **Giles, M.B.,** 1990, „Non-reflecting Boundary Conditions for Euler Equation Calculations“, AIAA Journal, Vol.28, No.12, 1990

[24] **Pieringer, P., 1999,** "Implementierung eines nichtreflektierenden Randalgorithmus in ein finite Volumen basiertes Strömungsrechenprogramm", Diploma Thesis at the Institute of Thermal Turbomachinery and Machine Dynamics, Technical University of Graz

[25] **Gehrer A., Paßrucker H., Jericha H., Lang J., 1996,** "Blade design and Grid generation for Computational Fluid Dynamics with Bézier-curves and Bézier-surfaces“, European Conference - Antwerpen - March ’97, Paper No. 54

8. Appendices

8.1 Machine train dynamics

8.1.1 Test rig tilting pad bearings

Turbine Front Radial Bearing TLL

Input		
TFL-Load	1660	N
Rotational Speed	1204.2772	rad/s
Bearing Diam. $d_b=2r_b$	100.0110	mm
Bearing Length	50.0000	mm
Bearing Clear. $c_r' = r_b-r$	0.0842	mm
Preload $m=1-c_r'/c_r$	0.5427	-
Pad Clearence $c_r=r_p-r$	0.1842	mm
Bearing Radius $r_b=d_b/2$	50.0055	mm
Journal Radius $r=r_b-c_r'$	49.9213	mm
Pad Radius $r_p=r+c_r$	50.1055	mm
Number of Segments	5	-
Arc	62	°
Tilting Pad Mode	1	-
$\alpha_1=$	-31	°
T-inlet =	60	°C
Tilting Start Angle =	0	°

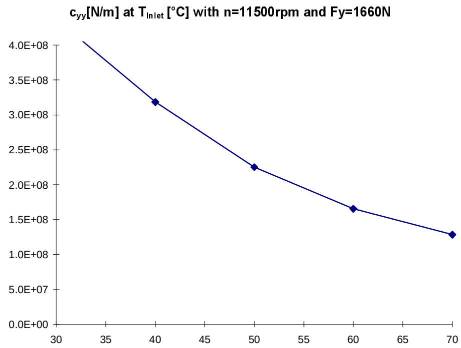

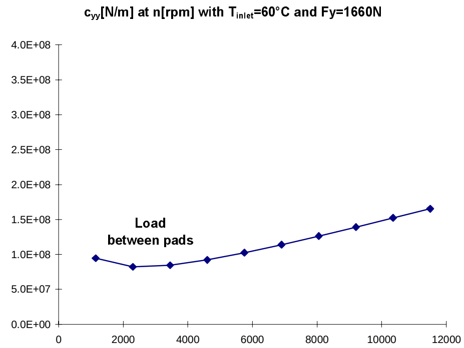

Variation of pad inlet temperature T_{Inlet} [°C]

T_{inlet} [°C]	n [rpm]	w_x [µm]	w_y [µm]	F_x [N]	F_y [N]	Q_r [kW]	p_{av} [bar]	T_{av} [°C]	η_{av} [mPas]	c_{xx} [N/m]	c_{xy} [N/m]	c_{yx} [N/m]	c_{yy} [N/m]	D_{xx} [Ns/m]	D_{xy} [Ns/m]	D_{yx} [Ns/m]	D_{yy} [Ns/m]
30	**11500**			0.0	**1660.0**								**4.37E+08**				
40	**11500**	0.0	**5.3**	0.0	**1660.0**	18.8	15.5	47.6	30.9	3.15E+08	5.00E+05	-4.45E+05	**3.18E+08**	1.80E+05	7.27E+04	-7.29E+04	1.82E+05
50	**11500**	0.0	**7.5**	0.0	**1660.0**	13.5	10.4	55.4	22.5	2.20E+08	3.54E+05	-2.50E+05	**2.25E+08**	1.24E+05	5.23E+04	-5.26E+04	1.26E+05
60	**11500**	0.0	**10.5**	0.0	**1660.0**	9.8	7.3	63.9	16.4	1.58E+08	3.59E+05	-1.62E+05	**1.65E+08**	8.73E+04	3.80E+04	-3.86E+04	9.02E+04
70	**11500**	0.0	**14.1**	0.0	**1660.0**	7.3	5.4	72.9	12.2	1.17E+08	1.34E+05	-1.42E+05	**1.28E+08**	6.40E+04	2.83E+04	-2.93E+04	6.81E+04

Variation of shaft speed n [rpm]

T_{inlet} [°C]	n [rpm]	w_x [µm]	w_y [µm]	F_x [N]	F_y [N]	Q_r [kW]	p_{av} [bar]	T_{av} [°C]	η_{av} [mPas]	c_{xx} [N/m]	c_{xy} [N/m]	c_{yx} [N/m]	c_{yy} [N/m]	D_{xx} [Ns/m]	D_{xy} [Ns/m]	D_{yx} [Ns/m]	D_{yy} [Ns/m]
60	**11500**	0.0	**10.5**	0.0	**1660.0**	9.8	7.3	63.9	16.4	1.57E+08	1.87E+05	-1.73E+05	**1.65E+08**	8.74E+04	3.80E+04	-3.86E+04	9.03E+04
60	**10350**	0.0	**11.6**	0.0	**1660.0**	8.0	6.6	63.5	16.6	1.43E+08	1.69E+05	-1.56E+05	**1.52E+08**	8.80E+04	3.84E+04	-3.93E+04	9.16E+04
60	**9200**	0.0	**12.8**	0.0	**1660.0**	6.4	5.9	63.2	16.8	1.29E+08	1.54E+05	-1.40E+05	**1.39E+08**	8.88E+04	3.89E+04	-4.00E+04	9.34E+04
60	**8050**	0.0	**14.4**	0.0	**1660.0**	5.0	5.3	62.9	17.0	1.14E+08	1.35E+05	-1.23E+05	**1.26E+08**	8.97E+04	3.95E+04	-4.09E+04	9.58E+04
60	**6900**	0.0	**16.4**	0.0	**1660.0**	3.7	4.6	62.5	17.3	9.99E+07	1.12E+05	-1.03E+05	**1.14E+08**	9.09E+04	4.01E+04	-4.20E+04	9.91E+04
60	**5750**	0.0	**19.1**	0.0	**1660.0**	2.6	4.0	62.1	17.5	8.53E+07	9.62E+04	-9.77E+04	**1.02E+08**	9.24E+04	4.08E+04	-4.37E+04	1.04E+05
60	**4600**	0.0	**22.8**	0.0	**1660.0**	1.7	3.3	61.8	17.7	7.06E+07	8.28E+04	-8.12E+04	**9.21E+07**	9.46E+04	4.17E+04	-4.62E+04	1.13E+05
60	**3450**	0.0	**28.1**	0.0	**1660.0**	1.0	2.7	61.4	17.9	5.57E+07	7.22E+04	-6.36E+04	**8.44E+07**	9.79E+04	4.30E+04	-5.09E+04	1.29E+05
60	**2300**	0.0	**36.0**	0.0	**1660.0**	0.5	2.2	61.1	18.1	4.04E+07	6.33E+04	-4.80E+04	**8.22E+07**	1.04E+05	4.50E+04	-6.13E+04	1.67E+05
60	**1150**	-0.1	**48.9**	0.0	**1660.0**	0.1	1.6	60.8	18.4	2.35E+07	6.88E+04	-4.10E+04	**9.45E+07**	1.16E+05	4.89E+04	-9.37E+04	3.06E+05

Turbine Coupling Radial Bearing TFL

Input		
TFL-Load	140	N
Rotational Speed	1204.2772	rad/s
Bearing Diam. $d_b=2r_b$	90.0110	mm
Bearing Length	45.0000	mm
Bearing Clear. $c_r' = r_b-r$	0.0743	mm
Preload $m=1-c_r'/c_r$	0.5739	-
Pad Clearence $c_r=r_p-r$	0.1743	mm
Bearing Radius $r_b=d_b/2$	45.0055	mm
Journal Radius $r=r_b-c_r'$	44.9313	mm
Pad Radius $r_p=r+c_r$	45.1055	mm
Number of Segments	5	-
Arc	62	°
Tilting Pad Mode	1	-
$\alpha_1=$	5	°
T-inlet =	60	°C
Tilting Start Angle =	0	°

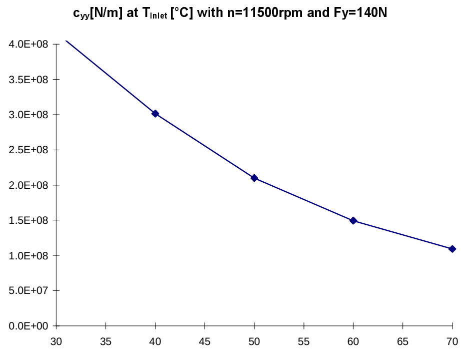

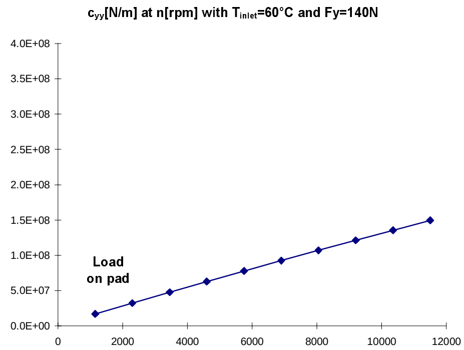

Variation of pad inlet temperature T_{Inlet} [°C]

T_{inlet} [°C]	n [rpm]	w_x [µm]	w_y [µm]	F_x [N]	F_y [N]	Q_r [kW]	p_{av} [bar]	T_{av} [°C]	η_{av} [mPas]	c_{xx} [N/m]	c_{xy} [N/m]	c_{yx} [N/m]	c_{yy} [N/m]	D_{xx} [Ns/m]	D_{xy} [Ns/m]	D_{yx} [Ns/m]	D_{yy} [Ns/m]
30	**11500**			0.0	**140.0**								**4.16E+08**				
40	**11500**	0.0	**0.5**	0.0	**140.0**	13.9	16.6	47.8	30.6	3.01E+08	4.07E+05	-4.03E+05	**3.01E+08**	1.65E+05	6.32E+04	-6.32E+04	1.65E+05
50	**11500**	0.0	**0.7**	0.0	**140.0**	10.0	11.0	55.5	22.3	2.10E+08	2.68E+05	-2.61E+05	**2.10E+08**	1.13E+05	4.54E+04	-4.54E+04	1.13E+05
60	**11500**	0.0	**0.9**	0.0	**140.0**	7.3	7.6	64.0	16.4	1.49E+08	1.78E+05	-1.76E+05	**1.49E+08**	7.97E+04	3.30E+04	-3.30E+04	7.97E+04
70	**11500**	0.0	**1.3**	0.0	**140.0**	5.4	5.5	72.9	12.2	1.09E+08	1.27E+05	-1.24E+05	**1.09E+08**	5.78E+04	2.44E+04	-2.44E+04	5.78E+04

Variation of shaft speed n [rpm]

T_{inlet} [°C]	n [rpm]	w_x [µm]	w_y [µm]	F_x [N]	F_y [N]	Q_r [kW]	p_{av} [bar]	T_{av} [°C]	η_{av} [mPas]	c_{xx} [N/m]	c_{xy} [N/m]	c_{yx} [N/m]	c_{yy} [N/m]	D_{xx} [Ns/m]	D_{xy} [Ns/m]	D_{yx} [Ns/m]	D_{yy} [Ns/m]
60	**11500**	0.0	**0.9**	0.0	**140.0**	7.3	7.6	64.0	16.4	1.49E+08	2.38E+05	-2.03E+05	**1.49E+08**	7.97E+04	3.30E+04	-3.30E+04	7.97E+04
60	**10350**	0.0	**1.0**	0.0	**140.0**	5.9	6.9	63.6	16.6	1.35E+08	1.61E+05	-1.58E+05	**1.35E+08**	8.01E+04	3.33E+04	-3.33E+04	8.02E+04
60	**9200**	0.0	**1.2**	0.0	**140.0**	4.8	6.2	63.2	16.8	1.21E+08	1.43E+05	-1.41E+05	**1.21E+08**	8.06E+04	3.37E+04	-3.37E+04	8.06E+04
60	**8050**	0.0	**1.3**	0.0	**140.0**	3.7	5.4	62.9	17.0	1.07E+08	1.25E+05	-1.23E+05	**1.07E+08**	8.10E+04	3.41E+04	-3.41E+04	8.11E+04
60	**6900**	0.0	**1.5**	0.0	**140.0**	2.7	4.6	62.5	17.3	9.23E+07	1.07E+05	-1.05E+05	**9.25E+07**	8.15E+04	3.44E+04	-3.45E+04	8.15E+04
60	**5750**	0.0	**1.8**	0.0	**140.0**	1.9	3.9	62.1	17.5	7.76E+07	8.91E+04	-8.68E+04	**7.77E+07**	8.19E+04	3.48E+04	-3.49E+04	8.20E+04
60	**4600**	0.0	**2.2**	0.0	**140.0**	1.2	3.1	61.7	17.8	6.26E+07	7.11E+04	-6.89E+04	**6.27E+07**	8.24E+04	3.53E+04	-3.53E+04	8.25E+04
60	**3450**	0.0	**3.0**	0.0	**140.0**	0.7	2.4	61.3	18.0	4.73E+07	5.33E+04	-5.11E+04	**4.76E+07**	8.29E+04	3.57E+04	-3.58E+04	8.31E+04
60	**2300**	0.0	**4.4**	0.0	**140.0**	0.3	1.6	60.9	18.3	3.19E+07	3.55E+04	-3.34E+04	**3.23E+07**	8.35E+04	3.62E+04	-3.63E+04	8.41E+04
60	**1150**	0.0	**8.6**	0.0	**140.0**	0.1	0.8	60.4	18.6	1.64E+07	1.78E+04	-1.63E+04	**1.70E+07**	8.49E+04	3.69E+04	-3.75E+04	8.72E+04

Brake Compressor Inlet Radial Bearing GFL

Input		
GLL-Load	2100	N
Rotational Speed	1204.277	rad/s
Bearing Diam. $d_b=2r_b$	89.61	mm
Bearing Length	40	mm
Bearing Clear. $c_r' = r_b-r$	0.06	mm
Preload $m=1-c_r'/c_r$	0.5	-
Pad Clearence $c_r=r_p-r$	0.12	mm
Bearing Radius $r_b=d_b/2$	44.805	mm
Journal Radius $r=r_b-c_r'$	44.745	mm
Pad Radius $r_p=r+c_r$	44.865	mm
Number of Segments	5	-
Arc	43.38	°
Tilting Pad Mode	1	-
α_1=	14.31	°
T-inlet =	60	°C
Tilting Start Angle =	0	°

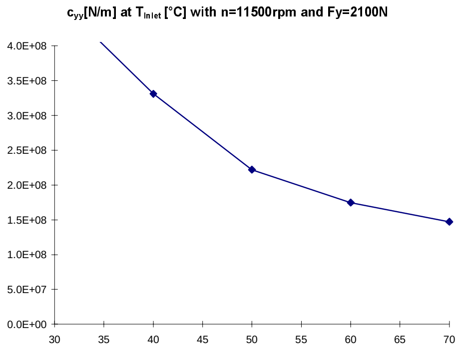

Variation of pad inlet temperature T_{Inlet} [°C]

T_{inlet} [°C]	n [rpm]	w_x [µm]	w_y [µm]	F_x [N]	F_y [N]	Q_r [kW]	p_{av} [bar]	T_{av} [°C]	η_{av} [mPas]	c_{xx} [N/m]	c_{xy} [N/m]	c_{yx} [N/m]	c_{yy} [N/m]	D_{xx} [Ns/m]	D_{xy} [Ns/m]	D_{yx} [Ns/m]	D_{yy} [Ns/m]
30	**11500**			0.0	**2100.0**								**4.70E+08**				
40	**11500**	0.0	**7.3**	0.0	**2100.0**	10.6	23.1	48.4	29.8	3.21E+08	-1.23E+08	1.26E+08	**3.31E+08**	1.20E+05	-4.77E+04	1.04E+04	1.82E+05
50	**11500**	0.0	**10.1**	0.0	**2100.0**	7.6	15.9	56.1	21.9	2.08E+08	3.40E+05	-1.64E+04	**2.22E+08**	7.36E+04	1.60E+04	-1.63E+04	7.71E+04
60	**11500**	0.0	**13.7**	0.0	**2100.0**	5.6	11.5	64.5	16.1	1.56E+08	2.08E+05	1.13E+05	**1.75E+08**	5.36E+04	1.19E+04	-1.24E+04	5.85E+04
70	**11500**	0.0	**17.7**	0.0	**2100.0**	4.3	8.9	73.5	12.0	1.23E+08	1.55E+05	1.92E+05	**1.47E+08**	4.09E+04	9.11E+03	-9.76E+03	4.72E+04

Brake Compressor Exit Radial Bearing GLL

Input		
GLL-Load	2570	N
Rotational Speed	1204.28	rad/s
Bearing Diam. $d_b=2r_b$	109.62	mm
Bearing Length	50	mm
Bearing Clear. $c_r' = r_b-r$	0.07	mm
Preload $m=1-c_r'/c_r$	0.5	-
Pad Clearence $c_r=r_p-r$	0.14	mm
Bearing Radius $r_b=d_b/2$	54.81	mm
Journal Radius $r=r_b-c_r'$	54.74	mm
Pad Radius $r_p=r+c_r$	54.88	mm
Number of Segments	5	-
Arc	43.61	°
Tilting Pad Mode	1	-
α_1=	14.195	°
T-inlet =	60	°C
Tilting Start Angle =	0	°

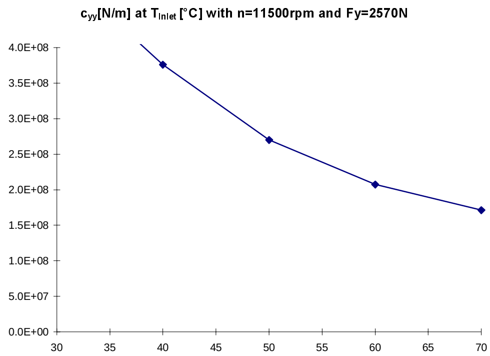

Variation of pad inlet temperature T_{Inlet} [°C]

T_{inlet} [°C]	n [rpm]	w_x [µm]	w_y [µm]	F_x [N]	F_y [N]	Q_r [kW]	p_{av} [bar]	T_{av} [°C]	η_{av} [mPas]	c_{xx} [N/m]	c_{xy} [N/m]	c_{yx} [N/m]	c_{yy} [N/m]	D_{xx} [Ns/m]	D_{xy} [Ns/m]	D_{yx} [Ns/m]
30	**11500**			0.0	**2570.0**								**5.13E+08**			
40	**11500**	0.0	**7.0**	0.0	**2570.0**	19.8	18.2	49.2	28.8	3.67E+08	4.07E+05	-4.31E+05	**3.76E+08**	2.28E+05	7.95E+04	-8.01E+04
50	**11500**	0.0	**10.1**	0.0	**2570.0**	14.4	12.0	56.7	21.4	2.56E+08	2.15E+05	-2.87E+05	**2.70E+08**	1.57E+05	5.96E+04	-6.07E+04
60	**11500**	0.0	**14.0**	0.0	**2570.0**	10.7	8.5	65.0	15.9	1.86E+08	-2.91E+05	4.54E+05	**2.07E+08**	1.12E+05	4.48E+04	-4.66E+04
70	**11500**	0.0	**18.4**	0.0	**2570.0**	8.1	6.5	73.8	11.9	1.44E+08	9.67E+04	-1.48E+05	**1.71E+08**	8.42E+04	3.44E+04	-3.70E+04

8.1.2 Shaft models

Model of Brake Compressor Shaft

Brake Comp. Shaft, C=2.07 / 1.75E08, TSJE0420 with 4.5kg

1	1				
0	25000	50	4	8	66
0	0	0	0	0	0
4	0	4.5	0	0	0
7	0.02462	0	6.15E+06	0	0
7	0.0055	0	7.53E+06	0	0
7	0.0065	0	1.87E+06	0	0
4	0	1.3	0	0	0
7	0.011	0	2.44E+06	0	0
7	0.003	0	3.20E+06	0	0
8	0.0354	47.2711	6.06E+05	0	0
4	0	7.04	0	0	0
8	0.01085	47.2711	6.06E+05	0	0
8	0.04625	52.3967	7.45E+05	0	0
8	0.0375	56.8201	8.76E+05	0	0
8	0.0935	73.2508	1.46E+06	0	0
8	0.0575	74.601	1.51E+06	0	0
4	0	0	**2.07E+08**	0	0
8	0.065	74.601	1.51E+06	0	0
8	0.0237	104.1948	2.94E+06	0	0
4	0	2.278	0	0	0
8	0.0403	104.1948	2.94E+06	0	0
8	0.047	120.8414	3.96E+06	0	0
4	0	3.148	0	0	0
8	0.043	120.8414	3.96E+06	0	0
8	0.0595	143.3835	5.58E+06	0	0
8	0.0225	153.9124	6.42E+06	0	0
4	0	1.763	0	0	0
8	0.0465	153.9124	6.42E+06	0	0
5	0.0829	24.583	0	0	0
8	0.0545	153.9124	6.42E+06	0	0
8	0.0228	154.3999	6.46E+06	0	0
5	0.1216	36.744	0	0	0
8	0.0712	154.3999	6.46E+06	0	0
8	0.023	154.8881	6.51E+06	0	0
4	0	3.669	0	0	0
8	0.054	154.8881	6.51E+06	0	0
8	0.01	188.8146	9.67E+06	0	0
8	0.0326	156.8487	6.67E+06	0	0
5	0.1225	39.006	0	0	0
8	0.0414	156.8487	6.67E+06	0	0
8	0.071	155.8669	6.59E+06	0	0
4	0	3.959	0	0	0
8	0.051	155.8669	6.59E+06	0	0
8	0.019	150.0406	6.11E+06	0	0
8	0.0506	171.9462	8.02E+06	0	0
5	0.1288	117.5	0	0	0
8	0.1224	171.9462	8.02E+06	0	0
8	0.019	147.9833	3.42E+06	0	0
8	0.0691	112.364	3.42E+06	0	0
4	0	7.71	0	0	0
8	0.0719	112.364	3.42E+06	0	0
8	0.094	91.7655	2.28E+06	0	0
4	0	5.444	0	0	0
8	0.098	91.7655	2.28E+06	0	0
8	0.0405	61.6538	1.03E+06	0	0
4	0	1.808	0	0	0
8	0.0235	61.6538	1.03E+06	0	0
8	0.065	49.9395	6.76E+05	0	0
4	0	0	**1.75E+08**	0	0
8	0.0575	49.9395	6.76E+05	0	0
8	0.028	48.8359	6.47E+05	0	0
8	0.0306	39.4584	4.22E+05	0	0
4	0	4.373	0	0	0
8	0.0564	39.4584	4.22E+05	0	0
4	0	0.774	0	0	0
8	0.0115	39.4584	4.22E+05	0	0
0	0	0	0	0	0

Mode Shapes of Brake Compressor Shaft

I. Brake Compressor Bending Mode

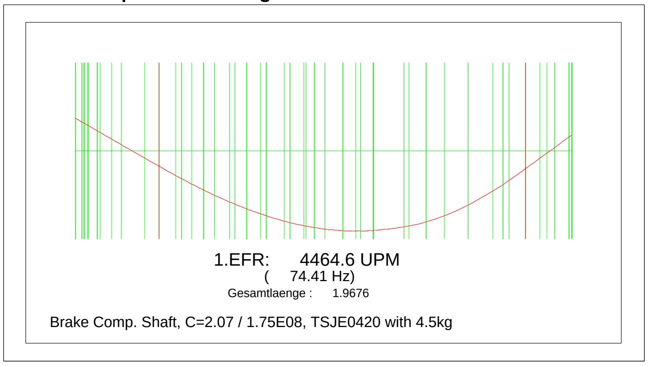

II. Brake Compressor Bending Mode

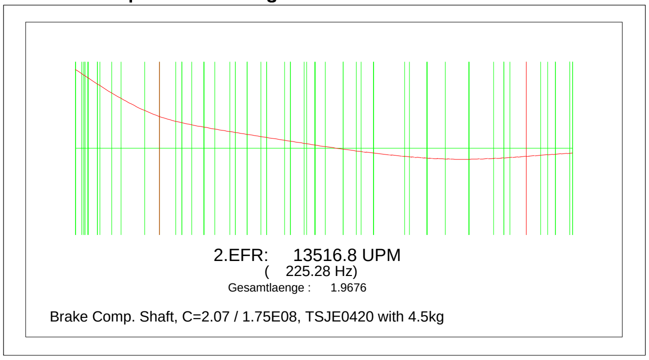

III. Brake Compressor Bending Mode

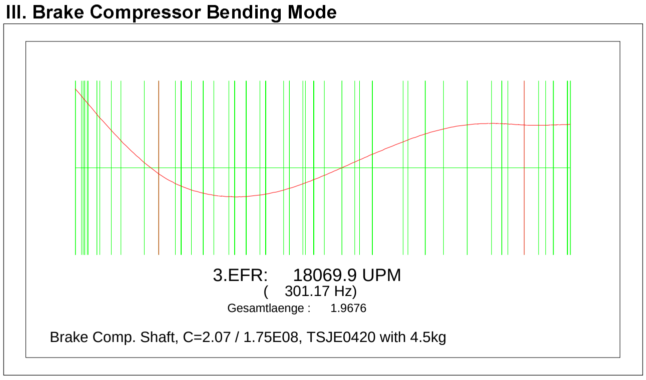

Model of Turbine Shaft

Turbine Shaft, C=1.65 / 1.49E08, TSJE0420 with 4.5kg					
1	1				
0	35000	50	3	8	29
0	0	0	0	0	0
5	0.108	65.72	0	0	0
7	0.01	0	1.57E+06	0	0
4	0	3.26	0	0	0
7	0.053	0	1.57E+06	0	0
5	0.092	31.84	0	0	0
7	0.022	0	1.57E+06	0	0
8	0.006	181.262	2.75E+07	0	0
8	0.029	370.0767	3.71E+07	0	0
8	0.003	88.7814	2.14E+06	0	0
8	0.007	71.9129	1.40E+06	0	0
8	0.08	61.6538	1.03E+06	0	0
4	0	0	**1.65E+08**	0	0
8	0.08	61.6538	1.03E+06	0	0
8	0.482	67.9733	1.25E+06	0	0
8	0.0386	61.6538	1.03E+06	0	0
8	0.0074	105.1589	3.00E+06	0	0
8	0.0185	257.3335	1.80E+07	0	0
8	0.0485	49.9395	6.76E+05	0	0
4	0	0	**1.49E+08**	0	0
8	0.0485	49.9395	6.76E+05	0	0
8	0.0185	257.3335	1.80E+07	0	0
8	0.0074	105.1589	3.00E+06	0	0
8	0.0369	61.6538	1.03E+06	0	0
8	0.0127	94.7988	2.44E+06	0	0
8	0.006	190.9787	9.89E+06	0	0
7	0.02462	0	6.15E+06	0	0
4	0	4.5	0	0	0
0	0	0	0	0	0

Mode Shapes of Turbine Shaft

I. Turbine Bending Mode

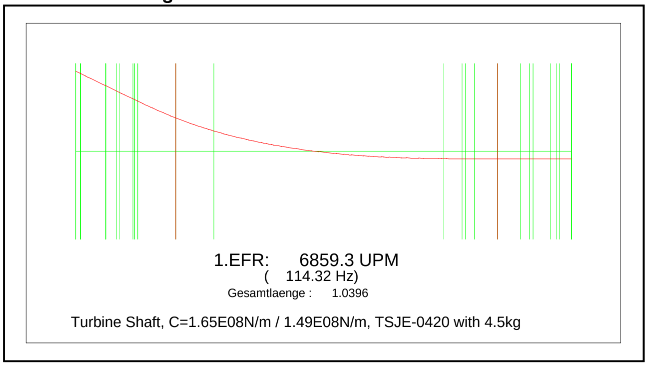

II. Turbine Bending Mode

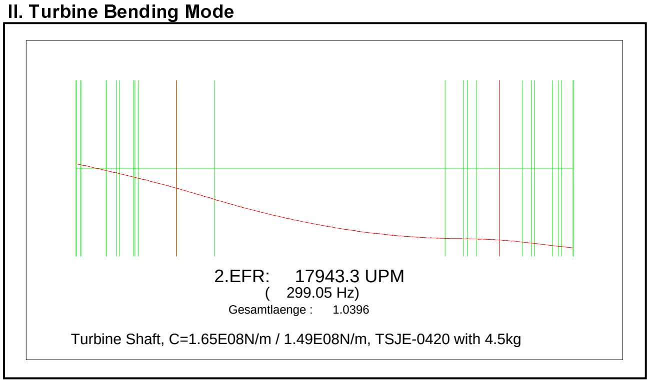

III. Turbine Bending Mode

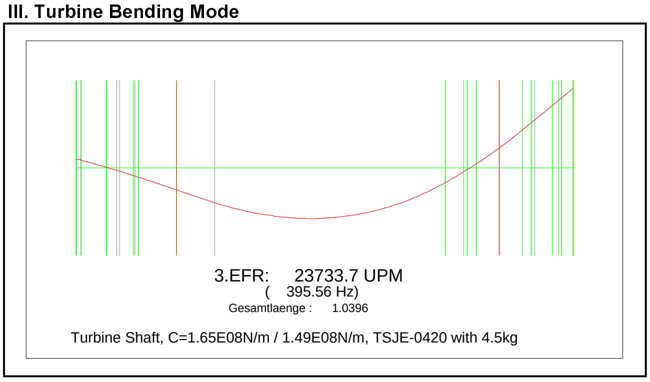

Model of TSJE-0420

TSJE-0420					
1	1				
0	500000	100	4	8	9
0	0	0	0	0	0
3	0	0	0	2005	0
8	0.0145	84.3423	3.92E+06	0	0
8	0.1865	6.4367	1.63E+05	0	0
4	0	0.612	0	0	0
8	0.1865	6.4367	1.63E+05	0	0
8	0.0145	84.3423	3.92E+06	0	0
3	0	0	0	2005	0
0	0	0	0	0	0

Mode Shape of TSJE-0420

I. Coupling Bending Mode

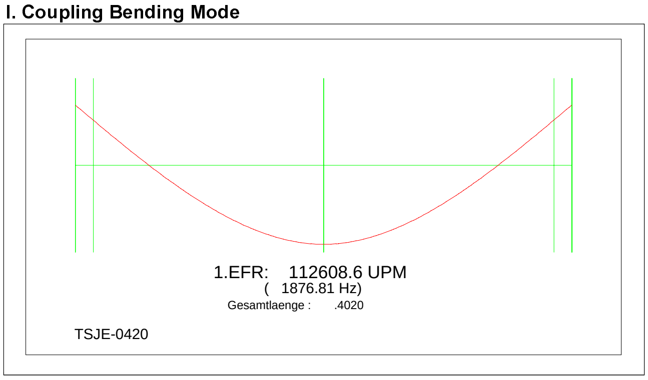

8.2 Test parameter variations

8.2.1 Test parameter checklist

To have a good matching of the TTM-stage test conditions wirh the GHH-brake compressor and TTM compressor station characteristics some help is given by a general part load behaviour overview in chapter 4.2.3 Quasi 3D simulation for different load conditions. For further investigations the results of the 58 Navier Stokes jobs on the TTM-stage mid section are given in the following chapter 8.2.2. The results from this Quasi 3D simulations agree quite well in terms of power, mass flow and flow angles, but since these values were calculated only at the midspan section the higher losses of the hub section had no influence on the TTM-stage efficiency values. So I would suggest to believe the qualitative behaviour but not the quantitative values of these TTM-Stage efficiencies.

To check for test condition capability of the test rig the following simplified procedure may run for example:

(1) Looking at the power generation capability P = f (n, $t_{0\ tot}$, $p_{0\ tot}$) of the test stage at test condition
(2) Checking for IGV´s angle of the GHH for equal braking power and test stage pressure ratio on test speed
  (a) test stage pressure ratio can be reached -> use of the brake compressor for multiplying mass flow
  (b) test stage pressure ratio is impossible -> throttling mode of the brake compressor
(3) With the brake compressor mass flow and exit temperature the compressor station operation can be calculated
(4) Additional checks for the test flow situation in the test stage regarding rotor inlet angle matching, exit swirl, rotor exit static temperature may help in the measurement task

Test Turbine TTM-stage :

air gas constant R = 287.0 J/kgK

Data of Quasi 3-D Navier Stokes Simulation

turbine inlet temperature t_0 [°C]

t_0 [°C]	T_0 [K]
181.3	454.4
159.1	432.2
137.0	410.1
116.0	389.1
95.0	368.1

speed n [rpm]

n [rpm]	n π/30	n [%]
11550	1209.5	105
11000	1151.9	100
10450	1094.3	95
9900	1036.7	90

90
95
100
105

turbine inlet pressure p_0 =

p_0 = pressure ratio π

p_0 [bar]	π
4.0	4.0
3.5	3.5
3.0	3.0
2.5	2.5
2.0	2.0

turbine outlet pressure p_{2stat} [bar] 1.0

GHH Brake Compressor :

air (70% humidity) gas constant R = 289.8 J/kgK

Model of measured performance at 11175rpm at ÖMV

speed n [rpm]

n [rpm]	n [%]
11550	105
11000	100
10450	95
9900	90
9350	85
8800	80

Inlet guide vanes α [°]

α [°]
-15
0
20
35
50

-15
0
20
35
50

brake compressor outlet pressure p_{ex}

(including overflow pipe and mixer losses)

p_{ex} [bar]
4.0
3.5
3.0
2.5
2.0

brake compressor inlet pressure p_{in} [bar] 0.95

brake compressor inlet temperature t_{in} [°C] 15

Compressor Station TTM :

Example (see 4.2.3.2 and Fig. 44) :

turbine inlet temperature t_0 [°C]	137.0						
speed n [rpm]	10450	=	speed n [rpm]	10450			
turbine inlet pressure p_0 [bar]	2.75	=	brake compressor outlet pressure p_{ex} [bar]	2.75			
power [kW]	1365	=	power [kW]	1365			
			brake compressor inlet guide vanes α [°]	39		mass flow m_{CS} [kg/s]	
mass flow m_0 [kg/s]	15.2		mass flow m_{GHH} [kg/s]	8.2		(m_0 - m_{GHH}) [kg/s]	7.0
			brake compressor outlet temperature t_{GHH} [°C]	176		outlet temperature t_{CS} [°C]	91
rotor inlet (48) β_1 [°]	48					(t_0 m_0 - t_{GHH} m_{GHH})/m_{CS} [kg/s]	
exit swirl α_2 [°]	8						
rotor exit static temperature t_2 [°C]	43						
stator exit Mach number M_{1abs}	1.10						
rotor exit Mach number M_{2rel}	0.77						

8.2.2 Additional TTM-Stage results (t_{0tot} =181.3°C, 137.0°C, 95.0°C)

$t_{0\ tot}$ = 181.3°C

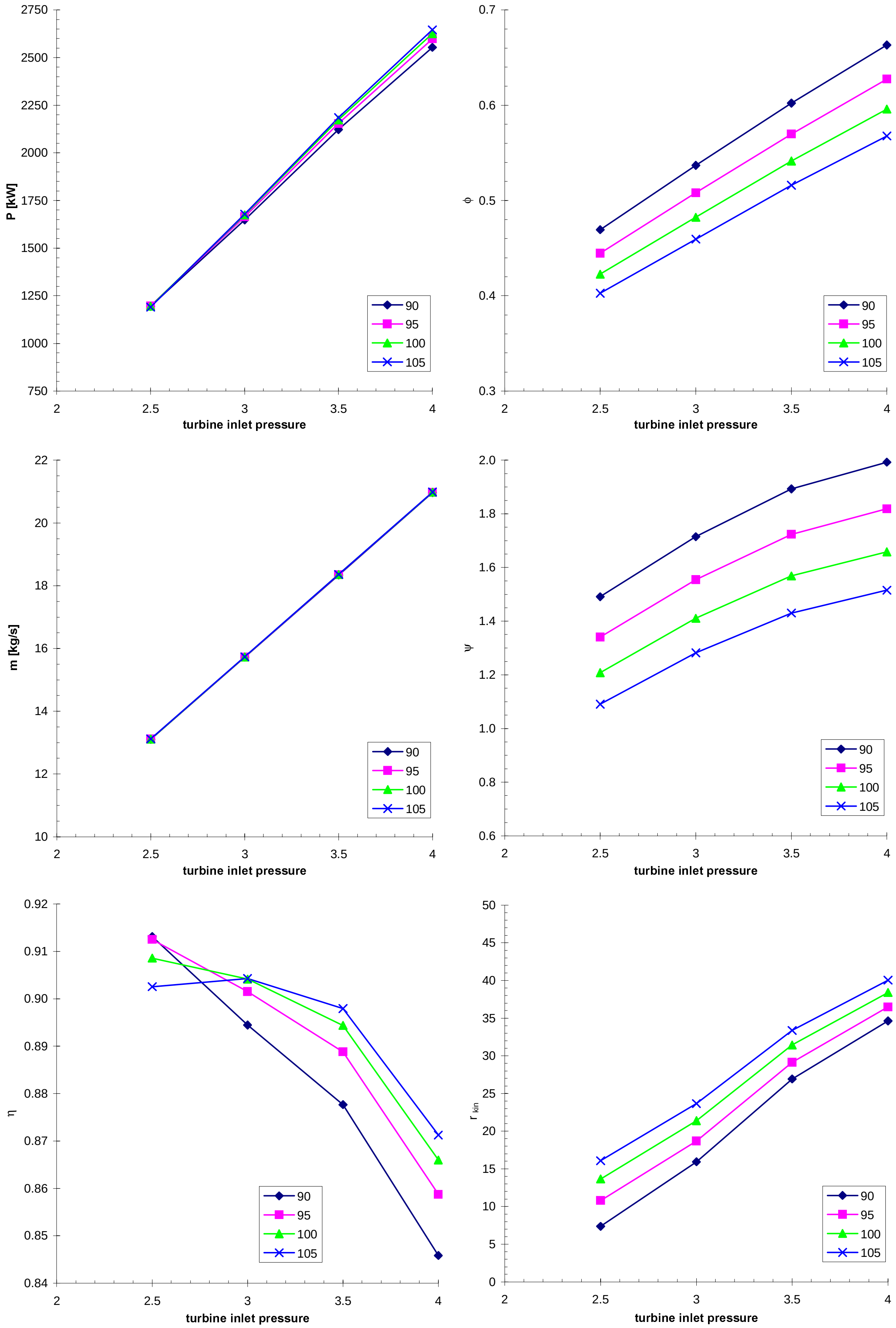

$t_{0\ tot}$ = 181.3°C

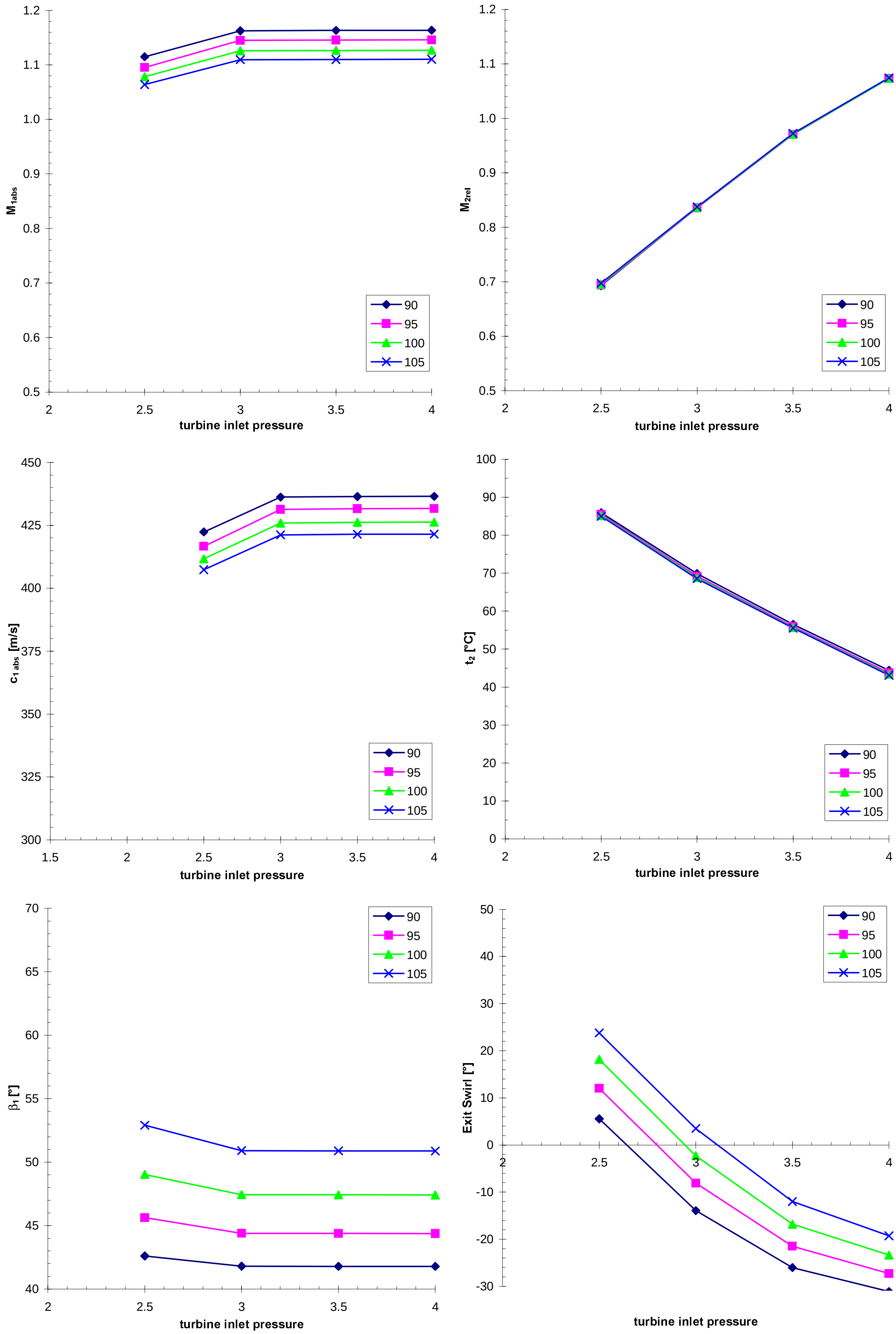
M1abs
M2rel
c1 abs [m/s]
t2 [°C]
β1 [°]
Exit Swirl [°]
turbine inlet pressure
90
95
100
105

$t_{0\ tot}$ = 137.0°C

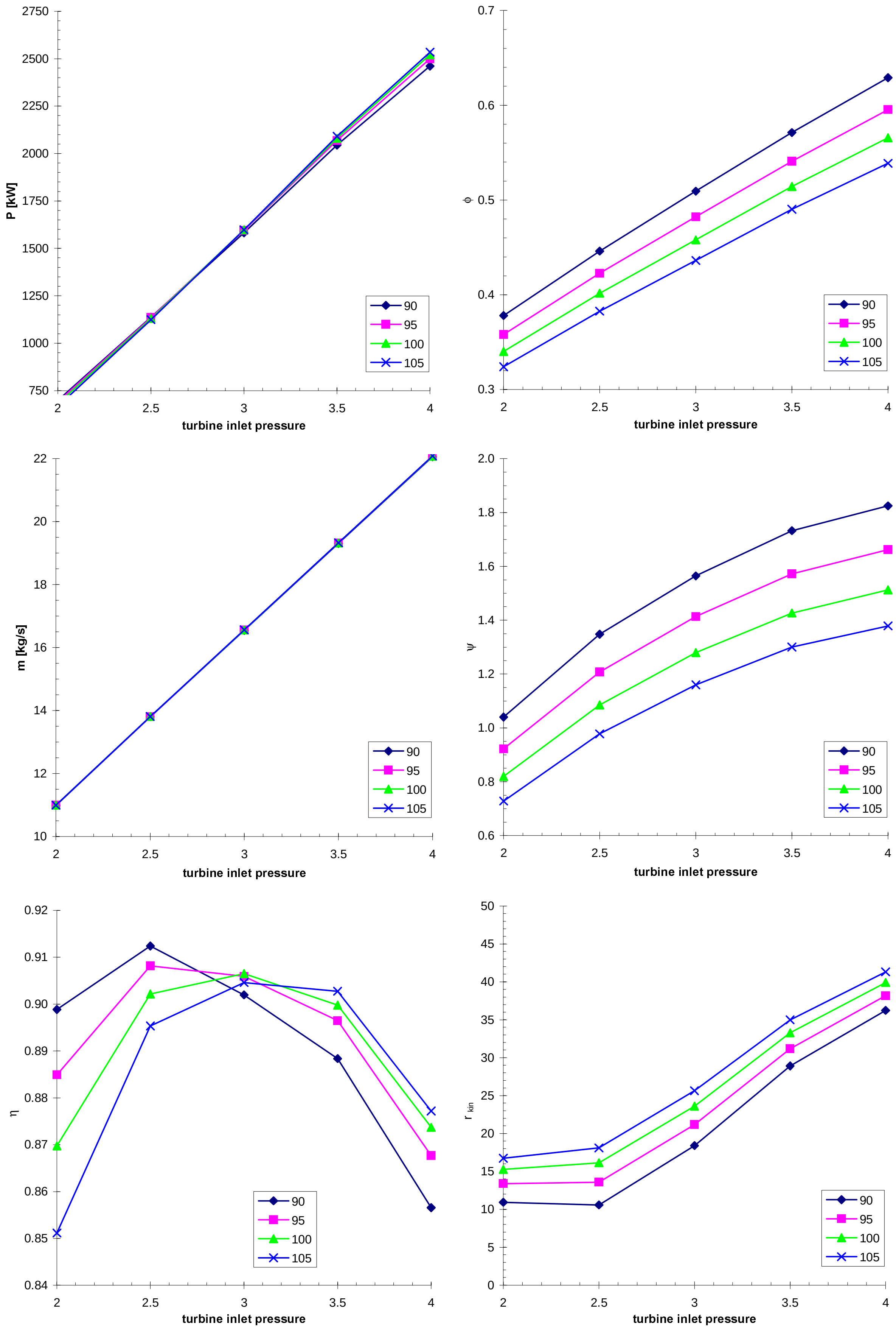

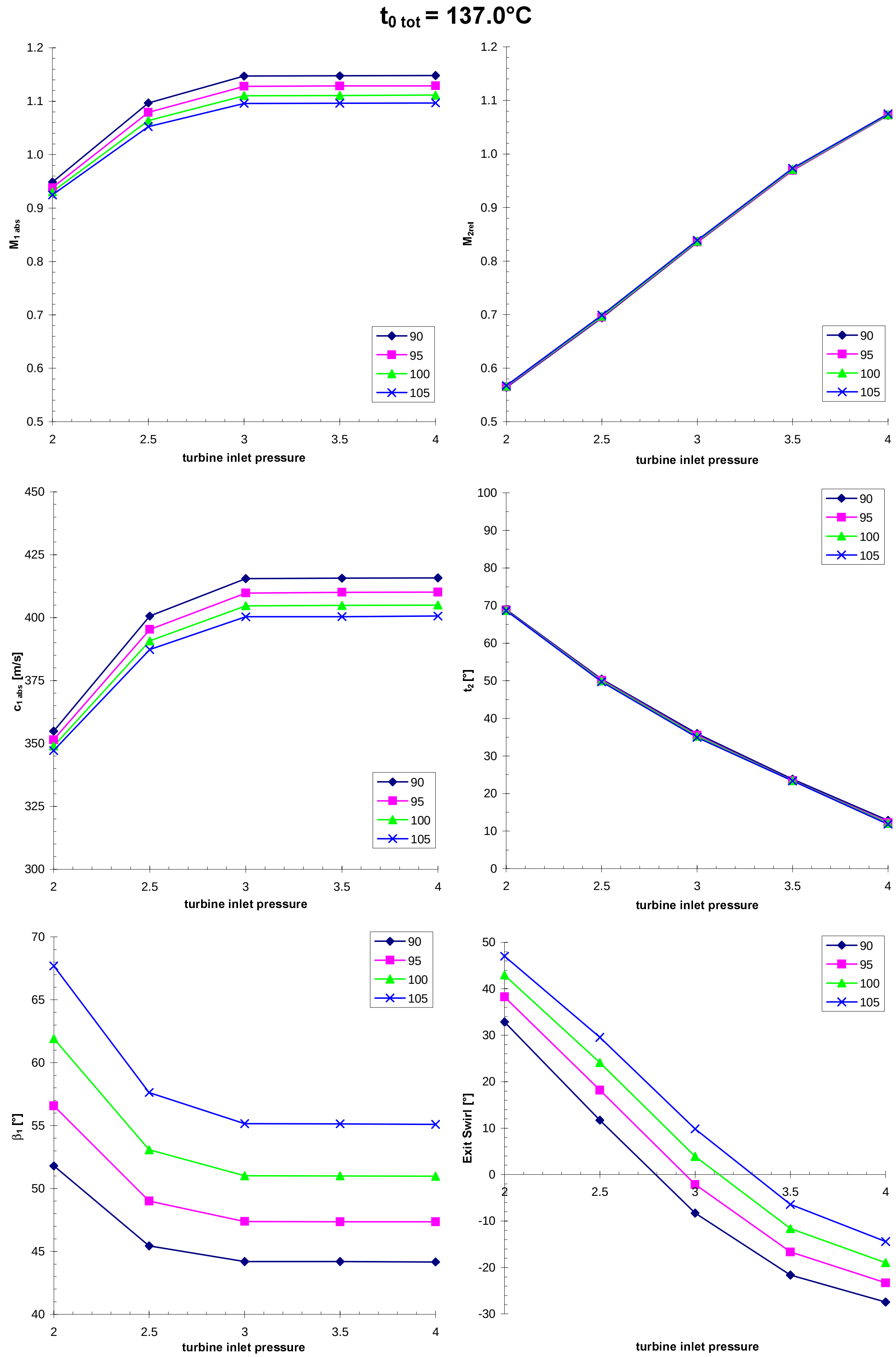
$t_{0\ tot}$ = 137.0°C
$M_{1\ abs}$
M_{2rel}
$c_{1\ abs}$ [m/s]
t_2 [°]
β_1 [°]
Exit Swirl [°]
turbine inlet pressure
90
95
100
105

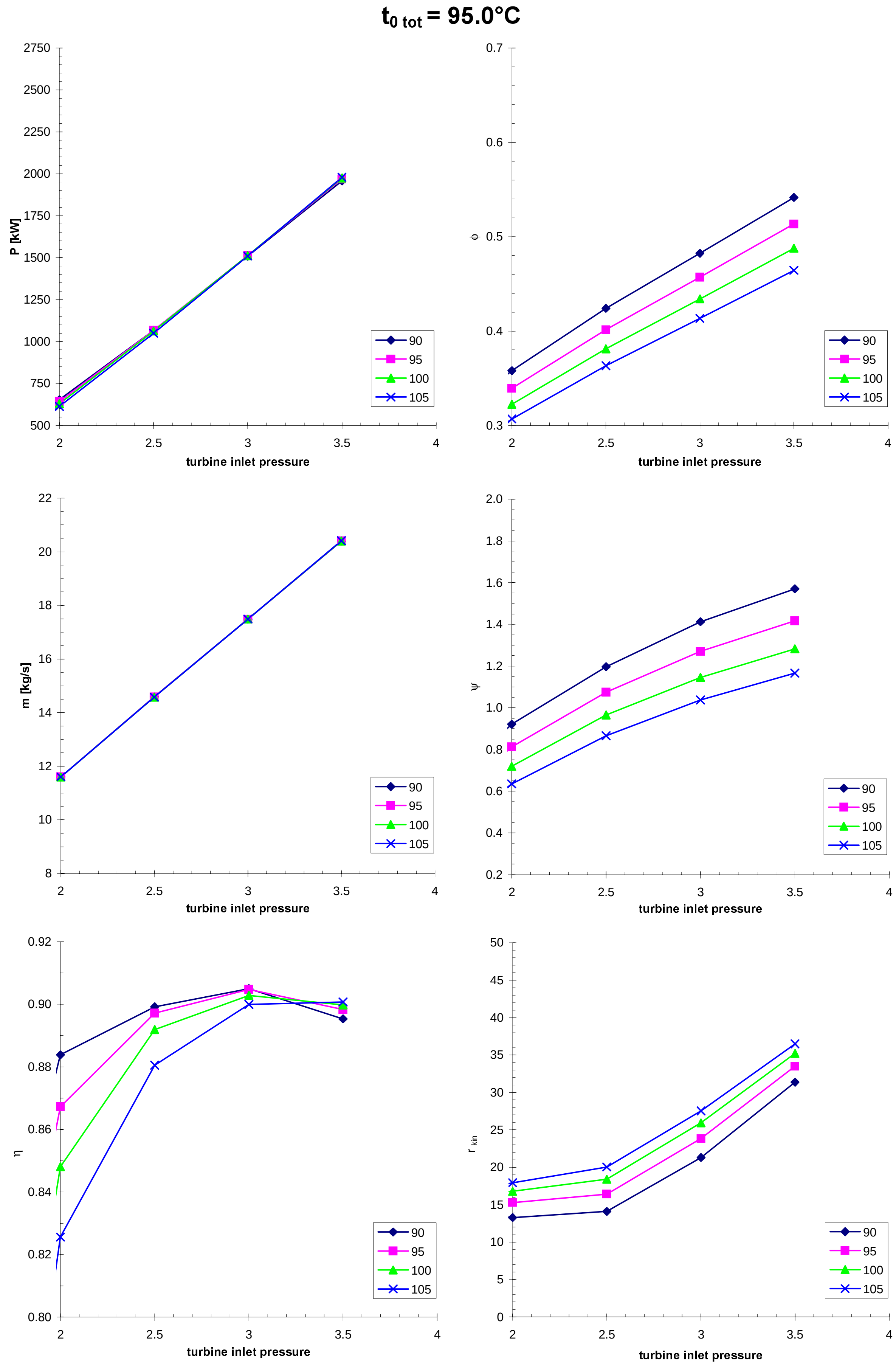

t0 tot = 95.0°C
P [kW]
ϕ
m [kg/s]
ψ
η
r kin
turbine inlet pressure
90
95
100
105

$t_{0\ tot} = 95.0°C$

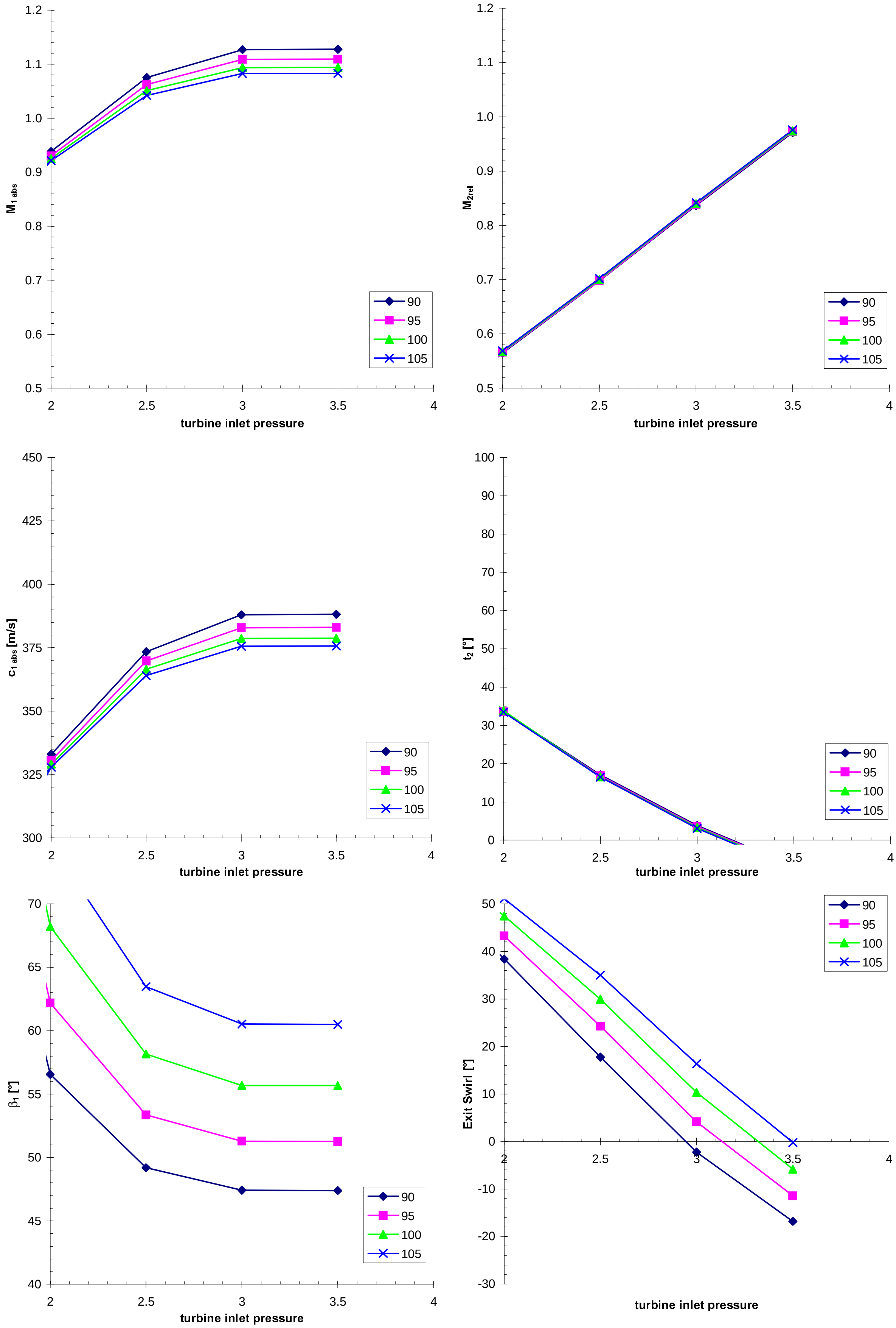
M1 abs
M2rel
c1 abs [m/s]
t2 [°]
β1 [°]
Exit Swirl [°]
turbine inlet pressure
90
95
100
105

8.2.3 GHH brake compressor (inlet condition: 0.95bar, 15°C, R=289.82J/kgK)

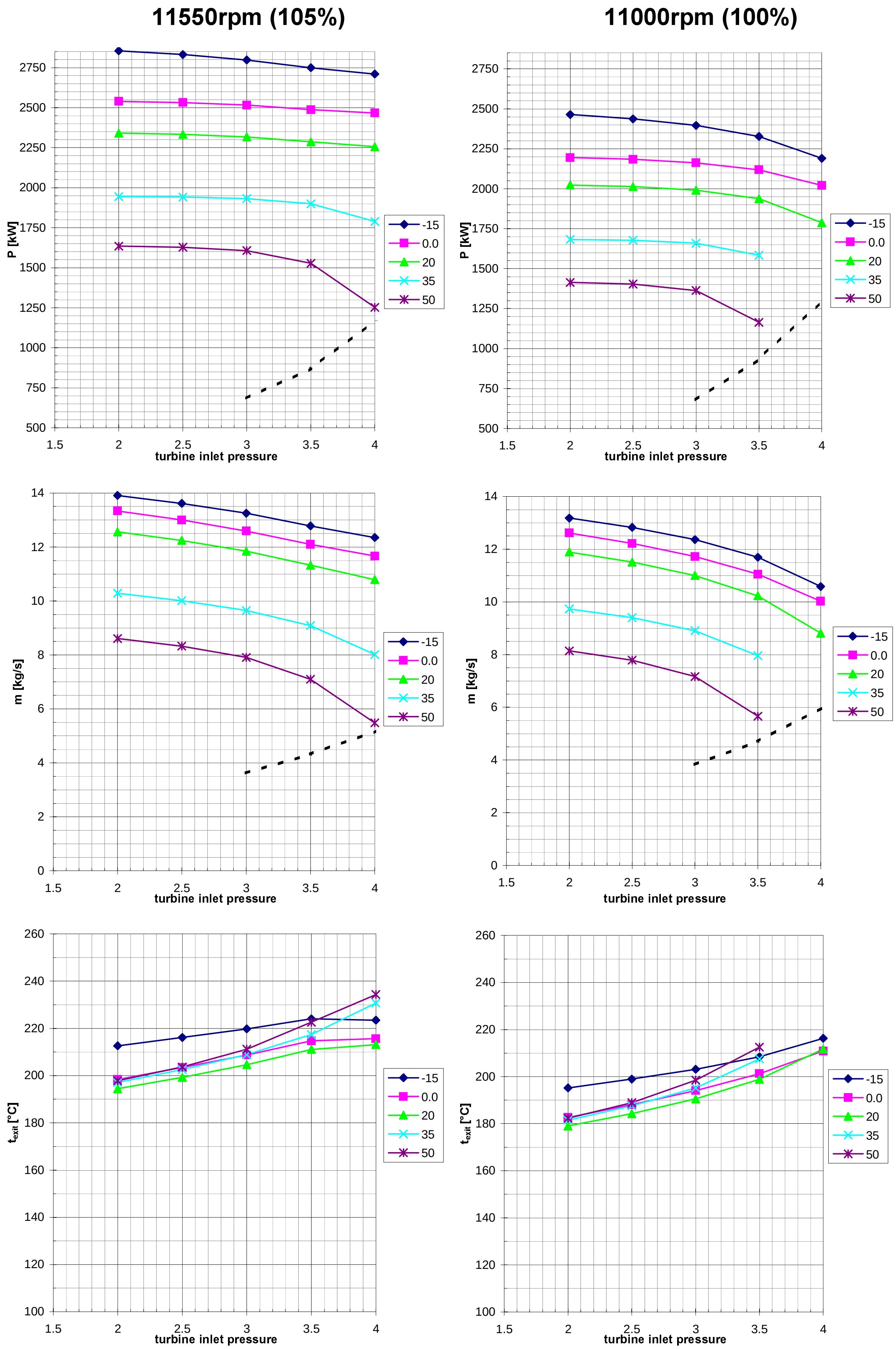

10450rpm (95%) | 9900rpm (90%)

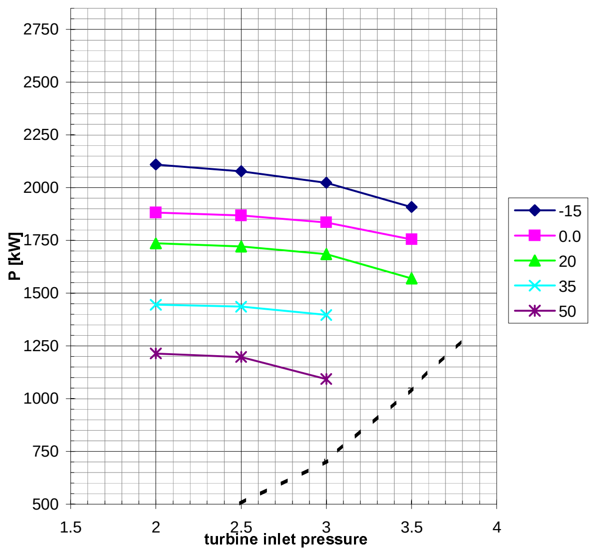

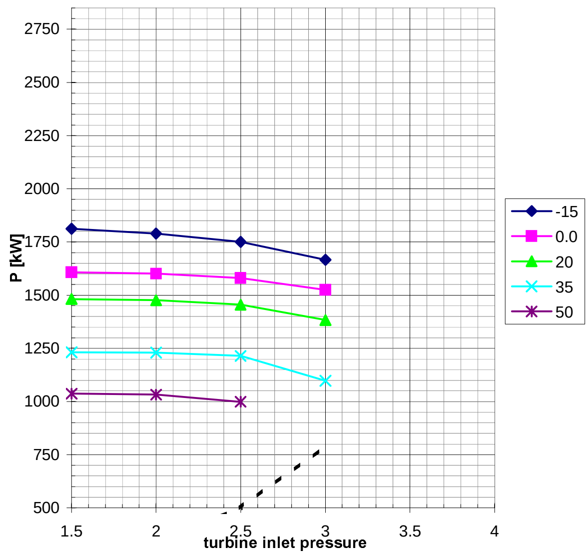

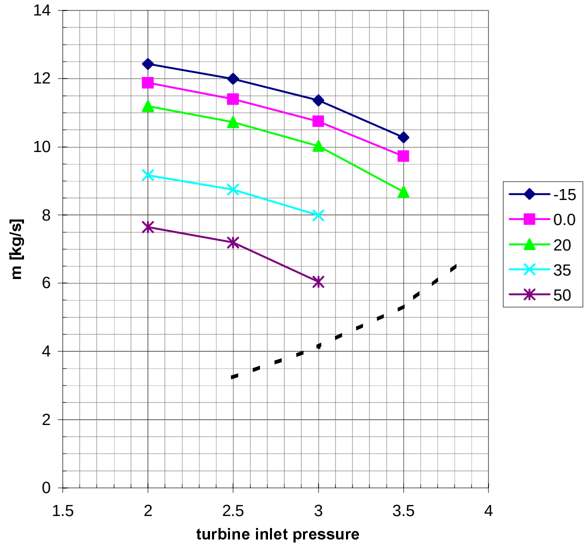

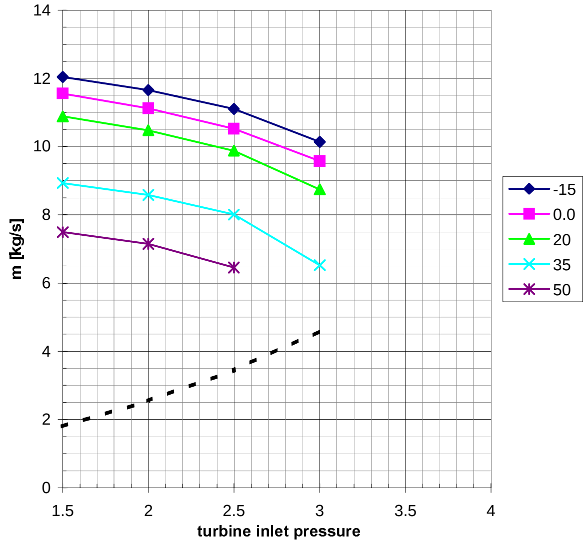

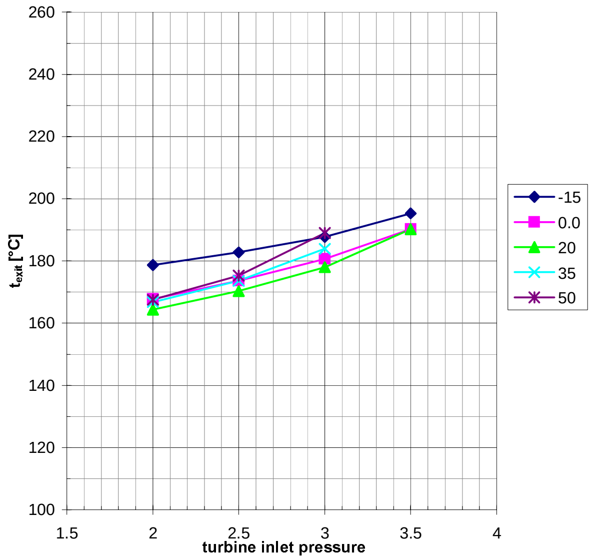

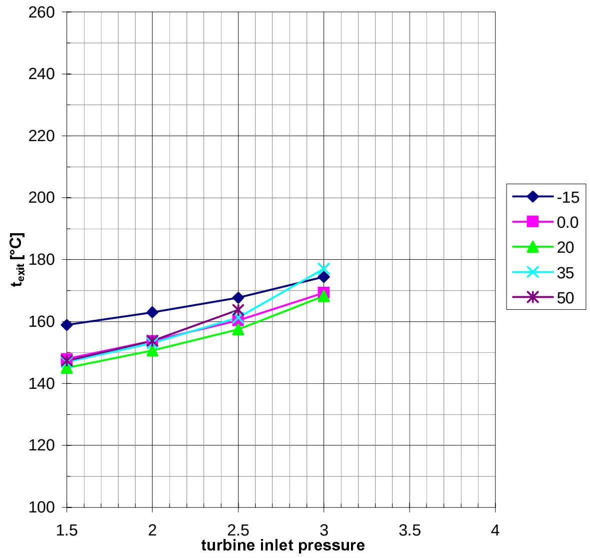

9350rpm (85%)

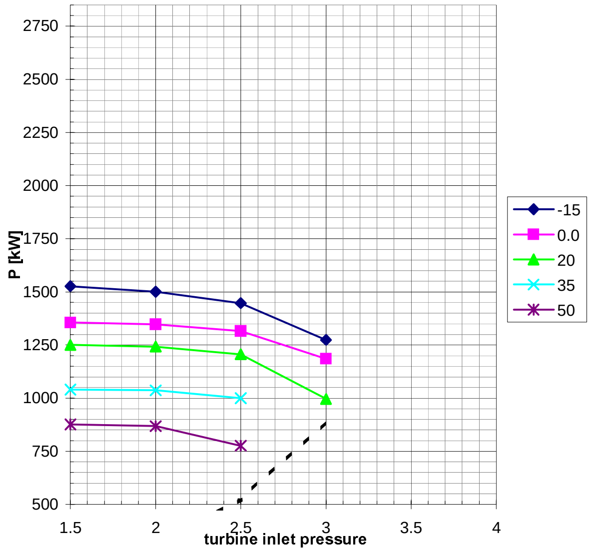

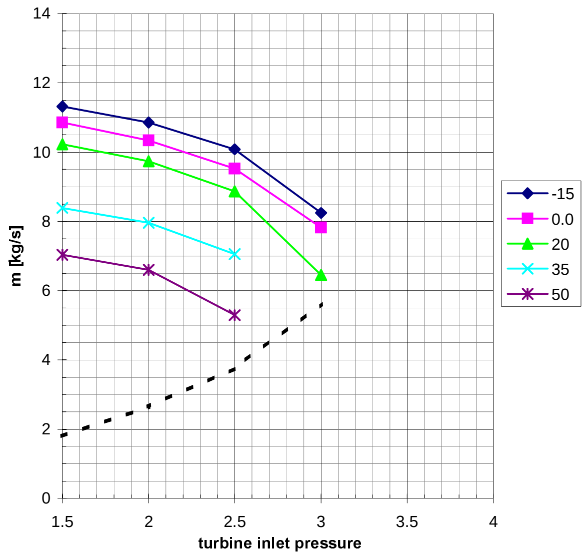

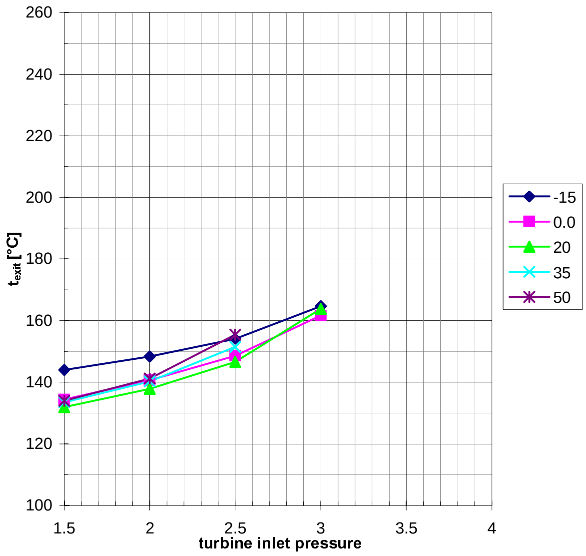

8800rpm (80%)

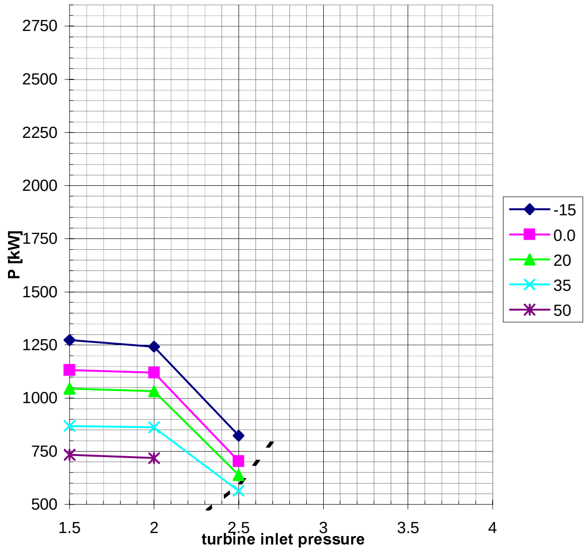

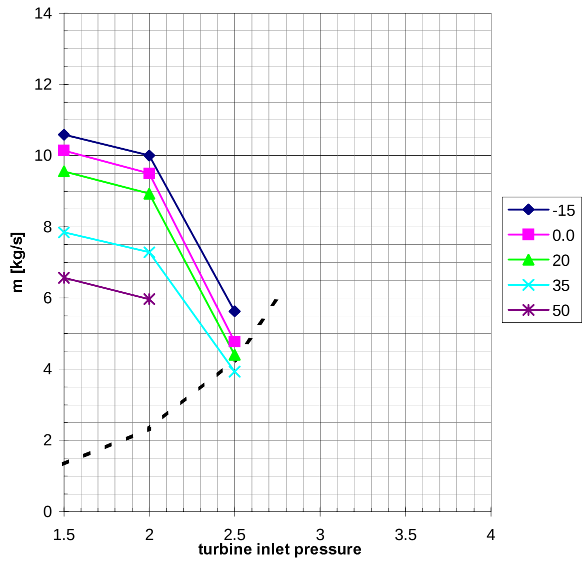

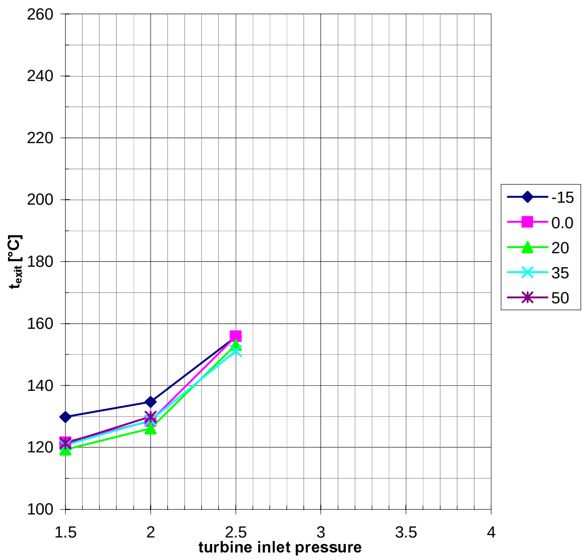

8.3 Test turbine drawings

8.3.1 Test turbine assembly drawing

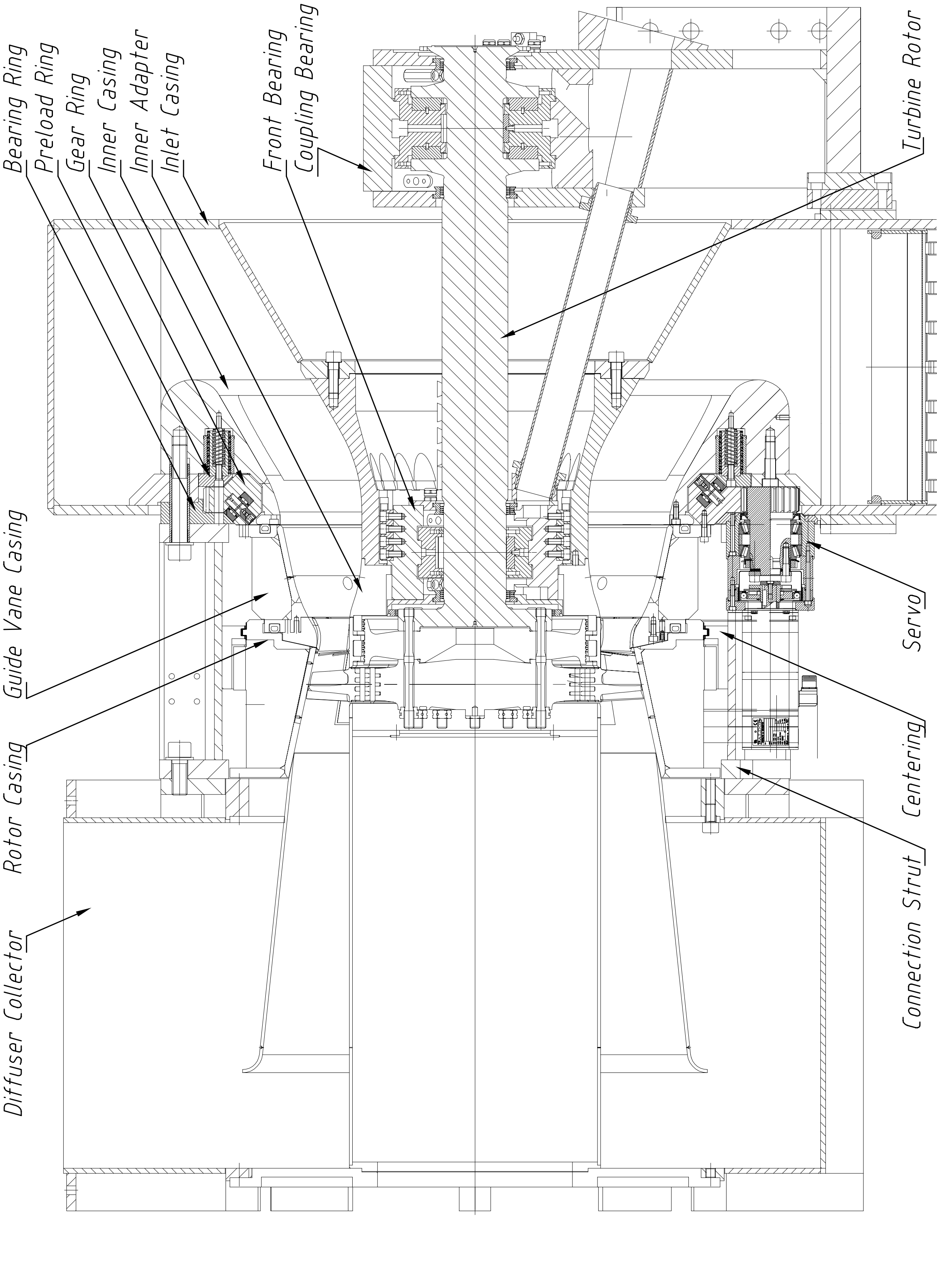

8.3.2 Inlet casing

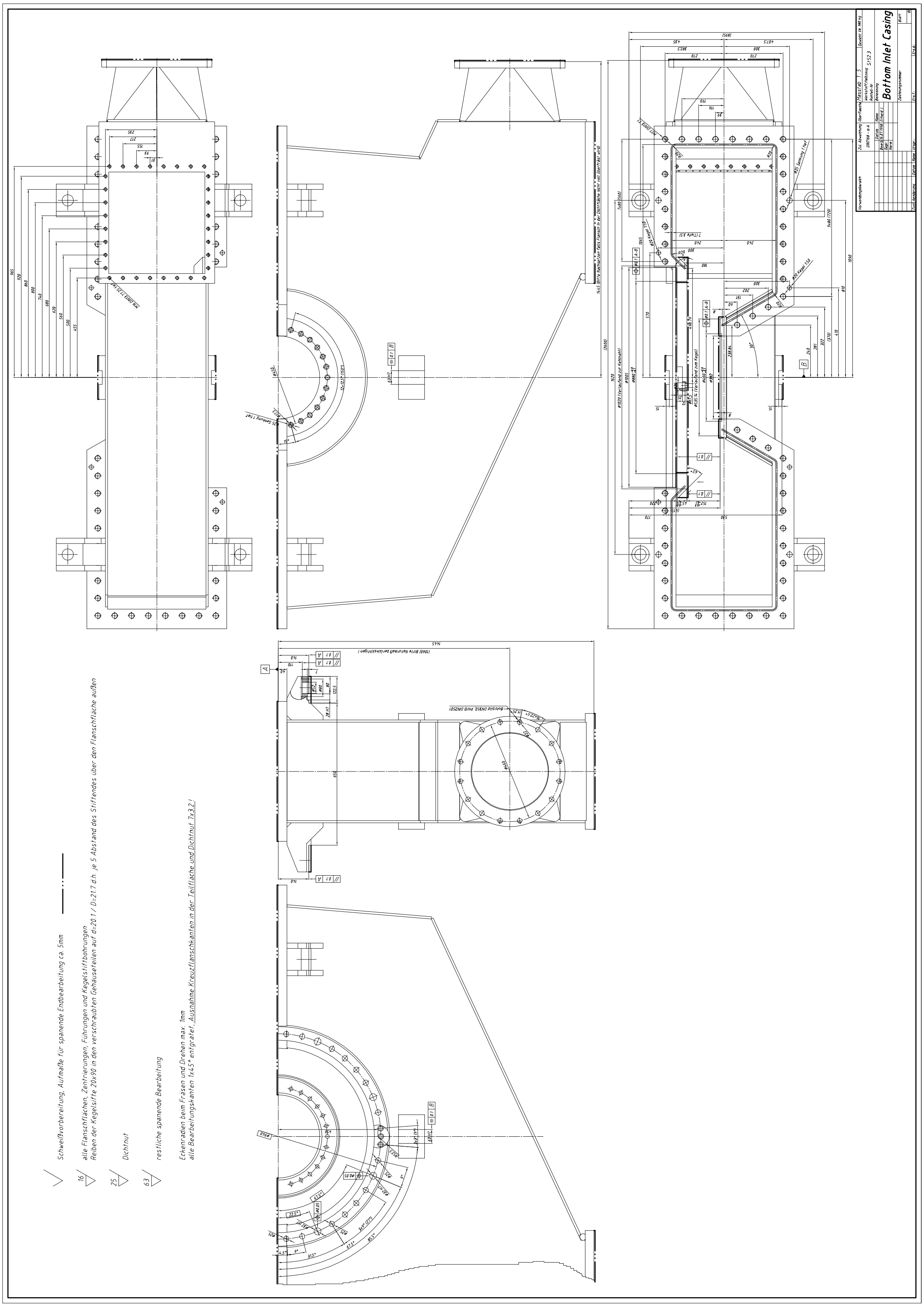

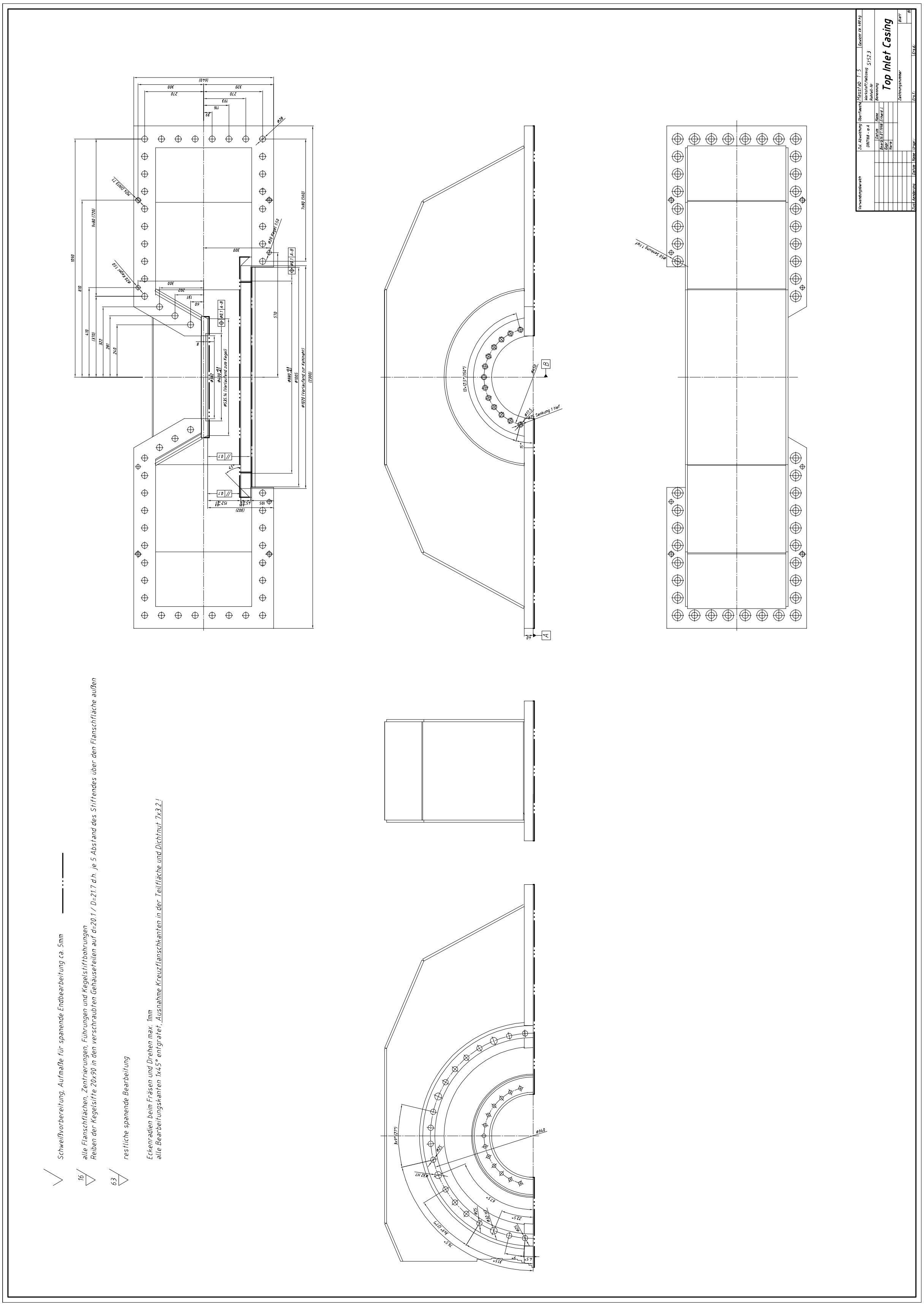
Top Inlet Casing
Schweißvorbereitung, Aufmaße für spanende Endbearbeitung ca. 5mm
16
alle Flanschflächen, Zentrierungen, Führungen und Kegelstiftbohrungen
Reiben der Kegelsifte 20x90 in den verschraubten Gehäuseteilen auf d=20.1 / D=21.7 d.h. je 5 Abstand des Stiftendes über den Flanschfläche außen
63
restliche spanende Bearbeitung
Eckenradien beim Fräsen und Drehen max. 1mm
alle Bearbeitungskanten 1x45° entgratet, Ausnahme Kreuzflanschkanten in der Teilfläche und Dichtnut 7x3.2 !

8.3.3 Inner casing

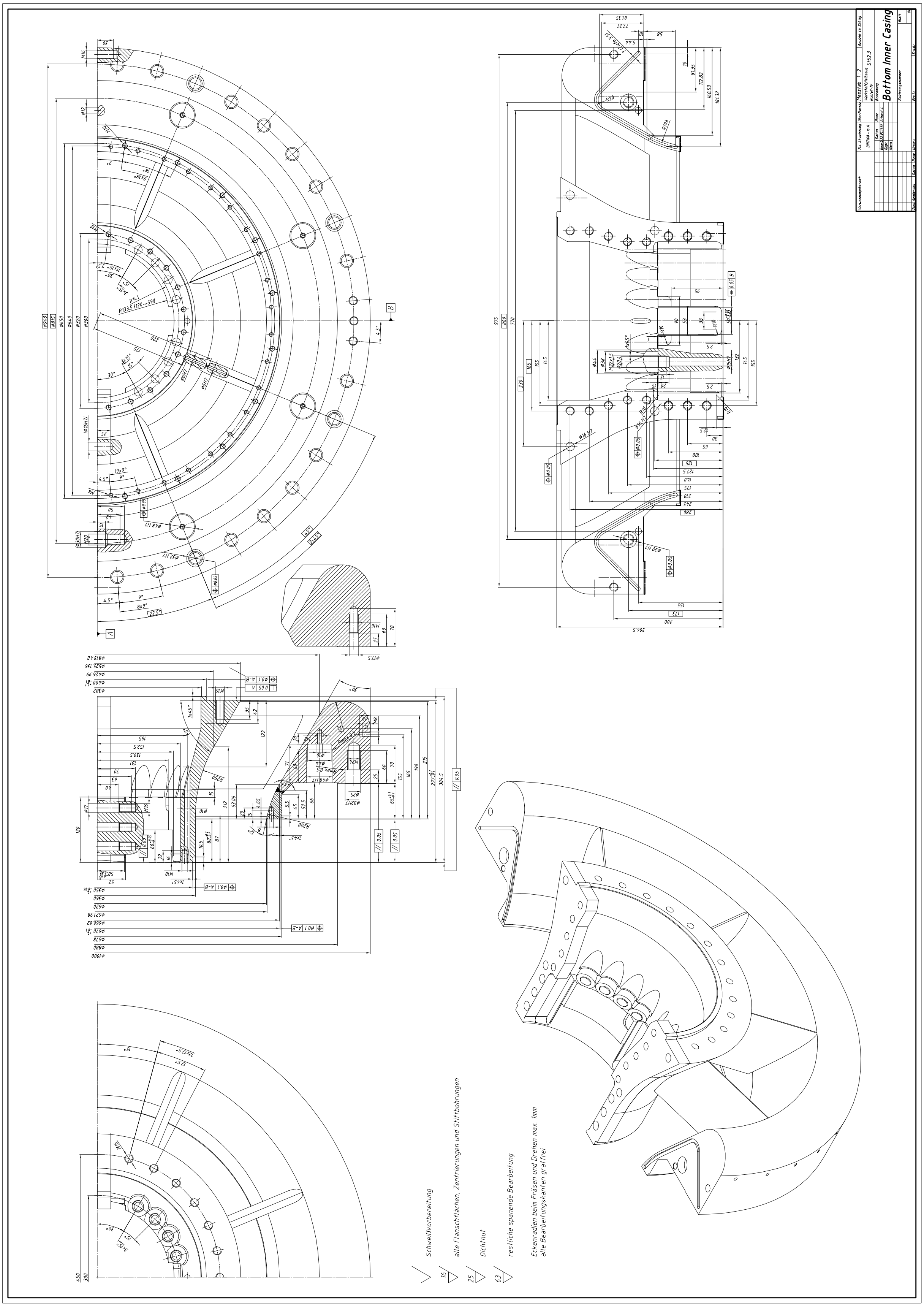

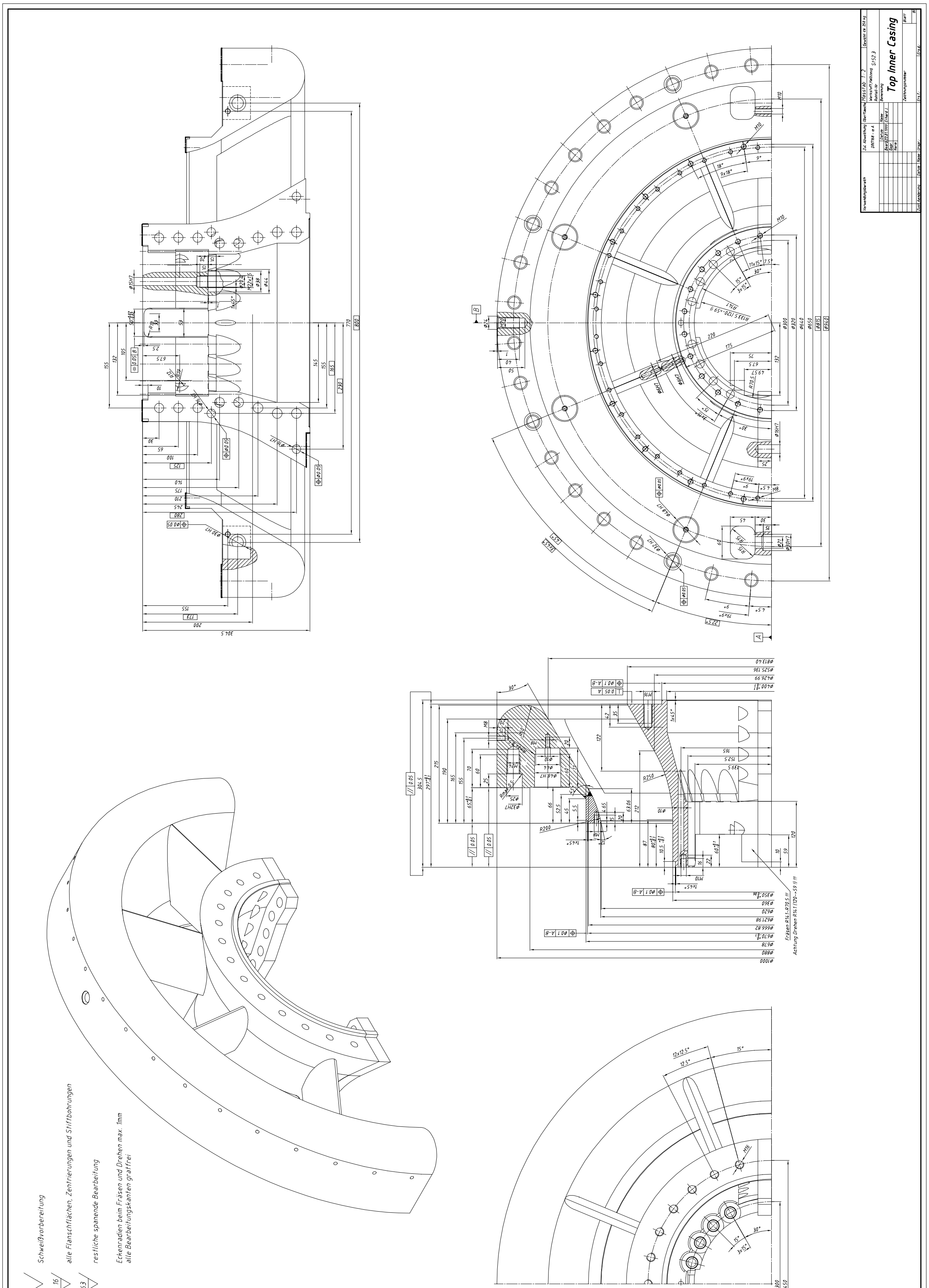
Top Inner Casing
Schweißvorbereitung
alle Flanschflächen, Zentrierungen und Stiftbohrungen
restliche spanende Bearbeitung
Eckenradien beim Fräsen und Drehen max. 1mm
alle Bearbeitungskanten gratfrei

8.3.4 Front bearing

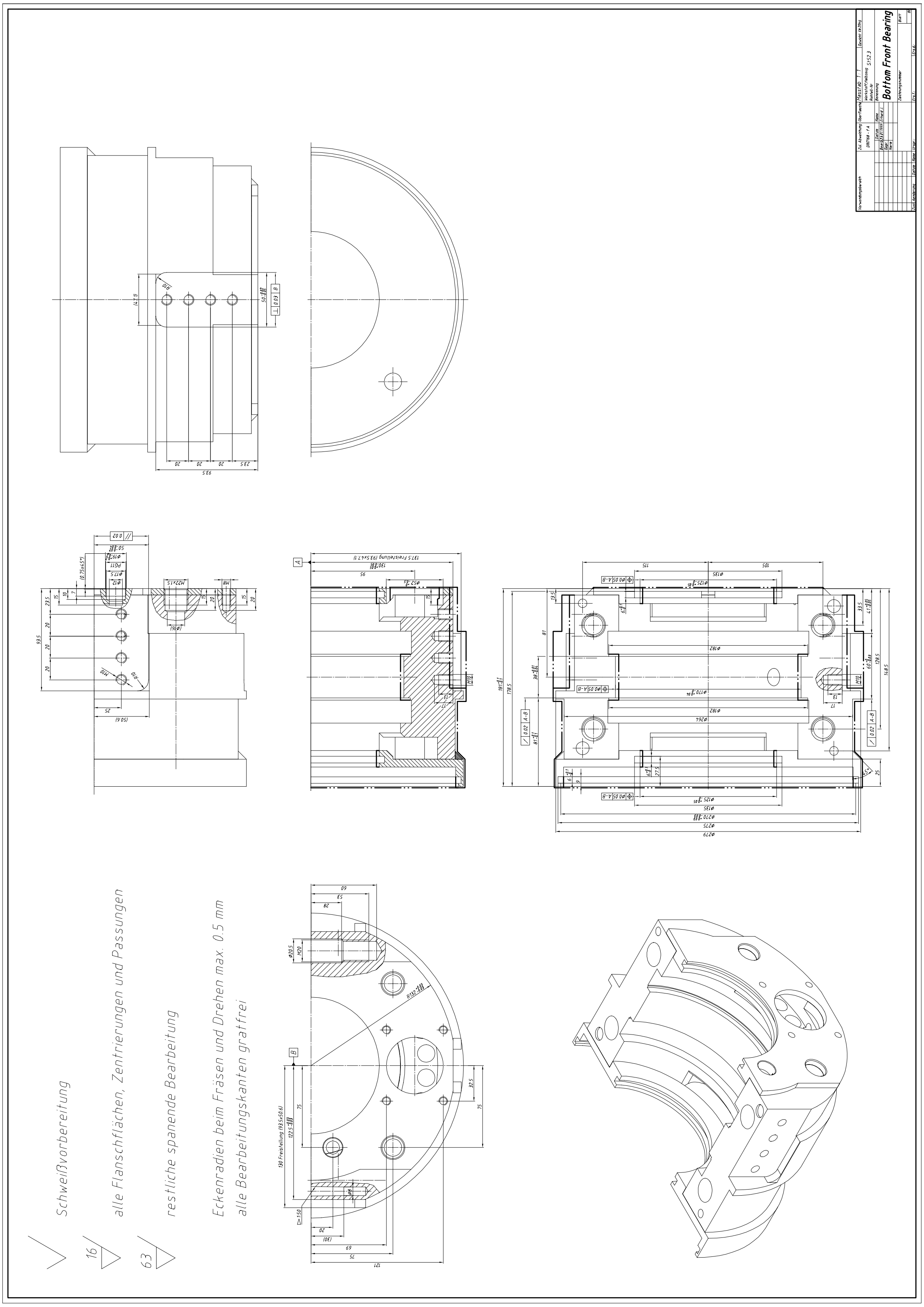

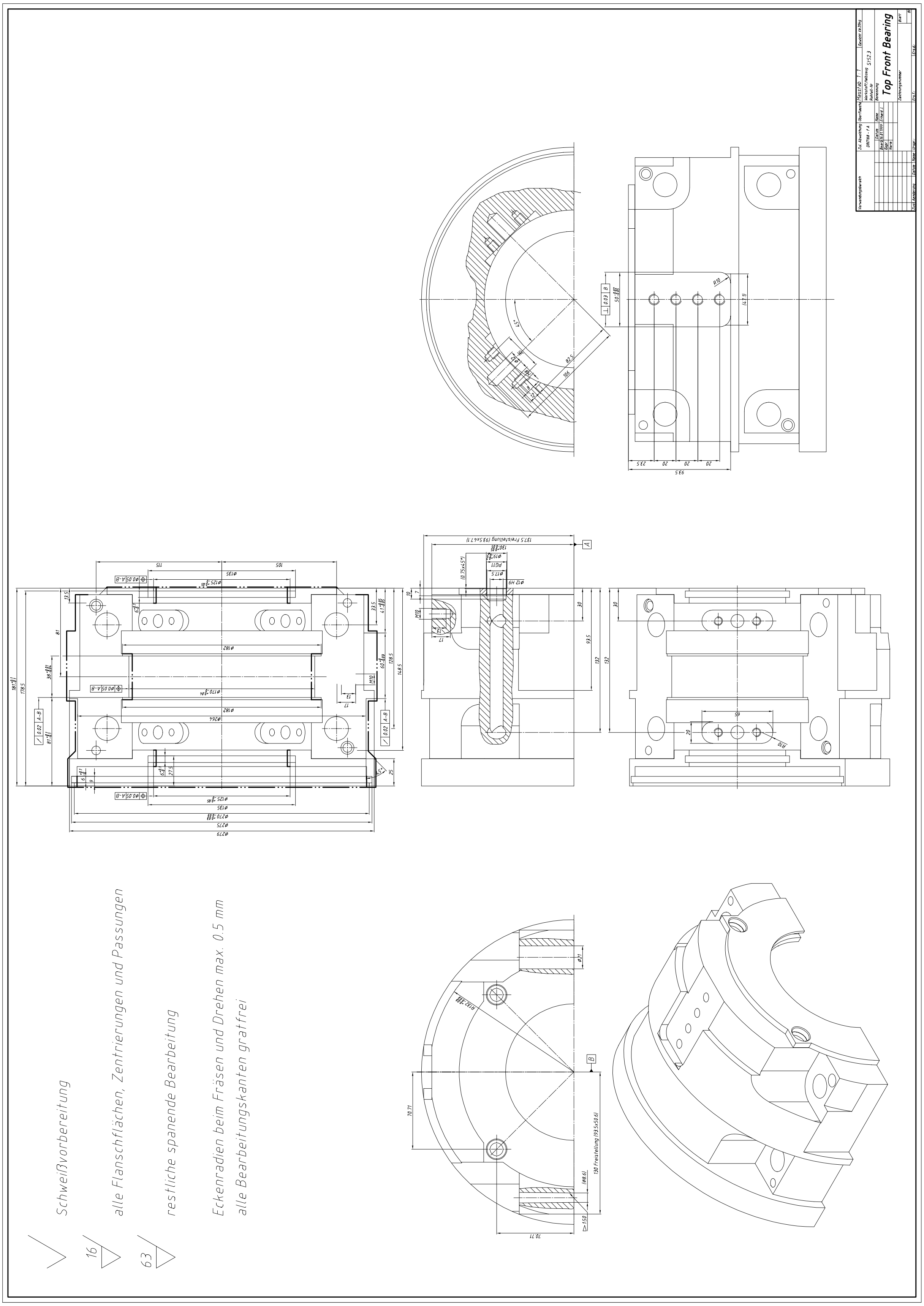
Top Front Bearing
Schweißvorbereitung
16
alle Flanschflächen, Zentrierungen und Passungen
63
restliche spanende Bearbeitung
Eckenradien beim Fräsen und Drehen max. 0.5 mm
alle Bearbeitungskanten gratfrei

8.3.5 Coupling bearing

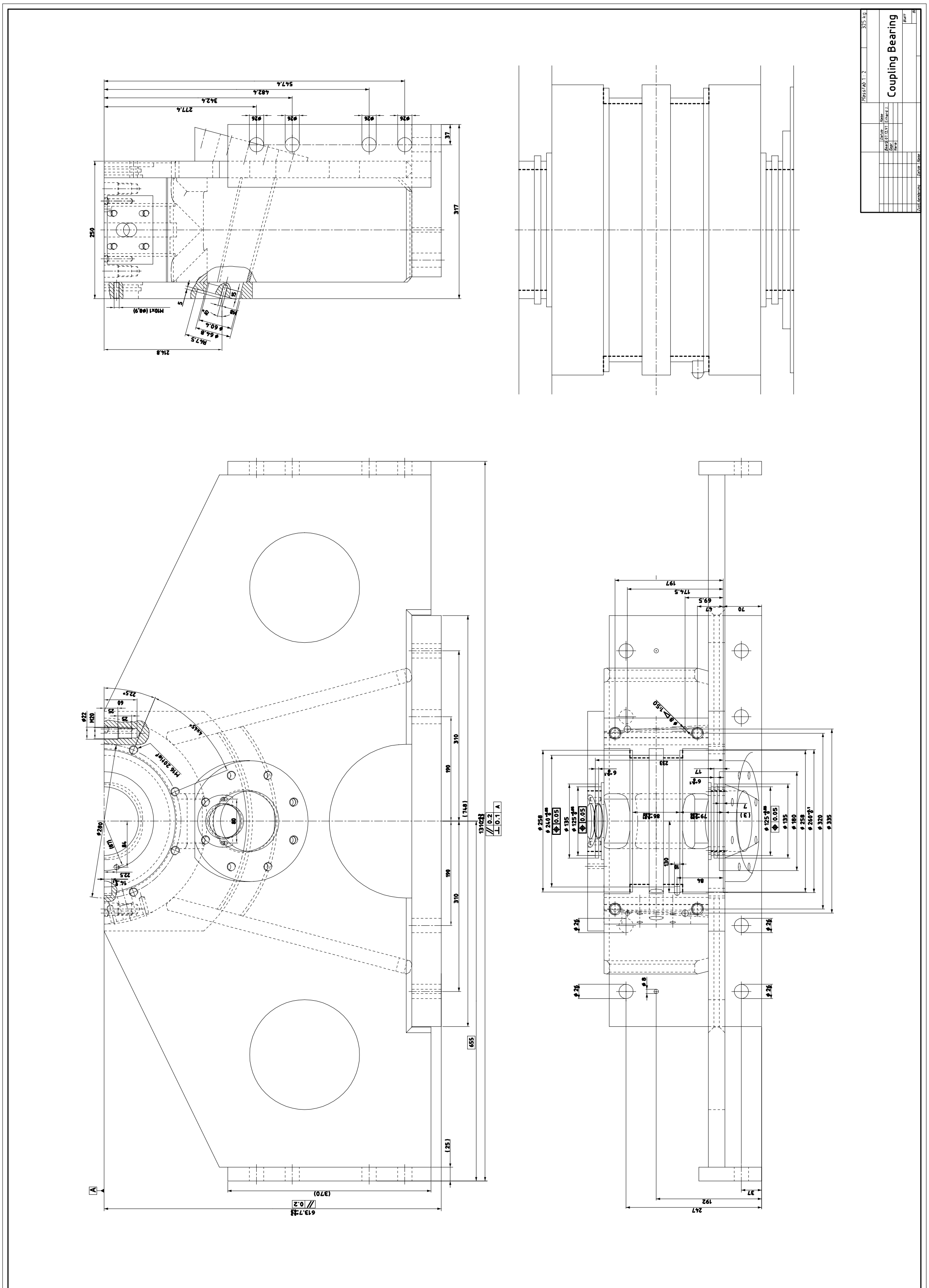

8.3.6 Turbine shaft

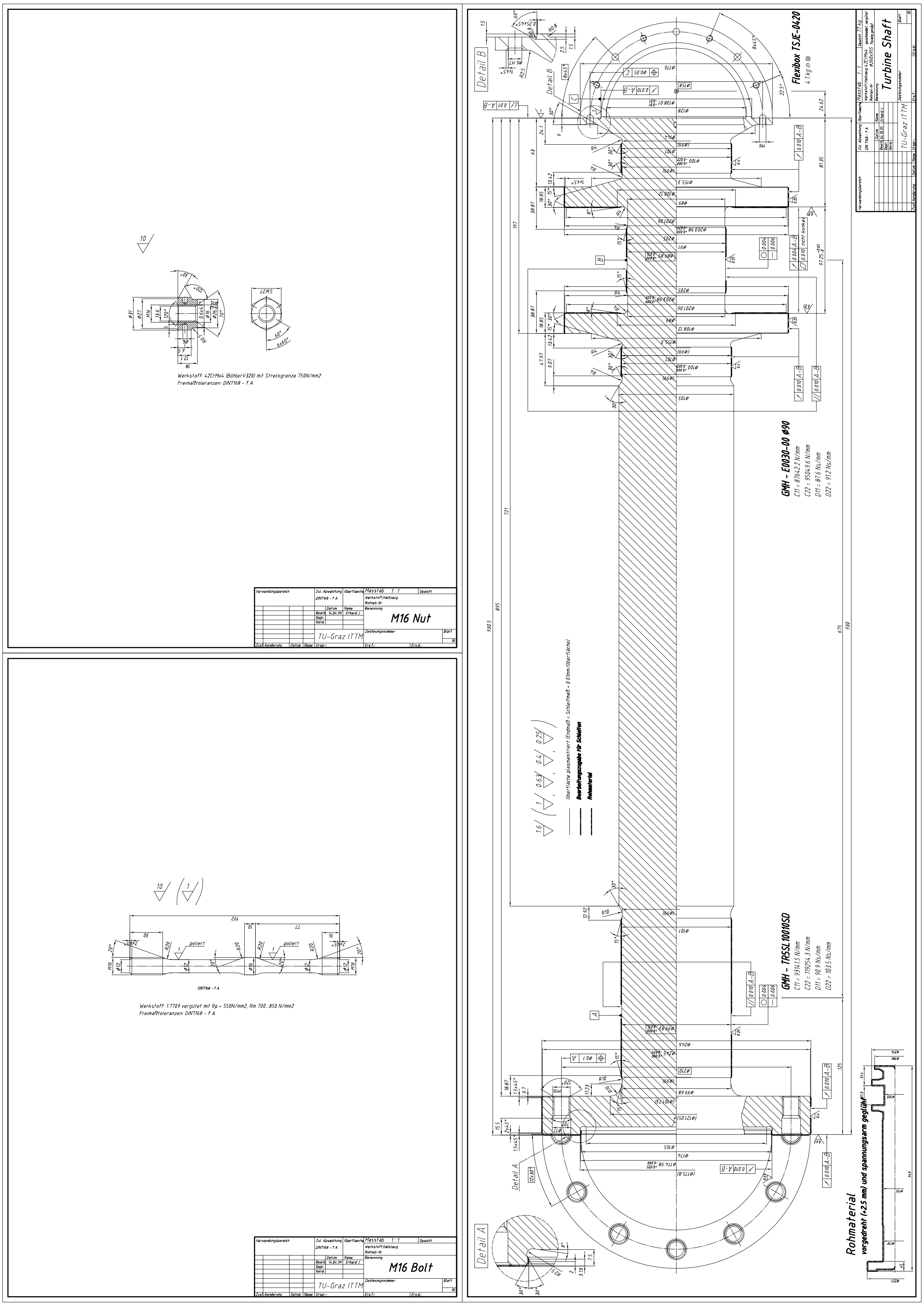

8.3.7 Preload ring

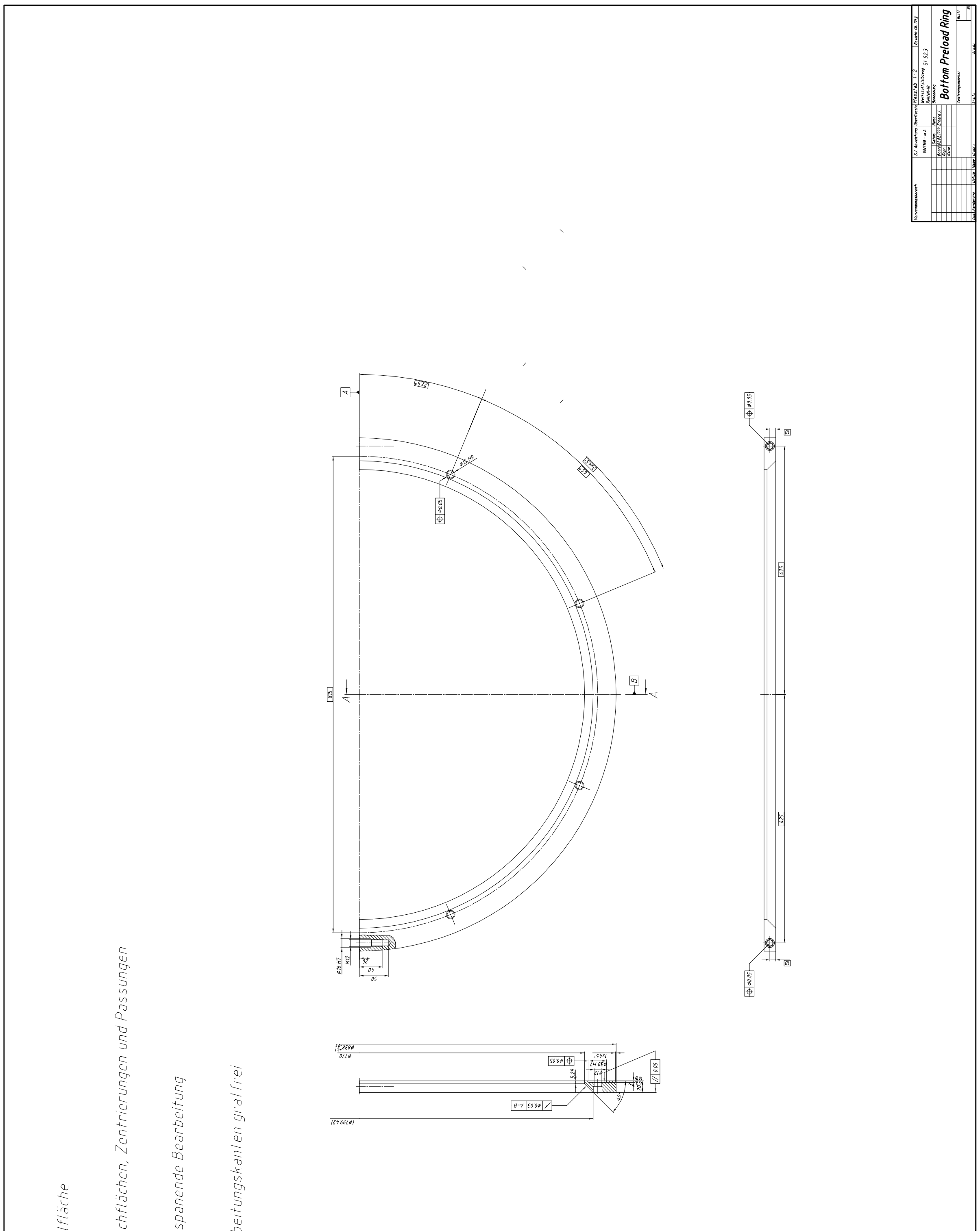

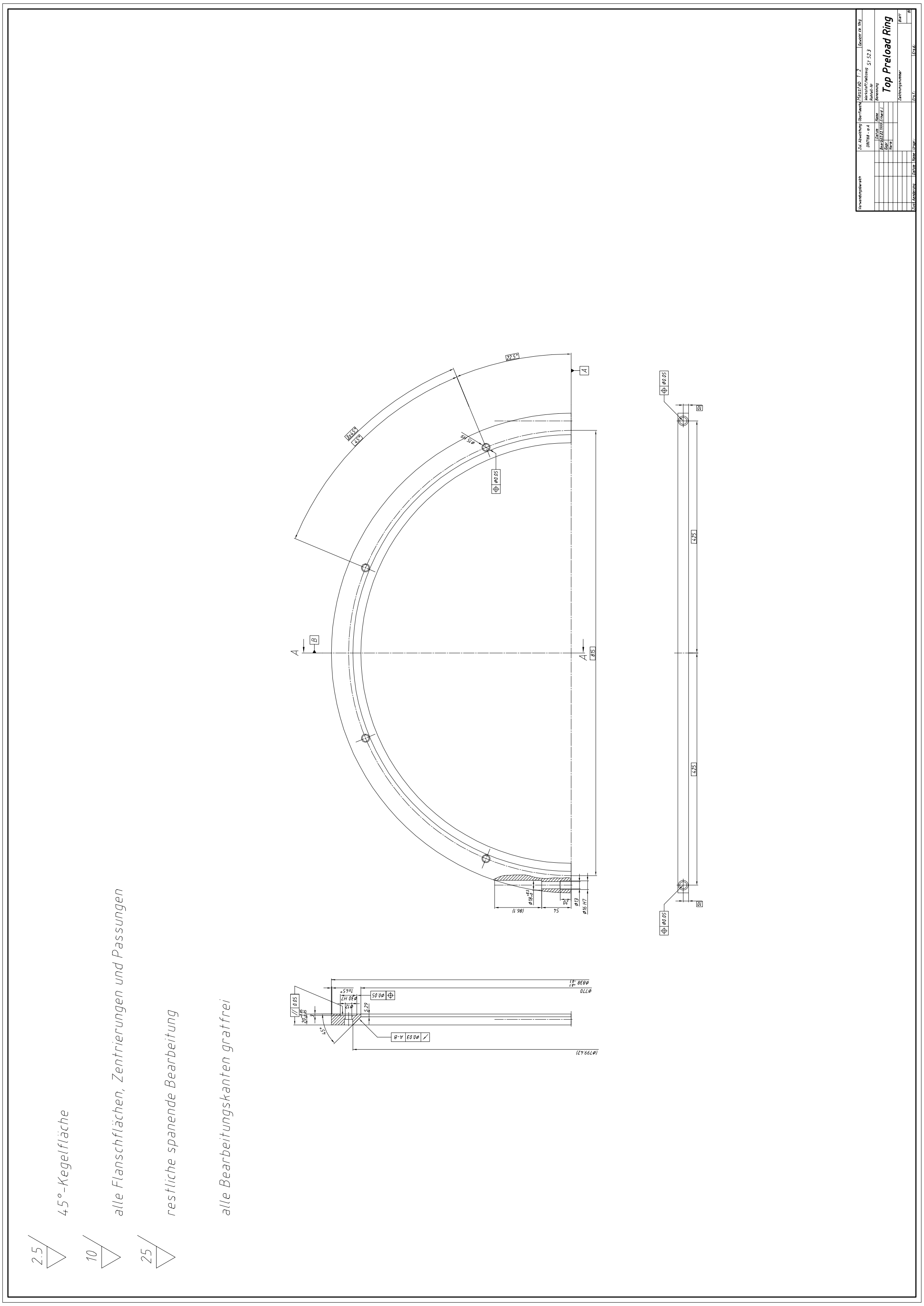
Top Preload Ring
45°-Kegelfläche
alle Flanschflächen, Zentrierungen und Passungen
restliche spanende Bearbeitung
alle Bearbeitungskanten gratfrei

8.3.8 Gear ring

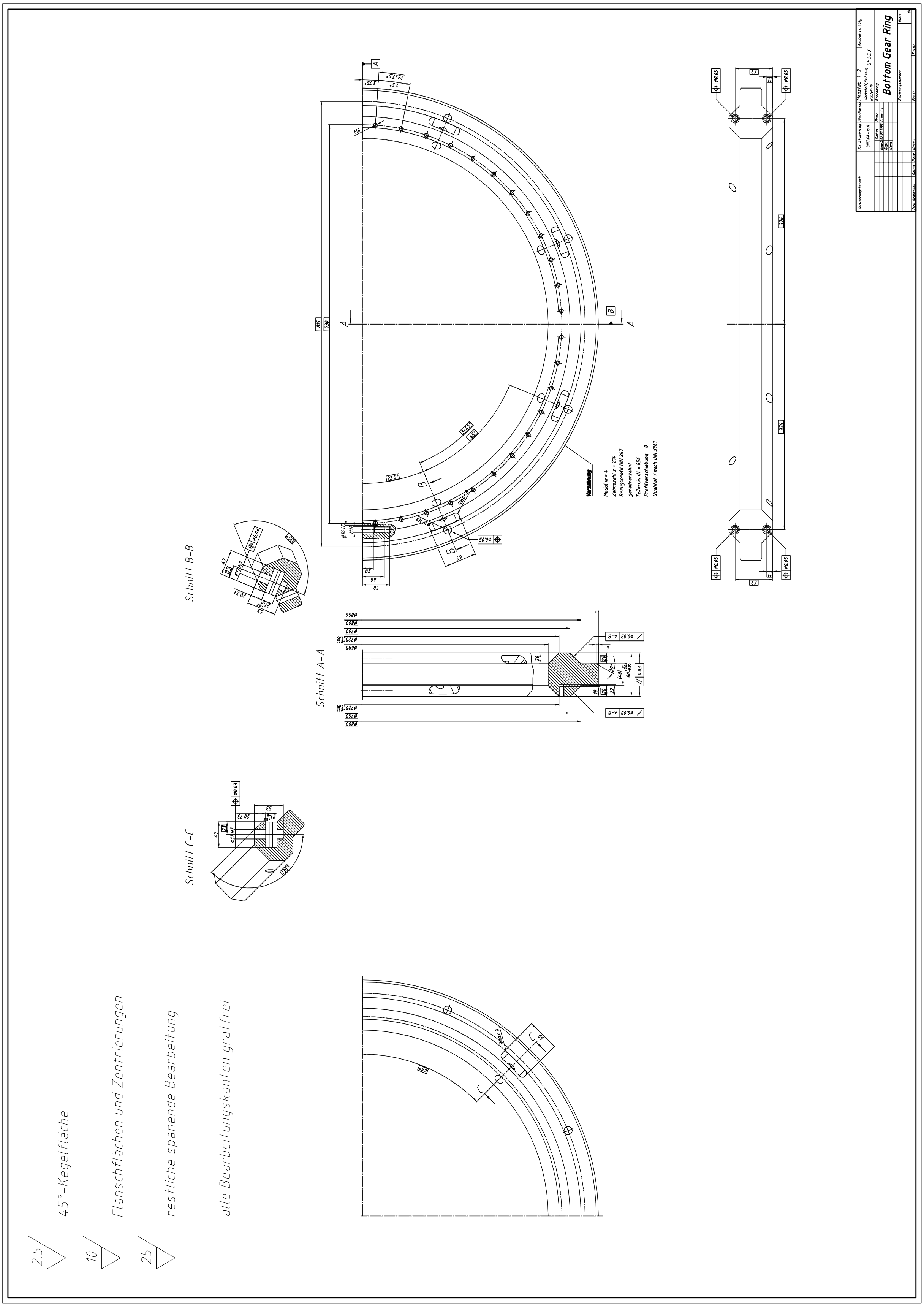

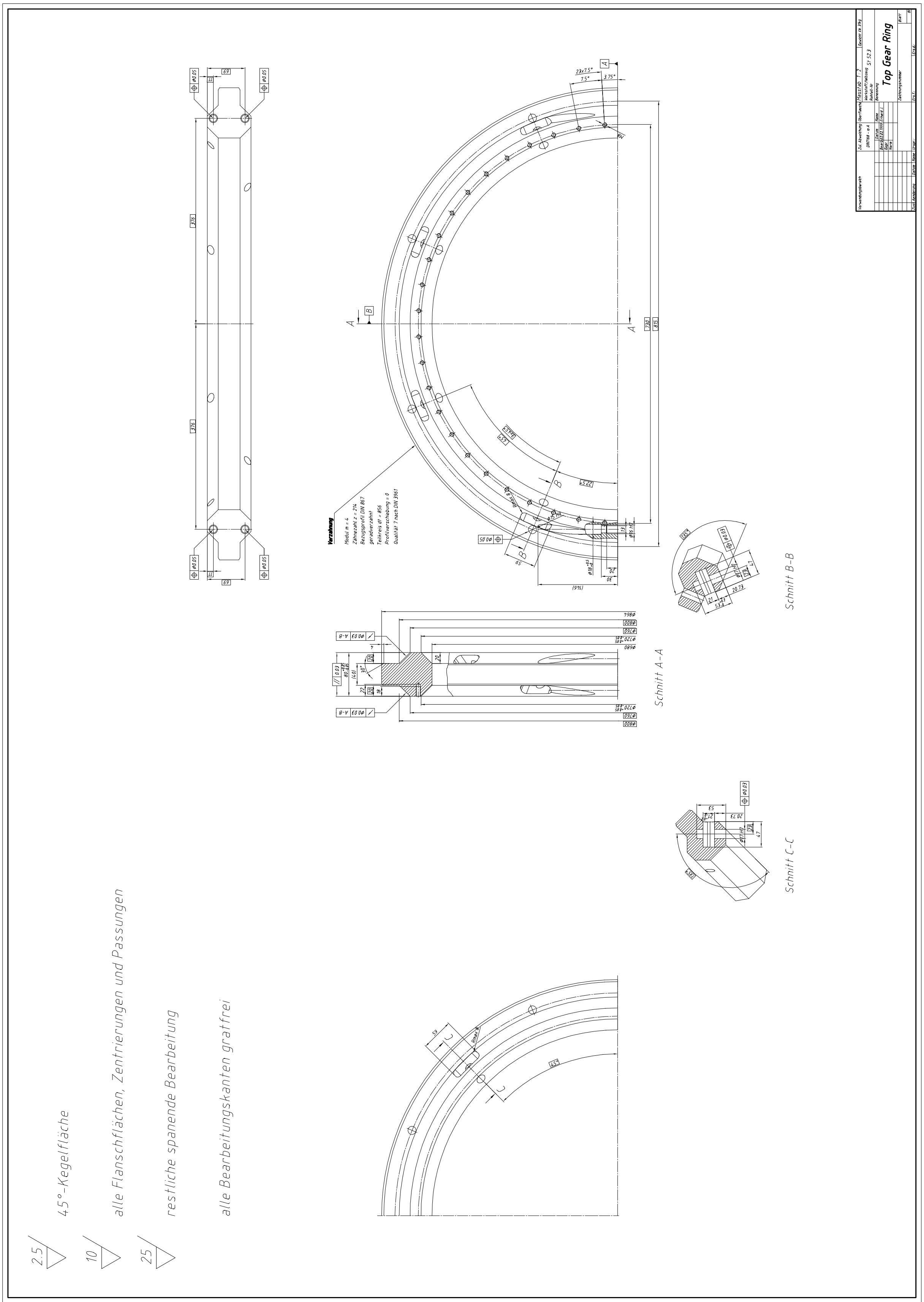
Top Gear Ring
Schnitt A-A
Schnitt B-B
Schnitt C-C
45°-Kegelfläche
alle Flanschflächen, Zentrierungen und Passungen
restliche spanende Bearbeitung
alle Bearbeitungskanten gratfrei

8.3.9 Bearing ring

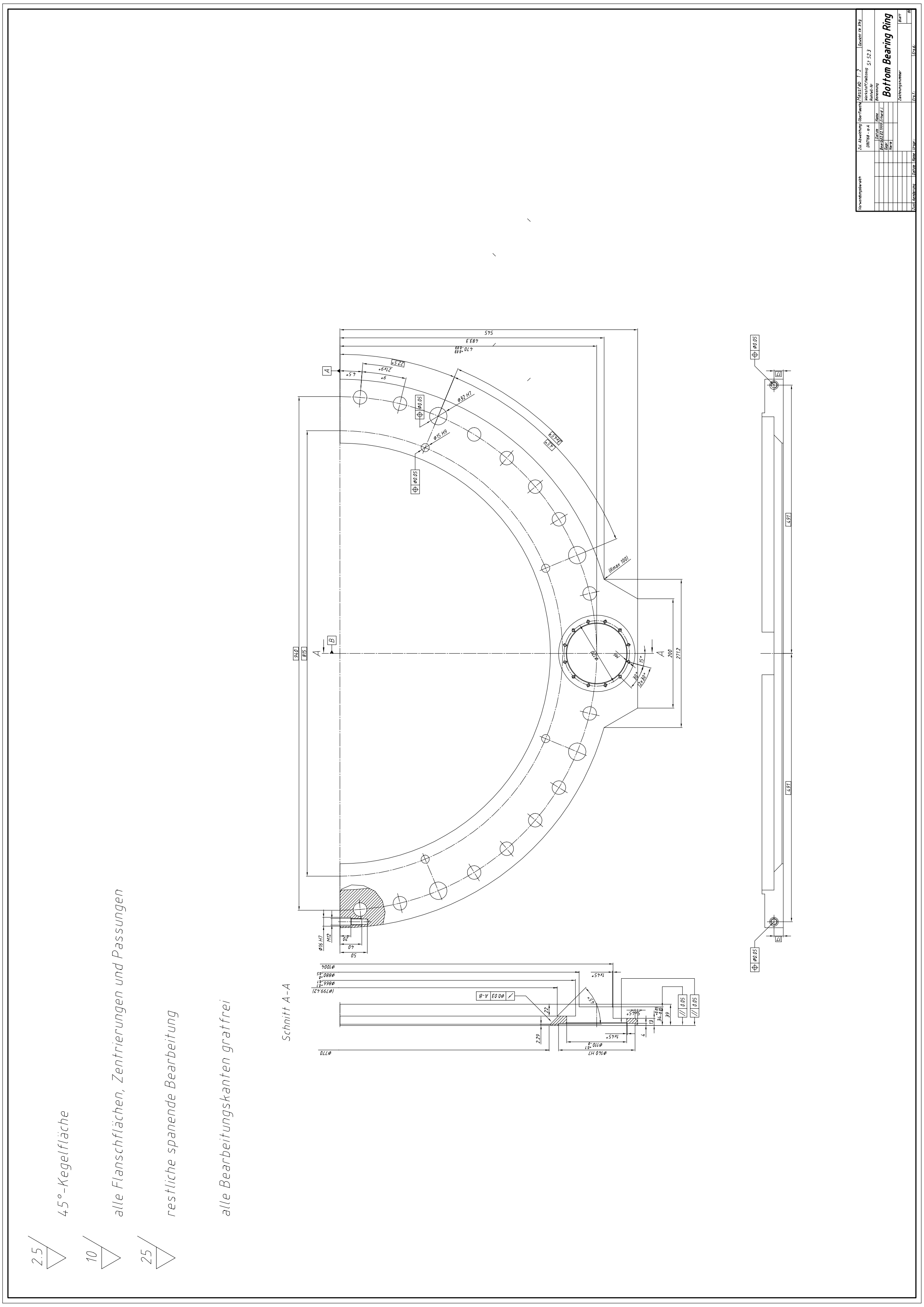

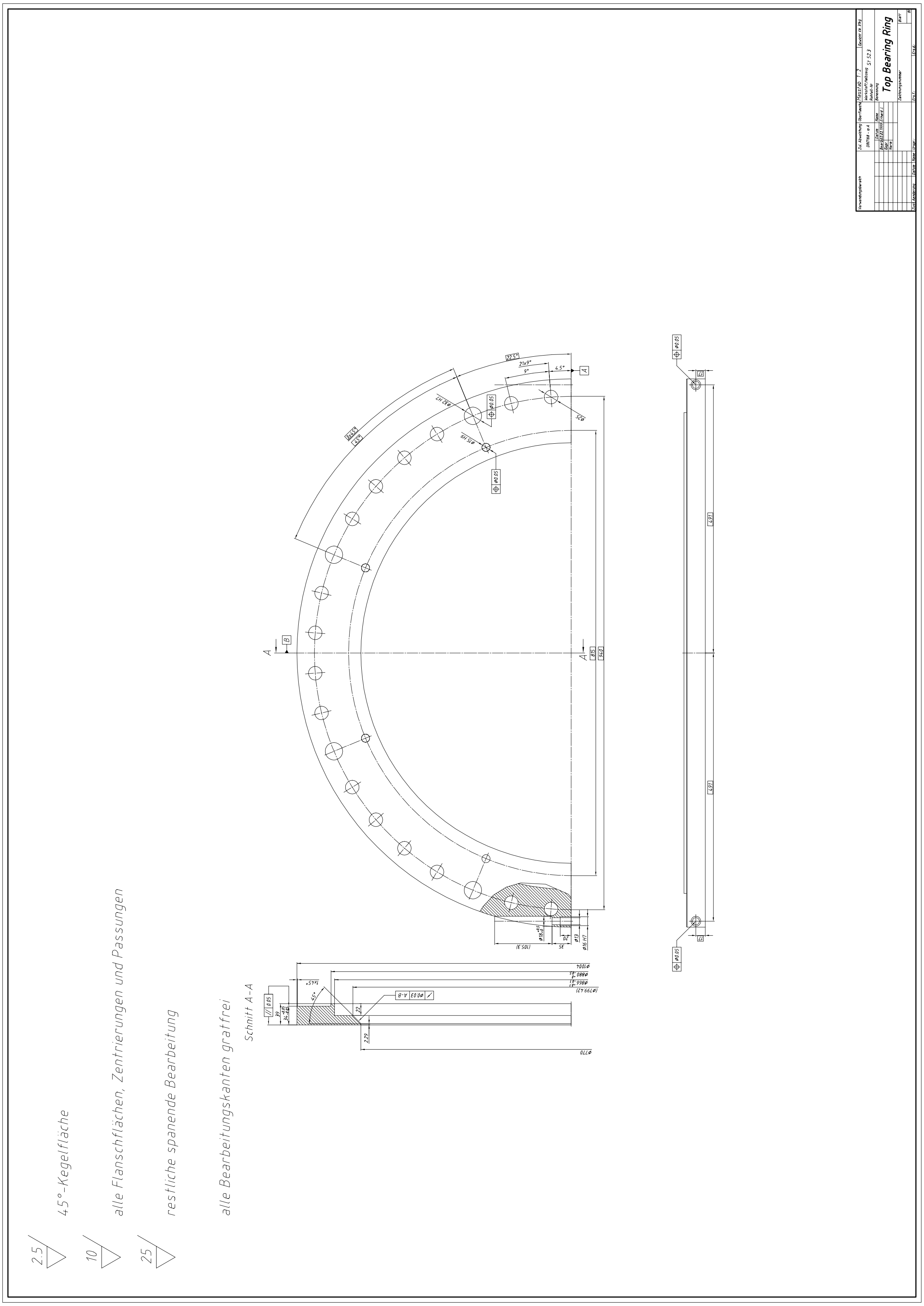
Top Bearing Ring
45°-Kegelfläche
alle Flanschflächen, Zentrierungen und Passungen
restliche spanende Bearbeitung
alle Bearbeitungskanten gratfrei
Schnitt A-A

8.3.10 Servo

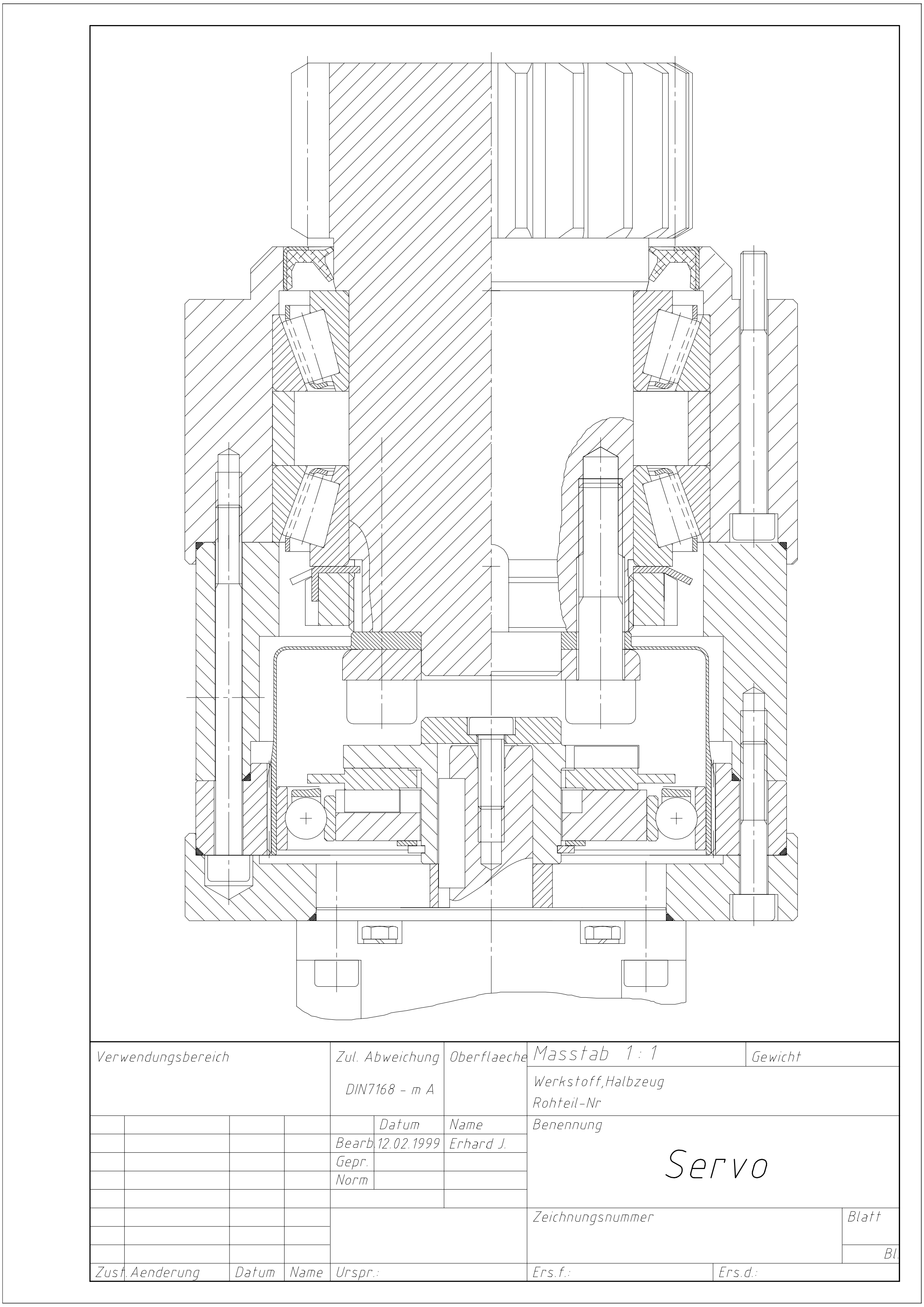
Verwendungsbereich
Zul. Abweichung
Oberflaeche
Masstab 1 : 1
Gewicht
DIN7168 - m A
Werkstoff,Halbzeug
Rohteil-Nr
Datum
Name
Benennung
Bearb
12.02.1999
Erhard J.
Gepr.
Norm
Servo
Zeichnungsnummer
Blatt
Bl
Zust.
Aenderung
Datum
Name
Urspr.:
Ers.f.:
Ers.d.:

8.3.11 Connection strut

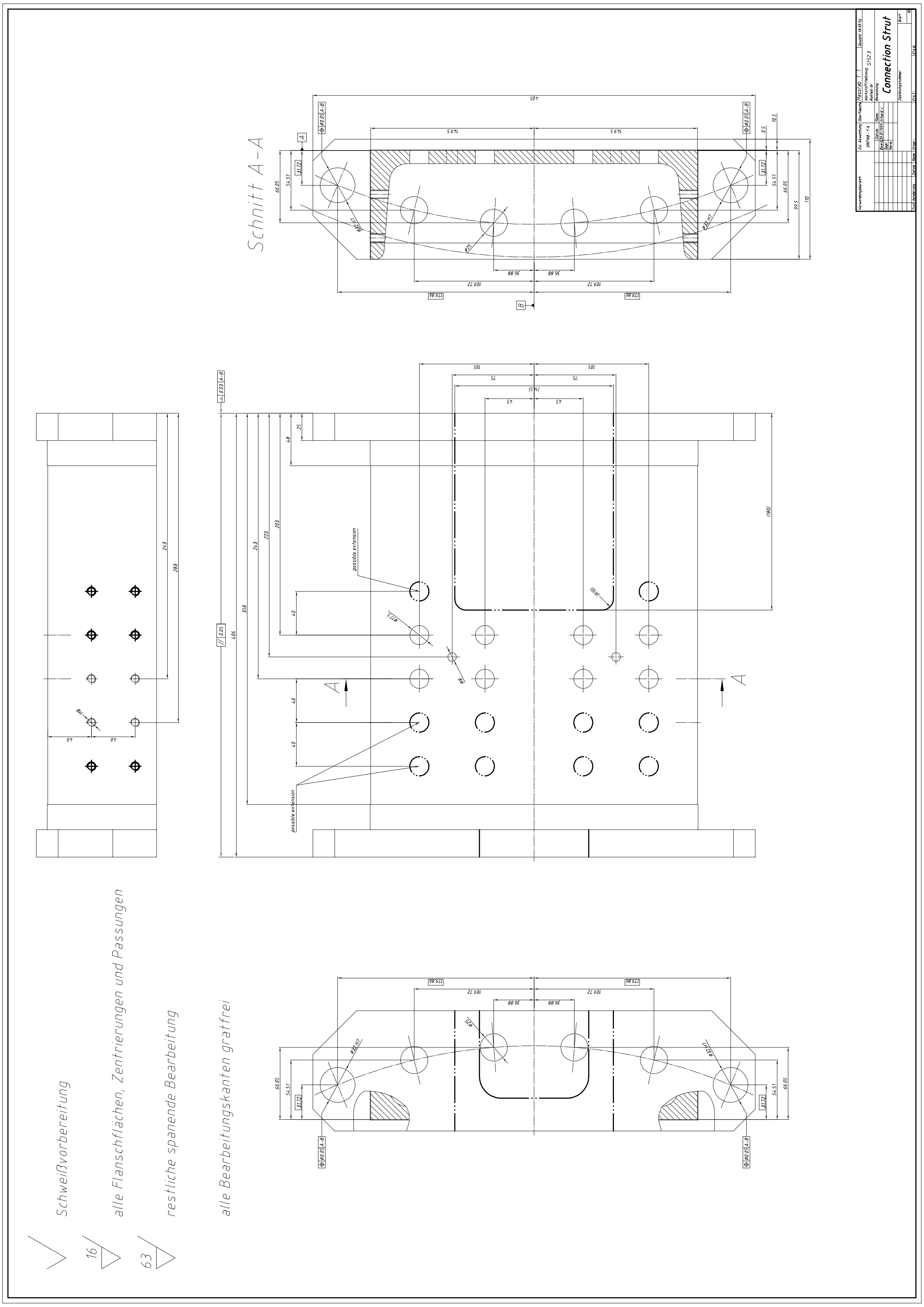

8.3.12 Centerline support

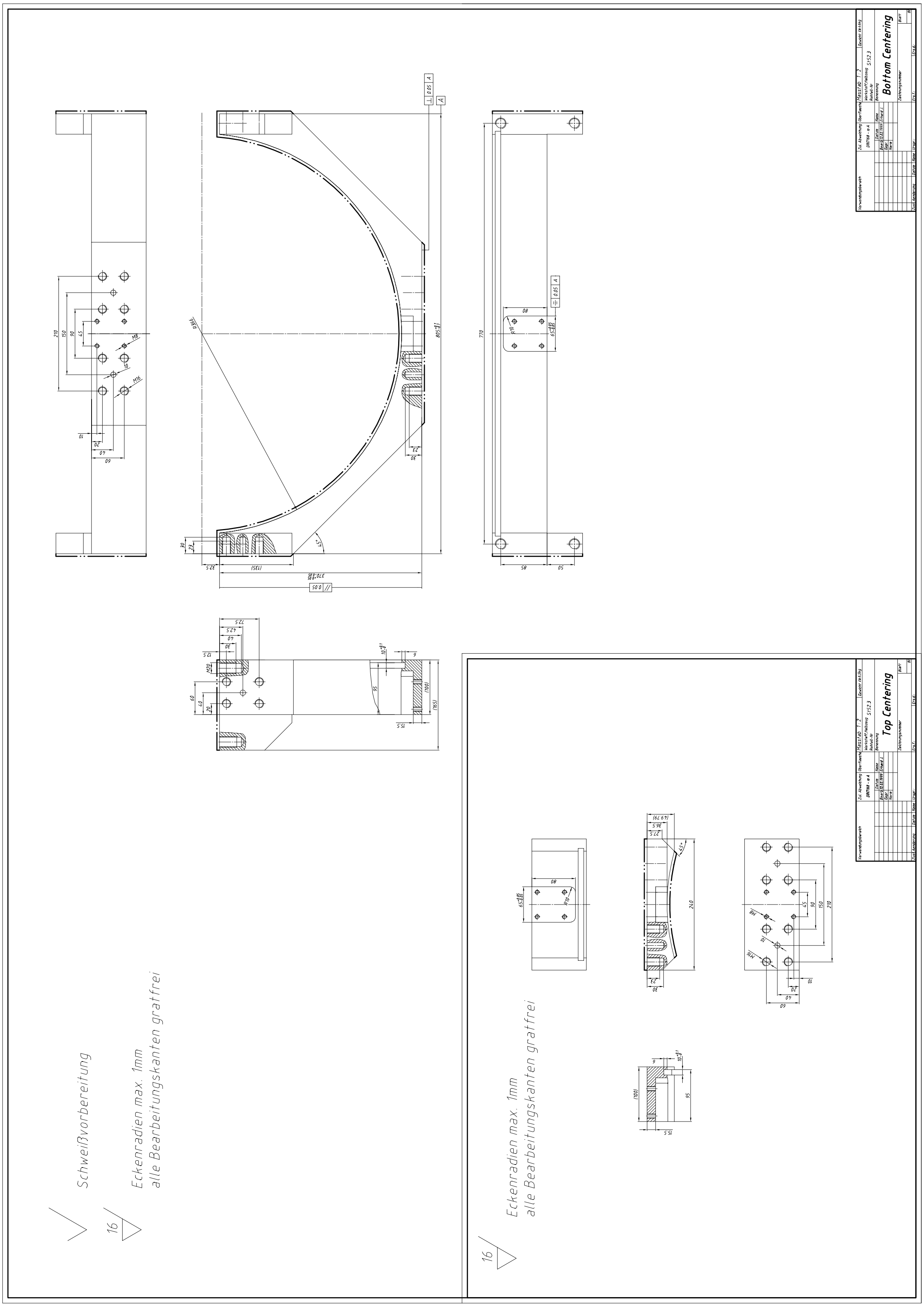

8.3.13 Guide vane casing

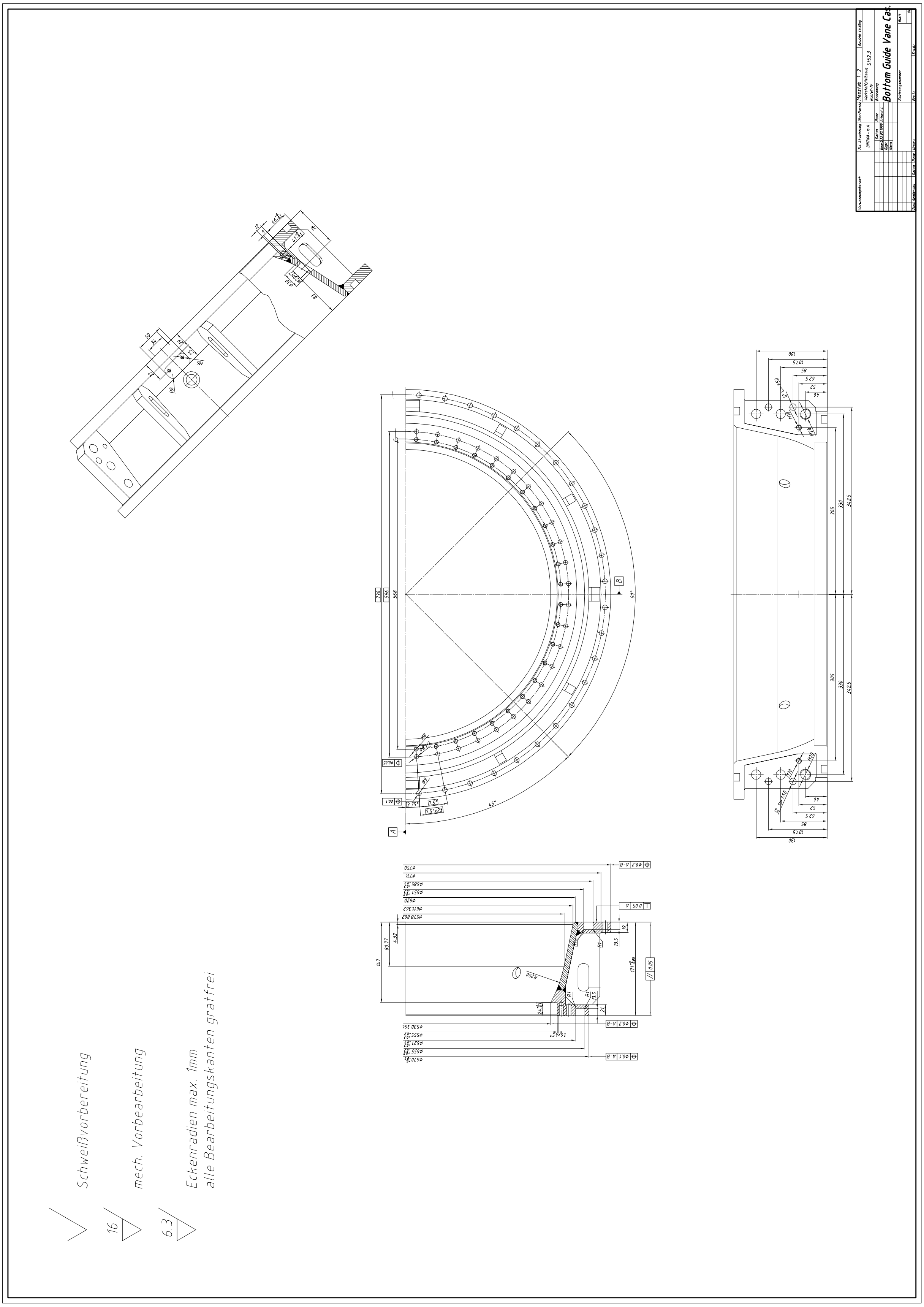

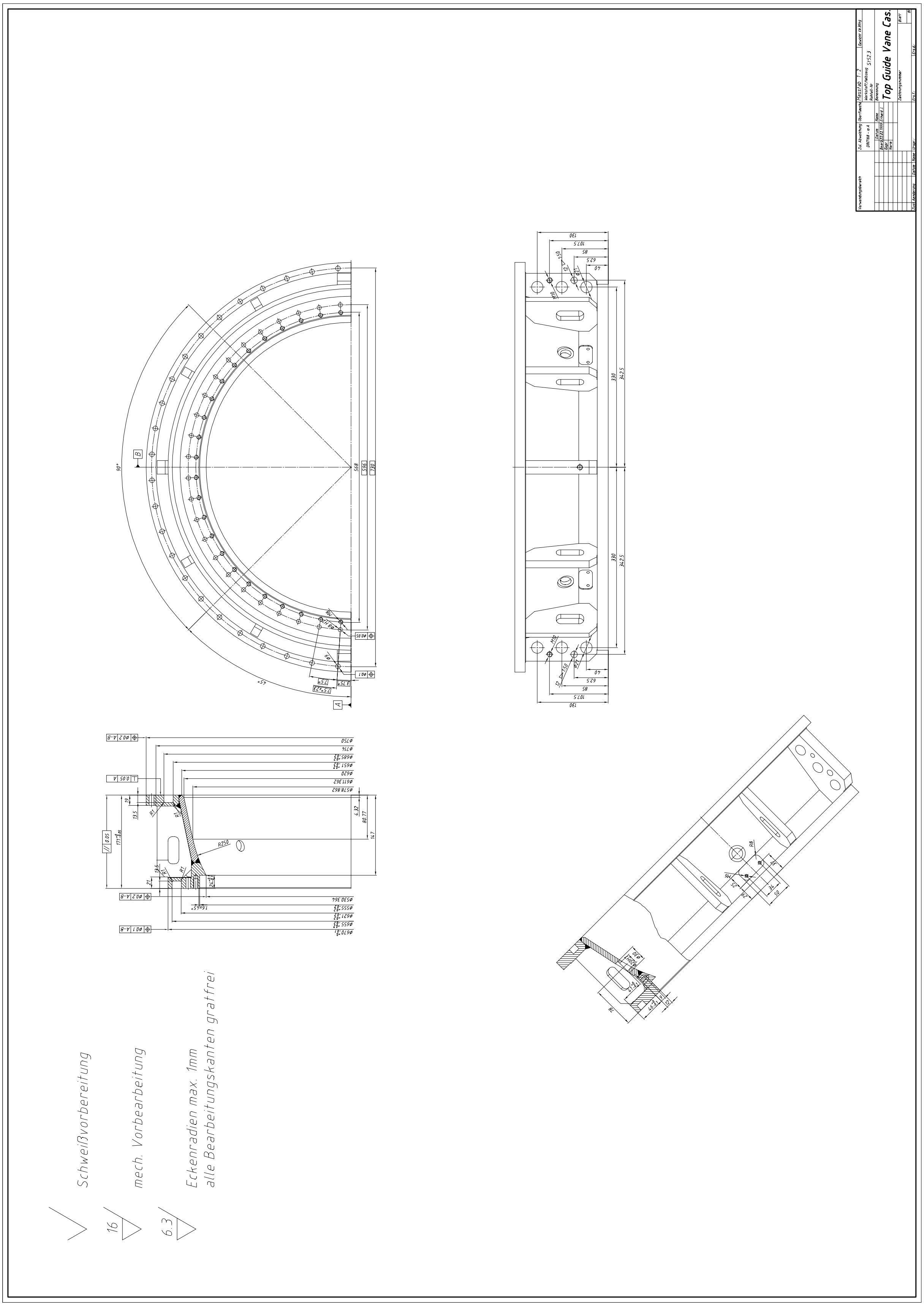
Top Guide Vane Cas.
Schweißvorbereitung
16 mech. Vorbearbeitung
6,3 Eckenradien max. 1mm
alle Bearbeitungskanten gratfrei

8.3.14 Rotor casing

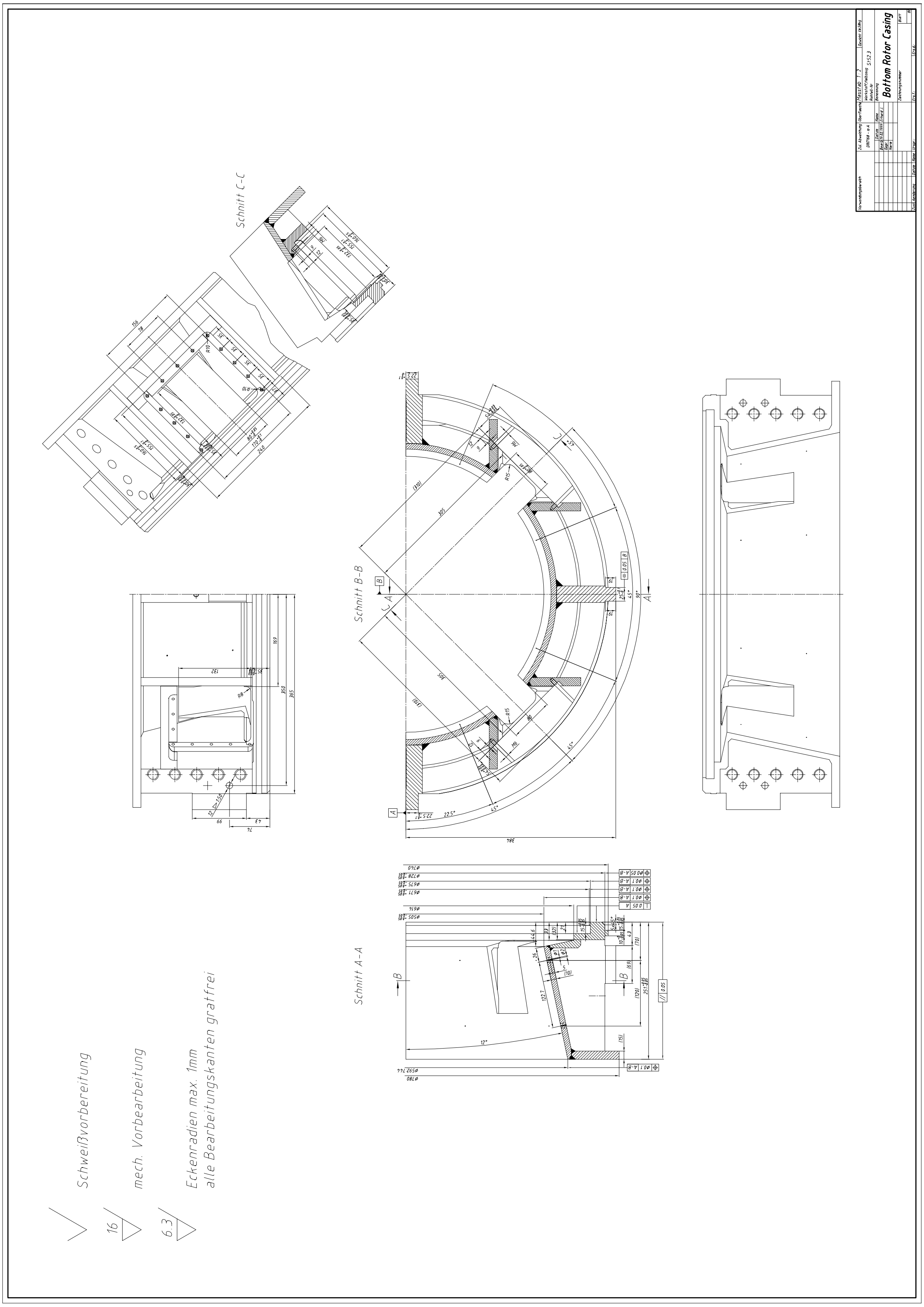

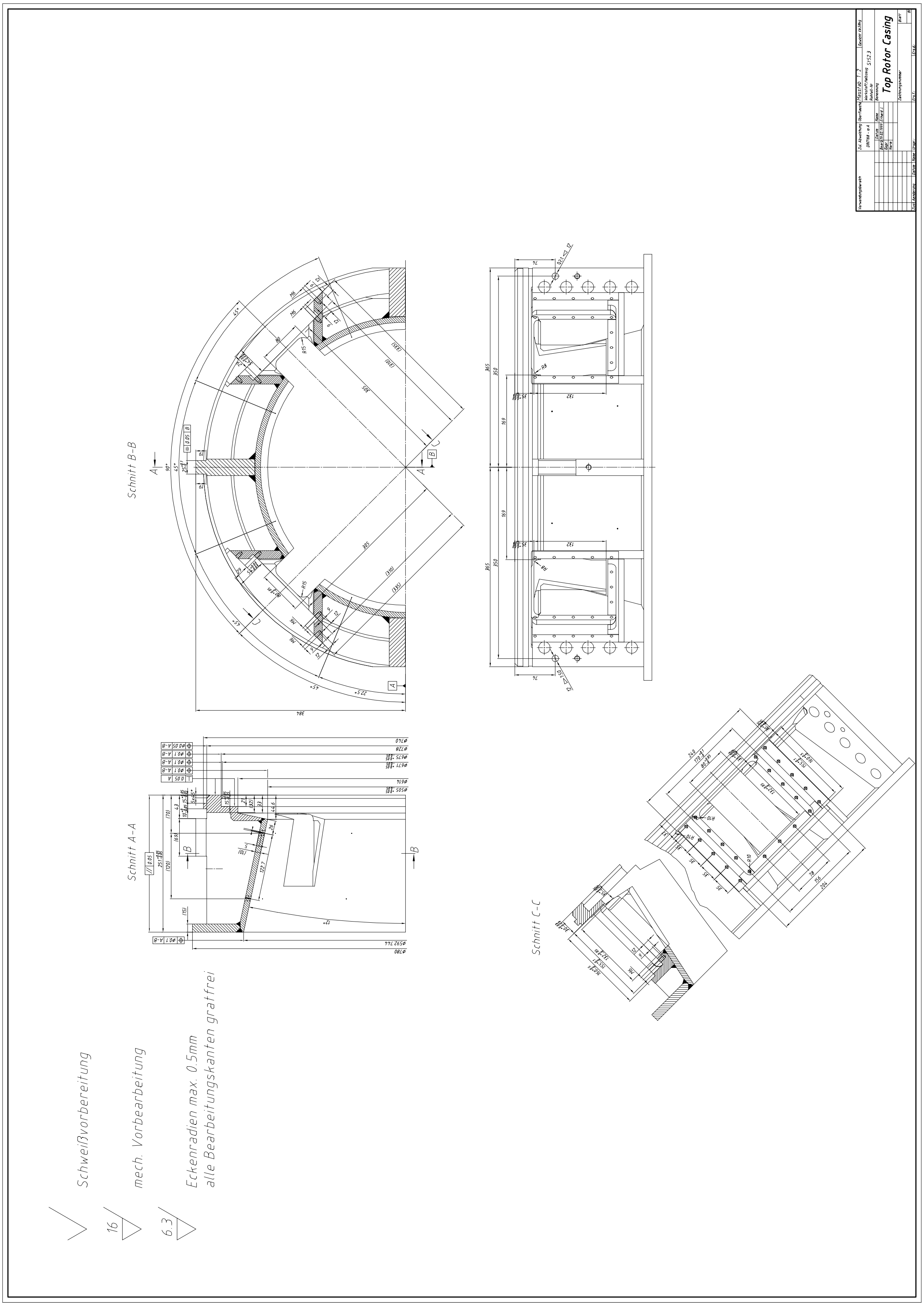
Top Rotor Casing
Schnitt B-B
Schnitt A-A
Schnitt C-C
Schweißvorbereitung
mech. Vorbearbeitung
Eckenradien max. 0.5mm
alle Bearbeitungskanten gratfrei

8.3.15 Diffuser collector

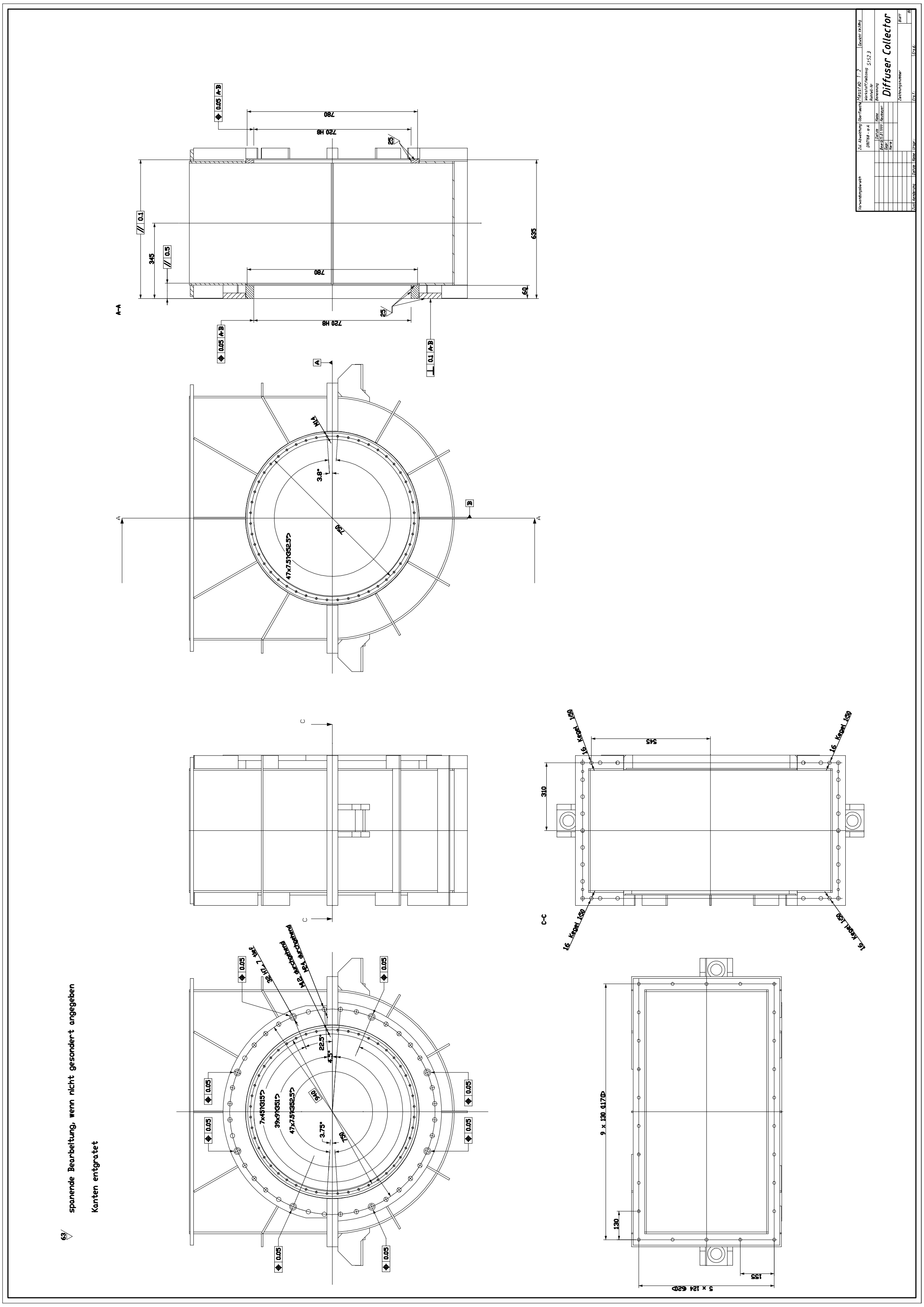

8.3.16 TTM-Stage discs

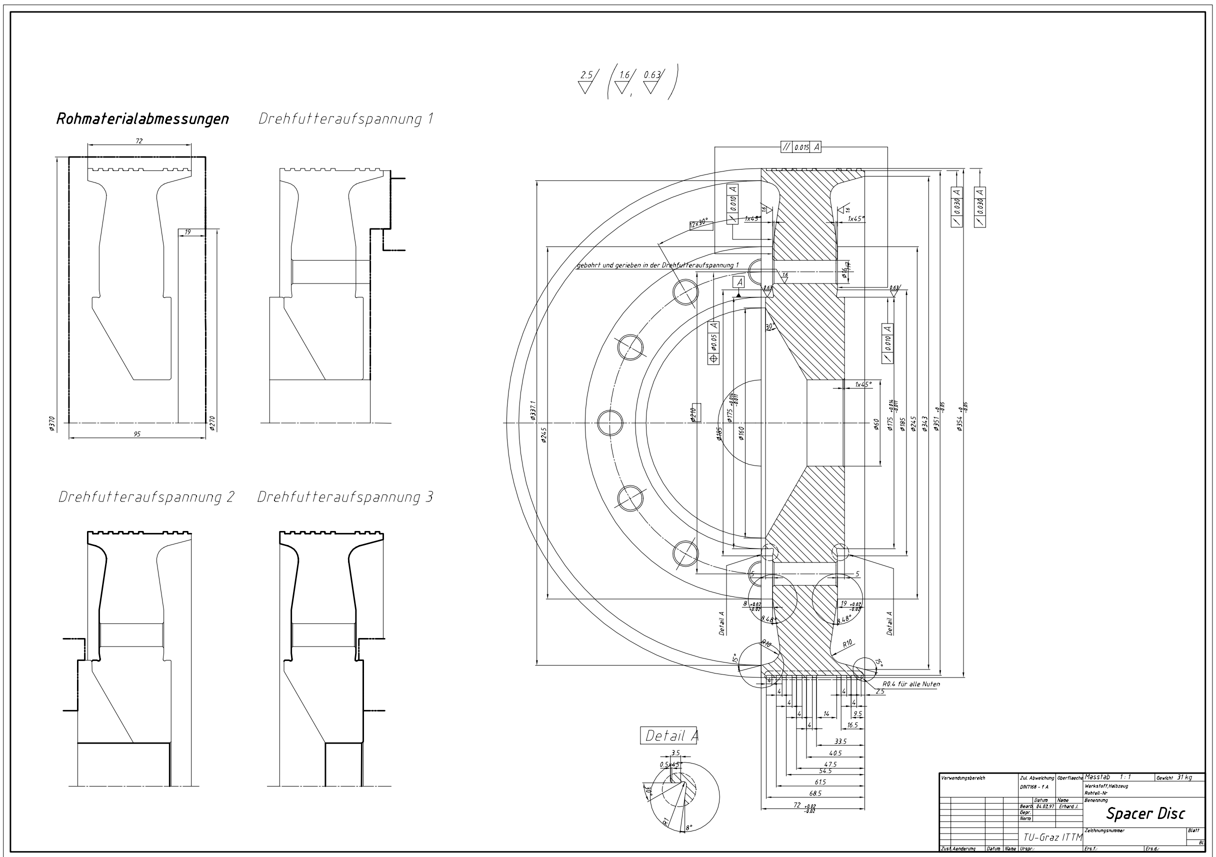

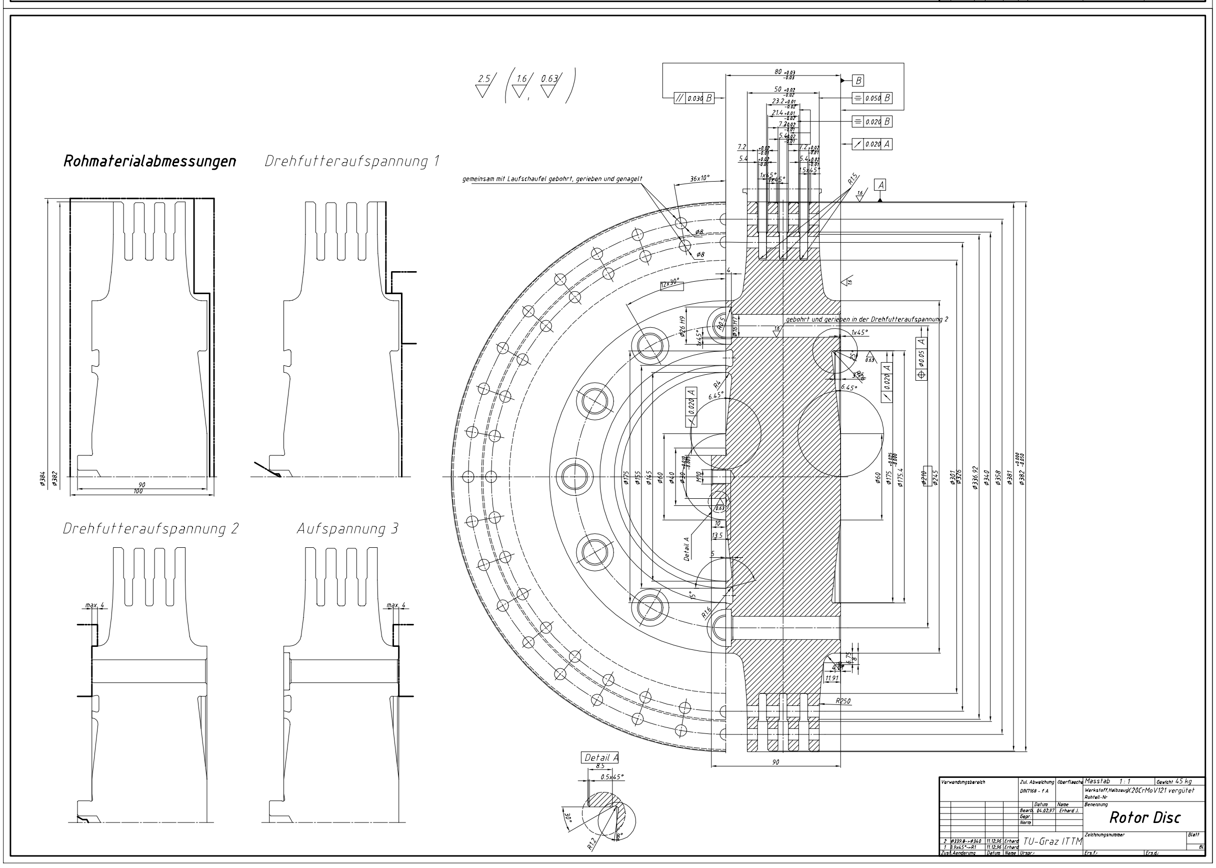

8.4 TTM-Stage blading

8.4.1 TTM-Stage guide vane

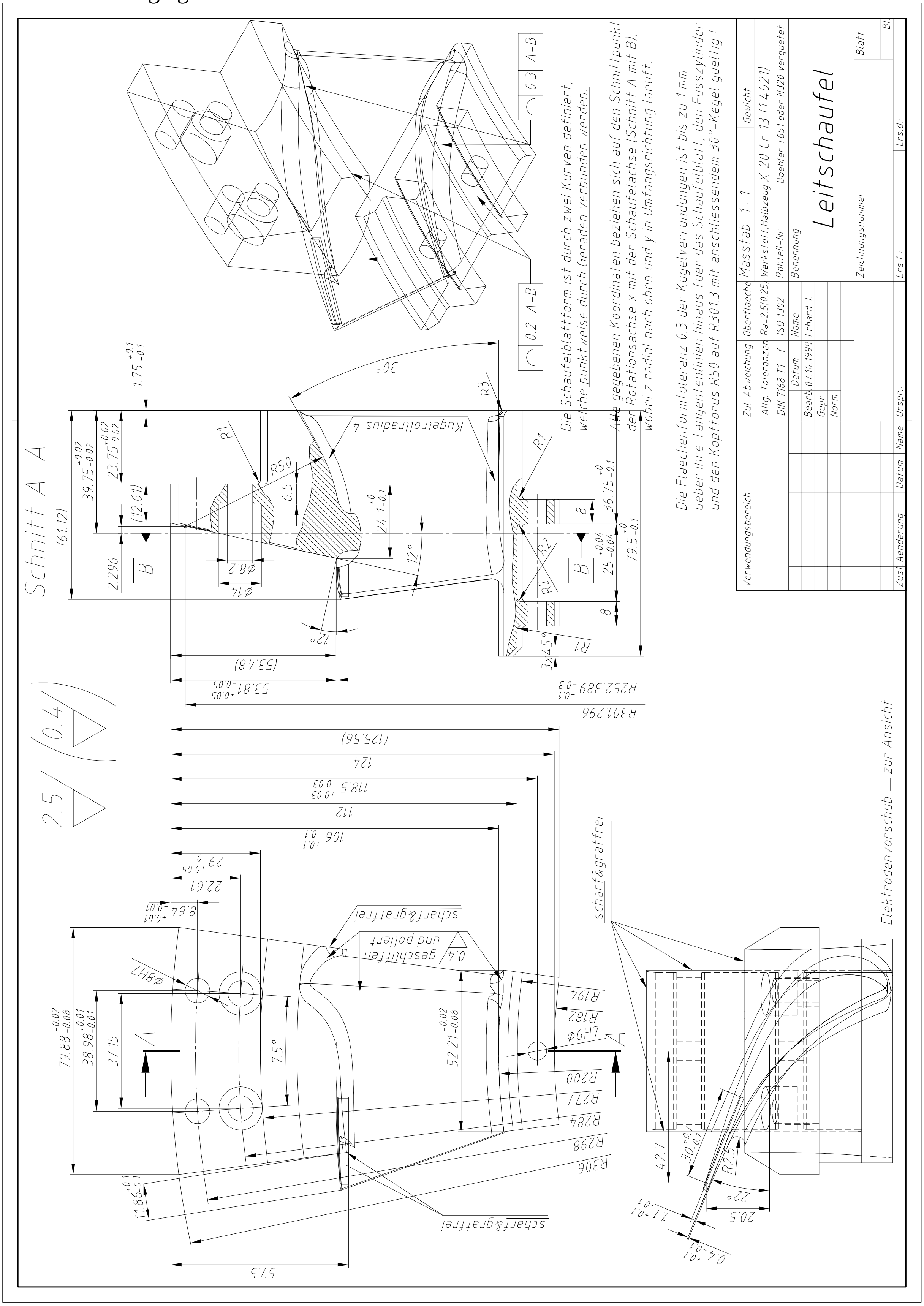

TTM-Stage Vane Sections								
Hub	200.000	0.000	Mean	229.000	0.000	Tip	258.000	0.000
pitch =	52.360					pitch =	67.500	
x_inlet =	-58.000					x_inlet =	-58.000	
x_outlet =	34.500					x_outlet =	34.500	
n =	82.000					n =	82.000	
i	x	y				i	x	y
					Midspan			
0	-0.038000	-0.018500		-0.038000	-0.020050		-0.038000	-0.021600
1	-0.037967	-0.018973		-0.037984	-0.020687		-0.038000	-0.022400
2	-0.037478	-0.019946		-0.037439	-0.021973		-0.037400	-0.024000
3	-0.036684	-0.020757		-0.036592	-0.023078		-0.036500	-0.025400
4	-0.035631	-0.021479		-0.035465	-0.024039		-0.035300	-0.026600
5	-0.034097	-0.022433		-0.033798	-0.025316		-0.033500	-0.028200
6	-0.032326	-0.023278		-0.031913	-0.026439		-0.031500	-0.029600
7	-0.030767	-0.023719		-0.030233	-0.027060		-0.029700	-0.030400
8	-0.028969	-0.024064		-0.028284	-0.027532		-0.027600	-0.031000
9	-0.027435	-0.024253		-0.026668	-0.027827		-0.025900	-0.031400
10	-0.025639	-0.024305		-0.024719	-0.027902		-0.023800	-0.031500
11	-0.024105	-0.024242		-0.023052	-0.027871		-0.022000	-0.031500
12	-0.022354	-0.024076		-0.021177	-0.027688		-0.020000	-0.031300
13	-0.020511	-0.023710		-0.019205	-0.027255		-0.017900	-0.030800
14	-0.018644	-0.023151		-0.017222	-0.026575		-0.015800	-0.030000
15	-0.017042	-0.022508		-0.015471	-0.025804		-0.013900	-0.029100
16	-0.015200	-0.021591		-0.013500	-0.024646		-0.011800	-0.027700
17	-0.013619	-0.020639		-0.011809	-0.023419		-0.010000	-0.026200
18	-0.011776	-0.019310		-0.009843	-0.021755		-0.007910	-0.024200
19	-0.009763	-0.017579		-0.007671	-0.019590		-0.005580	-0.021600
20	-0.007919	-0.015756		-0.005694	-0.017278		-0.003470	-0.018800
21	-0.006122	-0.013736		-0.003761	-0.014668		-0.001400	-0.015600
22	-0.004280	-0.011417		-0.001788	-0.011759		0.000703	-0.012100
23	-0.002482	-0.008866		0.000144	-0.008488		0.002770	-0.008110
24	-0.000639	-0.005959		0.002121	-0.004789		0.004880	-0.003620
25	0.000940	-0.003190		0.003810	-0.001262		0.006680	0.000665
26	0.002737	0.000250		0.005744	0.003130		0.008750	0.006010
27	0.004352	0.003467		0.007476	0.007233		0.010600	0.011000
28	0.005726	0.006389		0.008913	0.010894		0.012100	0.015400
29	0.007306	0.009931		0.010603	0.015416		0.013900	0.020900
30	0.008886	0.013613		0.012293	0.020107		0.015700	0.026600
31	0.010297	0.016867		0.013798	0.024184		0.017300	0.031500
32	0.011874	0.020575		0.015487	0.028888		0.019100	0.037200
33	0.013237	0.023755		0.016968	0.032928		0.020700	0.042100
34	0.013379	0.024078		0.017140	0.033339		0.020900	0.042600
35	0.013521	0.024401		0.017261	0.033801		0.021000	0.043200
36	0.013664	0.024724		0.017432	0.034212		0.021200	0.043700
37	0.013806	0.025047		0.017603	0.034623		0.021400	0.044200
38	0.013948	0.025370		0.017774	0.035085		0.021600	0.044800
39	0.014090	0.025693		0.017895	0.035496		0.021700	0.045300
40	0.014032	0.026241		0.017816	0.036120		0.021600	0.046000
41	0.013756	0.026497		0.017428	0.036399		0.021100	0.046300
42	0.013283	0.026480		0.016992	0.036340		0.020700	0.046200
43	0.012824	0.026254		0.016512	0.036077		0.020200	0.045900
44	0.012629	0.025946		0.016315	0.035673		0.020000	0.045400
45	0.012435	0.025638		0.016117	0.035269		0.019800	0.044900
46	0.012240	0.025330		0.015870	0.034915		0.019500	0.044500
47	0.012045	0.025022		0.015673	0.034511		0.019300	0.044000
48	0.011851	0.024714		0.015475	0.034107		0.019100	0.043500
49	0.011656	0.024406		0.015278	0.033703		0.018900	0.043000
50	0.010096	0.021748		0.013598	0.030374		0.017100	0.039000
51	0.008471	0.018965		0.011835	0.026832		0.015200	0.034700
52	0.006714	0.016059		0.010007	0.023180		0.013300	0.030300
53	0.005133	0.013561		0.008316	0.019981		0.011500	0.026400

54	0.003553	0.011239	0.006601	0.017020	0.009650	0.022800
55	0.001993	0.009120	0.004942	0.014310	0.007890	0.019500
56	0.000171	0.006835	0.002996	0.011367	0.005820	0.015900
57	-0.001430	0.004944	0.001275	0.008922	0.003980	0.012900
58	-0.003009	0.003233	-0.000420	0.006716	0.002170	0.010200
59	-0.004852	0.001390	-0.002394	0.004375	0.000064	0.007360
60	-0.006450	-0.000098	-0.004115	0.002456	-0.001780	0.005010
61	-0.008294	-0.001672	-0.006092	0.000444	-0.003890	0.002560
62	-0.009894	-0.002948	-0.007812	-0.001194	-0.005730	0.000560
63	-0.011736	-0.004309	-0.009783	-0.002925	-0.007830	-0.001540
64	-0.013356	-0.005433	-0.011533	-0.004366	-0.009710	-0.003300
65	-0.015200	-0.006623	-0.013500	-0.005866	-0.011800	-0.005110
66	-0.016780	-0.007584	-0.015190	-0.007067	-0.013600	-0.006550
67	-0.018622	-0.008649	-0.017161	-0.008400	-0.015700	-0.008150
68	-0.020320	-0.009596	-0.019010	-0.009568	-0.017700	-0.009540
69	-0.022289	-0.010651	-0.021094	-0.010876	-0.019900	-0.011100
70	-0.024131	-0.011576	-0.023066	-0.011988	-0.022000	-0.012400
71	-0.025487	-0.012213	-0.024543	-0.012756	-0.023600	-0.013300
72	-0.026824	-0.012829	-0.025962	-0.013515	-0.025100	-0.014200
73	-0.028423	-0.013547	-0.027712	-0.014373	-0.027000	-0.015200
74	-0.029759	-0.014122	-0.029129	-0.015061	-0.028500	-0.016000
75	-0.031359	-0.014796	-0.030879	-0.015848	-0.030400	-0.016900
76	-0.032833	-0.015407	-0.032467	-0.016553	-0.032100	-0.017700
77	-0.034294	-0.015962	-0.033997	-0.017181	-0.033700	-0.018400
78	-0.035631	-0.016454	-0.035465	-0.017727	-0.035300	-0.019000
79	-0.036684	-0.016924	-0.036592	-0.018262	-0.036500	-0.019600
80	-0.037497	-0.017481	-0.037449	-0.018891	-0.037400	-0.020300
81	-0.037913	-0.018182	-0.037907	-0.019691	-0.037900	-0.021200
82	-0.038000	-0.018500	-0.038000	-0.020050	-0.038000	-0.021600

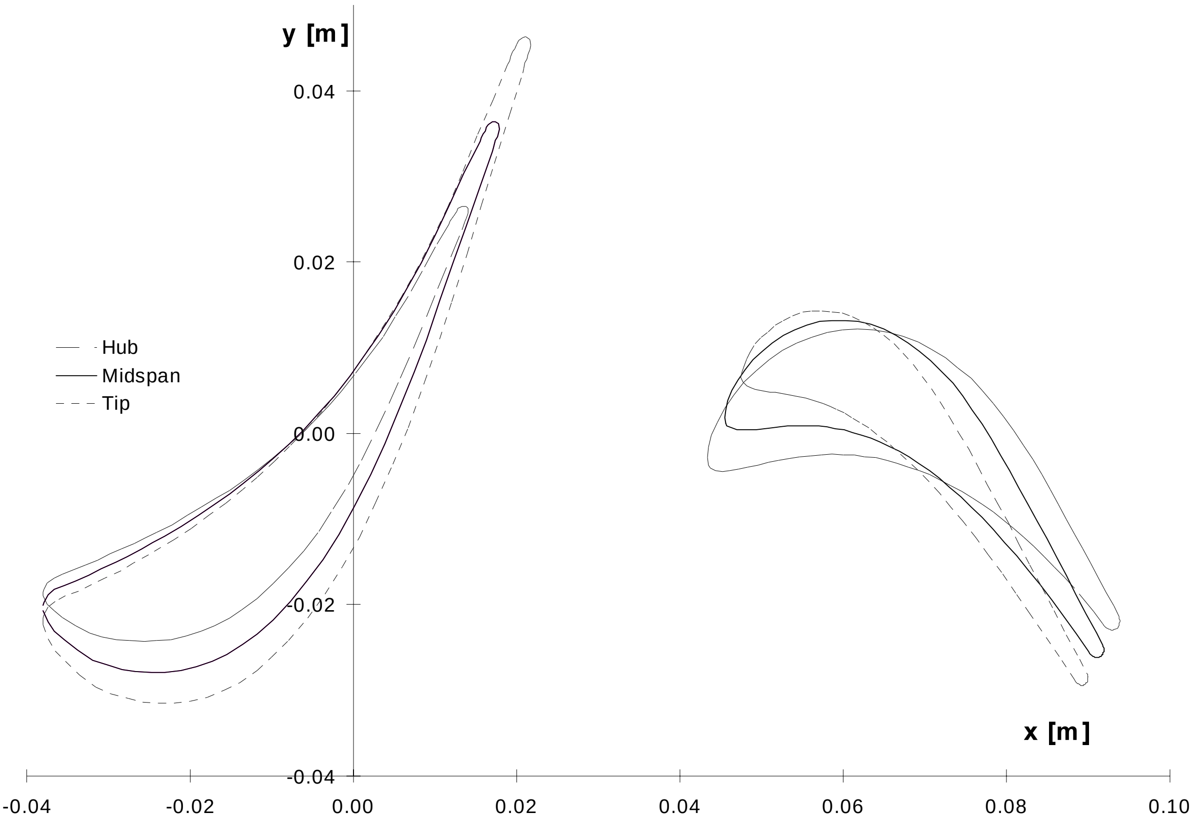

8.4.2 TTM-Stage rotor blade

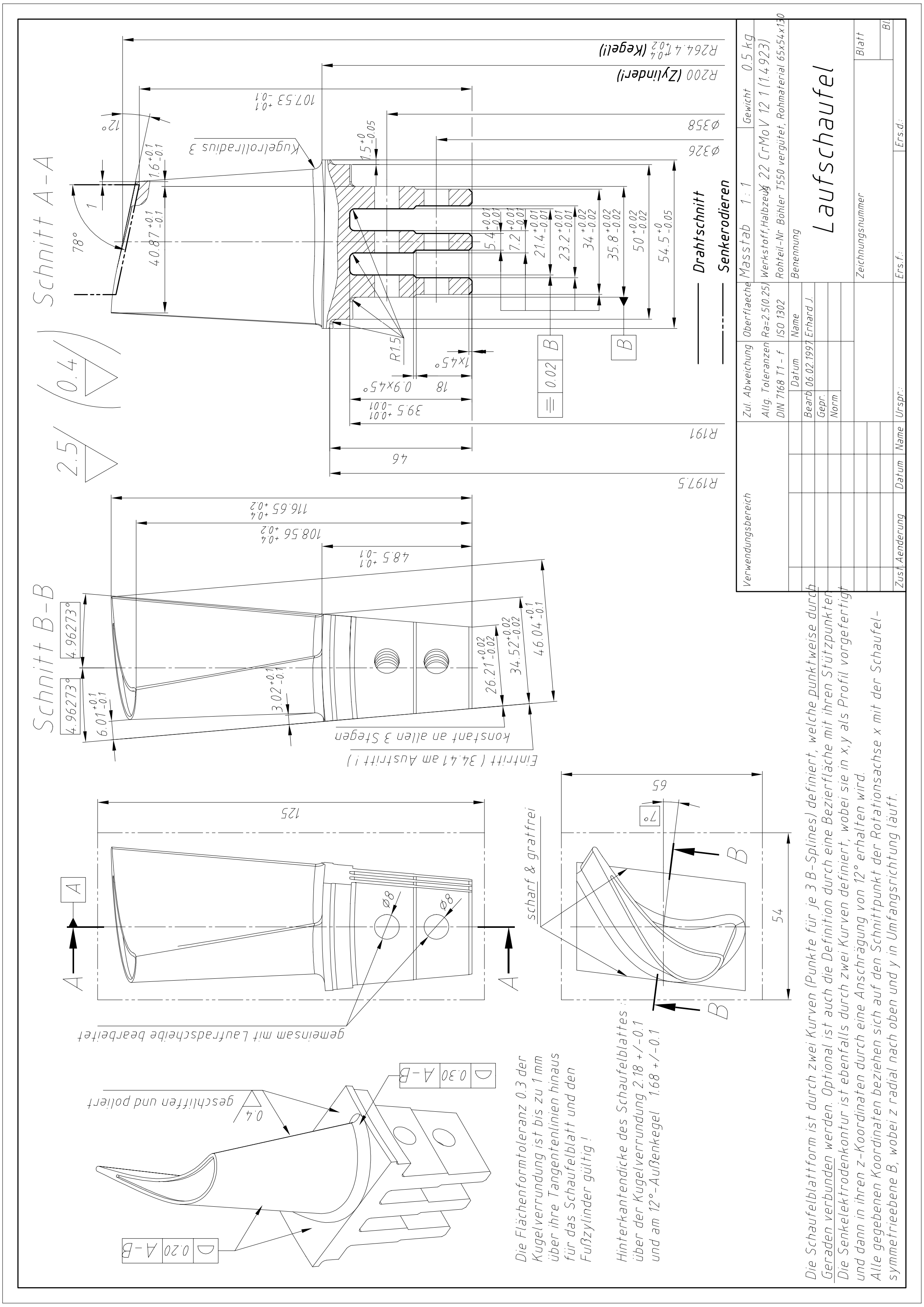

TTM-Stage Blade Sections								
Hub	200.000	67.000	Mean	232.789	67.000	Tip	265.577	67.000
pitch =	34.907					pitch =	46.400	
x_inlet =	-32.500					x_inlet =	-32.500	
x_outlet =	55.000					x_outlet =	55.000	
n =	207.000					n =	207.000	
i	x	y				i	x	y
		Hub			Midspan			Tip
0	0.043523	-0.003727		0.045612	0.001141		0.047700	0.006010
2	0.043324	-0.002851		0.045412	0.001819		0.047500	0.006490
4	0.043457	-0.001639		0.045528	0.002736		0.047600	0.007110
6	0.043882	-0.000213		0.045841	0.003819		0.047800	0.007850
8	0.044565	0.001330		0.046382	0.004995		0.048200	0.008660
10	0.045476	0.002911		0.047038	0.006206		0.048600	0.009500
12	0.046586	0.004469		0.047893	0.007435		0.049200	0.010400
14	0.047872	0.005956		0.048936	0.008578		0.050000	0.011200
16	0.049308	0.007333		0.050054	0.009616		0.050800	0.011900
18	0.050873	0.008570		0.051287	0.010585		0.051700	0.012600
20	0.052544	0.009646		0.052622	0.011423		0.052700	0.013200
22	0.054301	0.010543		0.054050	0.012121		0.053800	0.013700
24	0.056122	0.011250		0.055561	0.012675		0.055000	0.014100
26	0.057989	0.011759		0.057095	0.013030		0.056200	0.014300
28	0.059882	0.012067		0.058636	0.013184		0.057390	0.014300
30	0.061782	0.012172		0.060211	0.013186		0.058640	0.014200
32	0.063673	0.012076		0.061792	0.013038		0.059910	0.014000
34	0.065540	0.011782		0.063360	0.012691		0.061180	0.013600
36	0.067369	0.011297		0.064909	0.012149		0.062450	0.013000
38	0.069147	0.010629		0.066423	0.011465		0.063700	0.012300
40	0.070866	0.009789		0.067903	0.010595		0.064940	0.011400
42	0.072517	0.008789		0.069338	0.009594		0.066158	0.010400
44	0.074097	0.007641		0.070726	0.008481		0.067354	0.009320
46	0.075603	0.006363		0.072067	0.007212		0.068530	0.008060
48	0.077035	0.004970		0.073357	0.005825		0.069680	0.006680
50	0.078394	0.003480		0.074612	0.004330		0.070830	0.005180
52	0.079685	0.001909		0.075823	0.002740		0.071960	0.003570
54	0.080913	0.000276		0.076997	0.001068		0.073080	0.001860
56	0.082085	-0.001403		0.078148	-0.000681		0.074210	0.000042
58	0.083208	-0.003112		0.079279	-0.002496		0.075350	-0.001880
60	0.084288	-0.004839		0.080399	-0.004365		0.076510	-0.003890
62	0.085335	-0.006573		0.081517	-0.006287		0.077700	-0.006000
64	0.086354	-0.008305		0.082627	-0.008258		0.078900	-0.008210
66	0.087351	-0.010030		0.083775	-0.010265		0.080200	-0.010500
68	0.088332	-0.011745		0.084916	-0.012323		0.081500	-0.012900
70	0.089301	-0.013450		0.086050	-0.014425		0.082800	-0.015400
72	0.090261	-0.015145		0.087280	-0.016573		0.084300	-0.018000
74	0.091216	-0.016833		0.088508	-0.018767		0.085800	-0.020700
76	0.092167	-0.018516		0.089734	-0.021008		0.087300	-0.023500
78	0.093118	-0.020196		0.091009	-0.023298		0.088900	-0.026400
80	0.093646	-0.021132		0.091723	-0.024566		0.089800	-0.028000
82	0.093734	-0.021324		0.091817	-0.024712		0.089900	-0.028100
84	0.093799	-0.021509		0.091849	-0.024905		0.089900	-0.028300
86	0.093841	-0.021687		0.091871	-0.025044		0.089900	-0.028400
88	0.093863	-0.021857		0.091882	-0.025179		0.089900	-0.028500
90	0.093866	-0.022018		0.091883	-0.025309		0.089900	-0.028600
92	0.093850	-0.022170		0.091875	-0.025485		0.089900	-0.028800
94	0.093817	-0.022310		0.091858	-0.025605		0.089900	-0.028900
96	0.093768	-0.022440		0.091834	-0.025720		0.089900	-0.029000
98	0.093704	-0.022557		0.091752	-0.025828		0.089800	-0.029100
100	0.093626	-0.022661		0.091663	-0.025880		0.089700	-0.029100
102	0.093536	-0.022751		0.091618	-0.025975		0.089700	-0.029200
104	0.093435	-0.022826		0.091518	-0.026063		0.089600	-0.029300
106	0.093324	-0.022886		0.091412	-0.026093		0.089500	-0.029300

108	0.093204	-0.022929	0.091302	-0.026165	0.089400	-0.029400
110	0.093076	-0.022955	0.091188	-0.026178	0.089300	-0.029400
112	0.092942	-0.022963	0.091071	-0.026182	0.089200	-0.029400
114	0.092803	-0.022953	0.090951	-0.026176	0.089100	-0.029400
116	0.092660	-0.022922	0.090830	-0.026111	0.089000	-0.029300
118	0.092513	-0.022871	0.090707	-0.026086	0.088900	-0.029300
120	0.092365	-0.022799	0.090583	-0.025999	0.088800	-0.029200
122	0.092217	-0.022704	0.090458	-0.025952	0.088700	-0.029200
124	0.092069	-0.022587	0.090335	-0.025843	0.088600	-0.029100
126	0.091924	-0.022445	0.090162	-0.025723	0.088400	-0.029000
128	0.091781	-0.022279	0.090040	-0.025540	0.088300	-0.028800
130	0.090627	-0.020850	0.088514	-0.023475	0.086400	-0.026100
134	0.088271	-0.018122	0.085535	-0.019561	0.082800	-0.021000
136	0.087070	-0.016827	0.084085	-0.017714	0.081100	-0.018600
138	0.085856	-0.015580	0.082628	-0.015940	0.079400	-0.016300
140	0.084630	-0.014383	0.081215	-0.014292	0.077800	-0.014200
142	0.083393	-0.013238	0.079807	-0.012719	0.076220	-0.012200
144	0.082146	-0.012145	0.078423	-0.011223	0.074700	-0.010300
146	0.080890	-0.011106	0.077055	-0.009863	0.073220	-0.008620
148	0.079625	-0.010122	0.075707	-0.008576	0.071790	-0.007030
150	0.078352	-0.009195	0.074376	-0.007382	0.070400	-0.005570
152	0.077071	-0.008324	0.073066	-0.006282	0.069060	-0.004240
154	0.075785	-0.007511	0.071772	-0.005275	0.067760	-0.003040
156	0.074492	-0.006756	0.070500	-0.004353	0.066508	-0.001950
158	0.073193	-0.006061	0.069246	-0.003524	0.065300	-0.000988
160	0.071889	-0.005425	0.068019	-0.002778	0.064150	-0.000131
162	0.070580	-0.004850	0.066815	-0.002113	0.063050	0.000624
164	0.069267	-0.004336	0.065634	-0.001528	0.062000	0.001280
166	0.067950	-0.003884	0.064480	-0.001012	0.061010	0.001860
168	0.066630	-0.003493	0.063350	-0.000566	0.060070	0.002360
170	0.065306	-0.003164	0.062243	-0.000192	0.059180	0.002780
172	0.063979	-0.002897	0.061159	0.000121	0.058340	0.003140
174	0.062650	-0.002693	0.060100	0.000379	0.057550	0.003450
176	0.061318	-0.002550	0.059059	0.000580	0.056800	0.003710
178	0.059986	-0.002469	0.058043	0.000730	0.056100	0.003930
180	0.058654	-0.002449	0.057027	0.000831	0.055400	0.004110
182	0.057322	-0.002487	0.056061	0.000886	0.054800	0.004260
184	0.055995	-0.002582	0.055047	0.000904	0.054100	0.004390
186	0.054673	-0.002729	0.054086	0.000881	0.053500	0.004490
188	0.053360	-0.002923	0.053130	0.000829	0.052900	0.004580
190	0.052063	-0.003156	0.052181	0.000752	0.052300	0.004660
192	0.050786	-0.003417	0.051243	0.000656	0.051700	0.004730
194	0.049541	-0.003693	0.050271	0.000558	0.051000	0.004810
196	0.048339	-0.003964	0.049369	0.000463	0.050400	0.004890
198	0.047196	-0.004204	0.048498	0.000393	0.049800	0.004990
200	0.046134	-0.004379	0.047667	0.000371	0.049200	0.005120
202	0.045179	-0.004446	0.046940	0.000427	0.048700	0.005300
204	0.044369	-0.004347	0.046284	0.000591	0.048200	0.005530
206	0.043746	-0.004012	0.045773	0.000909	0.047800	0.005830
207	0.043523	-0.003727	0.045612	0.001141	0.047700	0.006010

8.4.3 Formulas for Quasi 3D Navier Stokes evaluation

These formulas were used for the evaluation of the Quasi 3D Navier Stokes simulation jobs in capter 4.2.3 :

$T = p / (\rho \cdot 287)$

$c_{abs} = (c_{ax}{}^2+c_u{}^2+c_r{}^2)^{0.5}$

$w_{rel} = (c_{ax}{}^2+(c_u-u)^2+c_r{}^2)^{0.5}$

$a = (1.4 \cdot 287 \cdot T)$

$\alpha = \arctan(c_{ax}/c_u)$, $\beta = \arctan(c_{ax}/(c_u-u))$

$T_{tot} = T \cdot [1 + (1.4-1)/2 \cdot c_{abs}{}^2 / (1.4 \cdot p / \rho)]$

$p_{tot} = p \cdot [1 + (1.4-1)/2 \cdot c_{abs}{}^2 / (1.4 \cdot p / \rho)]$^(1.4/(1.4-1))

$M_{1is} = [\ 2 / (1.4-1) \cdot ((p_{0tot} / p_{1stat})$^((1.4-1)/1.4) - 1)]$^{0.5}$

$T_{1is} = T_{1tot}\ (p_1 / p_{0tot})$^((1.4-1)/1.4)

$c_{is} = M_{is}\ (1.4 \cdot 287 \cdot T_{is})^{0.5}$

$\rho_{is} = p / (287 \cdot T_{is})$

$\mu_{is} = \mu_s \cdot (T_{is}/T_s)^{1.5} \cdot (1+110.4/T_s) / (T_{is}/T_s+110.4/T_s)$ Sutherland law $\mu_s = 0.00001876$ Ns/m^2, T_s =303.15 K

$Re = c_{is} \cdot s \cdot \rho_{is} / \mu_{is}$

Zweiffel´s Coefficient = $2 \cdot c_{1ax} \cdot (c_{u1}-c_{u0}) / c_1{}^2 \cdot (t_1 / b_{1ax})$ respectively $2 \cdot c_{2ax} \cdot [(c_{u2}-u_2)-(c_{u1}-u_1)] / w_2{}^2 \cdot (t_2 / b_{2ax})$

$\pi = p_{0tot} / p_{2stat}$

$\eta = a_u / \Delta h_{is}$

$a_u = P / m = u_1 \cdot c_{1u} - u_2 \cdot c_{2u}$

$\Delta h_{is} = 1.4/(1.4-1) \cdot 287 \cdot T_{0tot} \cdot [1 - ((p_{2stat} / p_{0tot})$^((1.4-1)/1.4)]

$\psi = \Delta h / u_2{}^2$

$\phi = c_{2ax} / u_2$

$R_{kin} = 1 - (c_2{}^2 - c_1{}^2) / (2 \cdot (u_2 \cdot c_{2u} - u_1 \cdot c_{1u}))$